Targeting monocarboxylate transporters to reverse lactic acid-driven immunosuppression

DISSERTATION ZUR ERLANGUNG

DES DOKTORGRADES DER NATURWISSENSCHAFTEN (DR. RER. NAT.)

DER FAKULTÄT FÜR BIOLOGIE UND VORKLINISCHE MEDIZIN

DER UNIVERSITÄT REGENSBURG

vorgelegt von

Nathalie Babl, geb. Kauer

aus Marktredwitz

im Jahr 2023

The present work was carried out from October 2019 to April 2023 at the Clinic and Polyclinic of Internal Medicine III at the University Hospital Regensburg.

Die vorliegende Arbeit entstand im Zeitraum von Oktober 2019 bis April 2023 an der Klinik und Poliklinik für Innere Medizin III des Universitätsklinikums Regensburg.

Das Promotionsgesuch wurde eingereicht am: 04.04.2023

Die Arbeit wurde angeleitet von: Prof. Dr. Marina Kreutz

Unterschrift: _____

Table of contents

List of Figures

List of Tables

List of Abbreviations

µM	micromole per liter
2NBDG	2-Deoxy-2-[(7-nitro-2,1,3-benzoxadiazol-4-yl)amino]-D-glucose
3-BrPA	3-Bromopyruvate
3PG	3-Phosphoglyceric acid
7-AAD	7-Aminoactinomycin D
AA	Acrylamide
ACK	Ammonium chloride potassium
ADCC	Antibody-dependent cellular cytotoxicity
AM	Acetoxymethylester
AMPK	AMP-activated protein kinase
ANOVA	Analysis of variance
AO	Acridine orange
APCs	Antigen presenting cells
APS	Ammonium persulfate
Arg-1	Arginase 1
ASA	Acetylsalicylic acid
ATP	Adenosine triphosphate
BCR	B cell receptor
BM	Bone marrow
BSA	Bovine serum albumin
BV	Brilliant Violet
BW	Body weight
CAFs	Cancer-associated fibroblasts
CCL	CC-chemokine ligand
ccRCC	Clear cell renal cell carcinoma
CD	Cluster of differentiation
CG	Cathepsin G
CHC	α-cyano-4-hydroxy cinnamic acid
COX	Cyclooxygenase
CRC	Colorectal carcinoma
CSF	Colony stimulating factor
CTL	Cytotoxic T cell
CTLA4	Cytotoxic T lymphocyte-associated protein 4

CXCL2	CXC motif chemokine 2
CXCR2	CXC motif chemokine receptor 2
DC	Dendritic cell
DCA	Dichloroacetate
DCF	2',7'-Dichlorodihydrofluorescein
DCFDA	2',7'-Dichlorodihydrofluorescein diacetate
DFMO	Difluoromethylornithine
DHAP	Dihydroxyacetone phosphate
Diclo	Diclofenac
DMSO	Dimethyl sulfoxide
DNA	Deoxyribonucleic acid
DNase	Desoxyribonuclease
dNTPs	2'-Deoxyribonucleosid-5'-triphosphates
ECL	Enhanced chemiluminescence
ECM	Extracellular matrix
EDTA	Ethylene diamine tetra acetic acid
ELISA	Enzyme-linked immunosorbent assay
EMT	epithelial-mesenchymal transition
FCS	Fetal calf serum
FDG-PET	Fluorodeoxyglucose positron emission tomography
fMLP	N-Formylmethionyl-leucyl-phenylalanine
Foxp3	Forkhead box protein 3
FRET	Fluorescence resonance energy transfer
GA3P	Glyceraldehyde 3-phosphate
GA3P	Glyceraldehyde 3-phosphate
GAPDH	Glyceraldehyde 3-phosphate dehydrogenase
G-CSF	Granulocyte-colony stimulating factor
GFP	Green fluorescent protein
GLUT	Glucose transporter
H^+	Proton
HBSS	Hank's balanced salt solution
HIF	Hypoxia-inducible factor
HK	Hexokinase
HLA	Human leukocyte antigen
HRE	Hypoxia-responsive elements

HRP	Horse radish peroxidase
i.p.	Intraperitoneally
ICAM-1	Intracellular adhesion molecule 1
ICB	Immune checkpoint blockade
IFNγ	Interferon gamma
Ig	Immunoglobulin
IHC	Immunohistochemistry
IL	Interleukin
IMC	Immature myeloid cells
iNOS	Inducible nitric oxide synthase
$KHCO_3$	Potassium hydrogen carbonate
KIR	Killer Ig-like receptors
Km	Michaelis-Menten constant
KO	Knock-out
LA	Lactic acid
LBK1	Liver kinase B1
LDH	Lactate dehydrogenase
LPS	Lipopolysaccharide
Luc	Luciferase
MACS	Magnetic cell sorting
MCT	Monocarboxylate transporter
MCT1i	Inhibitor of monocarboxylate transporter 1
MCT4i	Inhibitor of monocarboxylate transporter 4
MDSCs	Myeloid-derived suppressor cells
MeTD	Metabolic tumor stroma score
MHC	Major histocompability complex
mM	millimole per liter
M-MLV	Moloney leukemia virus
MMRd	Mismatch repair deficit
MNCs	Mononuclear cells
mRNA	Messenger RNA
MSI	microsatellite instability
mTOR	Mechanistic target of rapamycin
NAD	Nicotinamide adenine dinucleotide
NADH	Nicotinamide adenine dinucleotide hydrogen

NE	Neutrophil elastase
NET	Neutrophil extracellular trap
NFAT	Nuclear Factor of Activated T Cells
NF-kB	Nuclear factor kappa b
NH_4Cl	Ammonium chloride
NK cell	Natural killer cell
NKG2D	Natural-killer group 2 member D
Nox	NADPH oxidase 2
NSAID	Non-steroidal anti-inflammatory drug
OVA	Ovalbumine
OXPHOS	Oxidative phosphorylation
P/S	Penicillin/streptomycin
PBS	Phosphate buffered saline
PCR	Polymerase chain reaction
PD-1	Programmed cell death protein 1
PDK	Pyruvate dehydrogenase
PDK1	Pyruvate dehydrogenase kinase 1
PD-L1	Programmed cell death ligand 1
PFK	Phosphofructokinase
PFKb3	Phosphofructokinase 2
PG	3-Phosphoglyceric acid
PI	Propidium iodide
PI3K	Phosphatidylinositol 3-kinase
PMBCs	Peripheral blood mononuclear cells
PMN	Polymorphonuclear cells
PPP	Pentose-phosphate pathway
PRR	Pattern recognition receptor
PVDF	Polyvinylidenfluoride
qRT-PCR	Quantitative real-time PCR
RCC	Renal cell carcinoma
RNA	Ribonucleic acid
ROS	Reactive oxygen species
SDS	Sodium dodecyl sulfate
SDS-PAGE	Sodium dodecyl sulfate polyacrylamide gel electrophoresis
SEM	Standard error of mean

SLC	Solute carrier
SOGC	Serine-glycine-one-carbon
TAMs	Tumor-associated macrophages
TANs	Tumor-associated neutrophils
TBS	Tris buffer saline
TBST	TBS + Tween 20
TCA	Tricarboxylic acid
TCR	T cell receptor
TECs	Tumor-associated endothelial cells
TEMED	Tetramethylethyldiamine
TGF	Transformation growth factor
Th	T helper cell
TIGAR	TP53-induced glycolysis and apoptosis regulator
TIL	Tumor infiltrating lymphocytes
TLR	Toll like receptor
TME	Tumor microenvironment
TNF	Tumor necrosis factor
TNM	Tumor-node-metastasis
Treg	Regulatory T cell
Tris	Tris-(hydroxymethyl)-aminomethane
VEGF	Vascular endothelial growth factor
VHL	von Hippel-Lindau
WT	Wildtype

1 Introduction

1.1 Hallmarks of cancer

We all come into contact with cancer in the course of our lives, either because we know someone who has cancer or because we ourselves are diagnosed. Despite the remarkable progress in cancer research, cancer remains a global burden on humanity, with an increasing incidence due to demographic changes and unhealthy lifestyle habits (1). The transformation of a normal cell into a tumor cell is a multistep process, which requires the acquisition of several characteristic capabilities to enable proliferation, survival and dissemination of tumor cells. These functional capabilities were summarized by Hanahan and Weinberg as "hallmarks of cancer" in one of the most cited publications in cancer research in 2000 (2). In the original article the authors described 6 hallmarks. Later, in 2011, two new emerging hallmarks and two enabling characteristics were added, including a dysregulated energy metabolism (3). Finally, in 2022, Hanahan published a revised version (4), as shown in Figure 1.

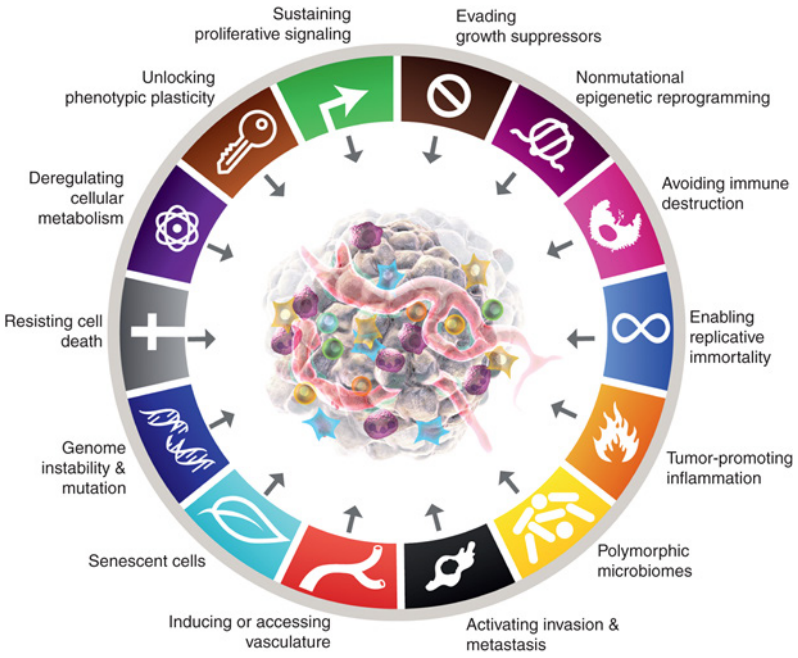

Figure 1. The Hallmarks of Cancer. Depiction of the functional capabilities of tumors acquired during tumorigenesis. (Modified from Hanahan, Cancer Discoveries 2022 (4))

Certainly, **continuous proliferation** is the most important function of tumor cells. While healthy cells tightly control cell division to ensure homeostasis of cell number and thus maintenance of normal tissue structure and function, tumor cells develop various mechanisms to achieve uncontrolled growth (4).

Genome instability and mutations promote the achievement of numerous hallmark functions. Most of the genetic alterations in cancer underlie either a gain-of-function mutation in proto-oncogenes or

a loss-of-function mutation in tumor-suppressor genes (3). Mutated oncogenes then foster cell division, growth and survival, whereas tumor-suppressors should protect against uncontrolled cellular growth, support DNA repair and control the cell cycle under physiological conditions (Figure 2).

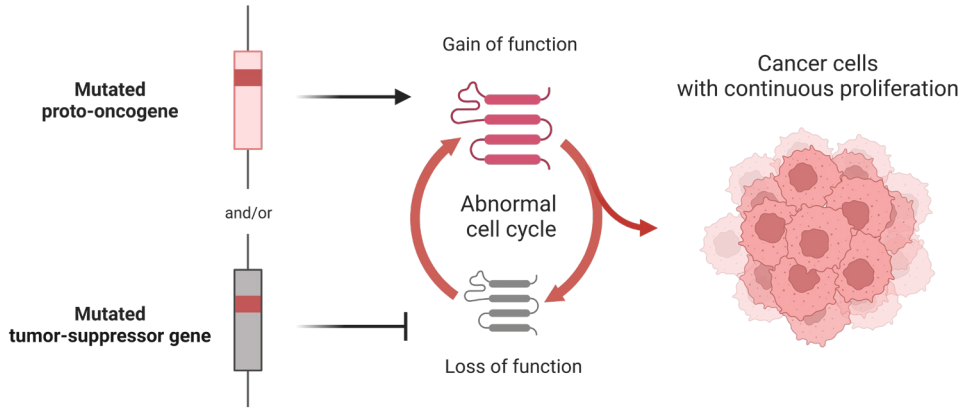

Figure 2. Gain-of-function of oncogenes and loss-of-function of tumor-suppressor genes. Mutations in proto-oncogenes or tumor-suppressor genes enable the sustained proliferation of tumor cells. Created with BioRender.com.

Evasion of growth suppressors is required to maintain proliferation and is mediated by dysfunction of tumor-suppressor genes or oncogenes, which are normally involved in powerful programs that limit uncontrolled cell growth. Two master regulators are the p53 protein and retinoblastoma protein (RB), which act as central checkpoints within two important, complementary cellular regulatory loops that determine proliferation or activation of senescence or apoptosis programs. Furthermore, **epigenetic reprogramming** accounts for pathological altered expression of proto-oncogenes and tumor-suppressor genes and has recently been added to the list of characteristics of cancer (3). Loss of PTEN due to promoter methylation is a prominent example of epigenetics promoting tumor progression. PTEN phosphatase antagonizes Phosphatidylinositol 3-kinase (PI3 kinase) by degrading its product, phosphatidylinositol trisphosphate (PIP3) (5,6).

Healthy cells have a kind of biological clock, an evolutionarily conserved repetitive nucleotide sequence called telomeres at the end of chromosomes that get shorter with each cell division (7). When telomeres reach a critical length, the cell can no longer perform further mitosis (8). Cancer cells **outsmart age-related death** by aberrant expression of telomerases. In addition, tumor cells develop a variety of strategies to **resist apoptosis**. Most commonly, tumor cells exhibit loss of function of tumor-suppressor p53, a critical damage sensor of the apoptosis-inducing circuit (9). Furthermore, tumor cells upregulate expression of anti-apoptotic regulators (Bcl-2) or survival signals (Igf1/2) and downregulate expression of pro-apoptotic factors (Bax, Bim, Puma) (3).

Tumor **angiogenesis** is essential for ongoing survival and progression of tumors. In the past, angiogenesis was considered important only when tumors grew macroscopically to receive nutrients and oxygen and to remove metabolic waste and carbon dioxide (3). However, there is emerging

evidence that angiogenesis also supports the microscopic premalignant phase of neoplastic progression, reinforcing its status as a hallmark of cancer. The process of growing new vessels is mostly regulated by oncogenic signaling and the expression of vascular endothelial growth factor A (VEGF-A). In addition to tumor cells, myeloid cells such as macrophages or neutrophils can promote pathological angiogenesis (10–12).

The response of the human body to cancer cells shows several analogies to **inflammation** and therefore Harold F. Dvorak considered tumors as “wounds that do not heal” (13–16). Nowadays, the inflammatory microenvironment with several infiltrating immune cells is actually declared as a hallmark of cancer (3).
Tumors as organs interface with their surroundings and moreover with the entire organism. There is increasing evidence that **polymorphic microbiomes** residing in the gut, skin or other mucosa and connected organs, or in tumors themselves can affect many of the characteristic capabilities in different ways (4).

Of fundamental importance for the prognosis of cancer patients is the **tissue invasion and metastasis behavior** of tumor cells. A multifaceted process involving several steps of wound healing and embryonic morphogenesis enables the "epithelial-mesenchymal transition" (EMT) of tumor cells. EMT allows tumor cells to migrate and lays the cornerstone for metastasis (17–19). However, stromal cells have also been shown to promote invasion and metastasis. For example, tumor-associated macrophages (TAMs) can foster penetration of adjacent tissue by secreting matrix-degrading enzymes (20,21). In addition, **phenotypic plasticity and impaired differentiation** are thought to represent independent capacity (4).

However, the continuous progress over the past decades has revisited the scope of the “hallmarks of cancer” (2–4). Rapid tumor growth requires **reprogramming of tumor metabolism**, shaping an intricate tumor microenvironment (TME). Metabolic adaption is most evident in accelerated glycolysis of tumor cells, even in the presence of oxygen, to produce adenosine triphosphate (ATP) and building blocks (22). As consequence, glucose is depleted from the TME while lactate and H^+, hereafter referred as lactic acid, accumulates. However, tumors are more and more considered as ‘organs’ that exhibit another level of complexity. They consist of tumor cells, metabolites and in addition of a whole recruitment of different cell types creating the intricate TME. Recently, **senescent cells of different origins** were included in the list of functionally important cell types in the TME. Remarkably, tumor-infiltrating immune cells are not only suppressed but also co-opted to promote tumor growth, resulting in **immune evasion** (23–28). Therefore, tumor biology can only be fully understood by investigation of the crosstalk between all cells types within the tumor as well as the TME (29). In recent decades, it has become clear that the two hallmarks “metabolic adaptation of tumor cells” and “immune evasion” are

closely linked, opening a therapeutic field that simultaneously target tumor metabolism and immunosuppression (30).

The following chapters will focus on the metabolic interplay between tumor cells and immune cells and discuss tumor metabolism as a target for cancer therapy.

1.2 The tumor microenvironment

The TME is an intricate network of different cell types and non-cellular soluble factors as shown in Figure 3. The composition and properties of the TME can diversify broadly and are critical in determining immune response against the tumor. The tumor stroma consists of various cell populations such as T cells, natural killer (NK) cells, dendritic cells (DCs), macrophages, myeloid-derived suppressor cells (MDSCs), fibroblasts, and endothelial cells. However, tumor-associated immune cells are a double-edged sword, as they can promote or inhibit tumor growth. Through various mechanisms cancer cells tend to evade immune surveillance. One mechanism of immunosuppression is based on tumor metabolism. Tumor cells, as well as activated T cells and NK cells, rely on glucose and amino acids to cover their energetic demands and generate building blocks for intracellular processes, leading to metabolic competition. In addition to nutrient restriction, tumor-induced accumulation of metabolites such as lactic acid inhibits immune cell function (31), which is addressed more in detail in the following sections.

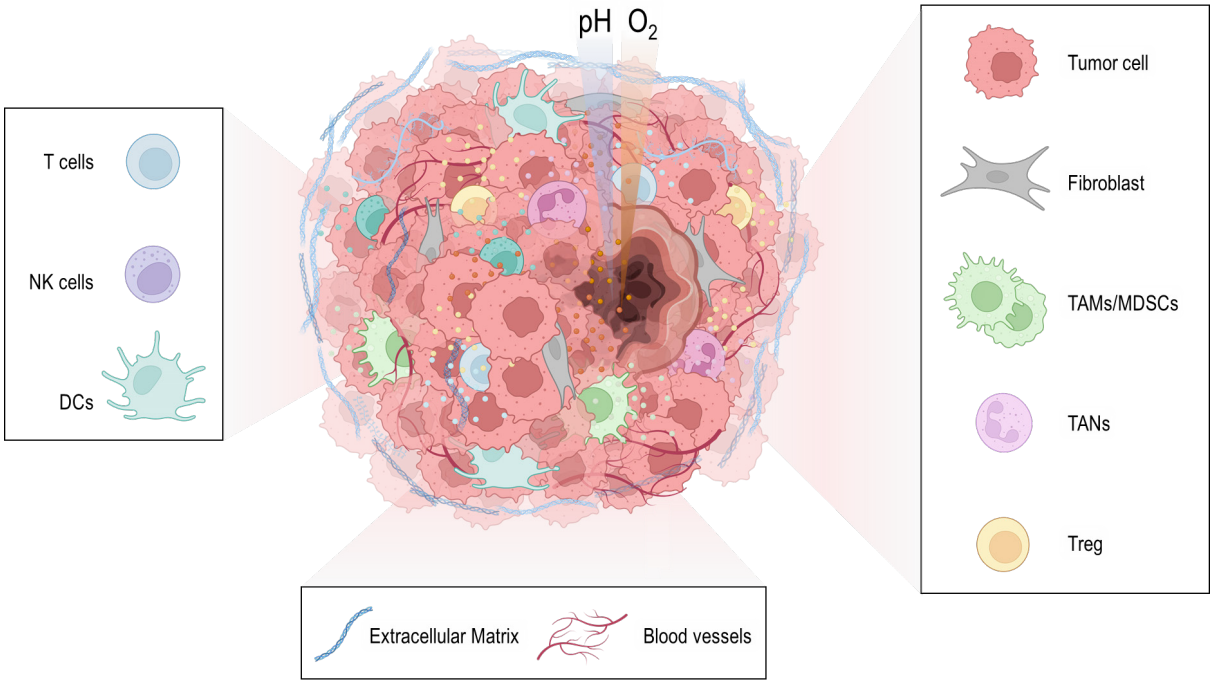

Figure 3. Schematic representation of the tumor microenvironment (TME), which comprises stromal and immune cells and extracellular matrix components. Abbreviations: MDSC, myeloid-derived suppressor cell; NK, natural killer; TAM, tumor-associated macrophage; TAN, tumor-associated neutropil; Treg, regulatory T cell. Created with BioRender.com.

1.2.1 Tumor cells

Carcinogenesis has several parallels to evolutionary development. Metabolic adaption of tumor cells is crucial for tumor development and progression. This includes alterations in amino acid and lipid metabolism but one of the key-metabolic alterations is an elevated glycolytic rate, termed Warburg effect. The Warburg effect of tumor cells leads to glucose depletion and accumulation of lactic acid within the TME. Lactic acidosis has severe consequences for immune cells and is a driving force for angiogenesis, metastasis and cancer progression (32–39). Thus, glucose metabolism represents an attractive target for anti-cancer therapy.

1.2.1.1 Tumor metabolism - the Warburg effect

The Warburg effect: 100 years on.

Glucose is the main source for energy production in most cells of the human body. In non-malignant cells, glucose is mainly introduced into the tricarboxylic acid cycle (TCA) cycle to generate 30-32 ATP per molecule glucose via oxidative phosphorylation (OXPHOS). However, tumor cells adapt their metabolism towards enhanced aerobic glycolysis (2 ATP/glucose) rather than the much more efficient OXPHOS to meet bioenergetic, biosynthetic, and redox requirements. We are now approaching the 100th anniversary of the first description of this phenomenon. The characteristic aerobic glycolysis of tumor cells was named “Warburg effect” after its discoverer Otto Warburg, who received the Nobel Prize in 1931 not for the Warburg effect but for his discovery of the nature and function of the respiratory enzyme cytochrome c oxidase (22).

As shown in Figure 4, glucose is taken up via glucose transporter 1 (GLUT1) and converted to pyruvate, which is metabolized into lactate by the lactate dehydrogenase (LDH). Constant glycolytic activity requires continuous export of the produced lactate out of the cells via monocarboxylate transporter (MCT) 1 and MCT4 in symport with a proton (H^+) in a concentration-dependent manner, resulting in lactate accumulation and acidification of the TME.

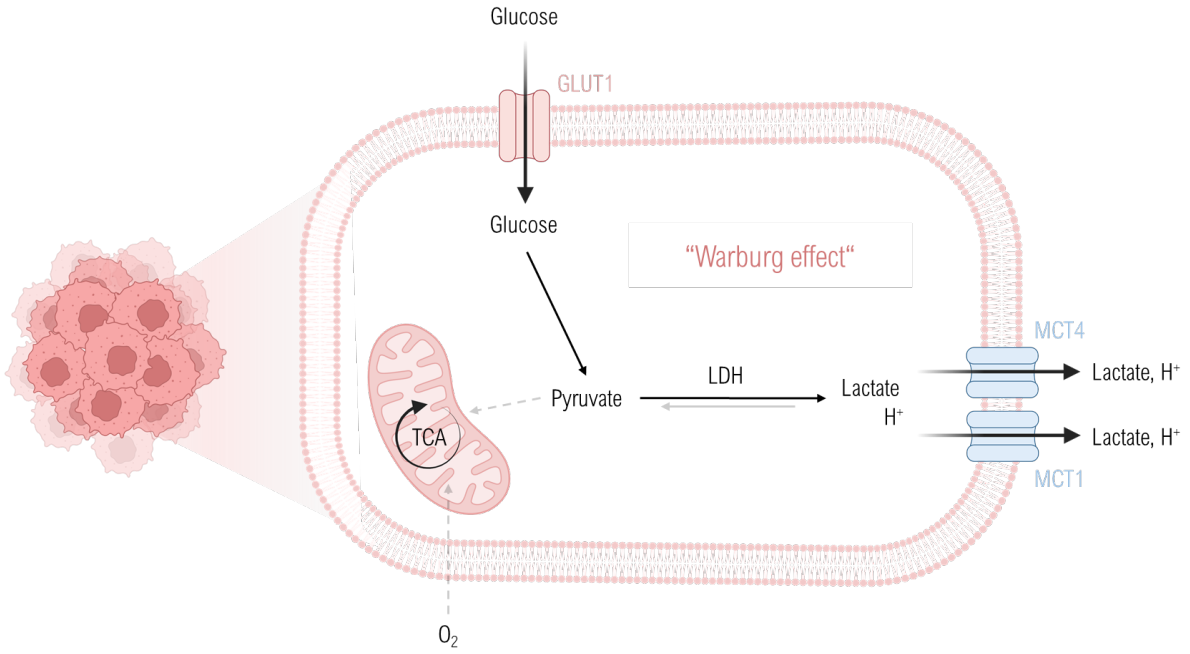

Figure 4. Tumor cells are characterized by accelerated aerobic glycolysis - the Warburg effect. Glucose transporter 1 (GLUT1) enables the uptake of glucose into the cell, which is followed by its conversion to pyruvate. In tumor cells, glucose-derived pyruvate is not introduced into the tricarboxylic acid cycle (TCA) and oxidative phosphorylation (OXPHOS) in the mitochondria but metabolized to lactate by lactate dehydrogenase (LDH) independently of the presence of oxygen (O_2) and exported from the cell via monocarboxylate transporters 1 and 4 (MCT1/4). As a result, lactic acidosis of the tumor microenvironment (TME) occurs. Created with BioRender.com.

But why do cancer cells switch to a less efficient metabolism?

Warburg thought that aerobic glycolysis is due to "the irreversible injury of respiration" in tumor cells (40). Nowadays, it is known that mitochondrial function is intact in most tumor cells and some even depend on mitochondrial respiration (41–43). In fact, solid tumors often represent a mosaic of cells with different metabolic properties (37). However, the answer to the question of why is that it is not fully understood. A correlation between accelerated glucose uptake and proliferation has been found in tumor cells, but also in non-malignant cells (44). In cell cultures, increased proliferation upon stimulation is accompanied by increased glycolysis, as evidenced by lactate accumulation in the medium. This simple observation raised the hypothesis that the Warburg effect provides glycolytic intermediates and building blocks fueling pathways that contribute to macromolecular synthesis as shown in Figure 5 (45). With each cell division, the cell must double its cell mass. Nourished pathways include the pentose-phosphate pathway (PPP) providing ribose for nucleotide synthesis and NADPH for reductive biosynthesis, the hexosamine pathway, which is important for protein glycosylation, the serine-glycine-one-carbon (SOGC) metabolism, which is required for glutathione, nucleotides and methylation processes and glycerol production for generation of lipids (42). These pathways are often upregulated in tumor cells by oncogenic signaling.

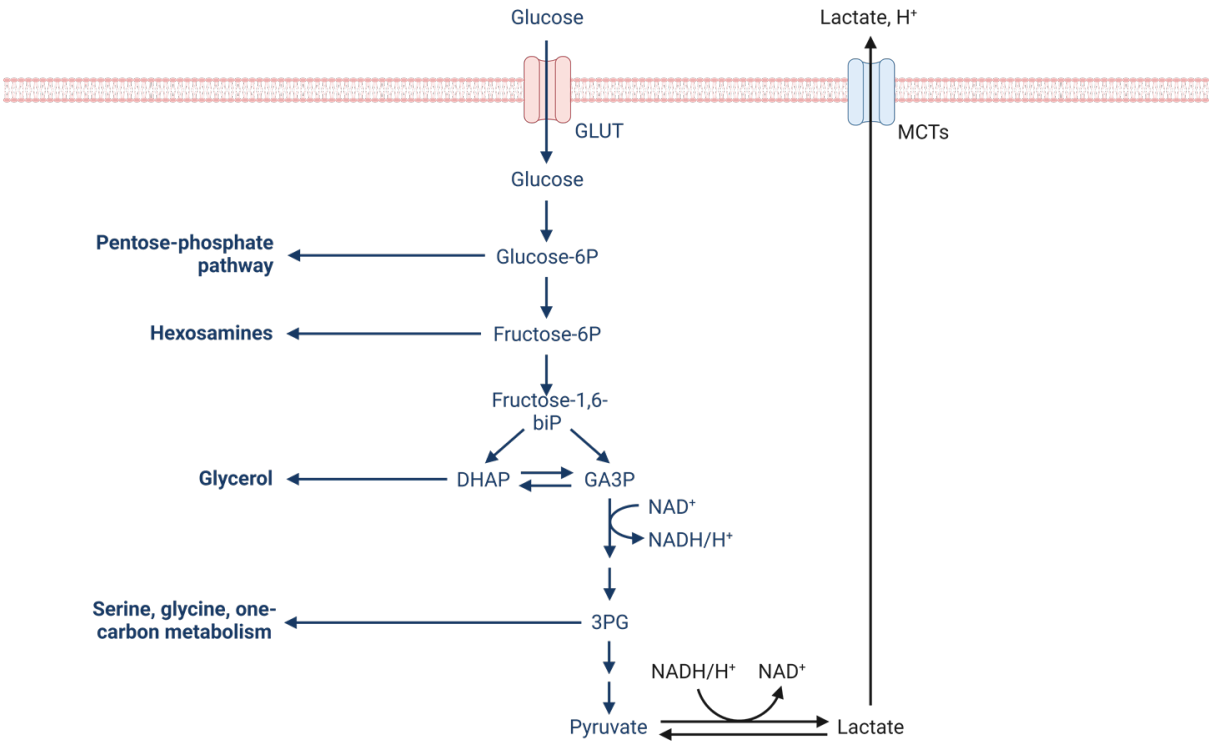

Figure 5. The Warburg effect provides building blocks for rapid tumor growth. Glycolytic intermediates fuel the pentose-phosphate pathway, hexosamine pathway, serine-glycine-one-carbon metabolism and provide glycerol for synthesis of lipids. GLUT, glucose transporter; MCTs, monocarboxylate transporter; P, phosphate; DHAP, dihydroxyacetone phosphate; GA3P, glyceraldehyde 3-phosphate; 3PG, 3-phosphoglyceric acid; NADH, nicotinamide adenine dinucleotide hydrogen; NAD, nicotinamide adenine dinucleotide. Created with BioRender.com.

However, the fact that tumor cells excrete enormous amounts of lactate due to the Warburg effect and thus loose three carbons/glucose molecule that could have been used for building blocks speaks against this hypothesis. In this context, Hosios et al. investigated the origin of carbon mass and found that neither glucose nor glutamine are the main source, but instead other amino acids, which are consumed to a much lesser extent, account for the majority of carbon mass (46). This indicates that there must be another reason for aerobic glycolysis besides generating building blocks for biosynthesis.

Luengo et al. recently postulated that cells engage aerobic glycolysis when the demand for NAD^+ is in excess of the demand for ATP (47). Finally, fitting the analogy to evolution, it has been hypothesized that the Warburg effect simply provides a selection advantage in hypoxic regions (48).

Tumor cells rely on the continuous export of lactate to maintain glycolytic flux, which is mediated by MCTs that export lactate along with protons (lactic acid). This leads to accumulation of lactate and concomitant acidification of the TME. Acidosis supports tumor growth in multiple ways by promoting invasion, angiogenesis, metastasis, and immune evasion (37,48). In line, buffering with bicarbonate reduced formation of spontaneous metastasis in a prostate cancer model (49). Studies reported that high lactate levels in primary lesions of human tumors correlate with occurrence of metastasis (50,51).

The formation of blood vessels enables extravasation and the formation of metastases. Interestingly, tumor-derived lactic acid induces angiogenesis by stimulating the production of VEGF by endothelial but also myeloid cells (38,39,52). Furthermore, lactic acid acts as an immune-regulatory molecule, which is discussed more in detail in chapter 1.2.1.3. Therefore, the Warburg effect of tumor cells facilitates invasion, metastasis, and immune escape by inducing lactic acidosis in the TME.

Which mechanisms are driving the Warburg effect?

Glycolysis-related genes have been found to be overexpressed in a set of 24 cancer entities representing more than 70 % of cancers worldwide (53). It is known that metabolic reprogramming of malignant cells is driven by genetically altered expression levels of different genes, dysfunctional oncogenes or tumor-suppressor genes (54,55). A schematic overview of the molecular mechanisms mediating the Warburg phenotype in tumor cells is given in Figure 6 and explained in more detail below.

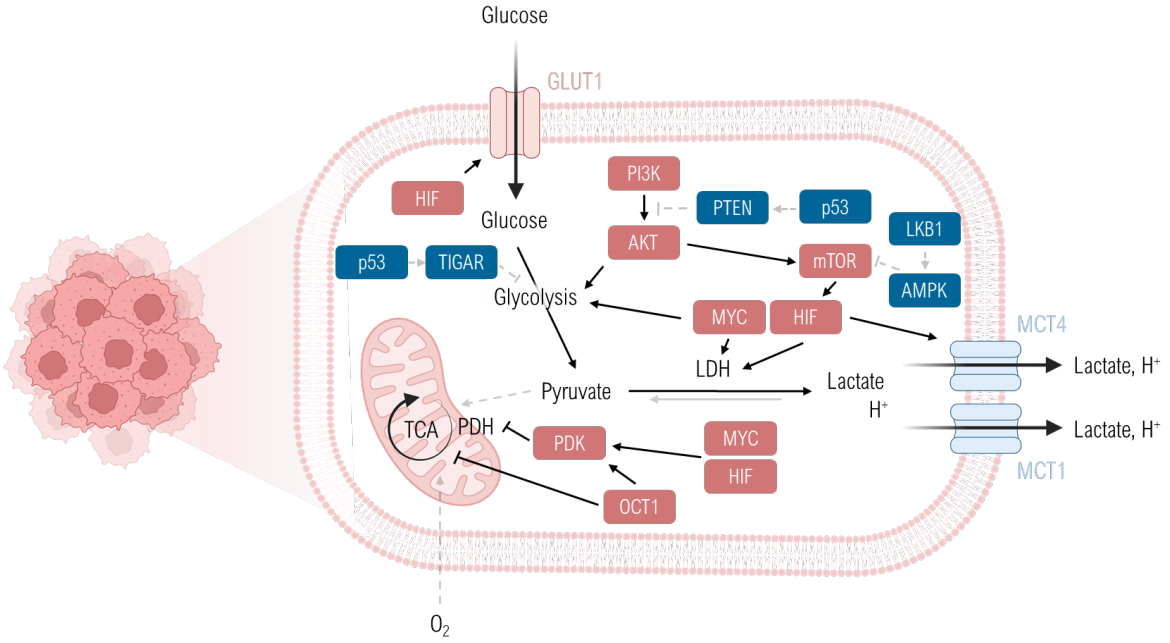

Figure 6. Molecular mechanisms driving the Warburg effect. The glycolytic switch of tumor cells is driven by multiple oncogenic signaling pathways. Phosphatidylinositol 3-kinase (PI3K) activates AKT, which in turn activates mTOR and directly regulates glycolytic enzymes, resulting in increased glycolysis. The tumor-suppressor liver kinase B1 (LKB1) normally counteracts the glycolytic phenotype by inhibiting mTOR through activation of AMP-activated protein kinase (AMPK). The mTOR pathway regulates many basic biological and physiological processes, but among others stimulates the glycolytic phenotype by activation of hypoxia-inducible factor 1 (HIF1), which induces a hypoxia-adapted transcriptional program. HIF1 upregulates the expression of glucose transporter 1 (GLUT1), different glycolytic enzymes, lactate dehydrogenase A (LDHA), monocarboxylate transporter 4 (MCT4) and pyruvate dehydrogenase kinase 1 (PDK1), which blocks the entry of pyruvate into the tricarboxylic acid (TCA) cycle. MYC cooperates with HIF in the transcription of several genes encoding glycolytic proteins, but also enhances mitochondrial metabolism. The tumor-suppressor p53 normally counteracts the glycolytic phenotype by suppressing glycolysis through TP53-induced glycolysis and apoptosis regulator (TIGAR) and supporting PTEN expression, opposing the PI3K/AKT pathway. OCT1 (also known as POU2F1) has an inhibitory effect on oxidative phosphorylation (OXPHOS). PDH, pyruvate dehydrogenase. The dashed grey lines indicate loss of function. According to Cairns et al. (55). Created with BioRender.com.

One pathway, which is heavily affected by activating mutations in several cancer entities is the PI3K-AKT-mTOR axis. Phosphatidylinositol 3-kinase (PI3K) downstream signaling involves AKT1, which in turn activates mTOR (mammalian Target of Rapamycin) and as well directly regulates glycolytic enzymes, in the end resulting in increased glycolysis. AKT1 is an important effector for glycolysis and upregulates expression of glucose transporters (GLUT1) and activates key-glycolytic enzymes by phosphorylation, such as hexokinase and phosphofructokinase 2 (PFKb3) (56,57).

Moreover, AKT1 activates mTOR, which is a master regulator and often constitutively activated in tumor cells. Activated mTOR induces protein and lipid biosynthesis for cell proliferation and activates the transcription factor hypoxia-inducible factor 1 (HIF1) even in the presence of adequate oxygen supply (55).

HIF1 is a major driver of the Warburg effect downstream of the PI3K/AKT and mTOR pathways. HIF1 and HIF2 are transcription factors that consist of a HIF1β subunit and either the HIF1α or HIF2α subunit forming a heterodimer and induce gene expression under hypoxia. HIFα is strictly regulated and connected to cellular oxygen availability, while the β-subunit is ubiquitously expressed. Under normoxic conditions, the HIFα subunits are hydroxylated in an oxygen dependent reaction, allowing the recognition by the von Hippel-Lindau tumor-suppressor (VHL), an ubiquitin ligase, and subsequent proteasomal degradation. Under hypoxia, oncogenic signaling or loss of-function of VHL, HIF1 is stabilized and binds to regulatory hypoxia responsive elements (HRE) in the DNA (58). Subsequently, expression of more than 70 genes is induced, including VEGF, GLUT1, most glycolytic enzymes, LDHA, and lactate transporter MCT4 (55,59). Overexpression and stabilization of HIF1 has been demonstrated in several cancers and is associated with aggressiveness and poor prognosis (59–63). In addition, HIF1 activates pyruvate dehydrogenase kinases (PDKs), which inactivate the mitochondrial pyruvate dehydrogenase complex by phosphorylation and thereby prevent the entry of pyruvate into the tricarboxylic acid (TCA) cycle (64–66). In consequence, the rate of OXPHOS is reduced, which enforces the glycolytic phenotype.

A collaborator of HIF is the transcription factor c-MYC. Whereas tightly regulated in normal cells, overexpression of MYC is found in about 30 % of human tumors. Together with HIF stabilization, MYC signaling leads to activation of various glucose transporters, LDH and PDK1, but also stimulates mitochondrial biogenesis and function as well as mitochondrial glutaminolysis (37,55,67–70).

Furthermore, AMP-activated protein kinase (AMPK) is a critical sensor of energy status and crucial in cellular response to metabolic stress. On molecular basis, AMPK normally antagonizes AKT1 and inhibits mTOR. Various oncogenic dysfunctions can suppress AMPK signaling, thereby uncoupling energy status from proliferation signaling (55,71). In healthy cells, the tumor-suppressor gene STK11,

encoding liver kinase b1 (LKB1), activates AMPK through phosphorylation and is mutated in Peutz-Jeghers syndrome (72). Loss of AMPK signaling allows mTOR activation and subsequent HIF stabilization, enforcing the glycolytic switch (55).

Overexpression of the transcription factor OCT1 has been reported in several human cancers. Studies in mice revealed that OCT1-induced gene expression leads to increased glucose metabolism and decreased mitochondrial respiration (73). Among the regulated genes is an isoform of the PDK, the PDK4, which exerts the same function as PDK enzymes activated via HIF1. However, clarifying the downstream pathways of OCT1 requires further investigation (55).

Implication of the Warburg effect in diagnostics

The discovery by Otto Warburg and colleagues had a fundamental impact on cancer diagnostics. The fact that cancer cells rely on increased glucose uptake has proven useful for tumor diagnosis, staging, and surveillance and provides the basis for clinical 18F-fluorodeoxyglucose positron emission tomography (FDG-PET) (37,55,74,75).

1.2.1.2 Monocarboxylate transporters – the Achilles' heel of Warburg?

Tumor cells are characterized by metabolic adaption towards a glycolytic phenotype known as the Warburg effect. Due to increased glycolysis, tumor cells produce lactate in the millimolar range. Maintenance of the Warburg phenotype requires continuous export mediated by proton-coupled MCTs. Expression of MCTs has been implicated in tumor aggressiveness and poor patient survival in across many cancers and hence deserves attention (76–79).

MCTs belong to the solute carrier (SLC) 16 gene family that implies 14 isoforms, each of them forming 12 transmembrane helices. Out of those, MCT1 (*SLC16A1*), MCT2 (*SLC16A7*), MCT3 (*SLC16A8*) and MCT4 (*SLC16A3*) mediate a proton-linked transmembrane transport of L-lactate, pyruvate and ketone bodies in a wide variety of tissues (80). MCTs are passive transporters and operate bidirectionally depending on the concentration gradient of their substrates. Furthermore, it was demonstrated that functional expression and correct translocation to the plasma membrane of MCT1 and 4 requires co-expression and interaction with the chaperone CD147 (basigin) (81–83). Besides the proton-coupled transporters, a second sodium-coupled class of MCTs has been identified, comprising two members, SLC5A8 and *SLC5A12* (84). However, this thesis focuses on MCT1 and MCT4, which are the key tumor-associated lactate transporters (85,86).

MCT1 mainly facilitates lactate entry under physiological conditions

MCT1 has a high affinity for lactate (Km = 3.5 - 10 mM), but also for pyruvate (Km = 0.7 mM) and is ubiquitously expressed. MCT1 is found in heart and red skeletal muscle fibers and facilitates the entry of lactate and ketone bodies into myocytes as fuel for OXPHOS (87–89). Indeed, a correlation between the abundance of MCT1 and the oxidative capacity of muscle fibers, as evidenced by mitochondrial content, has been noted (90,91). In the renal proximal tubule and liver parenchyma, MCT1 mediates the import of lactate into the cell for gluconeogenesis (92). In addition, MCT1 (or MCT2) is important for the transport of monocarboxylates across the blood-brain-barrier as nutrients for neurons, which use them for mitochondrial respiration (93). Especially in muscles and the brain, MCT isoforms are able to act as a kind of shuttles in the influx and efflux of lactic acid (93).

Furthermore, MCTs are essential for glycolytic cells such as erythrocytes, activated T cells, white muscle cells, but also tumor cells. Lactate, the end product of glycolysis, must be exported to maintain glycolysis. This is mediated in some cases by MCT1 in a gradient-dependent manner, while MCT4 is the main transporter for lactate efflux in highly glycolytic cells (94). MCT1 may play a role in the redox balance between reduced (NADH) and oxidized (NAD^+) nicotinamide adenine dinucleotide (95,96). At molecular level, this means that cytosolic NADH/NAD^+ ratio is linked to the lactate/pyruvate ratio and the mitochondrial NADH/NAD^+ ratio is linked to the hydroxybutyrate/acetoacetate ratio. MCT1 in the gut is thought to be involved in the uptake of short-chain fatty acids such as acetate, propionate, and butyrate produced by bacteria (95,96). Notably, all MCT isoforms, including MCT1, are completely absent in Langerhans β-cells, which is essential for preventing insulin secretion due to elevated blood lactate levels during exercise (97). MCT1 (and MCT3) is also important for the osmotic balance of the eye by transport of lactate and water in the retinal pigment epithelium. This process is required for retinal adhesion and pH regulation of the subretinal space (96). Finally, it is controversially discussed whether MCT1 is also found in the mitochondrial membrane acting as a lactate shuttle (89,96,98–100).

The regulation of MCT1 expression is not fully understood. MCT1 is thought to be upregulated by AMPK and calcineurin. Interestingly, the promoter of MCT1 contains the binding sequence of Nuclear Factor of Activated T Cells (NFAT) and calcineurin could dephosphorylate and activate the transcription factor NFAT (96). One study reported that the promoter of MCT1 can be silenced by methylation in breast cancer (101).

Micro RNAs (miRNA) might also be involved in regulation. Loss of translation repressors miR-29a and miR-29c increase MCT1 expression via oncogenic MYC signaling (102,103). Moreover, loss-of-function of tumor suppressor p53 and nuclear factor kappa b (NF-kB) might enhance MCT1 expression (104). Finally, extracellular acidosis can trigger MCT1 expression by HIF2 and MYC activation (105,106).

MCT4 is the Achilles' heel of glycolytic tumors – main lactate exporter

MCT4 has a lower affinity for lactate (Km = 22 - 28 mM), but - important for its function as main lactate exporter - an extremely low affinity for pyruvate (Km = 153 mM). This prevents the loss of pyruvate, which would hinder the regeneration of NAD from NADH produced during glycolysis by reduction of pyruvate to lactate (94). MCT4 is found in tissues that rely on glycolysis such as white skeletal muscle fibers, astrocytes, chondrocytes and myeloid cells, and especially in tumor cells (76,90,91,94,95). The meta-analysis of MCT4 expression by Bovenzi et al. revealed that MCT4 is overexpressed in tumor or stromal cells and is associated with poor patient outcome across various cancer types, whereas MCT1 expression was not clearly associated with survival (76).

The major regulatory mechanism of MCT4 expression is the induction of gene transcription by HIF1α. Cobalt treatment, a hypoxia mimetic inducing transcriptional regulation by HIF1α, induced mRNA expression of MCT4 as did hypoxia (96,107,108). It has been demonstrated that only the promotor of MCT4, but not MCT1, is stimulated by HIF1α, which binds to the hypoxia-response element (HRE) present in the promotor of MCT4, but absent in MCT1 (107). Thus, MCT4 joins a number of proteins regulated by HIF in tumors, such as most glycolytic enzymes or glucose transporters that maintain the Warburg phenotype. MCT4 is pivotal to tumor progression and emerges as an attractive target for cancer therapy, and the aim of this work was to clarify whether MCT4 as target is likely superior to MCT1.

1.2.1.3 Lactic acid - Warburg effect as metabolic immune checkpoint

The Warburg effect of tumor cells leads to an accumulation of lactate and a concomitant acidification of the TME. In solid tumors, lactate concentrations of up to 40 mM compared to 1-2 mM in blood have been measured (34,109). Several publications have demonstrated that lactic acid is not only a metabolic waste product but rather an immune-regulatory molecule and correlates with tumor progression and metastatic spread (Figure 7). Our group and others have shown that tumor-derived lactic acid inhibits effector functions of T cells and NK cells (32–35,110,111) and fosters the differentiation and activity of tumor-promoting immune cell populations, such as regulatory T cells (Tregs) or myeloid cells (36,38,39,112–114). This suggests that the tumor-promoting effect of lactic acidosis might be due its suppression of tumor immunity (37).

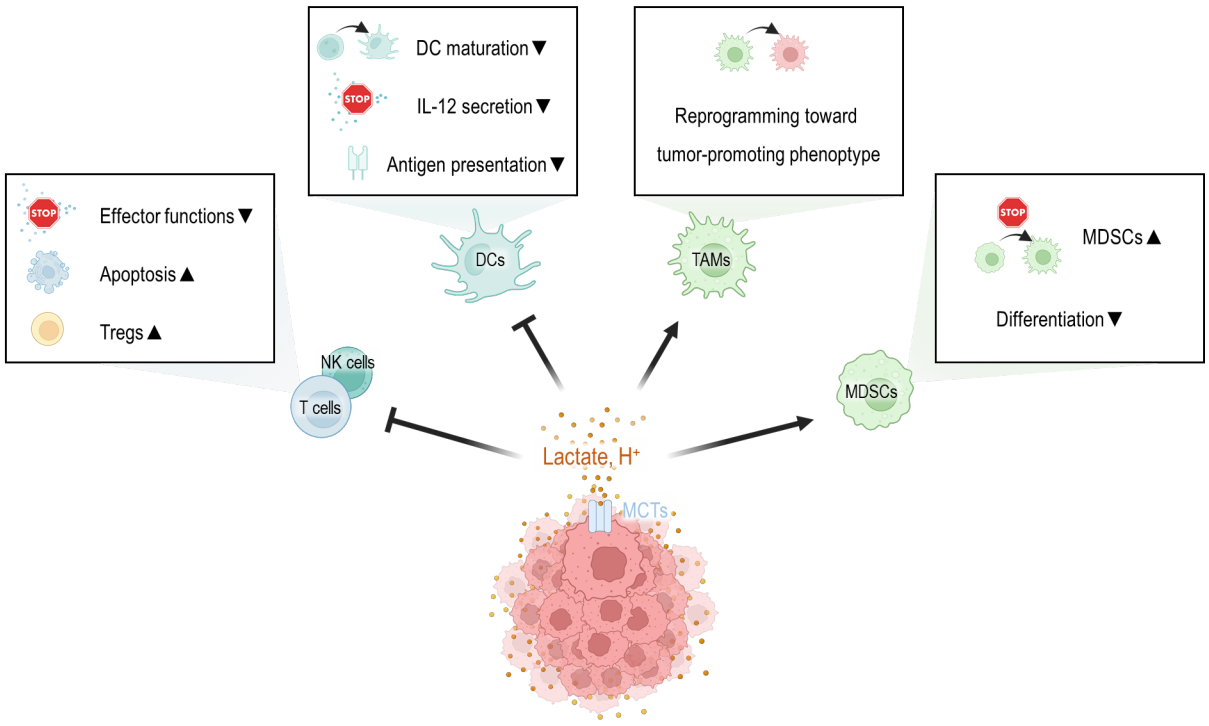

Figure 7. Lactic acid as immune-regulatory molecule suppresses immune cell function in the TME. Tumor-derived lactic acid contributes to immune escape and tumor progression as it severely impairs effector functions of T cell and natural killer (NK) cell and fosters the differentiation and activity of tumor-promoting immune cell populations, such as regulatory T cells (Tregs), dendritic cells (DCs), tumor-associated macrophages (TAMs) and myeloid-derived suppressor cells (MDSCs). Created with BioRender.com.

Vasaikar et al. found a negative correlation between the number of $CD8^+$ T cells and increased glycolysis in colorectal carcinoma (CRC) (115). Likewise, patients with low GLUT1 expression have a higher T cell infiltration, and T cells within the tumor are found in areas with low GLUT1 expression (37). Indeed, a highly glycolytic tumor metabolism has been linked to limited efficacy of immune checkpoint blockade (ICB) in melanoma and renal cell carcinoma and also to resistance to adoptive T cell transfer (32,116–120). Cytolytic function of NK cells was enhanced in Ldha-depleted tumors, and lactate treatment suppressed the cytotoxicity *in vitro* (34,121). Human T cell proliferation and cytokine production are also decreased by lactic acid treatment (33–35,122). After stimulation, T cells upregulate expression of MCT1 and MCT4, which can result in import of lactic acid when extracellular concentrations exceed intracellular levels. The intracellular lactate accumulation and acidosis leads to a metabolic blockade of T cells, which is manifested by a blocked respiration (33). At molecular level, lactic acid prevented phosphorylation of JNK, c-Jun, p38, and NFAT activation, which are crucial signaling pathways for IFNγ production (34,110). Our group has previously shown that LDHA expression in melanomas was negatively correlated with T cell function, and cytokine production by tumor-infiltrating T cells and NK cells was decreased by LDHA-associated lactic acid (34). An interplay tumor and immune cell metabolism has been reported in several studies showing that a TME with low glucose levels limits glycolysis of tumor-infiltrating T cells (TILs), which in turn inhibits tumor immunity of

cytotoxic T cells (123,124). Contrary, Tregs appear more resistant to glucose restriction and lactic acid exposure and keep their immunosuppressive function (113).

Similar severe effects of lactic acid were observed in myeloid cells. Differentiation of DCs is impaired by lactic acid, resulting in lowered antigen presentation, reduced IL-12 and TNF secretion and consequently a tolerogenic phenotype (112). Tumor-associated macrophages (TAMs) and MDSCs play an important role in the TME and are frequently associated with tumor progression. Husain et al. found fewer MDSCs in spleens of mice bearing Ldha depleted tumors (121). In addition, TAMs are polarized toward an immunosuppressive M2-like phenotype by sensing acidic pH via the G-protein-coupled receptor (GPR) 43 (125). Colegio et al. demonstrated a functional reprogramming of TAMs to a tumor-promoting state by lactic acid in a HIF1α-dependent manner. HIF1α induces secretion of VEGF, which is consistent with the observed angiogenesis in Warburg tumors (38,39,126). Furthermore, lactic acid increases production of IL-23 by TAMs, which is involved in differentiation of tumor-promoting Th17 cells (127).

Nowadays, it is widely accepted that tumor-derived lactic acid is highly immunosuppressive, suggesting the Warburg effect of tumors as a metabolic immune checkpoint.

1.2.2 Tumor stromal cells

Although the primary function of the immune system in evolution was to defend against infection, its role in combating endogenous malignant cells became equally important in advanced vertebrates (128). The response of the human body to cancer cells shows several analogies to inflammation and therefore Harold F. Dvorak considered tumors as ‘wounds that do not heal’ (13–16). A variety of immune cells are recruited to the TME and determine whether the tumor survives and affects neighboring cells. Several studies have shown that type, density and location of immune cells in the tumor have a prognostic value for overall patient survival (26–28,129). In consequence, Galon proposes an immunoscore classification in addition to classical tumor-node-metastasis TNM staging (130,131). On this basis, immunotherapy has gained increasing interest in recent years. However, response rates to immunotherapy are limited and is not yet a universally applicable method for predicting whether a patient will respond or not. This has led to a surge of research addressing tumor-intrinsic mechanisms of resistance. Increasing evidence points to contribution of the Warburg effect to immunosuppression. Therefore, our group proposed a metabolic tumor stroma score (MeTS) to determine the likelihood of an effective anti-tumor immune response (37).

The TME is orchestrated by an interplay between tumor cells and stromal cells. Stromal cells primarily include TILs, NK cells, TAMs, MDSCs, and DCs, but also cancer-associated fibroblasts (CAFs) and endothelial cells (TECs). Tumor-associated immune cells represent a double-edged sword in terms of

pro- and antitumor effects. A simplified overview of the crosstalk between immune and tumor cells is depicted in Figure 8.

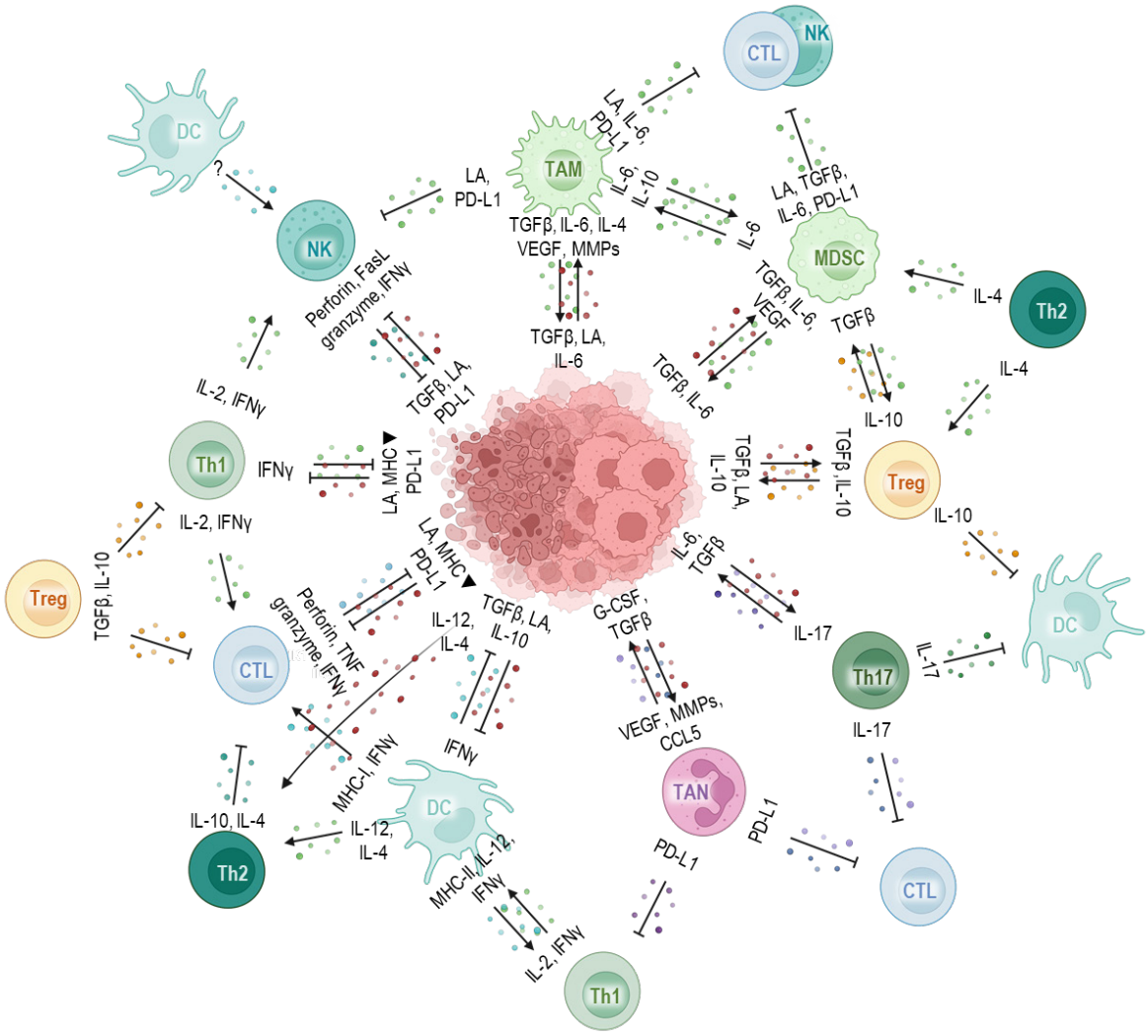

Figure 8. Crosstalk between tumor cells and immune cells in the TME. Abbreviations: CTL, cytotoxic T cell; Th, T helper cell; NK cell, natural killer cell; DC, dendritic cell; Treg, regulatory T cell; MDSC, myeloid-derived suppressor cell; Th, T helper cell; IL, interleukin; IFNγ, interferon γ; TNF, tumor necrosis factor; TGF, transforming growth factor; VEGF, vascular endothelial growth factor; PD-L1, programmed cell death ligand 1; MHC, major histocompatibility complex; CXCL, CXC motif chemokine ; CCL, CC-chemokine ligand. Created with BioRender.com.

But back to basics: The cellular immune system is divided into the innate (monocytes, macrophages, granulocytes, DCs, NK cells) and adaptive immune system (T cells, B cells). In general, immune cells can distinguish between healthy cells and tumor cells mainly by identification of so-called tumor antigens. Tumor antigens represent abnormal molecules solely produced by malignant cells such as mutated proteins, altered or aberrantly expressed proteins, glycolipids or foreign proteins encoded by oncoviruses. Their potential to induce an immune response depends on various factors, including accessibility to the immune cells, immunogenicity and grade of expression. The pro- and anti-tumor effects of tumor-associated immune cells are discussed in the following section (128).

1.2.2.1 Tumor-associated myeloid cells

All tumor-associated myeloid cells belong to the innate immune system include macrophages, granulocytes and DCs. Additionally, during tumorigenesis, an immature myeloid population appears, the so-called MDSCs. The role of these populations in tumor immunity is explained in the following sections.

1.2.2.1.1 Tumor-associated macrophages

TAMs are the most abundant immune cells within tumors and play a central role in tumor progression and metastasis (12,132–137). Both circulating monocytes and tissue resident macrophages are attracted by chemokines, which include CC-chemokine-ligand 2 (CCL2), VEGF, as well as colony-stimulating factor 1 (CSF1) (12). A oversimplified model classifies TAMs into M1 and M2 subtypes depending on their differentiation status and functional role (138,139). M1-like macrophages are classically activated by interferon γ (IFNγ) or microbial factors such as lipopolysaccharide (LPS) and are considered pro-inflammatory. They are thought to promote anti-tumor responses through the production of cytokines (interleukin (IL)-1, IL-12, IL-23), chemokines (CXCL9, CXCL10) tumor necrosis factor (TNF), the release of reactive oxygen species (ROS), and antigen presentation via major histocompatibility complex (MHC) molecules. TNF activates endothelial cells and provokes coagulation, leading to tumor necrosis and directly stimulating apoptosis. In contrast, macrophages can also be polarized to an M2 phenotype that preferentially accumulates in the TME of advanced and hypoxic tumors. M2 macrophages are alternatively activated by stimulation with IL-4, IL-6, IL-13, IL-10, IL-33 and transforming growth factor β (TGFβ). This results in the subsequent production of anti-inflammatory cytokines (IL-10, TGFβ), which have an inhibitory effect on cytotoxic $CD8^+$ T cells. In addition, M2-like macrophages downregulate their MHC-II, express surface molecules such as scavenger receptors or programmed cell death ligand 1 (PD-L1), and produce extracellular matrix proteins (ECM) (10,139,140). Therefore, M2 macrophages exhibit tissue remodeling, immune tolerance, and pro-tumor functions and are involved in angiogenesis, tumor invasion and metastasis, and immunosuppression (44). However, M1/M2 polarization is far too simplistic, because a diverse spectrum of these highly plastic myeloid cells has already been described and remains to be fully characterized.

Colegio et al. demonstrated that lactic acid induces a tumor-promoting phenotype in TAMs (38,39). On the other hand, apart from tumor cells, TAMs are highly glycolytic and produce high amounts of lactic acid, which in turn promotes tumor progression (141,142). In line, depletion of TAMs reduced 18F-FDG uptake of tumor, resulting in improved T cell infiltration (142). This suggests that not only tumor metabolism but also a highly glycolytic phenotype of myeloid cells, termed “reverse Warburg effect”, can suppress anti-tumor immune response (37). Efficacy of immunotherapy was correlated

with dynamic change of TAM subpopulations during tumor development (143–147). The fact that TAMs can exert several anti-tumor and immunosuppressive effects and their phenotypic plasticity depending on the environment make them a potential manipulative target for cancer therapies (148-151).

1.2.2.1.2 Tumor-associated neutrophils

To date, most other immune cells have overshadowed the role of neutrophil granulocytes in cancer. Neutrophils are the most abundant class of leukocytes in human blood and play a central role in the TME (136,152). Similar to the classification of TAMs, TANs are divided into an antitumor N1 and a pro-tumor N2 phenotype (153,154). IFNγ or blockade of TGFβ signaling stimulate N1 polarization, which produce increased immune-stimulatory chemokines and cytokines (e.g. TNF), intracellular adhesion molecule 1 (ICAM-1), and Fas (154). In contrast, TANs polarize into the N2 phenotype upon stimulation with granulocyte colony-stimulating factor (G-CSF) or TGFβ. N2 TANs are characterized by increased expression of pro-tumor and immunosuppressive factors, including CC-chemokine ligand 2 (CCL2), CC-chemokine ligand 5 (CCL5), neutrophil elastase (NE), cathepsin G (CG), and arginase (153,154). In cancer, granulocytes are recruited by binding of CXC-motif-chemokine 2 (CXCL2) to the neutrophil CXC-motif-chemokine-receptor (CXCR2). CXCL2 is released into the circulating system by various cell types within the tumor such as tumor cells, immune cells, or fibroblasts (155–158). TANs are mostly considered as tumor-promoting due to release of proteases, ROS, pro-tumor cytokines, chemokines and promoting immunosuppression and angiogenesis (159–161). Gentles and colleagues observed that higher infiltration of polymorphonuclear cells (PMNs, including neutrophils) resulted in lower overall survival compared with other leukocytes, studying over 5000 cases of 25 different cancers (159). In addition, a higher neutrophil-to-lymphocyte-ratio creates a pre-metastatic niche for malignant cells and worsen the prognosis of patients (162–167). However, some studies showed contrary evidence that TANs may also have anti-tumor effects in certain cases (168,169). For example, TANs can release H_2O_2 after direct contact with tumor cells, leading to intracellular Ca^{2+} influx and subsequent cell death of the tumor cell (170). Moreover, physical contact between tumor cells and neutrophils isolated from healthy donors resulted in suppression of tumor cell growth through the interaction between Fas ligand and Fas receptor (171). Recent preclinical studies showed that virus-stimulated neutrophils enhanced the T cell mediated anti-tumor response to B16-F10 melanoma mouse model (71). This suggests that the pro- and antitumor functions of TANs are highly dependent on their environment and opens the possibility of manipulating the phenotype of TANs for anti-cancer therapy.

1.2.2.1.3 Myeloid-derived suppressor cells

Myeloid-derived suppressor cells (MDSCs) represent an immature myeloid cell type that has not yet transformed into macrophages, granulocytes or dendritic cells, but shares characteristics with M2 TAMs and M2 TAMs. More precisely, in mice MDSCs express the classical myeloid lineage marker CD11b as well as the Gr-1 and build to subsets: neutrophilic $Ly6G^+$ $Ly6C^{low}$ (PMN) and monocytic $Ly6G^-$ $Ly6C^+$ (M) (172–176). In humans PMN-MDSCs are defined as $CD11b^+$ $CD14^-$ HLA-DR^{low} $CD15^+$/$CD66b^+$ and M-MDSCs as $CD11b^+$ $CD14^+$ HLA-DR^{low} $CD15^-$ (172,173). MDSCs are closely related to monocytes and neutrophils, but arise only under pathological conditions, including chronic inflammation or stress, and display remarkable immunosuppressive and tumorigenic activities (174–179). Among the inhibitory activities are ROS and nitric oxide (NO) production harming T cells and NK cells, secretion of IL-10, IL-6 and TGFβ, depletion of essential amino acids for T cells such as arginine and cysteine, high expression of PD-L1 suppressing T cells, secretion of growth factors and VEGF, matrix metalloproteinases and promotion of Tregs (172,174–176,180–187). Increased cytokine levels of IL-6 and IL-10 in the TME stimulate formation and recruitment of MDSCs to the tumor side, which in turn enables MDSC self-activation by secretion of IL-6 and IL-10 in an autocrine manner (188). Overall, MDSCs are major players of immunosuppression.

1.2.2.1.4 Dendritic cells

DCs are professional antigen-presenting cells (APCs) and mediators between innate and adaptive immune system. DCs play a key role in anti-tumor immunity by migrating in the lymph node and presenting tumor antigens to $CD4^+$ and $CD8^+$ T cells through MHC-dependent cross-presentation. Some studies even report cytotoxic functions of DCs against tumor cells, so-called “NK killer DCs” sharing characteristics of DCs and NK cells (189–192). NK cells also interact with DCs, leading to activation of NK cells and promoting anti-tumor effects (189). On the other hand, tumor cells have the ability to reprogram DCs into an immunosuppressive and angiogenic phenotype that promotes tumor growth (193). Tumor cells release factors such as VEGF or IL-10 and lactic acid that promote a phenotype switch to immature tolerogenic DCs (112,194). However, no clear correlation between DC infiltration and prognosis has yet been established in human tumors (189).

1.2.2.2 Tumor-infiltrating lymphocytes

Lymphocytes are the predominant tumor killers in the TME and essential for tumor defense. T cells and B cells belong to the adaptive immune system and NK cells to the innate immune system. The capabilities of each lymphocyte population and how they are influenced by various factors in TME are discussed below.

1.2.2.2.1 Tumor-infiltrating T cells

Cytotoxic T cells (CTLs) are the key players of anti-tumor immunity, and the number of TILs has been associated with a better prognosis (26,27,129) and prediction of response to immunotherapy (195,196). T cells mature in the thymus from a common lymphoid precursor. They are characterized by the expression of a T cell receptor (TCR) responsible for the recognition of antigens presented on MHC molecules. Unlike myeloid cells, which express many different pattern recognition receptors (PRRs), each T cell expresses TCRs that are specific for only one antigen. This distinguishes matured lymphocytes from each other by the specificity of TCRs.

Classically, T cells are differentiated into either $CD8^+$ T cells or $CD4^+$ T cells, with $CD8^+$ cells recognizing MHC-I molecules and $CD4^+$ T cells recognizing MHC-II (197). Activated CTLs form the primary machinery for killing tumor cells within the adaptive immune system. DCs (or other APCs) present tumor antigens in MHC class I and class II molecules to activate $CD4^+$ T helper cells (Th cells) and induce and clonally expand CTLs ($CD8^+$ T cells) (Figure 9). However, a second co-stimulatory signal is required for activation of naïve T cells. According to the classical two-signal hypothesis, CD28 is constitutively expressed on the cell surface of naïve T cells and represents an essential co-stimulatory signal for the activation and expansion of T cells after ligation with CD80/86 on APCs (198–201). Nowadays, a whole repertoire of co-stimulatory but also co-inhibitory molecules is known. Once activated, the T cell does not necessitate further co-stimulation for cytotoxic functions. Activated T cells express CXCR3, which drives the migration of T cells into the tumor. T cells follow the gradient of CXCL9, CXCL10, and CXCL11 (202-204).

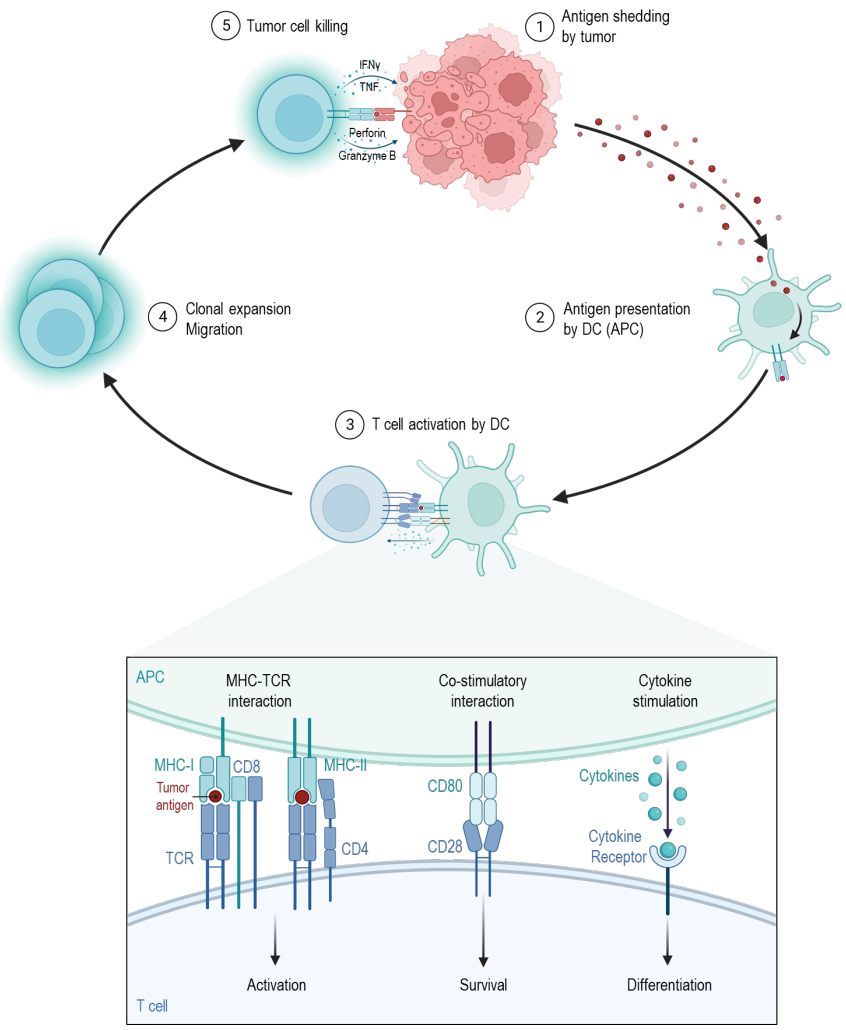

Figure 9. T cell activation. Tumor antigens are taken up by dendritic cells (DC) and presented via major histocompatility complex (MHC) molecules. $CD8^+$ T cells recognize MHC-I and $CD4^+$ T cells MHC-II. Antigen-presenting cells (APC) mediate three signals for T cell activation: interaction of MHC and T cell receptor (TCR), co-stimulatory interaction of CD80 and CD28 and secretion of cytokines. The co-stimulatory cytokine pattern is particularly important for differentiation of T helper cells. Once T cells are activated, clonal expansion and migration is induced. $CD8^+$ cytotoxic T cells kill tumor cells directly, while $CD4^+$ indirectly contribute by secretion of cytokines. Created with BioRender.com.

$CD8^+$ cytotoxic T cells

$CD8^+$ CTLs can directly lyse tumor cells by secreting cytolytic granules containing perforin and granzymes and produce the anti-tumor cytokines IFNγ and TNF (205,206) (Figure 9).

$CD4^+$ T helper cells

The $CD4^+$ T cell population differentiate into T helper 1 (Th1) cells and T helper 2 (Th2) cells, which require IL-12 and IL-4 stimulation, respectively, and T helper 17 (Th17) cells that differentiate upon IL-6 and TGFβ. Th1 cells primarily support tumor cell killing indirectly by secreting cytokines such as IL-2 (stimulation of CTL development and proliferation) and IFNγ (e.g. stimulation of macrophage cytotoxic activity), whereas Th2 cells produce tumorigenic cytokines, such as IL-4, IL-5, and IL-13. IL-17, IL-21, and IL-22 are released by Th17 cells, whose function in tumorigenesis varies depending on the cancer type (197,207).

$CD4^+$ $FOXP3^{high}$ regulatory T cells

Tregs represent another specific $CD4^+$ T cell subpopulation that is thought to protect against autoimmunity by suppressing self-reactive T cells. Depletion of $Foxp3^+$ Treg populations in mice resulted in severe autoimmunity affecting the whole body (208–210). Tregs express CD4, CD25, and the transcription factor Forkhead Box P3 (FOXP3) as characteristic markers. Within the tumor, Tregs inhibit the immune response against tumor cells by secreting immunosuppressive cytokines such as IL-10 and TGFβ. In addition, TGFβ induces differentiation of conventional T cells into Tregs that compete with $CD8^+$ T cells for IL-2, thereby limiting T cell proliferation and activation (140,211).

Mechanisms of immune escape

Although T cell infiltrates are found in tumors, they often fail to kill the tumors. According to the immune editing hypothesis, the surviving tumor cells have acquired additional properties either by further mutations or by selection during the equilibrium phase, so that the immune system can no longer eliminate them (205). In the last decades, several mechanisms of immune escape have been described, and Figure 10 provides an overview of the most important mechanisms. First, tumor cells may have a low immunogenicity and are “invisible” for T cells. Tumors may not carry antigens that are recognized by T cells and downregulate the MHC-I expression (212). Furthermore, tumor-specific antigens may be presented by DCs in the form of a cross-presentation but without co-stimulatory signals, so that T cells adopt a tolerant state and treat tumor antigens as self-antigens. Antigens may be modulated over time and tumors may initially express antigens that are recognized by the immune system, but due to genetic instability of tumors, antigens may change or get lost. Furthermore, a major driver of immune escape is tumor-triggered immunosuppression through a variety of mechanisms. Tumors often suppress immune responses by secretion of lactic acid, TGFβ, IL-10, or express inhibitory molecules such as programmed cell death ligand 1 (PD-L1) or attract immunosuppressive cells such as Tregs (35,213). However, the TME consists of even more immunosuppressive cell types that inhibit immune cell function, which includes MDSCs, TAMs but also CAFs.

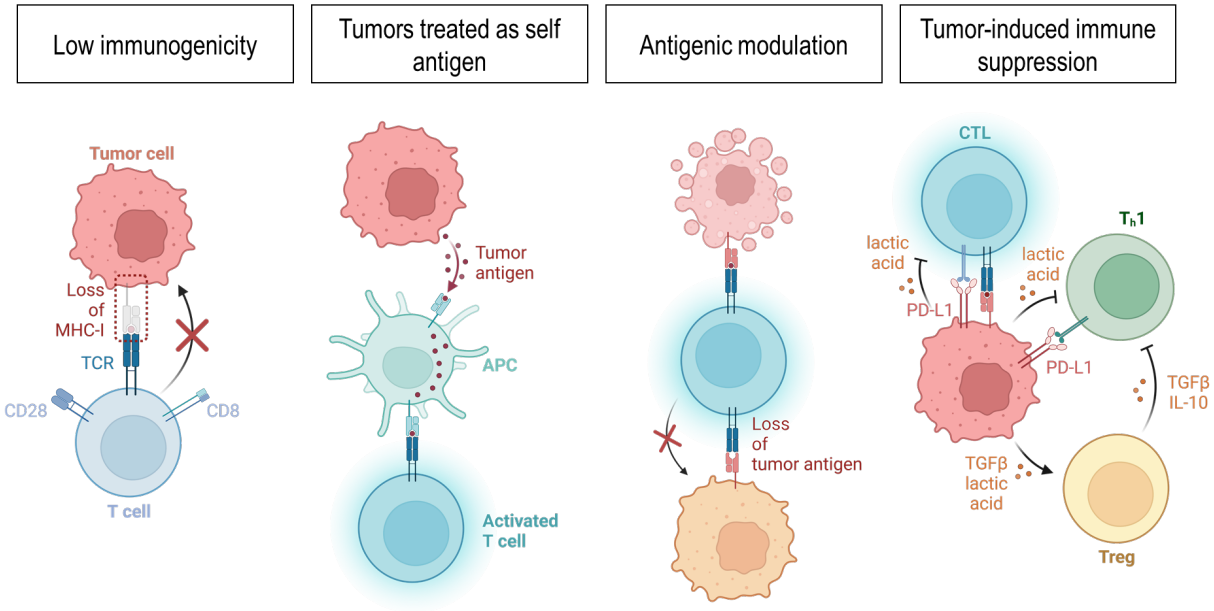

Figure 10. Mechanisms of immune escape. Low immunogenicity: Tumors may have a low immunogenic effect. Tumors may not carry antigens recognized by T cells, have lost their major histocompatility complex (MHC) molecules. Tumors treated as self-antigen: tumor-specific antigens can be presented by DCs via cross-presentation without co-stimulatory signals, so that T cells adapt a tolerant state. Antigen modulation: Tumors may initially express antigens that are recognized by the immune system. Such tumors can be destroyed. The genetic instability of tumors allows antigens to change during the equilibrium phase, when tumor cells can proliferate, to cells that do not possess immunogenic antigens. Tumor induced immune suppression: tumors often suppress immune responses or attract regulatory T cells (Treg) by secretion of lactic acid, TGFβ, IL-10, or express inhibitory molecules such as programmed cell death ligand 1 (PD-L1). Created with BioRender.com.

All in all, T cells are certainly the most important players in response against tumors. However, tumor cells pose several defined and well-targeted mechanisms to overcome immunosurveillance. Finding strategies to overcome T cell suppression could pave the way to a fight one of the humanity's toughest burden.

1.2.2.2.2 NK and NKT cells

NK cells are the only representative of lymphoid cells that belong to the innate immune system. In humans, there are two subpopulations of NK cells: $CD56^{high}$ NK cells, which account for the majority in peripheral blood and produce IL-12, IL-15 and IL-18, and $CD56^{dim}$ NK cells, which are cytotoxic, cytokine-producing and express CD16, an Fc receptor involved in antibody-dependent cellular cytotoxicity (ADCC) (214). Similar to T cells, NK cells are express several chemokine receptors, such as CXCR3, and are mainly recruited by tumor-derived CXCL9, CXCL10 and CXCL11 (215). As described above, loss of MHC-I expression is a mechanism by which tumors escape the immune system. However, this empowers tumor immunity by NK cells. NK cells kill tumor cells without prior activation when MHC-I is absent or expressed on a low level. Normally, recognition of MHC-I by NK cells acts as an inhibitory signal, but loss of MHC-I renders tumor cells vulnerable for NK cell killing (216,217). NK cell-mediated cytolysis by release of granules containing perforin and granzymes is controlled by surface receptors such as natural-killer-group-2-member-D (NKG2D), which recognizes stress-induced ligands on target

cells (218). Thus, tumors grew more aggressively and exhibited higher metastatic potential when NK cells were depleted before tumor inoculation (219–221). Moreover, NK cell density was linked to a better outcome in various cancers (222–226). Similar to T cell immunosuppression, NK cell function is inhibited by several factors in the TME, including lactic acidosis, IL-10 produced by Tregs, MDSCs, and tumor cells. In addition, NK cells express checkpoint molecules by which they can be inhibited, such as Killer Ig-like receptors (KIRs), PD-1 and cytotoxic T-lymphocyte-associated protein 4 (CTLA-4) (32,227,228). In addition to conventional NK cells, there is a unique subset of natural killer T cells (NKT cells). Like conventional T cells, NKT cells mature in the thymus and express a TCR to recognize specific antigens (229). However, unlike conventional T cells, NKT cells recognize lipid antigens presented by an alternative MHC-I like module CD1d (230). Additionally, NKT cells possess a repertoire of cytokine receptors similar to NK cells, through which NKT cells can be activated even in the absence of TCR signaling (231). Overall, apart from T cells, NK and NKT cells may also play a key role in tumor killing.

1.2.2.2.3 B cells

B cells are lymphocytes of the adaptive immune system, normally known for their humoral immune response. They are specialized in antibody production, but also in antigen presentation and cytokine production. Unlike T cells, B cells express a surface immunoglobulin called the B cell receptor (BCR). The BCR triggers a signaling cascade after binding an antigen, but also transports the antigen inside the cell, where it is processed and subsequently presented on an MHC-II molecule. T helper cells that have already differentiated in response to the same antigen can then recognize the peptide presented by MHC-II on the surface of the B cell. Effector T cells stimulate proliferation and differentiation of B cells through surface molecules and cytokines. By now, the importance of T cells in tumor immunity is widely recognized. However, there are relatively few B cells in tumors, and they are usually located at the margin or in the draining lymph nodes (232). Yet, some studies have reported that B cells play a role in the formation of tertiary lymphoid structures during tumorigenesis (233). These structures have been associated with a better prognosis in several cancers (234–237). Moreover, plasma cells produce large amounts of cytokines and antibodies in the TME even in small numbers, which promotes antibody-dependent cellular cytotoxicity (ADCC) and phagocytosis, as well as complement activation and enhanced antigen presentation by DCs (233,237–241). B cells shape tumor immunity through antigen presentation to T cells, but also through secretion of IFNγ. On the other hand, B cells can even worsen the prognosis of patients in some cancers (242–245). Similar to Tregs, immunosuppressive regulatory B cells can arise in the TME and produce inhibitory cytokines such as IL-10, IL-6, and TGFβ or PD-L1 (246–249). Briefly, the role of B cells in the TME is double-edged and requires more research.

1.2.2.3 Cancer-associated fibroblasts

CAFs are an important component of TME and have been shown to interact with tumor cells as well as immune cells in multiple ways. CAFs generally arise from tissue-derived quiescent fibroblasts that are recruited and activated by TGFβ, fibroblast growth factor 2, hepatocyte growth factor, platelet-derived growth factor (PDGF), or ROS (250–256). Furthermore, studies have reported that CAFs can originate from much more diverse origins such as mesenchymal stem cells or adipocytes (257–260). The role of CAFs in TME is mainly considered to be tumor-promoting and immunosuppressive due to the production and remodeling of the ECM as a physical barrier to immune cell infiltration, secretion of TGFβ, IL-6, and CXCL2, and MMPs (260–264). Moreover, CAFs are resistant to tumor-induced lactic acidosis and even utilize tumor-derived lactate to produce α-ketoglutarate, which induces the expression of inflammatory genes (265). In addition, CAFs themselves can contribute to a "reverse Warburg effect" by enhancing glycolysis, which in turn induces Tregs and inhibits T cells (37,266,267). It is reasonable to target glycolysis in both tumor and stromal cells to reduce immunosuppression.

1.2.2.4 Tumor endothelial cells

Blood vessels are usually lined with a unicellular layer of endothelial cells. Angiogenesis is acknowledged as hallmark of cancer because blood vessels are essential for tumor metabolic homeostasis and removal of waste products. Tumor cells, but also stromal cells induce vessel growth and migration of endothelial cells by VEGF or PDGF production. However, tumor endothelial cells are quite heterogeneric and distinguish from normal endothelial cells, which usually form monolayers with tight junctions, but tumor blood vessels remain leaky and immature due to delocalized tumor endothelial cells (268). Thus, TECs enable intravasation for tumor cells and thus play a key role for cancer invasion and metastasis (269–272). Upon TGFβ stimulation, TECs can differentiate to CAFs in a process called "endothelial-mesenchymal transition" (273).

1.3 Targeting the Warburg effect – potential for tumor- and immunotherapy

Alterations in the energy metabolism of tumor cells has been introduced as a hallmark of cancer (3). Accelerated glucose metabolism and a highly elevated turn-over of pyruvate into lactate even in the presence of oxygen, the Warburg phenotype, is a well-known metabolic feature of tumors of different entities and is linked to limited therapy response and worse patient prognosis (34,37,50,116,274–280). Moreover, the Warburg phenotype represents a metabolic checkpoint contributing to immune evasion and restricting the response to immunotherapeutic approaches. To sustain the glycolytic flux, lactate needs to be efficiently secreted and the main transporters found on glycolytic cells are the proton-coupled MCT1 and MCT4. Lactate secretion results, despite its accumulation, in a concomitant acidification ("lactic acid") of the TME, both fostering immunosuppressive cell populations. In such an environment, macrophages exhibit tumor-promoting characteristics as IL-6, TGF-β and VEGF secretion (134). Moreover, regulatory T cell function is preserved, whereas T and NK cell mediated anti-tumor immunity is severely impaired (32–35,110,111). The number of infiltrating CTLs is reduced as well as the expression of important mediators of anti-tumor immunity as IFNγ. Vice versa, reducing lactic acid secretion by lowering the expression of LDH in tumor cells improves T and NK cell infiltration, function and tumor growth control (34). Therefore, targeting glycolysis might be a promising strategy to overcome glycolysis-related immunosuppression and might support immune checkpoint blockade (ICB).

1.3.1 Anti-metabolic targeting to counteract the Warburg effect

1.3.1.1 Generations of anti-glycolytic agents

Generations of scientists have studied the Warburg effect and developed several compounds targeting tumor glycolysis (Figure 11) (281,282). Nevertheless, targeting aerobic glycolysis of tumor cells has not yet been successfully implemented into clinical practice. Some candidates have been tested in clinical trials with ambiguous results (282). Further development and testing of specific drugs against targets of the glycolytic pathway that are overexpressed in cancer, such as MCT4, is crucial to find a way to counteract the Warburg effect of tumors.

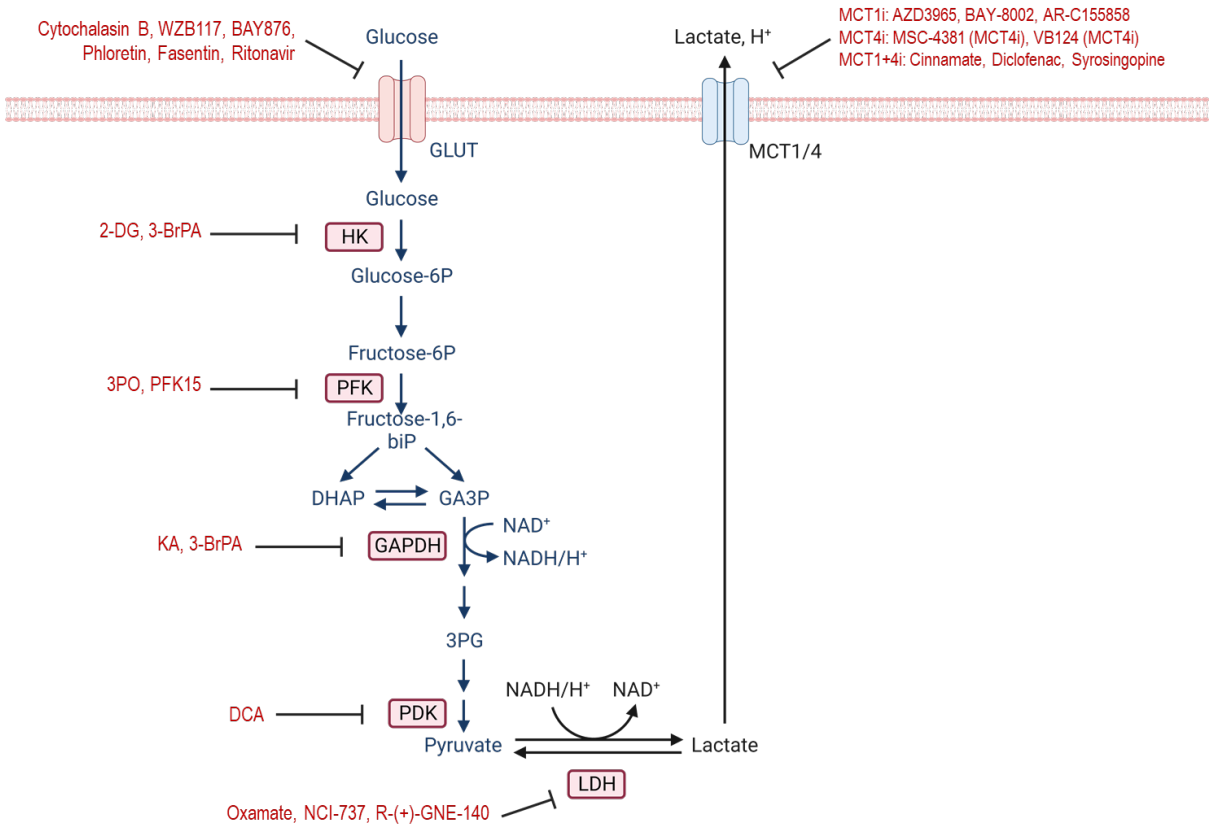

Figure 11. Anti-glycolytic agents. GLUT, glucose transporter; HK, hexokinase; PFK, phosphofructokinase; GAPDH, glyceraldehyde 3-phosphate dehydrogenase; PDK, pyruvate dehydrogenase; LDH, lactate dehydrogenase; MCT, monocarboxylate transporter; P, phosphate, 2-DG, 2-deoxyglucose; 3-BrPA, 3-bromopyruvate; DCA, dichloroacetate. DHAP, dihydroxyacetone phosphate; GA3P, glyceraldehyde 3-phosphate; 3PG, 3-phosphoglyceric acid; NADH, nicotinamide adenine dinucleotide hydrogen; NAD, nicotinamide adenine dinucleotide. Created with BioRender.com

1.3.1.2 Opening up a new era – specific inhibition of MCT4

Over the last years MCTs are emerging as an attractive target to restrict glucose metabolism. MCT1 and MCT4 are the key tumor-associated lactate transporters and essential for the glycolytic phenotype of tumor cells. Multiple compounds have been described to nonspecifically inhibit MCTs, such as cinnamate-based compounds (283,284), syrosingopine (285), or diclofenac (32). But none of these compounds has yet entered the clinic for anti-metabolic treatment of cancer. At this stage, only a few specific MCT1 inhibitors with clinical potential have been described, such as AZD3965 (286,287), AR-C155858 (288) and BAY-8002 (289). Currently, AZD3965 is the only MCT inhibitor that has been tested in a clinical trial (NCT01791595). However, while MCT1 is almost ubiquitously expressed, MCT4 is found predominantly in highly glycolytic cells. Moreover, unlike MCT1, MCT4 expression is triggered by HIF1α, a master regulator of the cellular response to hypoxia (290). Therefore, MCT4 may be a superior target than MCT1, as MCT4 has been implicated particularly in tumor aggressiveness and patient survival in various cancers. However, the range of selective MCT4 inhibitors is very limited. The

carboxylic acid AZ1422 (291), AZD0095 (292) and P-788 (293) were described as a selective MCT4 inhibitors but are still undisclosed. Currently, VB124 is a selective MCT4 inhibitor that can be purchased for research purposes (194). Fang et al. recently showed that VB124 is capable to improve the response to ICB *in vivo* in a hepatocellular carcinoma model system by increasing $CD8^+$ T cell infiltration and function. They demonstrated, that MCT4 knock down reduced glycolytic activity of the tumor cells and thereby extracellular acidification (294). Throughout this PhD project, we tested the recently described highly potent selective MCT4 inhibitor MSC-4381 (MCT4i) (293). The MSC-4381-MCT4 inhibitor belongs to a new class of selective MCT4 inhibitors that interact directly with the cytosolic domain of MCT4. Blocking MCT4 (and MCT1) might counteract tumor-derived lactic acidosis and improve anti-tumor response of T cells.

1.3.2 Immune checkpoint blockade

One approach of cancer immunotherapy is ICB. This attempts to influence the normal inhibitory signals that regulate lymphocytes. Immune responses are regulated by various positive and negative checkpoints (Figure 12). A positive checkpoint for T cells is controlled by the co-stimulatory CD80/86 receptors expressed by professional APCs, such as DCs. Negative immunological checkpoints are formed by inhibitory receptors, for example CTLA-4 and PD-1 on T cells. CTLA-4 is a crucial checkpoint for potentially autoreactive T cells, as the receptor binds to CD80 molecules on DCs and induces a negative signal restraining T cell activation. Blocking CTLA-4 with monoclonal ICB antibodies may lower the threshold for T cell activation. There is also evidence that anti-CTLA-4 antibodies can enhance immune responses by eliminating regulatory T cells that express CTLA-4 on their surface. Another immune checkpoint involves the inhibitory receptor PD-1 and its ligands PD-L1 and PD-L2. PD-L1 is expressed by most human tumors and a major strategy for immune escape (295).

Although ICB targeting PD-1 or PD-L1 have shown great progress in cancer treatment, only 20-40 % of patients respond to ICB (296).

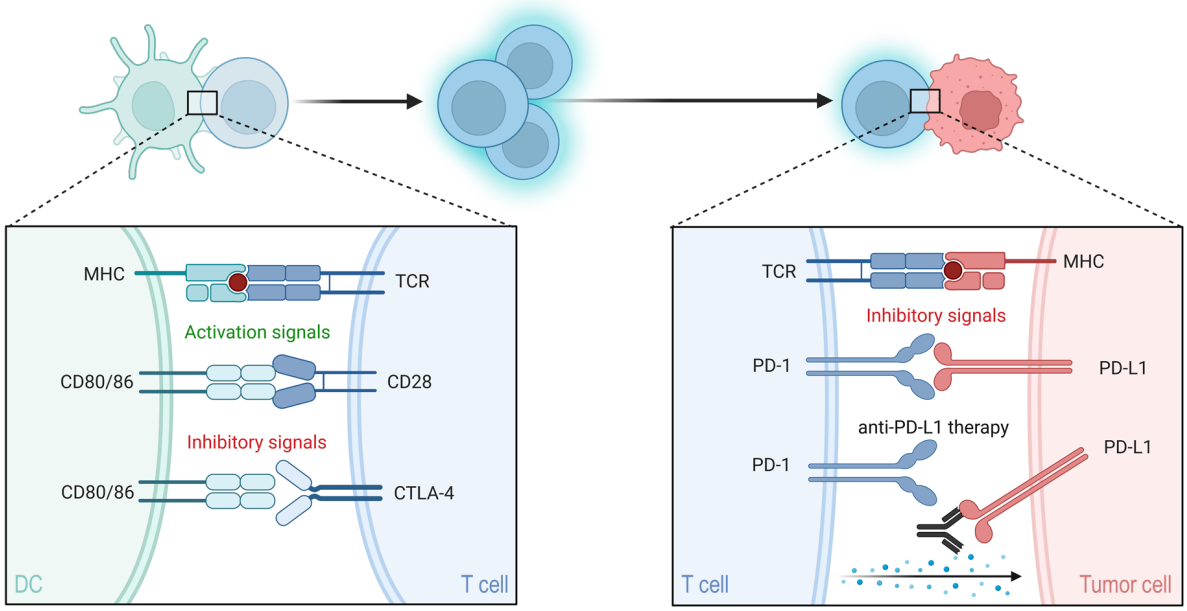

Figure 12. Immune checkpoint molecules and anti-PD-L1 therapy. T cells express stimulatory (CD28) and inhibitory immune checkpoint molecules (cytotoxic T-lymphocyte-associated Protein 4 (CTLA-4) and programmed cell death 1 (PD-1)). Many tumor cells express PD-L1 and thereby suppress T cell function. Anti-PD-L1 inhibitors target PD-L1 and support anti-tumor response. Created with BioRender.com.

At present, three PD-L1 inhibitors are approved by the US Food and Drug Administration for the treatment of non-small cell lung cancer to Merkel cell carcinoma: Atezolizumab, Durvalumab and Avelumab, of which the latter was used in this PhD project (295). It is essential to explore strategies to overcome resistance to ICB by testing combination therapies. Given its immunosuppressive role in immune cell differentiation and function, lactate metabolism has evolved as an attractive target for enhancing cancer immunotherapy (30).

1.4 Research objectives

Tumor cells are characterized by metabolic adaption towards a glycolytic phenotype, termed Warburg effect. Increased glucose uptake and its metabolism into lactate requires continuous export mediated by proton-coupled monocarboxylate transporters (MCTs), of which MCT1 and MCT4 are the dominant tumor-associated transporters. Accordingly, lactate and co-transported protons, herein named lactic acid, accumulates within the TME, and was shown to be immunosuppressive. In line, patients with high expression of glycolysis-related genes show a worse response to immunotherapy. Therefore, targeting glycolysis using specific MCT inhibitors might improve response to checkpoint inhibition therapy.

The aim of this project was to test whether specific blockade of MCT1 or MCT4 as monotherapy or in combination reverses the immunosuppressive effect of tumor-derived lactic acidosis in the TME. Efficacy and immunomodulatory role of specific MCT inhibitors (AZD3965, MCT1i; MSC-4381, MCT4i) and combinatory ICB should be investigated in colorectal carcinoma (CRC) *in vitro* cultures, tumor spheroid co-culture models, and *in vivo* mouse tumor studies. Furthermore, the impact of MCT inhibition should be studied in renal cell carcinoma (RCC) as second tumor model.

2 Material

2.1 Equipment

Autoclave	Systec, Linden, Germany
CASY Cell Counter	Roche Innovatis, Bielefeld, Germany
Centrifuge 5424R	Eppendorf, Hamburg, Germany
CFX Connect	BioRad, Hercules, CA, USA
Evos Cell Imaging System	AMG, Thermo Fisher Scientific, Waltham, MA, USA
FACSCalibur™ Flow Cytometer	BD Biosciences, Franklin Lakes, NJ, USA
FACSCelesta™ Flow Cytometer	BD Biosciences, Franklin Lakes, NJ, USA
Forceps	Aesculap, Tuttlingen, Germany
Fusion Pulse	Vilber Lourmat, Eberhardzell, Germany
Incubators	Haereus, Osterode, Germany
Incubators	Thermo Fisher Scientific, Waltham, MA, USA
Incucyte	Sartorius, Göttingen, Germany
Laminar Flow cabinet	Haereus, Osterode, Germany
Laminar Flow cabinet	Thermo Fisher Scientific, Waltham, MA, USA
LSRFortessa™ Flow Cytometer	BD Biosciences, Franklin Lakes, NJ, USA
MACSiMAG separator	Miltenyi Biotec, Bergisch Gladbach, Germany
Manual Micromanipulator	PreSens, Regensburg, Germany
Mastercycler nexus gradient	Eppendorf, Hamburg, Germany
Megafuge 16 R	Eppendorf, Hamburg, Germany
Microfuge	Haereus, Osterode, Germany and
Microscopes	Zeiss, Oberkochen, Germany
Multifuge X3 FR	Eppendorf, Hamburg, Germany
Multipette	Eppendorf, Hamburg, Germany
Nanodrop nd-1000	VWR International, Radnor, PA, USA
pH meter inolab 730	WTW, Weilheim, Germany
pH Needle Microsensor NTH-HP5	PreSens, Regensburg, Germany
Picofuge	Haereus, Osterode, Germany
Pipetboy	Integra, Biebertal, Germany
Pipettes	Gilson, Milddleton, WI, USA
Pipettes	Eppendorf, Hamburg, Germany
Pipettes	Thermo Fisher Scientific, Waltham, MA, USA

Power supplies Biometra	Biometra, Göttingen, Germany
QuadroMACS™	Miltenyi Biotec, Bergisch Gladbach, Germany
Repetitive Pipette HandyStep	Brand, Wertheim, Germany
SDR sensor dish reader	PreSens, Regensburg, Germany
Sepatech Megafuge 3.0R	Haereus, Osterode, Germany
ShakerVibrax-VXR	IKA, Staufen, Germany
Sonorex Ultrasonic bath	Branson, Danbury, CT, USA
TapeStation	Agilent Technologies, Santa Clara, CA, USA
Tecan Spark 10M	Tecan, Männedorf, Switzerland
Thermomixer	Eppendorf, Hamburg, Germany
Vortexer	Scientific Industries, Bohemia, NY, USA
Water purification system	Millipore, Eschbach, Germany
Waterbath	Julabo, Seelstadt, Germany
Wellwash 4 M2K	Thermo Fisher Scientific, Waltham, MA, USA
Western Blot chamber	Biometra, Göttingen, Germany
Western Blot chamber	BioRad, Hercules, CA, USA

2.2 Consumables

Casy Cups	OMNI Life Science, Bremen, Germany
Cell culture dish (96 well, U bottom)	BD Biosciences, Franklin Lakes, NJ, USA
Cell culture dish (96 well, U bottom)	Greiner, Kremsmünster, Austria
Cell culture dish (96 well, U bottom)	Sarstedt, Nümbrecht, Germany
Cell culture dishes, flat bottom	Eppendorf, Hamburg, Germany
Cell culture dishes, flat bottom	Greiner, Kremsmünster, Austria
Cell culture dishes, flat bottom	Sarstedt, Nümbrecht, Germany
Cell culture dishes, flat bottom	Eppendorf, Hamburg, Germany
Cell culture dishes, flat bottom	Greiner, Kremsmünster, Austria
Cell culture dishes, flat bottom	Sarstedt, Nümbrecht, Germany
Cell culture flasks	Eppendorf, Hamburg, Germany
Cell culture flasks	Greiner, Kremsmünster, Austria
Cell culture flasks	Sarstedt, Nümbrecht, Germany
Cell scrapers	Sarstedt, Nümbrecht, Germany
Cell strainer	BD Biosciences, Franklin Lakes, NJ, USA
ClipTip™ filter tips	Thermo Fisher Scientific, Waltham, MA, USA

Combitips for Multipette	Eppendorf, Hamburg, Germany
Combitips for Multipette	Brand, Wertheim, Germany
Cryo tubes	Corning Costar, Corning, NY, USA
Falcon tubes (15 ml, 50 ml, 225 ml)	BD Falcon, Franklin Lakes, NJ, USA
Flexible feeding tubes	Instechlabs, Plymouth Meeting, PA, USA
Hard-Shell 96 well PCR plates, low profile, skirted, clear	BioRad, Hercules, CA, USA
Hydrodish HD24 plates	PreSens, Regensburg, Germany
Immobilon-P PVDF membrane	Millipore, Eschbach, Germany
LS columns	Miltenyi Biotec, Bergisch Gladbach, Germany
Micro test tubes (1.5 ml)	Brand, Wertheim, Germany
Micro test tubes (1.5 ml, 2 ml)	Sarstedt, Nümbrecht, Germany
Micro test tubes, PCR-compatible (0.5 ml, 1.5 ml, 2 ml)	Sarstedt, Nümbrecht, Germany
Microseal B adhesive seal	BioRad, Hercules, CA, USA
Needles, disposable	BD Biosciences, Franklin Lakes, NJ, USA
Nunc™ Multidish (12 well) with UpCell surface	Thermo Fisher Scientific, Waltham, MA, USA
Oxodish OD24 plates	PreSens, Regensburg, Germany
Petri dishes	Greiner, Kremsmünster, Austria
Pipette tips	Eppendorf, Hamburg, Germany
Polystyrene test tubes	BD Biosciences, Franklin Lakes, NJ, USA
Polystyrene test tubes with cell strainer cap	BD Biosciences, Franklin Lakes, NJ, USA
Scalpels, disposable	Feather safety razor, Ozaka, Japan
Serological pipettes	Greiner, Kremsmünster, Austria
Serological pipettes	Sarstedt, Nümbrecht, Germany
Stericup vacuum filter bottles (0.2 µm)	Millipore, Eschbach, Germany
Stripwell microplates	Corning Costar, Corning, NY, USA
SurPhob SafeSeal® filter tips	Biozym Scientific, Hessisch Oldendorf, Germany
Syringe filters, sterile	Sartorius, Göttingen, Germany
Syringes, disposable	BD Biosciences, Franklin Lakes, NJ, USA
Ultra-low attachment microplates	Corning Costar, Corning, NY, USA
Whatman Chromatography Paper	GE Healthcare, Chicago, IL, USA

2.3 Media, buffer, solutions

Acrylamide/Bisacrylamide (30 %)	Carl Roth, Karlsruhe, Germany
RPMI1640, without L-Glutamine	Thermo Fisher Scientific, Waltham, MA, USA
Isoton II	Beckman Coulter, Brea, CA USA
2-Mercaptoethanol, for cell culture	Thermo Fisher Scientific, Waltham, MA, USA
2-Mercaptoethanol, for analyses	Sigma-Aldrich, St. Louis, MO, USA
MEM Essential vitamins	Thermo Fisher Scientific, Waltham, MA, USA
MEM Non-essential amino acids	Thermo Fisher Scientific, Waltham, MA, USA
Penicillin/Streptomycin	Thermo Fisher Scientific, Waltham, MA, USA
L-Glutamine	PAN Biotech, Aidenbach, Germany
AB-serum, human	Bavarian Red Cross, München, Germany
Fetal calf serum (FCS)	Sigma-Aldrich, St. Louis, MO, USA
Bovine serum albumin	Sigma-Aldrich, St. Louis, MO, USA
Dimethlysulfoxide (DMSO)	Carl Roth, Karlsruhe, Germany
Dimethlysulfoxide (DMSO)	Sigma-Aldrich, St. Louis, MO, USA
Ammonium persulfate (APS)	Sigma-Aldrich, St. Louis, MO, USA
RIPA buffer	Sigma-Aldrich, St. Louis, MO, USA
Cell Lysis Buffer	Cell Signalling Technology, Danvers, MA, USA
Sodium dodecyl sulfate (SDS)	Sigma-Aldrich, St. Louis, MO, USA
MEM Sodium Pyruvate	Thermo Fisher Scientific, Waltham, MA, USA
EDTA UltraPure	Thermo Fisher Scientific, Waltham, MA, USA
Trypsin/EDTA	Thermo Fisher Scientific, Waltham, MA, USA
Tween20	Sigma-Aldrich, St. Louis, MO, USA
Dulbecco's Phosphate Buffered Saline (DPBS)	PAN Biotech, Aidenbach, Germany
Hank's Balanced Salt Solution (HBSS)	PAN Biotech, Aidenbach, Germany
Casy Clean	Hoffmann-La Roche, Basel, Switzerland
Hydrogen peroxide (H_2O_2)	Sigma-Aldrich, St. Louis, MO, USA
Aqua bidest (H_2O)	Braun, Kronberg im Taunus, Germany
PCR-H_2O	Thermo Fisher Scientific, Waltham, MA, USA
Glycine	Carl Roth, Karlsruhe, Germany
ε-Amino-n-capronic acid	Sigma-Aldrich, St. Louis, MO, USA
Methanol	Merck, Darmstadt, Germany
Ethanol	Carl Roth, Karlsruhe, Germany

Acetic acid	Carl Roth, Karlsruhe, Germany
Trizma Base	United States Biological, Salem, MA, USA
Tetramethylethylendiamin (TEMED)	Merck, Darmstadt, Germany
FACS Flow	BD Biosciences, Franklin Lakes, NJ, USA
FACS Clean	BD Biosciences, Franklin Lakes, NJ, USA
FACS Rinse	BD Biosciences, Franklin Lakes, NJ, USA
Isopropanol (70%)	Braun, Kronberg im Taunus, Germany
Gelatine solution 0.1 %	PAN Biotech, Aidenbach, Germany
Pancoll, human	PAN Biotech, Aidenbach, Germany
Glycerin	Merck, Darmstadt, Germany
Bromphenole blue	Sigma-Aldrich, St. Louis, MO, USA
Sodium chloride	Merck, Darmstadt, Germany
Nuclease-free water	Thermo Fisher Scientific, Waltham, MA, USA
RIPA buffer	Sigma-Aldrich, St. Louis, MO, USA

2.4 Kits, reagents

10x Annexin V Binding buffer	BD Biosciences, Franklin Lakes, NJ, USA
2-NBD Glucose (2-NBDG)	Thermo Fisher Scientific, Waltham, MA, USA
7-Amino-Actinomycin D (7-AAD)	BD Biosciences, Franklin Lakes, NJ, USA
Acetyl salicylic acid (ASA) in medium	Fagron, Glinde, Germany
Agarose	Sigma-Aldrich, St. Louis, MO, USA
AZD0095	Provided by Merck, Darmstadt, Germany
AZD3965 (MCT1i)	Provided by Merck, Darmstadt, Germany
BD Comp Beads	BD Biosciences, Franklin Lakes, NJ, USA
BD Cytofix/Cytoperm	BD Biosciences, Franklin Lakes, NJ, USA
BD GolgiPlug (Brefeldin)	BD Biosciences, Franklin Lakes, NJ, USA
BD GolgiStop (Monensin)	BD Biosciences, Franklin Lakes, NJ, USA
Bio-Rad DC Protein assay kit	BioRad, Hercules, CA, USA
Brilliant Stain Buffer	BD Biosciences, Franklin Lakes, NJ, USA
Carboxy SNARF-1 AM acetate	Thermo Fisher Scientific, Waltham, MA, USA
CD3 T cell Isolation Kit (human)	Miltenyi Biotec, Bergisch Gladbach, Germany
CD4 MicroBeads (human)	Miltenyi Biotec, Bergisch Gladbach, Germany
CD8 MicroBeads (human)	Miltenyi Biotec, Bergisch Gladbach, Germany
Collagenase Type IA	Sigma-Aldrich, St. Louis, MO, USA

Cyclosporin A (Sandimmun®)	Novartis, Basel, Switzerland
Cyto3D™ Live-Dead Assay Kit	TheWell Bioscience, North Brunswick Township, NJ, USA
Dichlordihydrofluorescein-diacetat (DCFDA)	Thermo Fisher Scientific, Waltham, MA, USA
Diclofenac sodium salt in Medium	Sigma-Aldrich, St. Louis, MO, USA
DNase I	Sigma-Aldrich, St. Louis, MO, USA
dNTP-Mix	Hoffmann-La Roche, Basel, Switzerland
DuoSet ELISA human IFNγ	R&D systems, Minneapolis, MN, USA
DuoSet ELISA human IL-10	R&D systems, Minneapolis, MN, USA
DuoSet ELISA human IL-6	R&D systems, Minneapolis, MN, USA
DuoSet ELISA human IL-8	R&D systems, Minneapolis, MN, USA
DuoSet ELISA human TNF	R&D systems, Minneapolis, MN, USA
Dynabeads™ Human T-Activator CD3/CD28	Thermo Fisher Scientific, Waltham, MA, USA
ECL™ Prime Western Blot Detection Reagent	GE Healthcare, Chicago, IL, USA
FcR blocking reagent	Miltenyi Biotec, Bergisch Gladbach, Germany
FoxP3 staining kit	Thermo Fisher Scientific, Waltham, MA, USA
IL-15	PeproTech, Rocky Hill, NJ, USA
IL-2	PeproTech, Rocky Hill, NJ, USA
Intracellular pH Calibration Kit	Thermo Fisher Scientific, Waltham, MA, USA
Ionomycin	Enzo life sciences, Farmingdale, NY, USA
Kleptose HBP	Roquette, Lestrem, France
Lipopolysaccharide (LPS)	Enzo life sciences, Farmingdale, NY, USA
L-Lactic acid in Medium	Sigma-Aldrich, St. Louis, MO, USA
Methocel	DuPont de Nemours, Wilmington, DE, USA
Mitotracker Green FM	Thermo Fisher Scientific, Waltham, MA, USA
M-MLV Reverse Transcriptase	Promega, Madison, WI, USA
MSC-4381 MCT4 inhibitor (MCT4i)	Provided by Merck, Darmstadt, Germany
MycoAlert Mycoplasma Detection Kit	Cambrex, Rockland, ME, USA
NCI-737 in DMSO	Provided by Dr. Chi van Dang, Ludwig Institute for Cancer Research, Brussels, Belgium
PE MicroBeads (human)	Miltenyi Biotec, Bergisch Gladbach, Germany
Phorbol-12-myristate-13-acetate (PMA)	Calbiochem, Merck Millipore, Burlington, MA, USA
PolyHema	Sigma-Aldrich, St. Louis, MO, USA
Precision Plus Protein Kaleidsokop protein standard	BioRad, Hercules, CA, USA

Protease Inhibitor Cocktail	Hoffmann-La Roche, Basel, Switzerland
QuantiFast SYBR Green PCR Kit	Qiagen, Hilden, Germany
Qubit Protein Determination Kit	Thermo Fisher Scientific, Waltham, MA, USA
Random Decamer Primers	Thermo Fisher Scientific, Waltham, MA, USA
Reagent Diluent Concentrate	R&D systems, Minneapolis, MN, USA
ReBlot Plus Mild Antibody Stripping Solution	Merck, Darmstadt, Germany
RNAlater™	Qiagen, Hilden, Germany
RNeasy Mini Kit	Qiagen, Hilden, Germany
Substrate Reagent Pack	R&D systems, Minneapolis, MN, USA
Treg Expansion Kit	Miltenyi Biotec, Bergisch Gladbach, Germany
Trypan blue	Sigma-Aldrich, St. Louis, MO, USA
Zombia Aqua	BioLegend, San Diego, CA, USA
Zombie NIR Fixiable Viability Dye	BioLegend, San Diego, CA, USA

2.5 Antibiotics

Penicillin/streptomycin	Gibco, Carlsbad, CA, USA

2.6 Oligonucleotides

The listed oligonucleotides were designed as described below and synthesized by euorofins scientific, Luxemburg.

Gene	Sequence (forward and reverse)
18S rRNA	5'-ACCGATTGGATGGTTTAGTGAG-3' 5'-CCTACGGAAACCTTGTTACGAC-3'
IL-6	5'-ACCGATTGGATGGTTTAGTGAG-3' 5'-CCTACGGAAACCTTGTTACGAC-3'
SLC16A5	5'-ACCGATTGGATGGTTTAGTGAG-3' 5'-CCTACGGAAACCTTGTTACGAC-3'
SLC16A12	5'-ACCGATTGGATGGTTTAGTGAG-3' 5'-CCTACGGAAACCTTGTTACGAC-3'

2.7 Antibodies

2.7.1 Antibodies for Western Blot

Specificity	Source	Species reactivity	Molecular weight	Dilution	Company
α-Actin	Rabbit	Human, animals	42 kDa	1:2000	Sigma-Aldrich
α-Tubulin	Mouse	Human, animals	50 kDa	1:5000	Novus Bio
α-MCT1	Mouse	Human, mouse	40-48 kDa	1:1000	Santa Cruz Biotechnologies
α-MCT4	Rabbit	Human, mouse	43 kDa	1:1000	Santa Cruz Biotechnologies

2.7.2 Antibodies for flow cytometry

2.7.2.1 Anti-human antibodies

Antigen	Conjugation	Isotype	Clone	Company
α-CD3	PeCy7	Mouse IgG1	SK7	BioLegend
α-CD8	Pacific Blue	Mouse IgG1	RPA-T8	BD Bioscience
α-CD45	PerCP	Mouse IgG1	2D1	BioLegend
α-CD14	BV510	Mouse IgG2a	III329	BioLegend
α-CD66b	FITC	Mouse IgM	G10F5	BD Bioscience
α-IFNγ	FITC	Mouse IgG1	B27	BD Bioscience
α-Ki67	PE	Mouse IgG1	B56	BD Bioscience
α-FOXP3	APC	Rat IgG2a	PCH101	eBioscience
α-HLA-DR	PerCP	Mouse IgG2a	L423	BD Bioscience
α-TNF	APC	Mouse IgG1	MAb11	BioLegend
α-IL-6	BV421	Rat IgG1	MQ2-13A5	BD Bioscience

2.7.2.2 Anti-murine antibodies

Antigen	Conjugation	Isotype	Clone	Company
α-CD3	BV605	Rat IgG2b	17A2	BioLegend
α-CD4	BV510	Rat IgG2a	RM4-5	BioLegend
α-CD8	PeCy7	Rat IgG2a	53-6.7	BioLegend
α-CD45	PerCP	Rat IgG2b	30-F11	BD Bioscience
α-CD11b	BV510	Rat IgG2b	M1/70	BioLegend
α-Gr-1	BV711	Rat IgG2b	RB6-8C5	BioLegend
α-Ifnγ	APC	Rat IgG1	XMG1.2	BD Bioscience
α-F4/80	BV605	Rat IgG2a	BM8	BioLegend
α-NK1.1	BV421	Mouse IgG2a	PK136	BioLegend
α-PD-L1	PeCy7	Rat IgG2a	MIH6	BioLegend
α-IL-6	PE	Rat IgG1	MP5-20F3	BD Bioscience
α-CD19	BV711	Rat IgG2a	6D5	BioLegend

2.7.2.3 Other antibodies and dyes

Antigen	Conjugation	Function	Clone	company
Annexin V	FITC or APC	Viability	BB700	BD Biosciences
7-AAD		Viability		BD Biosciences
Cyto3D™ Live-Dead	Arcidine orange and propidium iodide	Viability		TheWell Bioscience
Carboxy-SNARF-1 AM		Intracellular pH		Thermo Fisher Scientific
2-NBDG		Glucose uptake		Thermo Fisher Scientific
DCFDA		Reactive oxygen species		Thermo Fisher Scientific
α-CD3/CD28 Dynabeads		T cell stimulation		BioLegend
In vivo mAb aPD-L1		Immune checkpoint inhibitor		BioXcell
In vivo mAb rat IgG2b		Isotype control		BioXcell
Human aPD-L1		Immune checkpoint inhibitor		Provided by Merck
Human mutated Isotype		Isotype control		Provided by Merck

2.8 Cell lines

HCT116	Provided by Merck, Darmstadt, Germany
HCT116 MCT4 Knock-Out	Provided by Merck, Darmstadt, Germany
MC38	Provided by Merck, Darmstadt, Germany
MC38 MCT4 Knock-Out	Provided by Merck, Darmstadt, Germany
MC38-OVA	Provided by Ramon Arens (297)
RJ494	Provided by Dr. Katrin Singer

2.9 Mice

C57BL/6N	Charles River, Wilmington, MA, USA
OT-I C57BL/6N	Provided by Christian Schmidl

2.10 Patient material

Collection of primary tumor samples and surrounding healthy tissue from ccRCC tumor patients was accomplished after approval of the ethics committee (University Regensburg, reference number 16-355-101) in accordance with the Helsinki Declaration and after signed informed consent of the patients.

2.11 Databases and software

CFX Maestro Software	Charles River, Wilmington, MA, USA
Citavi 6	Swiss Academic Software GmbH, Wädenswil, Switzerland
Evolution-Capt	Vilber Lourmat, Eberhardzell, Germany
FACSDiva	BD, Heidelberg, Germany
FlowJo v10.8.1	FlowJo, LLC, Ashland, OR, USA
Graph Pad Prism 9	GraphPad Software, La Jolla, CA, USA
Microsoft Excel	Microsoft Deutschland GmbH
PerlPrimer	Marshall, 2004
SensorDish-Reader Software	PreSens, Regensburg, Germany
UCSC genome browser	University of California, CA, USA
www.biorender.com	BioRender, Toronto, Canada
IncuCyte 2020B	Sartorius, Göttingen, Germany

Magellan	Tecan, Männedorf, Switzerland
pH1-View	PreSens, Regensburg, Germany

3 Methods

3.1 Cell culture

Cells were handled under a laminar air flow cabinet using sterile consumables and kept at 37 °C, 5 % CO_2, 95 % relative humidity. Unless otherwise specified, centrifugation was performed at 300 g, 4°C for 7 min.

3.1.1 Culture of cell lines

Tumor cell lines were cultured in tumor cell culture medium (Table 1). Cells were passaged every 3-4 days. Cells were rinsed with PBS and detached using 1 ml Trypsin/EDTA. Following, 9 ml culture medium was added to inactivate trypsin. Cells were centrifuged and seeded in fresh medium. Cells were passaged every 3-4 days in a ratio was 1:10 or 1:20 depending on the cell line and pellet size.

Table 1: Tumor cell culture medium

Component	Amount
RPMI1640	500 ml
FCS (heat inactivated)	10 %
L-glutamine	2 mM

For analysis of proliferation and viability, $0.15x10^6$/3 ml/well tumor cells were seeded in 6 well plates and measured after 72 hours. Lactate secretion was analyzed after 24 hours seeding $0.025x10^6$ cells/200 µl/well tumor cells in 96 well plates.

3.1.2 Cell freezing and thawing

For freezing of tumor cell lines, the volume of $1\text{-}3x10^6$ cells was mixed with freezing medium (80 % FCS, 20 % DMSO) in cryo tubes at a 1:2 ratio and slow-frozen in cryo freezing containers for short-term storage at -80°C and transferred to liquid nitrogen for long-term storage.

Frozen cells were thawed at room temperature and immediately transferred to warm medium. Cells were centrifuged and seeded in a cell culture flask containing pre-warmed culture medium.

3.1.3 Cell counting

CASY cell counter was used to determine cell count, viability and cell size. This method obtains signals when a cell passes in a low-voltage field through the system's high-precision measuring pore. The system was used according to manufacturer's instructions.

3.1.4 Isolation and culture of human immune cells

3.1.4.1 Isolation of human peripheral blood mononuclear cells

Human peripheral blood mononuclear cells (PBMCs) were isolated from either peripheral blood or thrombocyte cones (byproduct of leukocyte donation) of healthy donors. All participants provided written informed consent and the study was approved by the local ethics committee (vote numbers 13-101-0240 and 13-101-0238). Thrombocyte cones were obtained from the Transfusion Medicine Department of the University Hospital Regensburg. Blood was diluted with PBS to a final volume of 60 ml and 30 ml each were layered on top of 15 ml of Pancoll. PBMCs were enriched via ficoll density gradient centrifugation at 700 g, 20 min, RT without acceleration or break. The PBMC fraction was collected and washed twice with PBS. Cells were either used for spheroid co-culture experiments or subsequent isolation of T cells.

For spheroid co-culture experiments, PBMC were pre-stimulated for 24 hours in T cell medium (Table 2) containing 25 IU/ml IL-2. Cells were seeded in 24 well plates in a concentration of $1x10^6$ cells/ml/well and stimulated with anti-CD3/CD28 Dynabeads at a bead to cell ratio of 1:2.

3.1.4.2 Isolation and culture of human $CD3^+$ T cells

Human T cells were isolated from human PBMCs based on the magnetic cell sorting (MACS) technique from Miltenyi Biotec. $CD3^+$ cells were enriched by negative selection using the Pan T cell isolation kit according to the manufacturer's instructions. In brief, cells were washed with MACS wash buffer (PBS + 1 % FCS + 2 mM EDTA). All PBMCs except T cells were magnetically labeled with a cocktail of biotin-conjugated monoclonal antibodies against CD14, CD15, CD16, CD19, CD34, CD36, CD56, CD123, and CD235a (Glycophorin A) and anti-biotin MicroBeads. Next, the cell suspension was loaded onto a LS Column, which was placed in the magnetic field of a MACS Separator. The magnetically labeled cells were retained within the column. The untouched $CD3^+$ T cells are collected in the flowthrough. T cells were adjusted to a concentration of $10x10^6$/ml in T cell culture medium (Table 2) and stored over night or directly used for experiments.

Table 2: T cell culture medium

Component	Amount
RPMI1640	500 ml
Human serum (heat inactivated)	10 %
L-glutamine	2 mM
Penicillin	50 IU/ml
Streptomycin	50 µg/ml

Sodium pyruvate	1 mM
Non-essential amino acids	1 %
MEM essential vitamins	0.4 %
2-Mercaptoethanol	0.05 mM
Filtered through a 0.22 µm filter	

For experiments, $0.1x10^6$ cells/200 µl/well were seeded in round-bottom 96 well plates in T cell culture medium (Table 2) containing 25 IU/ml IL-2. Cells were stimulated using anti-CD3/CD28 coated Dynabeads at a ratio of one bead/cell. After 72 hours, T cells were passaged at a ratio of 1:2. For determination of oxygen consumption and extracellular acidification, T cells were seeded into 24 well HD24 and OD24 plates at a density of $0.8x10^6$ cells/ml/well. Measurements were performed using the PreSens technology.

3.1.4.3 Isolation of human $CD8^+$ T cells

Human $CD8^+$ T cells were isolated from PBMCs based on the magnetic cell sorting (MACS) technique from Miltenyi Biotec. $CD8^+$ T cells were enriched by positive selection using CD8 MicroBeads according to the manufacturer's instructions. In brief, cells were washed with MACS wash buffer (PBS + 1 % FCS + 2 mM EDTA). $CD8^+$ cells were magnetically labeled with CD8 MicroBeads. Following, the cell suspension was loaded onto a LS Column, which was placed in the magnetic field of a MACS Separator. The magnetically labeled $CD8^+$ cells were retained within the column and eluted as the positively selected cell fraction by removing the column from the magnetic field and flushing out of the column. T cells were adjusted to a concentration of $10x10^6$ cells/ml in T cell culture medium (Table 2) or directly used for experiments.

For experiments, $0.1x10^6$ cells/200 µl/well were seeded in round-bottom 96 well plates in T cell culture medium (Table 2) containing 25 IU/ml IL-2. Cells were stimulated using anti-CD3/CD28 coated Dynabeads at a ratio of one bead/cell. After 72 hours, T cells were passaged at a ratio of 1:2. For determination of oxygen consumption and extracellular acidification, T cells were seeded into 24 well HD24 and OD24 plates at a density of $0.8x10^6$ cells/ml/well. Measurements were performed using the PreSens technology.

3.1.4.4 Isolation of human granulocytes

Granulocytes were isolated from peripheral blood of healthy donors. Blood was diluted with PBS to a final volume of 60 ml and 30 ml each were layered on top of 15 ml of Pancoll. Granulocytes were separated via ficoll density gradient centrifugation at 700 g, 20 min, RT without acceleration or break.

The PBMC fraction was collected and washed twice with PBS. Subsequently, the white granulocyte layer on the erythrocyte pellet was transferred to a new Falcon tube. The erythrocytes were lysed by addition of 36 ml of ice-cold water for 40 seconds while carefully inverting the tube. Immediately after, 4 ml 10x PBS was added and cells were centrifuged. Another step of red cell lysis followed. The granulocyte fraction was washed twice with PBS and added to the PBMC fraction.

3.1.4.5 Isolation and differentiation of human monocytes

3.1.4.5.1 Isolation of monocytes by counterflow centrifugation

Monocytes were enriched from a lymphocyte donation obtained from voluntary donors in the Transfusion Medicine Department of the University Hospital Regensburg by elutriation. Elutriation is a process based on the principle of counterflow centrifugation that utilizes the balance between centrifugal force and counterflow drag force, allowing the separation of different cell types based on their size (Table 3). The first step was to assemble the separation chamber, connect it to the rotor, and sterilize the system by flushing with 6 % H_2O_2. The system was washed with PBS, and the peristaltic pump settings to achieve the required flow rates were determined by calibration with HBSS. PBMCs were enriched by gradient centrifugation as described in Section 3.1.4.1 and injected into the separation chamber at a flow rate of 52 ml/min. Different cell fractions were collected by applying appropriate pump flow rates (Table 3) at a rotor speed of 2500 rpm and a temperature of 4 °C. To increase cell viability, Hanks buffered salt solution (HBSS) supplemented with 6% donor plasma was used as vehicle.

Table 3: Elutriation settings

Cells	Cell size	Flow rate
B cells	7 µm	64 ml/min
T cells	7.5-8.5 µm	72-92 ml/min
Monocytes	9-10 µm	111 ml/min

Monocytes were collected in the final fraction. Purity was determined by flow cytometric analysis of surface markers CD3, CD14, and CD20. To confirm the unstimulated state of the enriched monocytes, IL-6 was measured in cell culture supernatants.

3.1.4.5.2 Differentiation and culture of monocyte-derived macrophages

For differentiation of monocyte-derived macrophages, monocytes were suspended in macrophage culture medium (Table 4) and seeded in Teflon-coated plastic bags and cultured at a concentration of $1x10^6$/ml for 6-7 days. For harvesting, cells were incubated at 4 °C for approximately 30 min and poured

into a 50 ml Falcon tube. After centrifugation, cells were suspended macrophage culture medium without AB serum.

Experiments were carried out in macrophage culture medium. AB serum was added directly to the wells after cell adherence to a final concentration of 2 %. For generation of RNA and protein lysates, $2.5x10^6$ cells/3 ml/well were seeded to 6 well cell culture plates and stimulated with 100 ng/ml LPS for 24 hours. For flow cytometric analyses, $0.5x10^6$ cells /1 ml/well were seeded in 12 well Up-Cell plates and stimulated with 100 ng/ml LPS. After 48 hours, plates were incubated at 4 °C for about 30 min to detach the cells. Plates were placed onto ice bags and cells were harvested by intensive flushing. For determination of lactate secretion, oxygen consumption and extracellular acidification, macrophages were seeded into 24 well plates at a concentration of $0.4x10^6$ cells/1ml/well.

Table 4: Macrophage culture medium

Component	Amount
RPMI1640	500 ml
AB-serum	2%
L-glutamine	2 mM
Penicillin	50 IU/ml
Streptomycin	50 µg/ml

3.1.5 Isolation and culture of murine splenocytes

C57BL/6N mice aged 12-20 weeks were used for experiments. Mice were provided by the central animal laboratories of the University Regensburg.

3.1.5.1 Spleen preparation

Mice were euthanized by CO_2 narcosis and cervical dislocation. The spleen was removed and stored in sterile PBS on ice for further processing. Spleens were scratched out in a petri dish containing 7 ml Tumor cell medium (Table 1) and cell suspension was filtered through a 100 µm cell strainer. The tissue remaining in the sieve was squeezed through with the plunge of a 2 ml syringe. Petri dish, plunge and cell strainer were rinsed with 10 ml medium. Cells were centrifuged. For erythrocyte lysis, pellet was diluted in 2 ml ACK buffer (Table 5) and incubated for 3 min at RT. 15 ml Tumor cell culture medium was added to stop the reaction. After centrifugation, the cell pellet was suspended in 1 ml murine T cell culture medium (Table 6) and filtered through a 100 µm cell strainer. Falcons and cell strainer were rinsed with 19 ml murine T cell culture medium, and cells were counted for subsequent B cell depletion.

Table 5: ACK lysis buffer

Component	Amount
NH_4Cl (Ammonium chloride)	49.64 g
$KHCO_3$ (Potassium bicarbonate)	16 g
EDTA (Ethylendiaminetetraacetate)	0.222 g
H_2O dest	Ad 1000 ml
pH adjusted to 7.4 Filtered through a 0.22 µm filter	

Table 6: Murine T cell culture medium

Component	Amount
RPMI1640	500 ml
FCS (heat inactivated)	10 %
L-glutamine	2 mM
Penicillin	50 IU/ml
Streptomycin	50 µg/ml
Sodium pyruvate	1 mM
Non-essential amino acids	1 %
MEM essential vitamins	0.4 %
2-Mercaptoethanol	0.05 mM
Filtered through a 0.22 µm filter	

3.1.5.2 B cell depletion and splenocyte culture

For live cell imaging (3.1.7.4), murine spheroid co-cultures were performed with B cell depleted splenocytes to increase the target to T cell ratio. Therefore, B cells were removed from splenocytes based on the magnetic cell sorting (MACS) technique from Miltenyi Biotec. B cells were stained with αCD19-PE antibodies. PE^+ B cells were then depleted by positive selection using PE MicroBeads according to the manufacturer's instructions. In brief, cells were washed with MACS wash buffer (PBS + 1 % FCS + 2 mM EDTA). Cells were labeled with beads and the suspensions was loaded onto a LS Column, which was placed in the magnetic field of a MACS Separator. The magnetically labeled PE^+ B cells were retained within the column. The unlabeled cells, B cell-depleted cells are collected in the flowthrough.

3.1.6 Mycoplasma test

All cell lines were routinely tested for mycoplasma contamination. Cell were cultured in antibiotic-free medium to a confluency of 100 %. Supernatant was collected and tested using the MycoAlert™ Mycoplamsa detection kit after manufacturer's instructions.

3.1.7 Spheroid co-culture

3.1.7.1 Spheroid formation

2D tumor cell culture based on the growth and proliferation of a monolayer of cells does not allow a complete understanding of the impact of the tumor microenvironment. In contrast, 3D spheroid culture models reflect the architecture and cellular composition of a tumor microenvironment with gradients of oxygen, nutrients and lactate. Tumor cell spheroids can be generated from tumor cell lines by preventing their adherence to a plastic surface. Therefore, 10.000 HCT116, MC38 or RJ494 tumor cells were either cultured in a hanging drop (30 µl per drop) on an inverted petri dish or in ultra-low-attachment 96 well plates (200 µl per well) coated with 50 µl PolyHEMA solution (Table 7) or 1 % agarose in PBS (Figure 13). After 4 days, robust spheroids have formed and were used for co-culture assay with immune cells as described in Chapter 3.1.7.2 and 3.1.7.3.

Table 7: PolyHEMA solution

Component	Amount
PolyHEMA	4.8 g
100% Ethanol	38 ml
H_2O dest	342 ml
8h at 65°C in 100% ethanol, then addition of H_2O	
Filtered through a 0.22 µm filter	

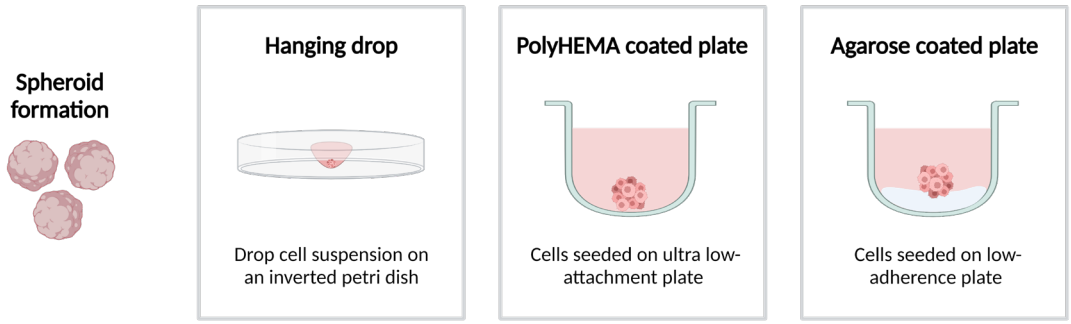

Figure 13. Spheroid formation assays. Created with BioRender.com.

3.1.7.2 Spheroid co-culture with human immune cells

HCT116 spheroids were generated as described in Chapter 3.1.7.1. To allow physiological acidification, spheroids were incubated for 7-10 days in coated 96 well plates. Prior to the addition of immune cells, 100 µl/well supernatant was removed and collected for lactate measurement. For co-culture, whole blood leucocytes were isolated from peripheral blood (3.1.4.1, 3.1.4.4). $0.1x10^6$ unstimulated whole leucocytes were directly added to the spheroids in a volume of 50 µl. In parallel, MNCs were pre-stimulated for 24 hours with αCD3/CD28 coated Dynabeads at a bead to cell ratio of 1:2 in T cell culture medium (Table 2) containing 25 IU/ml IL-2. Next day, $0.1x10^6$ pre-stimulated T cells were added in 50 µl T cell culture medium containing 100 IU/ml IL-2.

After 48 hours, co-cultures were either treated with GolgiStop for 3 hours to allow flow cytometric analysis of cytokine production or used for live cell imaging. Spheroids were harvested (12 spheroids per panel) and washed three times with PBS to remove remaining non-infiltrated immune cells. Afterwards, spheroids were dissembled by incubation with trypsin/EDTA. Reaction was stopped by addition of 2 ml tumor cell culture medium (Table 1) and flow cytometric staining was performed as described in Chapter 3.4. Experimental scheme is shown in Figure 14.

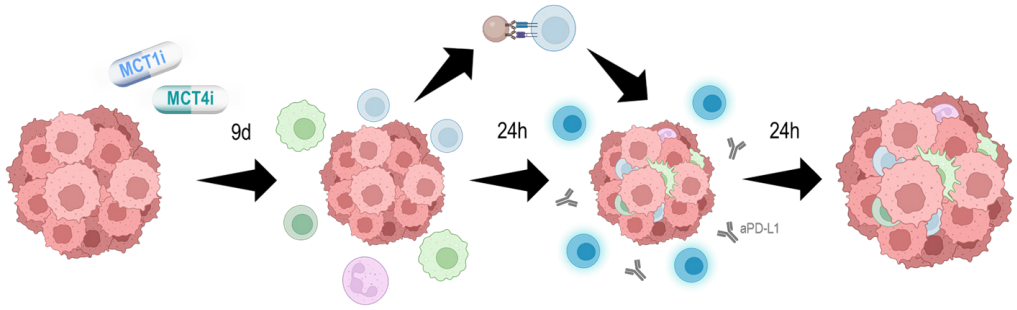

Figure 14. Spheroid co-culture scheme. Created with BioRender.com.

3.1.7.3 Spheroid co-culture with murine splenocytes

MC38 or MC38-OVA spheroids were generated as described in Chapter 3.1.7.1. To allow physiological acidification, spheroids were incubated for 7 days. Prior to the addition of immune cells, 100 µl supernatant was removed and collected for lactate measurement. For co-culture, splenocytes were isolated from C57BL/6N mice (3.1.5) and $0.1x10^6$ unstimulated bulk splenocytes were directly added to the spheroids in 50 µl. In parallel, splenocytes were pre-stimulated for 24 hours with αCD3/CD28 coated Dynabeads at a bead to cell ratio of 1:2 in murine T cell culture medium (Table 6) containing 50 IU/ml IL-2 and 50 ng/ml IL-15. Next day, $0.1x10^6$ pre-stimulated T cells were added in a volume of 50 µl T cell culture medium containing 200 IU/ml IL-2. After 48h, co-cultures were treated with GolgiStop for 3 hours to allow flow cytometric analysis of cytokine production. Spheroids were harvested (12 spheroids per panel) and washed three times in PBS to remove remaining non-infiltrated

immune cells. Afterwards, spheroids were dissembled by incubation with trypsin/EDTA. Reaction was stopped by addition of 2 ml tumor cell culture medium (Table 1) and flow cytometric staining was performed as described in Chapter 3.4.

3.1.7.4 Live cell imaging

IncuCyte ZOOM live cell imaging and analysis system, an incubator with integrated microscope, was used to analyze spheroid viability. Co-cultures for live-cell imaging were performed with B cell depleted splenocytes. Therefore, spheroids were co-cultured with immune cells as described in Chapter 3.1.7.2 and 3.1.7.3. After 48 hours co-culture, spheroids were washed and seeded in 96 ultra-low-attachment plates in 200 µl fresh medium containing 2 µl of Cyto3D™ Live-Dead viability dye. The viability dye consists of acridine orange (AO) and propidium iodide (PI). Both are nuclear staining (nucleic acid binding) dyes. AO is permeable to both live and dead cells and detects all nucleated cells by green fluorescence. PI enters only into the membranes of nucleated cells with damaged membranes and labels dead cells with red fluorescence. Double staining of nucleated cells with AO and PI results in a red fluorescence signal due to quenching of the AO signal (the PI reduces the fluorescence intensity of the AO by fluorescence resonance energy transfer (FRET)). Non-nucleated material such as red blood cells, platelets, and debris are not stained.

For co-cultures with MC38-OVA spheroids, no viability dye was added. Instead, viability was assessed by GFP fluorescence of MC38-OVA cells. Fluorescence signals of cells were monitored over time under cell culture conditions. Data were analyzed using the IncuCyte 2020B software.

3.1.8 Metabolic analysis of cell culture supernatants

3.1.8.1 Determination of lactate secretion

Cellular lactate secretion was assessed by enzymatic determination of lactate concentration in cell culture supernatants. Measurements were performed by the Department of Clinical Chemistry, University Hospital Regensburg, Germany.

3.1.8.2 Determination of extracellular acidification

The extracellular pH of cells was monitored under cell culture conditions over time using the PreSens technology. Cells were seeded in HD24 HydroDish plates with pre-calibrated pH sensors at the bottom of each well for non-contact reading by the SDR SensorDish® Reader through the transparent material of the plate.

3.1.8.3 Determination of oxygen consumption

Cell oxygen consumption was monitored over time under cell culture conditions using PreSens technology. Cells were seeded in OD24 OxoDish plates with pre-calibrated oxygen sensors at the

bottom of each well for non-contact reading by the SDR SensorDish® Reader through the transparent material of the plate.

3.1.8.4 Determination of cytokine secretion by ELISA

Cytokine concentrations in cell culture supernatants were determined by sandwich ELISA. The molecule of interest is captured in a "sandwich" of two specific antibodies, the lower of which is bound to the surface of a 96 well plate. The upper is biotinylated and can be labeled with a horseradish peroxidase that catalyzes a colorimetric reaction and allows subsequent absorbance measurement. A standard curve was used to calculate the absolute concentration of the cytokine of interest in cell culture supernatants.

For the quantification of cytokine levels, the respective DuoSet ELISA kits from R&D Systems were used according to the manufacturer's instructions.

3.2 Biochemical methods

3.2.1 Isolation of proteins

Isolation of proteins was performed on ice using pre-cooled chemicals and equipment. Lysates were centrifuged at 13.000 rpm for 15 min at 4 °C and protein concentration was determined by e the Qubit protein assay kit according to the manufacturer’s instructions. Samples were stored at -80 °C.

3.2.1.1 Preparation of RIPA lysates

For preparation of lysates from adherent cells, 1-2.5x10^6 cells were seeded into 3 ml medium in 6 well plates. After 24 hours, cells were washed twice with PBS, scraped down in 50 µl RIPA buffer and transferred to a fresh sample tube. In case of suspension cells, 1-2.5x10^6 cells were directly washed twice with PBS and cells were suspended in 50 µl of RIPA buffer. Lysates were vortexed for 1 min, then incubated at -20°C for 5 min, again vortexed and snap-frozen in liquid nitrogen.

3.2.1.2 Preparation of native lysates

For adherent cells, 1-2.5x10^6 cells were seeded into 3 ml medium in 6 well plates for 24 hours. Next day, cells were washed twice with PBS. Cells were scraped down in 50 µl CLB buffer and transferred in a fresh sample tube. In case of suspension cells, 1-2.5x10^6 cells were directly washed twice with PBS and cells were suspended in 50 µl of CLB buffer.

3.2.1.3 Preparation of phospho-lysates

Phospho-protein lysates were prepared to determine protein phosphorylation. 1x10^6 macrophages were seeded into 3 ml macrophage culture medium (Table 4) in 6 well plates for 24 hours. Afterwards, plates were placed on ice and wells washed twice with PBS. 500 µl of freshly prepared pre-equilibration

buffer (buffer B, Table 9) containing cytoplasmic extraction buffer (CEB) (also called buffer A in this setting, Table 8) was added to the culture plates. Cells were incubated on ice for 4 min, then scraped down and transferred to a fresh tube. Lysates were centrifuged, and the supernatant was carefully discarded. Subsequently, 60 µl of freshly prepared lysis buffer (buffer C, Table 10) was added to cell pellets and incubated on ice for 10 min. For denaturation of the secondary protein structure, 60 µl SDS sample buffer was added to the cell lysate and tubes were heated to a 95 °C for 10 min. Lysates were aliquoted, and stored at -80 °C.

Table 8: Buffer A for phospho-lysates

Component	Amount
Tris/HCl (pH 7.9)	10 mM
KCl	60 mM
EDTA	37 mg
H_2O dest	Ad 100 ml

Table 9: Buffer B for phospho-lysates

Component	Amount
EDTA	1.5 mM
Dithiothreitol	1 mM
EGTA	1 mM
β-Glycerophosphate	50 mM
Sodium fluoride	50 mM
Sodium pyrophosphate	25 mM
Sodium orthovanadate	1 mM
Leupeptin	2 µg/ml
Pepstatin A	2 µg/ml
Aprotinine	2 µg/ml
Buffer A	Ad 1000 µl
H_2O dest	1000 µl

Table 10: Buffer C for phospho-lysates

Component	Amount
Nonidet P40	0.4 %
Chymostatin	100 µg/ml
Bestatin	10 µg/ml
E64	3 µg/ml
1,10-Phenanthrolin	1 mM
Buffer B	Ad 1000 µl
H_2O dest	1000 µl

Table 11: SDS sample buffer

Component	Amount
Glycerine	20 %
Tris buffer (pH 6.8)	125 mM
Sodium dodecyl sulfate (SDS)	4 %
2-Mercaptoethanol	10 %
Bromphenol blue	0.02 %

3.2.2 Western blot analysis

Western blot is a technique used for detection of specific proteins in a whole cell lysate. For this purpose, proteins are separated by size using SDS (sodium dodecyl sulfate) polyacrylamide gel electrophoresis and then transferred to a PVDF membrane, where they can be visualized using specific antibodies and immunohistochemical detection methods.

3.2.2.1 SDS polyacrylamide gel electrophoresis

12 % separation gels and 5 % stacking gels were poured. The running gel was prepared as described below (Table 12, Table 13), immediately filled into the prepared glass plates in casting frames and covered with isopropanol. After polymerization, isopropanol was removed, glass plates were rinsed with water and the stacking gel solution was filled on top. A comb was placed into the solution and the gel was allowed to polymerize. The prepared gels were stored in a humid environment at 4 °C until electrophoresis.

Table 12: SDS polyacrylamide gels

Component	Running gel (12 %)	Stacking gel (5 %)
Running gel solution	11 ml	-
Stacking gel solution	-	5 ml
Tetramethylethyldiamin (TEMED)	11 µl	5 µl
APS (10 %)	55 µl	40 µl

Table 13: SDS polyacrylamide gel solution

Component	Running gel solution	Stacking gel solution
Running gel buffer (1.5 M Tris, pH 8.8)	25 ml	-
Running gel buffer (0.5 M Tris, pH 6.8)	-	25 ml
Acrylamide/Bis-Acrylamide (30 %)	40 ml	16.65 ml
SDS (10 %)	1 ml	1 ml
H_2O dest	Ad 100 ml	Ad 100 ml

For analysis, 10 µg protein were loaded per lane. The protein was diluted with PBS, mixed with 2x SDS sample buffer (Table 14) and heated for 10 min at 95 °C. Gels were placed into the running chamber filled with 1x Lämmli's running buffer (Table 15). Protein mixtures and a protein standard were loaded onto the gel. Electrophoresis was performed according to Table 16.

Table 14: 2x SDS sample buffer

Component	Amount
Glycerin	20 %
1.25 M Tris-HCl, pH 6.8	125 mM
SDS	4 %
2-Mercaptoethanol	10 %
Bromphenole blue	0.02 %
H_2O dest	Ad 50 ml

Table 15: 4x Lämmli's running buffer

Component	Amount
Glycine	0.95 M
Tris	40 mM

SDS	4 %
H_2O dest	Ad 3 l

Table 16: SDS PAGE voltage settings

Voltage	Time
80 V	20 min
100 V	30 min
120 V	90 min

3.2.2.2 Western blotting

Semi-dry blotting was used to transfer the separated proteins to a PVDF membrane. The membrane was pre-incubated in 70 % isopropanol and stored in buffer B until further usage. Three sheets of whatman paper was soaked with buffer A and placed onto the blotting chamber. Next, papers soaked in buffer B were placed on top. The membrane and following the gel was placed on top. The gel was covered with three sheets of whatman paper soaked with buffer C. Gel electrophoresis was carried out at 11 V for 1 hour. Blotting buffer formulations are shown in Table 17.

Table 17: Blotting buffers

Component	Amount
Buffer A	
Tris	0.3 M
Methanol	20 %
H_2O dest	Ad 1 l
Buffer B	
Tris	25 mM
Methanol	20 %
H_2O dest	Ad 1 l
Buffer C	
ε-Amino-n-Capronsäure	4 mM
Methanol	20 %
H_2O dest	Ad 1 l

After blotting, the membrane was directly transferred into 10 ml wash buffer (1x TBS (Table 18) + 0.1 % Tween, TBST). The membrane was washed two times (10 min each). Afterwards, unspecific antibody binding sites were blocked by incubation in a 5 % skimmed milk solution in TBST for 1 hour at RT under constant shaking. Membranes were incubated overnight at 4 °C in the primary antibody solution diluted in 5 % skimmed milk. Next day, blots were washed tree times with TBST and incubated for 1 hour at RT in the secondary antibody solution diluted in 5 % skimmed milk in TBST. After additional 3 washing steps, the enhanced chemiluminescence (ECL) detection solution was prepared according to the manufacturer's instructions for immunohistochemical detection. The membrane was carefully dried, placed on plastic foil, layered with the ECL solution and incubated for 5 min at RT. Afterwards, ECL was removed and the signal was detected using the chemiluminescence system Fusion Pulse 6 (Vilber Lourmat).

For the detection of additional proteins, antibodies were removed by membrane stripping. Therefore, the membrane was washed twice in TBST and incubated for 15 min with constant shaking in 1x mild or strong stripping solution. After three more washing steps, blocking and protein detection was performed as described above.

Table 18: 10x Tris buffered saline (TBS) buffer

Component	Amount
Tris	45.8 g
NaCl	175.5 g
H_2O dest	Ad 2 l
pH adjusted to 7.4	

3.3 Molecular biology methods

RNA samples were prepared and handled on ice using RNase-free plastic material and consumables. Samples were stored at -80 °C.

3.3.1 Preparation of ribonucleic acid

For the generation of RNA-lysates from adherent cells, 1-2.5x10^6 cells were seeded into 3 ml culture medium in 6 well plates. After 24 hours, medium was removed and cells were scraped down in 350 µl RLT-buffer supplemented with β-mercaptoethanol (1 ml RLT + 10 µl β-mercaptoethanol) according to manufacturer's instructions and sheared using a 20 G needle and syringe.

For the generation of RNA-lysates from suspension cells, up to $5x10^6$ cells were centrifuged and suspended in 350 µl RLT-buffer supplemented with β-meracptoethanol according to manufacturer's instructions and sheared using a 20 G needle and syringe.

RNA was isolated using the RNeasy Mini Kit according to the manufacturer's instructions. RNA concentration was assessed by NanoDrop.

3.3.2 Reverse transcription

For determination of gene expression levels, isolated RNA was transcribed into complementary DNA (cDNA) using a reverse transcriptase derived from the murine moloney leukemia virus (M-MLV), random decamer primers and 2'-deoxyribonucleosid-5'-triphosphates (dNTPs). The reaction was performed in a PCR thermocycler according to the following protocol (Table 19) with a total reaction volume of 20 µl.

Table 19: Reverse transcription protocol

Component	Volume/Reaction
Total RNA	500 ng
Random Decamer Primers (10 µM)	1 µl
dNTPs (10 mM)	1 µl
PCR H_2O	Ad 15 µl
Incubation: 5 min at 65°C	
5x Reverse transcription buffer	4 µl
Incubation: 2 min at 42°C	
M-MLV reverse transcriptase	1 µl
Incubation: 50 min at 42°C	
Incubation: 15 min at 70°C	

3.3.3 Primer design

Primers used for real-time PCR (RT-PCR) were designed to detect the genes of interest using an open-source software PerlPrimer and the UCSC genome browser based on the criteria in Table 20. The coding and genomic sequences were obtained from the UCSC database. Primer specificity was determined using the 'in-silico PCR' and the 'BLAT' function provided by the UCSC.

Table 20: Criteria for Primer design

Criteria	
GC content	40-60 %
Melting temperature	65-68 °C
Primer length	20-28 bp
Amplicon length	70-150 bp
Position	on 2 different exons

3.3.4 Quantitative real-time PCR

Gene expression was quantified by quantitative real-time polymerase chain reaction (qRT PCR). RNA content of cells is isolated and translated into cDNA by reverse transcription as described in Chapter 3.3.1 and 3.3.2. To determine gene expression, a fluorescent dye (SYBR Green) is added to the PCR mixture, which emits light only when bound to double-stranded DNA. During PCR, more double strands of the respective gene of interest are synthesized, which leads to an increase in the fluorescence signal and can be detected with a real-time PCR instrument. At a certain point in time, called Cq, the specific fluorescence exceeds the background fluorescence. The higher the abundance of RNA encoding the gene of interest was in the sample, the earlier this occurs. Using a standard curve included in each experiment, the absolute expression of the gene can be calculated and related to the expression of a housekeeping gene.

For qRT-PCR, a reaction mix was prepared in 96 well PCR microtiter plates with a total volume of 10 µl according to Table 21. Samples were pipetted in triplicates, standards were pipetted in duplicates. Plates were sealed with a PCR plate seal, briefly centrifuged, and the reaction was run in the BioRad CFX instrument according to the protocol given in Table 22. After the run, data were analyzed using the CFX software.

Table 21: qRT PCR reaction mix

Component	Amount
cDNA (diluted)	1 µl
QuantiFast SYBR Green PCR Kit	5 µl
Primer (10 pmol)	0.5 µl each
PCR H_2O	3 µl

Table 22: qRT PCR program

Process	Temperature	Duration
Initial denaturation	95 °C	5 min
Denaturation	95 °C	8 sec (40x)
Annealing/elongation	60 °C	20 sec (40x)
Melting curve	95 °C	15 sec
	65 °C	15 sec
	65-95 °C	10 min

3.4 Flow cytometry

Flow cytometry is the gold standard for cell analysis as it allows examination and sorting of not only surface markers, but also metabolic characteristics on individual cell level. Monoclonal antibodies conjugated to fluorochromes or fluorescent dyes allow labeling and detection of specific cell populations. Labeled cells individually pass through a laser beam, generating scattered light and fluorescence. Scattered light indicates the size (forward scatter, FSC) and granularity (side scatter, SSC) of the cells, fluorescence provides information about a specific cell type.

All centrifugation steps for flow cytometry staining were performed at 1600 rpm, 4 °C. When brilliant violet (BV) conjugated antibodies were used, antibodies were pre-incubated in BV staining buffer (10 µl buffer/antibody) for 10 min at RT before staining. Acquisition of stained cells was performed using the BD FACS Calibur, BD FACS Fortessa, or BD FACS Celesta instrument. Results were analyzed using the Flowjo_v10.8.1 software.

3.4.1 Viability staining

3.4.1.1 Live-Dead staining

To distinguish between live and dead cells, cells were stained with the fixable viability dye Zombie NIR or Zombie Aqua prior to surface staining. After washing twice with PBS, cells were incubated in 80 µl of diluted Zombie NIR dye (1:650 in PBS) or 50 µl of diluted Zombie Aqua dye (1:200) for 10 min at RT in the dark followed by subsequent surface staining (3.4.2) without additional washing step.

3.4.1.2 Annexin V/7-AAD staining

Early and late apoptosis was determined by Annexin V and 7-Aminoactinomycin D (7-AAD) staining. Annexin V is a phospholipid-binding protein that has a high affinity for the anionic phospholipid phosphatidylserine (PS). In viable cells, PS is located on the cytoplasmic side of the plasma membrane.

During apoptosis initiation, the plasma membrane undergoes structural changes that include translocation of PS from the inner- to the extracellular side, where Annexin V can bind it. 7-AAD is a membrane-impermeable fluorescent DNA intercalator that can only enter cells with membrane damage and undergoes a spectral shift after DNA binding. This allows differentiation of viable (double negative), early apoptotic (7-AAD negative, Annexin V positive) and late apoptotic cells (double positive). 0.5-1x10^6 cells were washed with PBS, suspended in 300 µl 1x Annexin Binding Buffer and stained with 5 µl Annexin V and 10 µl 7-AAD. After 20 min incubation at RT, cells were immediately measured.

3.4.2 Surface staining

For staining of cell surface markers, 0.5-1x10^6 cells were used per panel. If viability staining was included, it was performed as described in Chapter 3.4.1.1. Cells were washed once in 1ml FACS wash buffer (PBS + 2 % FCS) and the supernatant was discarded. When staining murine cells, 1 µl of Fc receptor blocking reagent was added and samples incubated for 10 min at 4 °C before further staining. Cells were then incubated with antibody cocktails for 20 min at 4 °C, washed in FACS wash buffer, resuspended in 250 µl FACS wash buffer and measured.

3.4.3 Intracellular staining

For staining markers located in in the cytoplasm or nucleus like cytokines or transcription factors, cells must be permeabilized before staining.

3.4.3.1 Staining for cytokines

For determination of intracellular cytokines, GolgiStop or GolgiPlug was added the cells for 2 hours before flow cytometric staining. Live-dead and surface staining preceded intracellular staining as described in Chapter 3.4.1.1 and 3.4.2. For cytokine staining, cells were fixed and permeabilized using the BD Fix/Perm Kit according to the manufacturer's instructions. Incubation with the respective antibodies was performed for 20 min at 4°C. Afterwards, the cells were resuspended in 250 µl FACS wash buffer and measured.

3.4.3.2 Staining for nuclear markers

Live-dead and surface staining preceded intracellular staining as described in Chapter 3.4.1.1 and 3.4.2. Afterwards, cells were washed in PBS and lysed using the Foxp3 staining Kit according to manufacturer's instructions. Incubation with the respective antibodies was performed at 4 °C for 30 min. Afterwards, the cells were resuspended in 300 µl FACS washing buffer and immediately measured.

3.4.4 Determination of glucose uptake

2-(N-(7-Nitrobenz-2-Oxa-1,3-Diazol-4-yl)-Amino)-2-Desoxyglucose (2NBDG) is a fluorescent glucose analog used to monitor glucose uptake in living cells. The 2NBDG staining was preceded by live-dead and surface staining. 200 µl of a 50 µM 2NBDG dilution in HBSS was directly added to the surface staining mix. Cells were incubated for 20 min under cell culture conditions, washed twice with FACS wash buffer and analyzed by flow cytometry.

3.4.5 Determination of cellular reactive oxygen species

The cell-permeable 2',7'-dichlorodihydrofluorescein diacetate (DCFDA) is a chemically reduced form of fluorescein used as an indicator of reactive oxygen species (ROS) in cells. After cleavage of the acetate groups by intracellular esterases and oxidation by abundant cellular ROS, the non-fluorescent DCFDA is converted to the highly fluorescent 2',7'-dichlorofluorescein (DCF).

After surface staining (3.4.2), cells were suspended in 500 µl FACS wash buffer and 12.5 µl of diluted DCFDA (1:50 dilution in FACS wash buffer of 400 µM stock) was added. Cells were incubated for 20 min under cell culture conditions, washed with cold PBS and immediately measured.

3.4.6 Determination of intracellular pH

Intracellular pH was determined by flow cytometry using the pH-sensitive dye 5-(and-6)-Carboxy SNARF™-1, Acetoxymethyl Ester (carboxy-SNARF-1-AM). The emission spectrum of carboxy-SNARF-1 is subject to a pH-dependent wavelength shift, so the ratio of the fluorescence intensities of the dye at two emission wavelengths can be used for a more accurate determination of pH.

Cells were harvested, and supernatants was kept under cell culture conditions for re-incubation after loading with the dye. Cells were washed with 1 ml HBSS and loaded with 10 µM carboxy SNARF-1 AM in 500 µl HBSS for 30 min under cell culture conditions. Cells were then washed with 1 ml of HBSS and the associated saved culture supernatant was added to readjust the intracellular pH. The cells were kept under cell culture conditions until measurement. The fluorescence response was calibrated with pH-controlled buffers and valinomycin/nigericin to equilibrate the intracellular pH with the controlled extracellular medium according to the manufacturer's recommendations. For analysis, the ratios of emission wavelength λ1 transmitted by a 575LP BP filter and wavelength λ2 transmitted by a 670LP filter were calculated.

3.4.7 Compensation

When performing multicolor immunofluorescence analyses with flow cytometry, the intrinsic spectral overlap of the different fluorochromes used, if not corrected, will result in the emission of a particular fluorochrome into an inappropriate detector. If this spectral overlap is not compensated for, it can

lead to misinterpretation of the data due to false-positive populations and artifactual populations in multicolor contour plots. However, by using appropriate single- and double-stained control samples, spectral overlap can be compensated for by electronic subtraction of unwanted signals so that accurate flow cytometric analysis of multicolor-stained cells can be successfully performed.
For antibody compensation, CompBeads, a compensation-particles set, was used according to the manufacturer's instructions. Unstained cells were used to adjust autofluorescence. Cells were used to compensate metabolic or viability staining.

3.5 Analysis of human tumor biopsies

3.5.1 Preparation and culture of patient-derived tumor cell suspensions

To obtain single-cell suspensions from human tissue, biopsies were minced with a scalpel and incubated in 1 ml digestion medium (Table 23) in 12 well plates for 2 hours. The suspension was passed through 70 µm cell sieves, and plates were rinsed with 20 ml of tumor cell culture medium (Table 1) to collect all cells. After centrifugation at 300 g for 7 min at 4 °C, cells were suspended in 1 ml tumor cell culture medium and counted. If erythrocytes were present as indicated by a red cell pellet, erythrocyte lysis was performed by incubation in 3 ml 1x ACK buffer (Table 5) for 2 min at RT before cell counting. Reaction was stopped by adding 10 ml of medium and cells centrifuged. For experiments, $0.1x10^6$ cells/200 µl/well were seeded in macrophage culture medium (Table 4) in 96 well plates. Next day, cells were harvested for flow cytometry staining (3.4).

Table 23: Human digestion medium

Component	Amount
RPMI1640	1 ml
DNase I (10 mg/mL)	45 µl
Collagenase IV (2100 U)	100 µl

3.5.2 Patient-derived tumoroids

Patient-derived tumor organoids (tumoroids) are tumor fragments with a mass of about 30 mg and serve as models to understand patient-specific drug responses of tumor and stroma. After determination of the wet weight, tumoroids were placed into 12 well UpCell plates in 1 ml macrophage culture medium (Table 4). After 48 hours, supernatant was collected.

3.6 Mouse experiments

C57/Bl6N mice were obtained from Charles River and housed at the conventional keeping at the animal facility of the University Hospital of Regensburg (ZTL Regensburg). All mice used for experiments were 10- to 12-week old females and were held for a minimum of 1-2 weeks for acclimation prior to the beginning of studies. Mice were housed with ad libitum access to food and water in a pathogen-free facility. All procedures were performed in accordance with institutional protocols approved by the government of Unterfranken (RUF-55.2.2-2532-2-1392-22) and the Institutional Animal Care and Use Committee of Merck/EMD Serono Research and Development Institute.

3.6.1 Study designs

The impact of MCT inhibitors as monotherapy or in combination with anti-PD-L1 (aPD-L1) on survival, tumoral immune infiltration and function, and intra-tumoral pH was investigated applying different study designs outlined in Figure 15. MC38 tumor cells were inoculated on day 0 (3.6.2). Mice were treated daily starting at day 6 throughout duration of each experiment (3.6.3). To test drug efficacy, mice were euthanized as soon as tumor volume reached 1700 mm^3. Analysis of immune infiltration and function by flow cytometry as well as determination of tumoral pH was carried out on day 11 to 13.

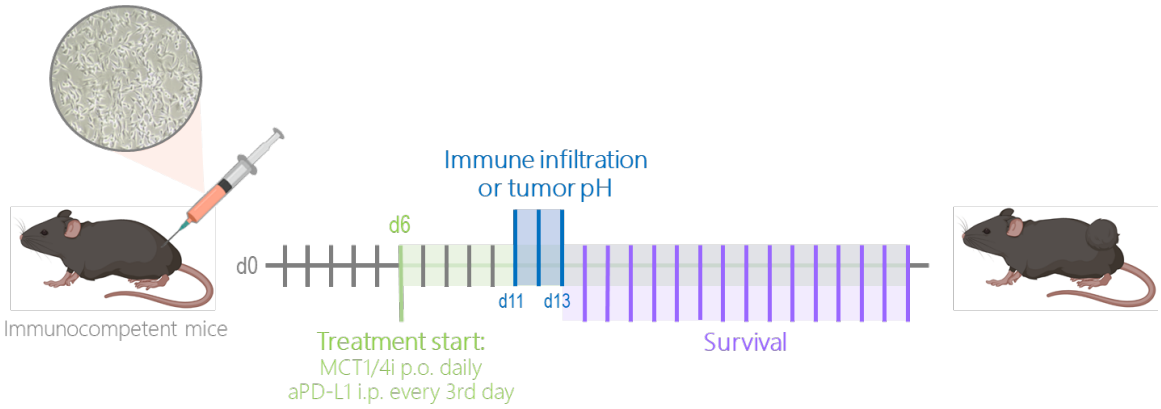

Figure 15. Experimental design of *in vivo* studies. Created with BioRender.com.

3.6.2 Tumor inoculation

Tumors in mice were generated by subcutaneous injection of $1x10^6$ MC38 wildtype or MCT4 Knock-Out tumor cells into the dorsal region. Using a manual caliper, tumor length was measured along the longest axis of the tumor and width was measured perpendicular to the length. Tumor volume was calculated using tumor length (l) and width (w) measurements with the equation l*w2*0,52, starting from the first day when tumors became visible. When the tumor volume reached 1700 mm^3, mice were killed and blood, spleen, and tumor were dissected for analysis.

3.6.3 Treatment and monitoring

Animals were monitored on a daily basis for tumor size and their general condition. Tumors were measured with a caliper starting at day 4. On day 6, when average tumor volume reached 50-75mm^3, mice were assigned to treatment groups. Each group was assigned to one of the treatment regimens as outlined in Table 24. Tumor volume was determined by using the tumor length (l) and width (w) measurements and calculating the volume with the equation $l \times w^2 \times 0.52$. The length was measured along the longest axis of the tumor and width was measured perpendicular to that length. Body weight was monitored every day, while administering the treatment to determine the volume of administration. Treatment was started on day 6 post cell implantation. All treatments were continued until humane endpoint (max tumor volume 1700 mm^3) in efficacy studies or study end of immune infiltration studies (Figure 15) was reached. MCT inhibitors were administered by oral gavage using flexible feeding tubes, aPD-L1 or isotype were injected intraperitoneally using insulin syringes. MCT1i was dissolved in vehicle 1 (Table 25) and MCT4i (Table 26) in vehicle 2, immune checkpoint blockade antibodies were diluted in PBS to a total volume of 120 µl.

Table 24: *In vivo* treatment

Groups	treatment	dose	schedule	volume	route
1	isotype	10 mg/kg BW	every 3rd day	120 µl	i.p.
	vehicle 1/2	-	daily	10 ml/kg BW	p.o.
2	isotype	10 mg/kg BW	every 3rd day	120 µl	i.p.
	MCT4i	3 mg/kg BW	daily	10 ml/kg BW	p.o.
3	aPD-L1	10 mg/kg BW	every 3rd day	120 µl	i.p.
	vehicle 1/2	-	daily	10 ml/kg BW	p.o.
4	aPD-L1	10 mg/kg BW	every 3rd day	120 µl	i.p.
	MCT4i	3 mg/kg BW	daily	10 ml/kg BW	p.o.
5	aPD-L1	10 mg/kg BW	every 3rd day	120 µl	i.p.
	MCT4i	3 mg/kg BW	daily	10 ml/kg BW	p.o.
	MCT1i	10 mg/kg BW	daily	10 ml/kg BW	p.o.

Table 25: Formulation vehicle 1

Component	Amount
Methocel	0.5 %
Tween20	0.25 %
H_2O dest	200 ml

Table 26: Formulation vehicle 2

Component	Amount
Kleptose	20 %
Phosphate buffer, pH 7.4	50 mM
H_2O dest	Ad 200 ml

3.6.4 Sample preparation for flow cytometry

Once humane endpoint (max 1700 mm^3) was reached, animals were euthanized by Ketamin/Xylazin (Ketamin 10 %: agent Ketaminhydrochloride, 90-120 mg/kg KG; Xylazin: 6-8 mg/kg KG) anesthesia followed by cervical dislocation.

3.6.4.1 Preparation of a single-cell suspension from tumors

Tumors were kept in cold PBS until processing. All preparations were performed on ice. All centrifugation steps were performed at 300 g for 8 min at 4 °C. Tumors were infused with 3 ml of digestion medium (Table 27), incubated in 6 well plates for 1 hour at 37 °C while minced with a scalpel after 30 min. Tumors were then passed through a 70 µm cell strainer and centrifuged. Erythrocytes were lysed by incubation with 2 ml of 1x ACK lysis buffer (Table 5) for 3 min at RT. The reaction was stopped with 10 ml medium. After centrifugation, cells were resuspended in 1-50 ml of medium depending on the pellet size, further passed through a 100 µm cell sieve and counted using the CASY system. $3x10^6$ cells were used for flow cytometric staining.

Table 27: Murine digestion medium

Component	Amount
RPMI1640	3 ml
DNase I (10 mg/ml)	12 µl
Collagenase IA (10 mg/ml)	15 µl

3.6.4.2 Spleen preparation

Spleens were scratched out in a petri dish containing 7 ml tumor cell culture medium (Table 1) and cell suspension was filtered through a 100 µm cell strainer. The tissue remaining in the sieve was squeezed through with the plug of a 2 ml syringe. Petri dish, plug and cell strainer were rinsed with 10 ml medium. Cells were centrifuged. For erythrocyte lysis, the pellet was diluted in 2 ml 1x ACK buffer (Table 5) and incubated for 3 min at RT. 15 ml Tumor cell culture medium was added to stop the reaction. After centrifugation, the cell pellet was suspended in 1 ml PBS and filtered through a 100 µm cell strainer. The tube and filter were rinsed with 19 ml PBS and cells were counted.

3.6.4.3 Blood preparation

Blood of the mice was collected from the vena cava abdominalis and immediately transferred into tubes filled with 4 ml PBS + 10 µl Heparin. Tubes were centrifuged and 1 ml 1x ACK lysis (Table 5) buffer was added for 5 min at RT. 2 ml FACS wash buffer was added to stop the reaction. Erythrocyte lysis was repeated. Cells were then resuspended 1 ml of FACS wash buffer for flow cytometry staining.

3.6.4.4 Lymph node preparation

Lymph nodes were placed on a 70 µm cell strainer, rinsed with 10 ml tumor cell culture medium (Table 1) and squeezed through with the plug of a 2 ml syringe. The cell sieve was rinsed with 30 ml culture medium, cells centrifuged and resuspended in 1 ml FACS wash buffer for flow cytometric staining.

3.6.5 *In vivo* tumor pH measurement

Tumor pH was measured in size-matched tumors using a fiber-optic pH meter consisting of a pH Needle Microsensor NTH-HP5 for measurement with high spatial resolution and using a manual micromanipulator. MCT inhibitors were administered 2 hours before pH determination. Microsensors were calibrated for at least 30 min, tumors were dissected, and the pH microsensor was inserted into the tumor at different depths, and pH was monitored between 1-3 min using the pH1-View software.

3.7 Graphics and statistics

Graphs were generated using GraphPad Prism software or the licensed program BioRender.com. Statistical analyses were performed using GraphPad Prism software.

4 Results

Metabolic reprogramming of tumor cells is acknowledged as hallmark of cancer in one of the most cited publications in cancer research by Hanahan and Weinberg (3). In contrast to non-transformed cells, tumor cells are characterized by metabolic adaption towards a glycolytic phenotype, termed Warburg effect (22,298). Increased glucose uptake and its conversion to lactate requires continuous export mediated by proton-coupled monocarboxylate transporters (MCTs), of which MCT1 and MCT4 are the major tumor-associated transporters (299,300). Accordingly, lactate and co-transported protons, herein named lactic acid, accumulate within the tumor microenvironment (TME). In metastasized tumors, lactate levels can reach up to concentrations of 40 mM (109,301).

The immunosuppressive effect of lactic acidosis on immune cells has been increasingly studied in recent years (33,35,117,121,301–305). Previous studies have shown that the acidic TME is associated with lower anti-tumor immune response and may contribute to immune checkpoint inhibitor failure in many patients (124,302,306–308). However, less attention has been paid to the fundamental differences in the sensitivity of lymphoid and myeloid cells to lactic acid. Moreover, although the Warburg phenotype has been studied as a metabolic immune checkpoint for years, there is still no approved anti-glycolytic drug for cancer therapy in the clinic. Therefore, our goal was to compare the sensitivity of different immune cells to lactic acid and provide a possibility for immunomodulatory treatment of solid Warburg tumors. Parts of this project were conducted in cooperation with Merck KGaA, Darmstadt, Germany.

4.1 Sensitivity of immune cells to lactic acid *in vitro*

As a consequence of the elevated glycolytic activity of tumor cells, immune cells encounter high levels of lactic acid in the TME. Several studies reported an immunomodulatory effect of lactic acid on lymphocytes (33,35,121) and myeloid cells (112,121). Besides tumor cells, highly proliferating effector T cells, tumor-associated macrophages and neutrophil granulocytes rely on glycolysis to cover their energetic demands. However, not much is known about the expression of the lactate transporters MCT1 and MCT4 in different kinds of immune cells or the differences in the susceptibility of lymphocytes and myeloid cells to lactic acidosis. Therefore, the basal MCT expression level, intracellular acidification, and viability of T cells and myeloid cells under lactic acid exposure were investigated.

4.1.1 T cells are sensitive to lactic acid

Lactic acid has been reported to impair murine as well as human T cell function (33,35,301). To confirm this, T cells were isolated from the peripheral blood of healthy donors and stimulated with αCD3/CD28

coated beads to study the sensitivity of T cells to lactic acid. As previously shown, 20 mM of lactic acid induced apoptosis in human $CD4^+$ T cells (experiments performed by Dr. Sonja Decking) (Figure 16A,B). MCT1 and MCT4 are the major lactate transporters and form the concentration dependent entry port for extracellular lactic acid into the cytoplasm of cells, which is required for the maintenance of the glycolytic flux. Indeed, T cells express lactate transporters MCT1 and MCT4 upon activation with anti-CD3/CD28 Dynabeads. Since lactate is imported together with protons, lactate import might be associated with intracellular acidification. Therefore, we examined the intracellular pH upon exposure to lactic acid and found a strong intracellular acidification in T cells, where pH dropped almost to 4.5 with 20 mM lactic acid.

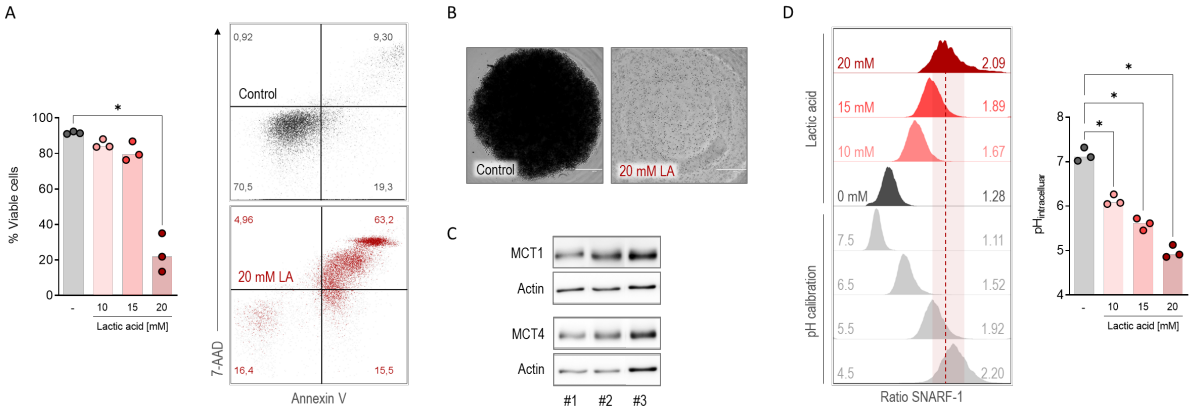

Figure 16. Lactic acid induces intracellular acidification and apoptosis in human T cells. $CD4^+$ T cells were isolated from MNCs of healthy donors, stimulated with αCD3/CD28 beads at a cell-to-bead ratio of 1:1 in the presence of 25 IU/ml IL-2. (A) Viability was assessed after 72 h of lactic acid treatment by Annexin V/7-AAD staining followed by flow cytometric analysis. Viable cells were designated as Annexin V^- 7-AAD^-. This work was conducted by Dr. Sonja Decking. Depicted are representative plots (n = 3) and median values with single data points. Significance was determined using one-way ANOVA and post-hoc Bonferroni multiple comparison test (*$p < 0.05$). (B) The morphology of treated cells was assessed after 48 h and images were acquired using the EVOS system. (C) Expression of MCT1 and MCT4 was analyzed in whole-cell lysates after 48 h by Western blot analysis. Three independent donors are shown. (D) To assess intracellular acidification, T cells were loaded with the pH-sensitive dye SNARF-1 AM and afterwards treated with lactic acid (graduated red colors). To evaluate the pH values, a standard curve was plotted using buffers with a fixed pH (shown in gray). Shown is a representative histogram (n = 3) and median values with single data points. Significance was determined using one-way ANOVA and post-hoc Bonferroni multiple comparison test (*$p < 0.05$). The red dashed line marks the signal peak of cells treated with 20 mM lactic acid.

4.1.2 Macrophages are resistant to lactic acid

Tumor-associated macrophages (TAMs) represent the most abundant immune cell type within tumors and play a central role in tumor progression and metastasis. Myeloid cells such as monocytes have been shown to be impaired in function by lactic acid but, unlike T cells, survive concentrations up to 20 mM lactic acid (36). As professional phagocytes and antigen-presenting cells, the original role of macrophages is first-line pathogen defense. At the site of infection, acidosis is a hallmark of infected tissue (309). Therefore, we investigated whether macrophages have an advantage in withstanding lactic acidosis (Figure 17A,B).

In contrast to T cells, monocyte-derived macrophages survived 20 mM lactic acid exposure like it has been demonstrated for monocytes (36). Interestingly, macrophages constitutively express high levels of lactate transporters MCT1 and MCT4 (Figure 17C), but show less intracellular acidification upon lactic acid exposure compared with T cells (Figure 17D) and maintain a pH between 6.5 and 5.5 upon 20 mM lactic acid, which hints towards a compensatory mechanism.

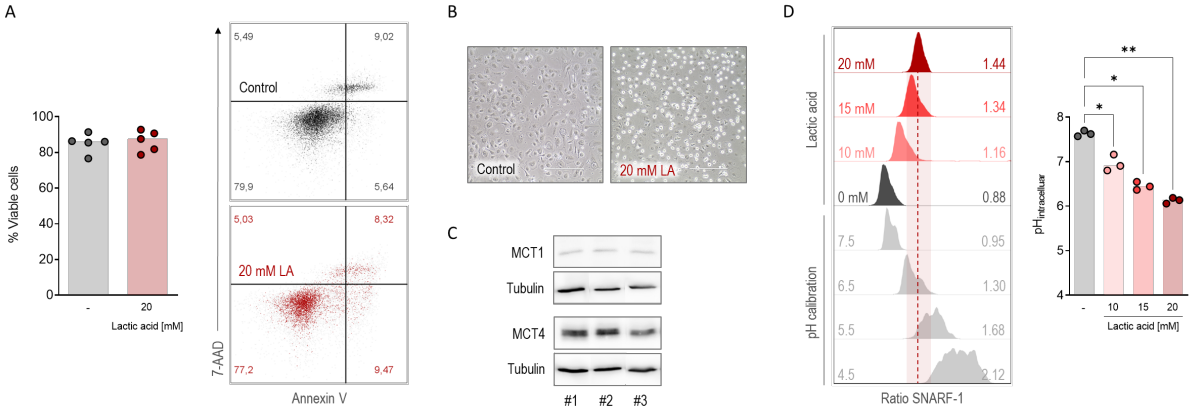

Figure 17. Macrophages survive lactic acidosis and show limited intracellular acidification. Monocyte-derived macrophages were generated as described in Chapter 3.1.4.5. (A) Viability was assessed after 48 h of lactic acid treatment by Annexin V/7-AAD staining followed by flow cytometric analysis. Viable cells were designated as Annexin V^- $7\text{-}AAD^-$. Depicted are representative plots (n = 3) and median values with single data points. (B) The morphology of treated cells was assessed after 48 h and images were acquired using the EVOS system. (C) Expression of MCT1 and MCT4 was analyzed in whole-cell lysates by Western blot analysis. Three independent donors are shown. (D) To assess intracellular acidification, macrophages were loaded with the pH-sensitive dye SNARF-1 AM and afterwards treated with lactic acid (graduated red colors). To evaluate the pH values, a standard curve was plotted using buffers with a fixed pH (shown in gray). Shown is a representative histogram (n = 3) and median values with single data points. Significance was determined using one-way ANOVA and post-hoc Bonferroni multiple comparison test (*$p < 0.05$; **$p < 0.01$). The red dashed line marks the signal peak of cells treated with 20 mM lactic acid.

4.1.3 Granulocytes are resistant to lactic acid

Neutrophil granulocytes display the most abundant leucocyte class in the blood and additionally play a pivotal role in the TME (136). Like macrophages, neutrophils are part of the innate immune system and involved in immunity against invading pathogens. Nevertheless, infiltrating neutrophils were found in many solid tumors and are considered tumor-promoting, although contrary observations have been made (310–312). Neutrophils have comparatively few mitochondria and cover their energy demands mainly by glycolysis (313) and have been shown to express the lactate transporters MCT1 and MCT4 (314). These cells have an incredibly short half-life of about 12.5-19 hours once these cells enter the bloodstream and maximum 5 hours after isolation *in vitro* (315,316). Unlike most other cells, acidic pH has been shown to delay apoptosis and prolong the functional lifespan of neutrophils (317–319). Therefore, we were interested how neutrophils respond to lactic acidosis.

Consistent with the described resistance towards acidic pH, neutrophils survived exposure to 20 mM lactic acid (Figure 18A,B). Interestingly, on the one hand, neutrophils showed similar resistance to lactic

acid as macrophages in terms of survival, but intracellular acidification was more comparable to T cells with a decrease in pH to 5 upon 20 mM lactic acid (Figure 18C). These results suggest that the intracellular pH itself is not harmful to immune cells.

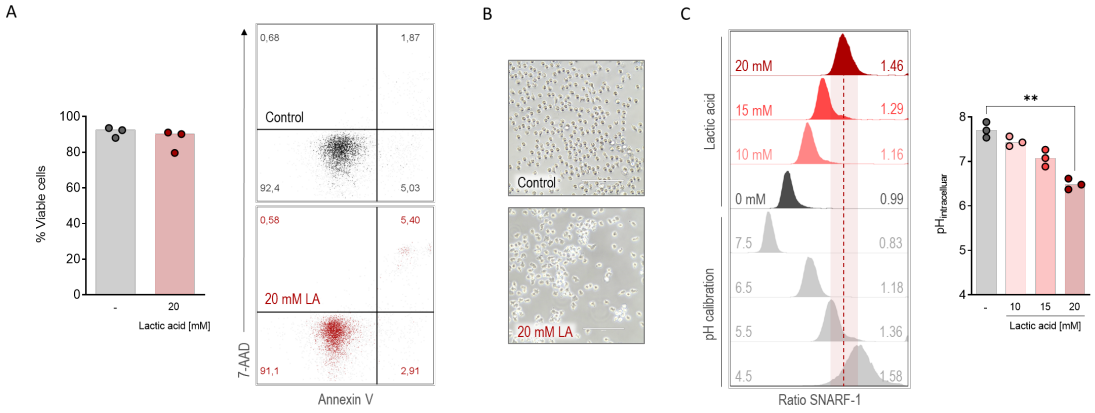

Figure 18. Neutrophils survive lactic acid but show intracellular acidification. Neutrophils were isolated from MNCs of healthy donors and stimulated with fMLP for 5 h. (A) Viability was assessed after 5h of lactic acid treatment by Annexin V/7-AAD staining followed by flow cytometric analysis. Viable cells were designated as Annexin V$^-$7-AAD$^-$. Depicted are representative plots (n = 3) and median values with single data points. (B) The morphology of treated cells was assessed after 48 h of treatment and images were recorded using the EVOS system. (C) To assess intracellular acidification, neutrophils were loaded with the pH-sensitive dye SNARF-1 AM and afterwards treated with lactic acid (graduated red colors). To evaluate the pH values, a standard curve was plotted using buffers with a fixed pH (shown in gray). Shown is a representative histogram (n = 3) and median values with single data points. Significance was determined using one-way ANOVA and post-hoc Bonferroni multiple comparison test (**p < 0.01). The red dashed line marks the signal peak of cells treated with 20 mM lactic acid.

4.2 Impact of MCT inhibition on tumor and immune cells *in vitro*

T lymphocytes are the most potent mediators of adaptive anti-tumor immune response (320). In the TME, T cells are exposed to lactic acidosis, resulting in intracellular acidification followed by cell death, as described above. Although viability of macrophages and neutrophils turned out insensitive to lactic acid, it was proven that lactic acid skews myeloid cells into a tumor-promoting phenotype (36,39,112,121,304,305,319). Therefore, lactic acid is not only a waste product of tumor metabolism, but rather an immunosuppressive and immunoregulatory molecule negatively influencing the anti-tumor immune response. Accordingly, one strategy to improve immunosurveillance might be to avoid tumor-derived lactic acidosis of the TME.

MCT1 and MCT4 are the key tumor-associated lactate transporters. They are overexpressed in most cancer entities and often correlated with worse outcome (275,299,321,322). Therefore, MCTs represent a promising target to prevent lactic acid accumulation in the TME and thereby augment immune cell function (102,111,293,300,302,321,323–327). Multiple compounds have been described to non-specifically inhibit MCTs, but only VB124 (194) and MSC-4381 (293) are the only selective MCT4 inhibitor that can be purchased for research purposes.

Here, we introduce the novel, highly potent MCT4 inhibitor MSC-4381 (MCT4i) provided by Merck within the framework of a collaborative project (293). Co-expression of MCT1 and MCT4 in tumor cells might require the contemporaneous use of both MCT1 and MCT4 inhibitors to sufficiently reduce tumoral lactic acid secretion. Therefore, in addition to MCT4i, we also used AZD3965 as an MCT1 inhibitor.

Importantly, highly proliferating effector T cells, macrophages, and neutrophil granulocytes also rely on glycolysis to meet their energetic needs and express MCT1 and MCT4, as shown previously. This raises the question of the applicability of MCT1 and MCT4 inhibitors in terms of negatively affecting immune cell function. Since only limited data on the effects of single or dual MCT1 and MCT4 inhibition in tumor and immune cells are available, we studied the effect of this treatment on tumor and immune cells.

4.2.1 Reduction of tumor-derived lactic acid by MCT inhibition

First, we wanted to study the efficacy of MCT inhibitors (MCTi) on a human tumor cell line. With the idea of being able to finally test the drugs in an *in vivo* mouse model in case of successful *in vitro* studies, we decided to use the colorectal carcinoma HCT116 (MC38 colorectal model for mouse) for these experiments. To confirm the baseline expression of MCT1 and MCT4 in HCT116 Wildtype (WT) cells, we performed western blot analysis. In addition, MCT expression was examined after 72 h of treatment with MCT1 and MCT4 inhibitor to determine whether their function might be mediated in part by downregulation of MCT1 or MCT4. HCT116 cells express both MCT1 and MCT4, but expression is not regulated by the indicated MCT inhibitors (Figure 19A). It has been demonstrated that appropriate expression and localization of MCT1 and MCT4 in the cell membrane requires co-expression and interaction with CD147 (basigin). Therefore, HCT116 cells were incubated with MCT inhibitory drugs for 24 hours and stained for CD147 expression. Neither MCT1i nor MCT4i affected expression levels of the co-factor CD147 Figure 19B.

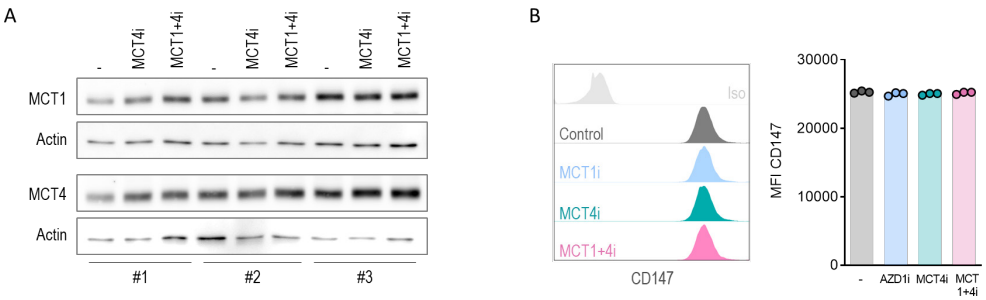

Figure 19. MCT inhibition has no impact on MCT or CD147 protein expression in HCT116 cells. HCT116 Wildtype cells were treated with 0.1 µM MCT1 inhibitor (MCT1i) and MCT4 inhibitor (MCT4i). (A) Expression of MCT1 and MCT4 was analyzed in whole-cell lysates by Western blot analysis after 24 h of treatment. Three independent donors are shown. (B) CD147 expression was determined by flow cytometry after 24 h of treatment. Representative plots and median values with single data points are shown.

Considering MCTs as the major transporters for lactate, we were interested whether MCT inhibitors could decrease tumor-derived lactic acid. HCT116 produced approximately 6 mM lactate within 24 hours (data not shown), but only combined MCT1 and MCT4 inhibition reduced lactate secretion by 50 %, no matter if we used the Astra Zeneca MCT4 inhibitor (AZD4i) or the Merck MCT4 inhibitor (MCT4i). Interestingly, treatment with 0.1 µM MCT4i was almost as effective as 20 times the amount (2 µM), so we decided to continue with 0.1 µM. In accordance with the co-expression of MCT1 and MCT4, targeting one of the MCT transporters alone had no effect (Figure 20A). Efficacy of treatment with MCT1i and MCT4i was confirmed using several tumor cell lines expressing both MCT1 and MCT4 lactate transporters, such as Mel285 (human melanoma), MC38 (murine colorectalcarcinoma), and B16 (murine melanoma), and resulted in a distinct reduction of tumor-induced lactate secretion when treated with both inhibitors (data not shown).

Regarding the role of acidic pH in inhibitory lactic acid effects on T cells, controversial views can be found in the literature. While a few authors reported suppression of T cells by sodium lactate (113,122), most other authors demonstrated that only lactic acid, which is associated with an acidification, impaired T cell function (35,301,328). Tumor cells maintain their glycolytic flux by exporting lactate in co-transport with protons via MCT1 and MCT4, resulting in extracellular acidification. Indeed, HCT116 showed a strong acidification with a pH decreasing from 7.35 to 6.6 within 48 hours, which was prevented with dual MCT1 and MCT4 inhibition (Figure 20B). Monitoring of oxygen concentration revealed that HCT116 cells not only relied on glycolysis but also consumed oxygen (Figure 20C). Nevertheless, inhibition of MCT showed no effect on the respiration of HCT116 cells.

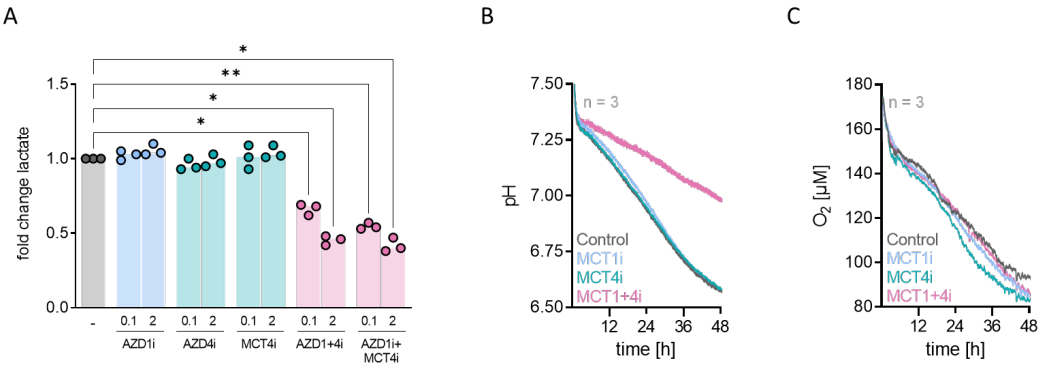

Figure 20. Dual MCT1 and 4 inhibition lowers lactate accumulation and acidification. HCT116 Wildtype cells were treated with 0.1 µM (A,B,C) or 2 µM (A) MCT inhibitors from Astra Zeneca (MCT1 inhibitor = AZD1i and MCT4 inhibitor = AZD4i) and Merck (MCT4 inhibitor = MCT4i). (A) Lactate concentrations in culture supernatants were measured after 48 h. Depicted are median values and single data points. Significance was determined using one-way ANOVA and post-hoc Bonferroni multiple comparison test (*p < 0.05; **p < 0.01). (B) Extracellular pH was monitored over time using the PreSens technology. (C) Cellular respiration was monitored over time using the PreSens technology. (B,C) Shown are median values (n = 3).

Glucose metabolism is crucial for highly proliferating cells. Targeting MCT1 and MCT4 in tumor cells diminished lactate efflux in HCT116 tumor cells, which might promote intracellular lactate accumulation and acidification, thereby negatively affecting tumor cell growth. Indeed, combined MCT1 and MCT4 blockade reduced HCT116 cell proliferation to 60 % after 72 h (Figure 21A). However, viability of HCT116 cells was not affected by any MCT inhibitory drug (Figure 21B,C).

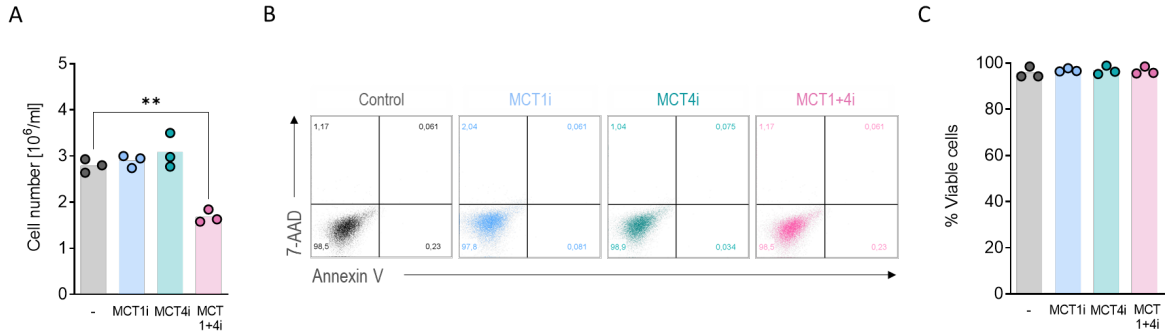

Figure 21. Only limited direct anti-cancer effect by MCT1 and MCT4 inhibition. HCT116 Wildtype cells were treated with 0.1 µM MCT1 inhibitor (MCT1i) and MCT4 inhibitor (MCT4i). (A) Cell number was analyzed after 72 h using the CASY system. Depicted are median values and single data points. Significance was determined using one-way ANOVA and post-hoc Bonferroni multiple comparison test (**$p < 0.01$). (B,C) Viability was assessed after 72 h by Annexin V/7-AAD staining followed by flow cytometric analysis. Viable cells were designated as Annexin V^- 7-AAD^-. Representative plots (A) and median values with single data points (C) are shown.

Taken together, in tumor cells expressing MCT1 and MCT4, dual MCT inhibition is required to sufficiently reduce lactate secretion *in vitro*. However, only modest direct anti-tumor effects were observed with respect to tumor cell proliferation and viability.

4.2.2 Preserved T cell effector functions upon MCT inhibition

MCT inhibitors are considered not only as anti-tumor agents but also as immunotherapeutic approach by preventing lactic acidosis of the TME. However, the adverse effects of such anti-metabolic drugs on T cells need to be carefully investigated. Upon activation, T cells undergo metabolic reprogramming towards aerobic glycolysis and upregulate expression of MCT1 and MCT4 (Figure 16C). In addition, the antiglycolytic agent 2-deoxyglucose is known to impair T cell effector functions when applied in high concentrations (329,330). Therefore, MCT inhibition might negatively affect T cell function. To assess this, bulk $CD3^+$ and $CD8^+$ T cells were investigated regarding the impact of MCT1 and MCT4 blockade on MCT and CD147 expression, lactate levels, proliferation, apoptosis, and effector functions.

In contrast to tumor cells, combined MCT1i and MCT4i decreased expression of MCT1 but not MCT4 in $CD8^+$ T cells (Figure 22A,C). CD147 (basigin), the co-factor of MCT1 and MCT4, mediates trafficking of MCT1 and MCT4 to the plasma membrane (83,327,331). Consistent with the kinetics of MCT expression after stimulation, quiescent T cells did not express CD147, the known MCT chaperone, but expression was induced upon stimulation. Similar to MCT expression levels, surface expression of

CD147 was decreased upon combined MCT1 and MCT4 restriction in bulk CD3⁺ and CD8⁺ T cells (Figure 22B,C).

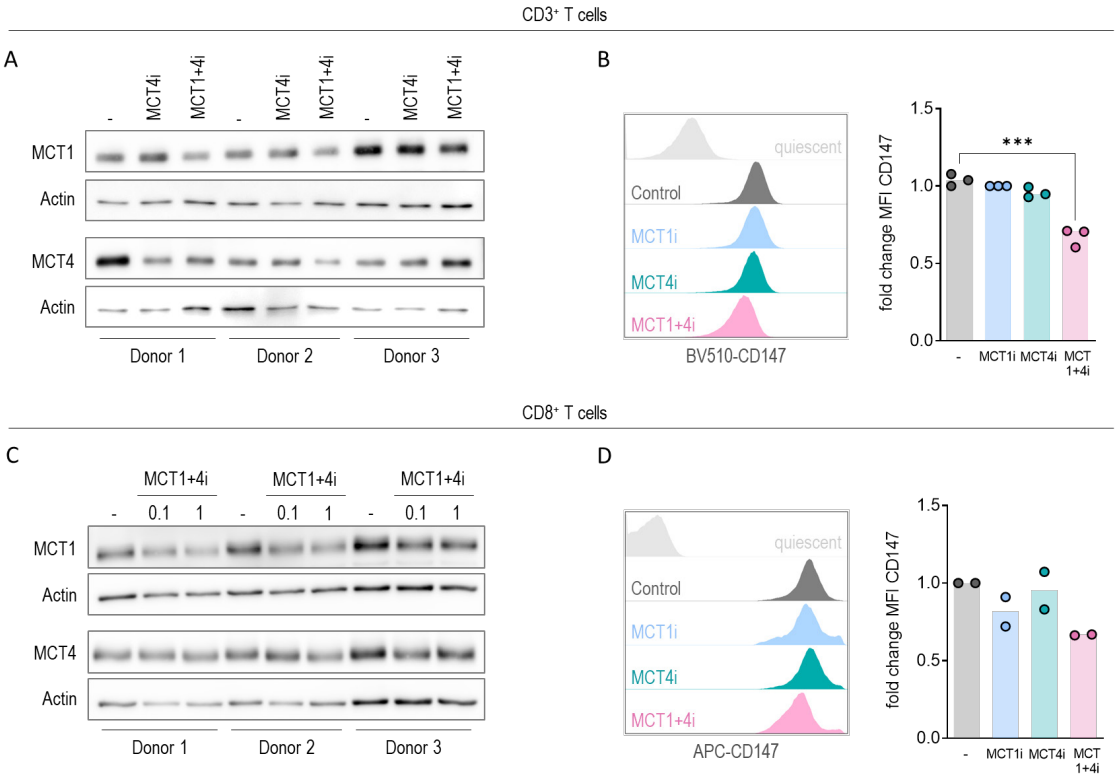

Figure 22. CD147 expression is downregulated by inhibition of MCT1 and MCT4 in human T cells. CD3⁺ (A,B) or CD8⁺ (C,D) T cells were isolated from MNCs of healthy donors, stimulated with αCD3/CD28 beads at a cell-to-bead ratio of 1:1 in the presence of 25 IU/ml IL-2 and treated with 0.1 µM MCT1 inhibitor (MCT1i) and/or MCT4 inhibitor (MCT4i). (A,C) Expression of MCT1 and MCT4 was analyzed in whole-cell lysates by Western blot analysis after 48 h (A) or 72 h (C). Three independent donors are shown. (B,D) CD147 expression was determined by flow cytometry after 48 h. Representative plots and median values with single data points are shown. Significance was determined using one-way ANOVA and post-hoc Bonferroni multiple comparison test (***$p < 0.001$).

T cells become glycolytic upon stimulation. CD3⁺ and CD8⁺ T cells produced lactate levels of 4 to 7 mM within 48 h (data not shown). In line with the MCT expression, MCT1 and MCT4 inhibitor treatment reduced lactate secretion in stimulated CD8⁺ and CD3⁺ T cells. According to MCT expression kinetics with delay of MCT4 (302), single MCT1i treatment lowered the lactate efflux of 48 h stimulated T cells, whereas single MCT4i had no effect (Figure 23A,D). Lactate efflux via MCTs is linked to proton efflux. Corresponding to lactate secretion, extracellular pH was increased when MCT1i was used alone and even more so in combination with MCT4i in CD3⁺ and CD8⁺ T cells (Figure 23B,E). However, combined targeting of MCT1 and MCT4 blocked respiration in CD3⁺ T cells, whereas the effect was much weaker in CD8⁺ T cells (Figure 23C,F).

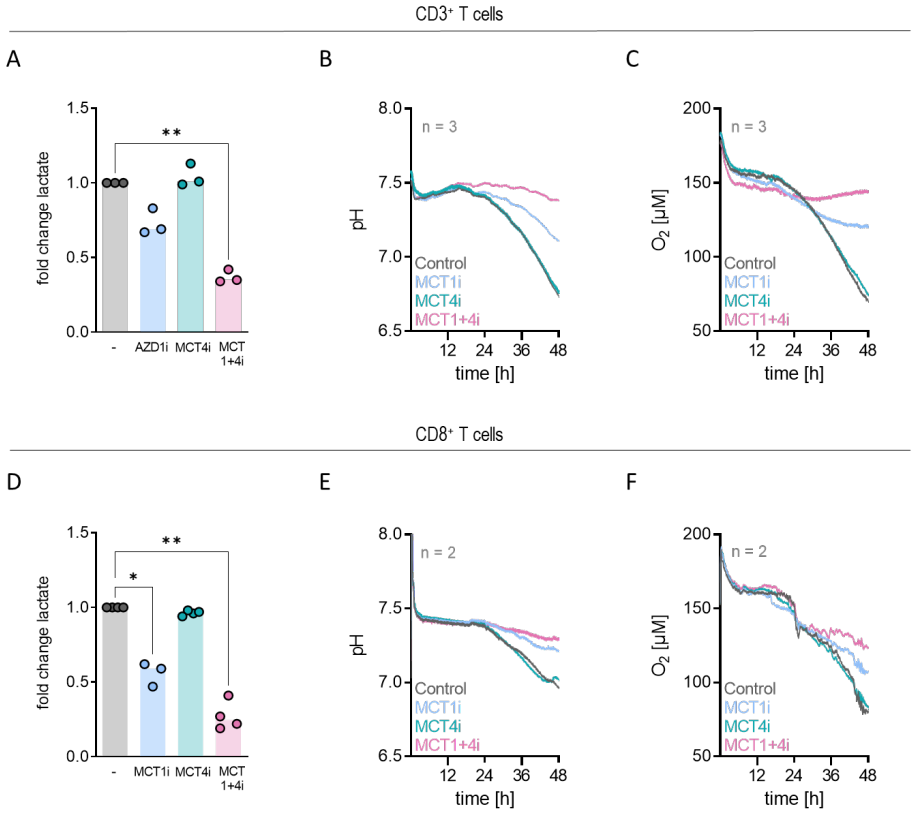

Figure 23. Dual MCT1 and 4 inhibition lowers lactate accumulation and acidification of human T cells. $CD3^+$ (A-C) or $CD8^+$ (D-F) T cells were isolated from MNCs of healthy donors, stimulated with αCD3/CD28 beads at a cell-to-bead ratio of 1:1 in the presence of 25 IU/ml IL-2 and treated with 0.1 µM MCT1 inhibitor (MCT1i) and/or MCT4 inhibitor (MCT4i). (A,D) Lactate concentration was measured after 48 h in culture supernatants. Depicted are median values and single data points. Significance was determined using one-way ANOVA and post-hoc Bonferroni multiple comparison test (*$p < 0.05$; **$p < 0.01$). (B,E) Extracellular pH was monitored over time using the PreSens technology. (C,F) Cellular respiration was monitored over time using the PreSens technology. (B,C,E,F) Shown are median values (B,C: n = 3; D,F: n = 2).

After activation, T cells start to produce cytokines, followed by clonal expansion. Only combined MCT1 and MCT4 inhibition reduced $CD3^+$ and $CD8^+$ T cell proliferation (Figure 24A,D). However, viability of $CD3^+$ and $CD8^+$ T cells was not affected by the anti-glycolytic treatment (Figure 24B,C,E,F).

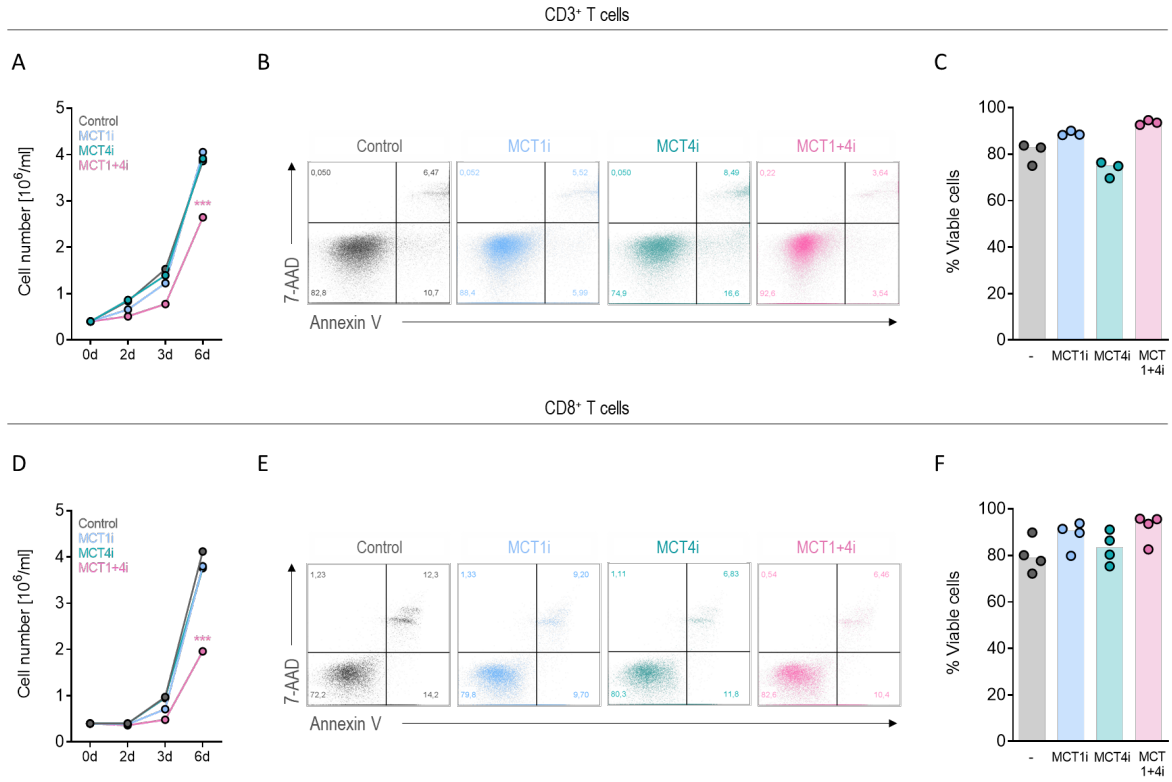

Figure 24. T cell viability is preserved upon MCT1 and MCT4 inhibition. $CD3^+$ (A-C) or $CD8^+$ (D-F) T cells were isolated from MNCs of healthy donors, stimulated with αCD3/CD28 beads at a cell-to-bead ratio of 1:1 in the presence of 25 IU/ml IL-2 and treated with 0.1 µM MCT1 inhibitor (MCT1i) and/or MCT4 inhibitor (MCT4i). (A,D) Cell number was analyzed after 2 d, 3 d and 6 d using the CASY system. Depicted are median values and (A: n = 3; D: n = 4). Significance was determined using two-way ANOVA and post-hoc Bonferroni multiple comparison test (***$p < 0.001$) referring to control. (B,C) Viability was assessed after 72 h by Annexin V/7-AAD staining followed by flow cytometric analysis. Viable cells were designated as Annexin V^- 7-AAD^-. Representative plots (B,E) and median values with single data points (C,F) are shown (B,C: n = 3; D,F: n = 4).

With regard to MCT inhibitors as anti-tumor immune boosting drug, the aim would be to efficiently target lactic acid efflux but preserve the T cell effector functions.

Therefore, we analyzed T cell related activation markers such as CD25, CD137 and CD69. CD25 is the alpha chain of the IL-2 receptor, CD137 is part of the TNF receptor family providing co-stimulatory signals required for T cell activation and CD69 an early activation marker involved in lymphocyte proliferating and perform signal-transmission. Whereas CD137, CD25 and CD69 were not found in quiescent $CD3^+$ and $CD8^+$ T cells, they were upregulated after stimulation. MCT inhibition did not affect activation marker expression in $CD3^+$ or $CD8^+$ T cells (Figure 25A-E). More importantly, interferon γ (IFNγ) production was maintained upon MCT1i and MCT4i treatment (Figure 25C,F).

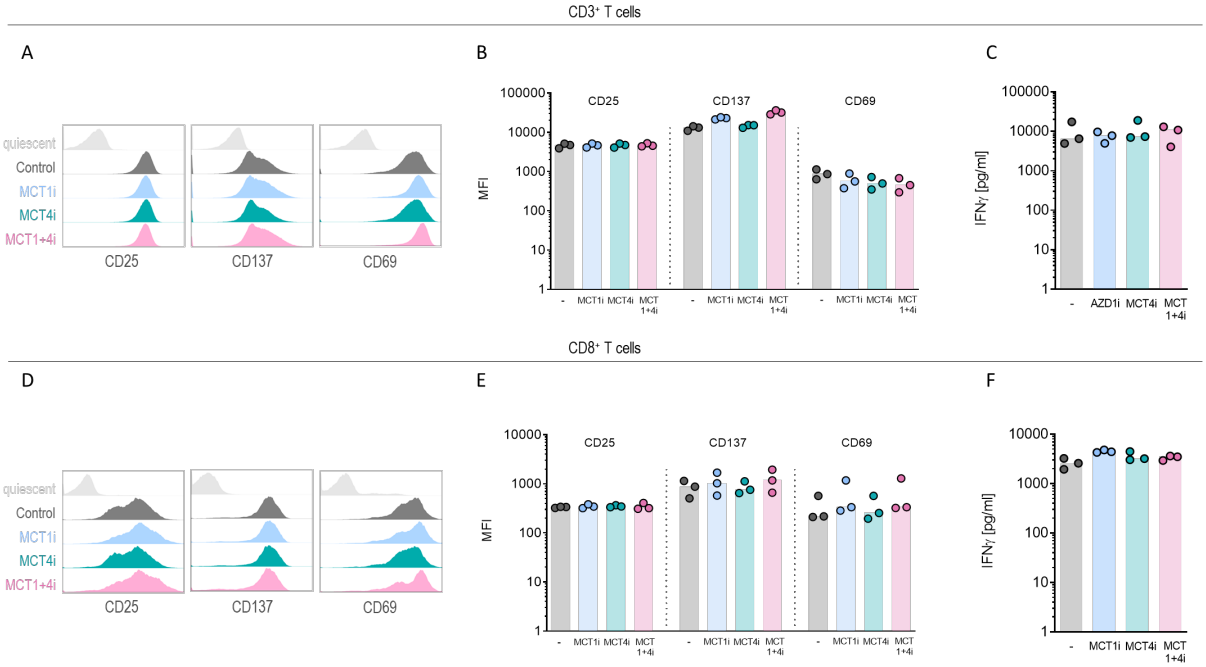

Figure 25. T cell effector functions are not affected by MCT 1 and MCT4 inhibition. $CD3^+$ (A-C) or $CD8^+$ (D-F) T cells were isolated from MNCs of healthy donors, stimulated with αCD3/CD28 beads at a cell-to-bead ratio of 1:1 in the presence of 25 IU/ml IL-2 and treated with 0.1 µM MCT1 inhibitor (MCT1i) and/or MCT4 inhibitor (MCT4i). (A-D) Activation marker CD25, CD137 and CD69 expression were determined by flow cytometry after 48 h. Representative plots (A,D) and median values with single data points are shown. (C,F) Cytokine levels in culture supernatants were measured by ELISA.

In summary, MCT1 and MCT4 inhibition impairs metabolism and proliferation of bulk $CD3^+$ and $CD8^+$ T cells but does not affect effector functions.

4.2.3 Immunocompetent phenotype of macrophages upon MCT inhibition

Macrophages express lactate transporters MCT1 and high levels of MCT4 even without activation (Figure 17C). When classically stimulated with LPS, glycolysis is triggered via the Toll-like receptor 4 TLR4. Besides tumor cells, macrophages also contribute to lactate acidosis of TME. In addition, it has been estimated that 80 % of studies linking tumor-associated macrophage (TAM) density to prognosis in any type of cancer have found a negative correlation, whereas less than 10 % have found a positive correlation (137,332,333). By blocking MCT1 and MCT4, we therefore might target not only tumor cells but also tumor-resident macrophages.

However, TAMs are not a homogeneous population but are composed of multiple subpopulations whose characteristics overlap depending on their environment. Thus, we differentiated monocytes to macrophages by adding human serum for 7 d, followed by stimulation with LPS to induce a mixed-phenotype. We examined the impact of MCT1 and MCT4 inhibition on MCT and CD147 expression, metabolism, viability and functional properties of monocyte-derived macrophages.

Neither MCT1 and MCT4 nor CD147 expression were influenced by MCT1 and MCT4 inhibition (Figure 26A,B). From previous work by our group using diclofenac as an MCT inhibitor, we knew that macrophages are more resistant than most other cells to MCT-inhibiting drugs. Thus, we also applied 200-fold concentration of MCT1i and MCT4i, but still could not detect any expression changes.

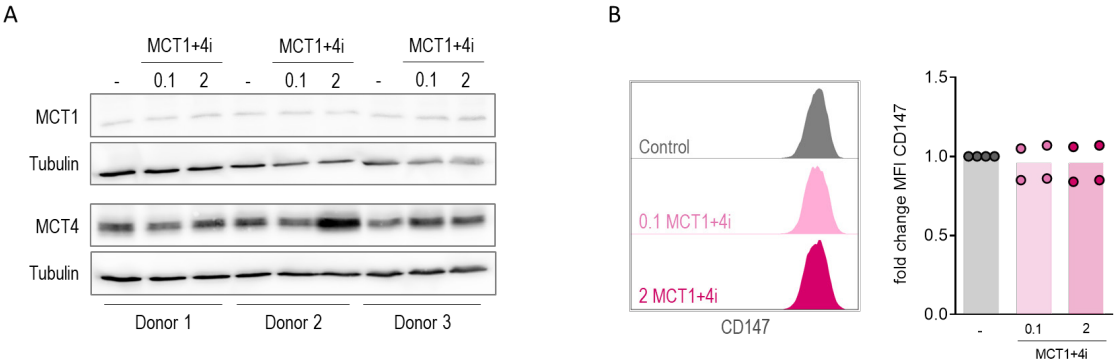

Figure 26. MCT inhibition has no impact on MCT or CD147 protein expression of human macrophages. Monocyte-derived macrophages were generated as described in Chapter 3.1.4.5, stimulated with 100 ng/ml LPS and treated with 0.1 µM MCT1 inhibitor (MCT1i) and/or MCT4 inhibitor (MCT4i). (A) Expression of MCT1 and MCT4 was analyzed in whole-cell lysates by Western blot analysis after 24 h. Three independent donors are shown. (B) CD147 expression was determined by flow cytometry after 48 h. Representative plots and median values with single data points are shown.

Consistent with our previous findings using diclofenac, lactate secretion was reduced by combined treatment with MCT1i and MCT4i, but only to about 70 % of the untreated control (Figure 27A). Inhibition of MCT1 or MCT4 alone showed no effect. Corresponding to lactate reduction, extracellular pH was increased upon combined MCT inhibition (Figure 27B). MCT1 and MCT4 blockade had no clear effect on macrophage respiration (Figure 27C).

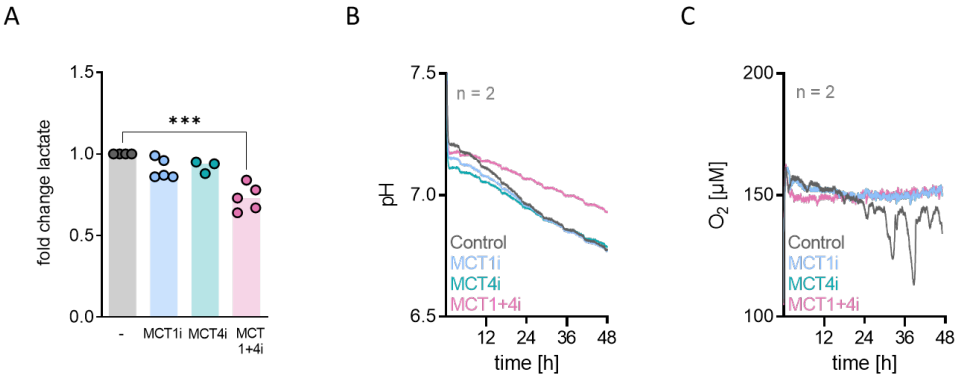

Figure 27. Dual MCT1 and MCT4 inhibition lowers lactate secretion of human macrophages. Monocyte-derived macrophages were generated as described in Chapter 3.1.4.5, stimulated with 100 ng/ml LPS and treated with 0.1 µM MCT1 inhibitor (MCT1i) and/or MCT4 inhibitor (MCT4i). (A) Lactate concentrations were measured after 48 h in culture supernatants. Depicted are median values and single data points. Significance was determined using one-way ANOVA and post-hoc Bonferroni multiple comparison test (***p < 0.001). (B) Extracellular pH was monitored over time using the PreSens technology. (C) Cellular respiration was monitored over time using the PreSens technology. (B,C) Shown are median values (n = 2).

MCT inhibition did not induce apoptosis in tumor cells or T cells. Likewise, viability of macrophages was not altered upon MCT1 and MCT4 inhibition even when applying a high concentration of 2 µM (Figure 28).

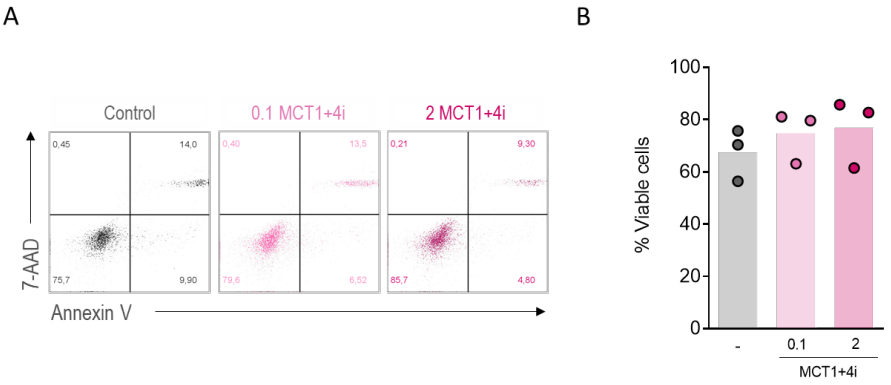

Figure 28. Viability of human macrophages is not affected by MCT1 and MCT4 inhibition. Monocyte-derived macrophages were generated as described in Chapter 3.1.4.5, stimulated with 100 ng/ml LPS and treated with 0.1 µM MCT1 inhibitor (MCT1i) and/or MCT4 inhibitor (MCT4i). (B) Viability was assessed after 72 h by Annexin V/7-AAD staining followed by flow cytometric analysis. Viable cells were designated as Annexin V^- $7\text{-}AAD^-$. Representative plots (A) and median values with single data points (B) are shown.

Macrophages seem to have an innate resistance to lactic acid as they also survive high concentrations up to 20 mM. Moreover, macrophages exhibit a high plasticity and are able to change their phenotype from pro-inflammatory to anti-inflammatory, but also from tumor-promoting to tumor-suppressive. Thereby, they change their cytokine patterns and surface marker expression in response to the environment (334). As also lactic acid has been shown to act as a signaling molecule on macrophages, leading to functional polarization to tumor-promoting state (38,39), we were interested whether targeting lactate metabolism in macrophages could be a way to regulate macrophage polarization.

IL-6 secretion has been associated with TAM frequency and poor prognosis in patients with non-small cell lung cancer (69), colorectal cancer (70), and renal cell carcinoma (Figure 70D). Strikingly, we found a strong decrease in IL-6 secretion (Figure 29A) upon MCT inhibition. TNF levels tended to be slightly reduced (Figure 29B). With regards to the effects on reactive oxygen (ROS) production, no clear trend was evident (Figure 27C). Furthermore, we investigated expression of molecules involved in the regulation of T cell immunity, such as programmed cell death ligand 1 (PD-L1) and major histocompatibility complex class II (MHC-II/HLA-DR). While PD-L1 mediates suppression of T cells as an immune checkpoint, MHC-II is responsible for antigen-presentation and boosters CD4 T cell response. Interestingly, treatment with MCT1 and MCT4 resulted in a decreased PD-L1 expression and an upregulation of MHC-II expression in macrophages (Figure 27D,E).

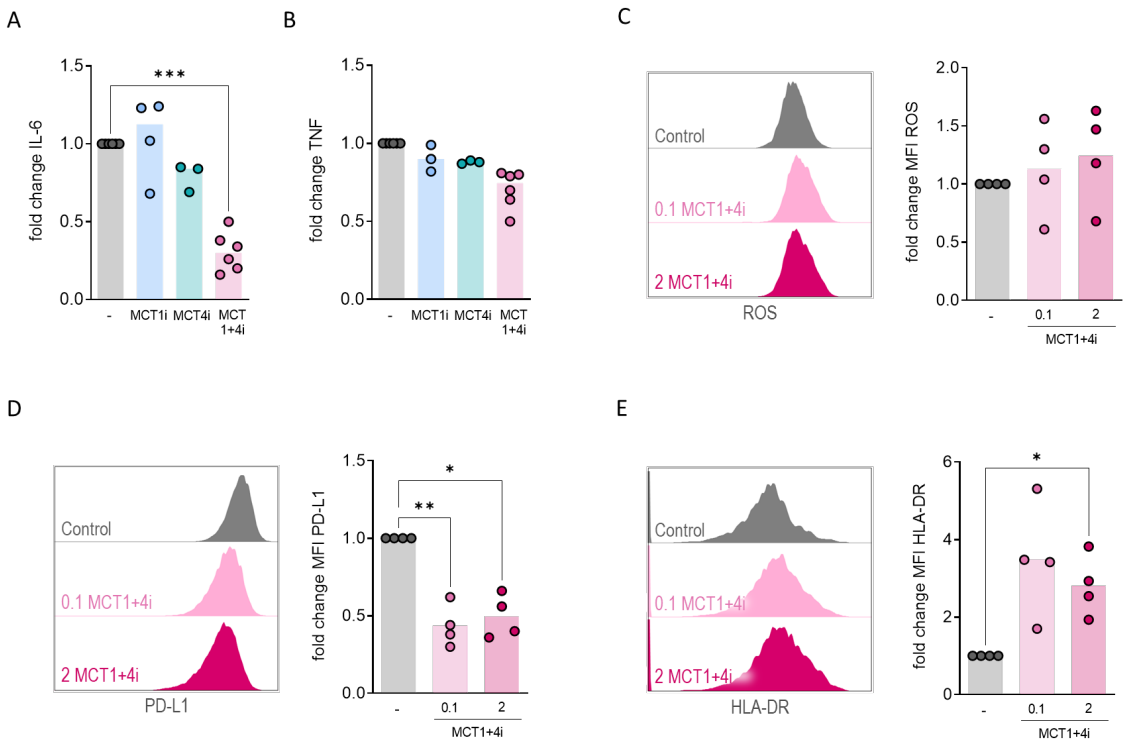

Figure 29. MCT1 and MCT4 inhibition skews human macrophages into an immunocompetent phenotype. Monocyte-derived macrophages were generated as described in Chapter 3.1.4.5, stimulated with 100 ng/ml LPS and treated with 0.1 µM MCT1 inhibitor (MCT1i) and/or MCT4 inhibitor (MCT4i). (A, B) Cytokine levels in culture supernatants were measured by ELISA. Median values with single data points are shown. (C) Reactive oxygen species (ROS) was determined by DCFDA staining, followed by flow cytometric analysis. (D,E) PD-L1 (D) and HLA-DR (E) expression were determined by flow cytometry after 48 h. Representative plots and median values with single data points are shown. Significance was determined using one-way ANOVA and post-hoc Bonferroni multiple comparison test (*p < 0.05; **p < 0.01; ***p < 0.001).

In brief, combination of MCT1 and MCT4 showed a limited decrease of lactate efflux in human macrophages but induced a favorable phenotype with low IL-6 secretion, attenuated PD-L1, and enhanced MHC-II expression.

4.2.4 No impact on granulocytes by MCT inhibition

In tumor immunology research, neutrophils are often overlooked because they are terminally differentiated, non-proliferative and short-lived. However, neutrophils are abundant in many tumors. It has been reported that depending on polarization, pro-tumoral N2-like or anti-tumoral N1-like tumor-associated neutrophils (TANs) can affect T cell subsets (310–312). Neutrophils contain few mitochondria and cover their energetic demands primarily through glycolysis (313). Furthermore, neutrophils are considered to express MCT1 and MCT4 (314). However, to our knowledge, nothing is known about the effects of targeting glycolysis in neutrophils. Due to the short lifetime of maximum 6h after isolation, experiments with neutrophils were limited. Yet, we analyzed viability, surface marker expression and ROS production upon MCT1 and MCT4 blockade and found that treatment with MCT1 and MCT4 did not induce apoptosis in human granulocytes (Figure 30).

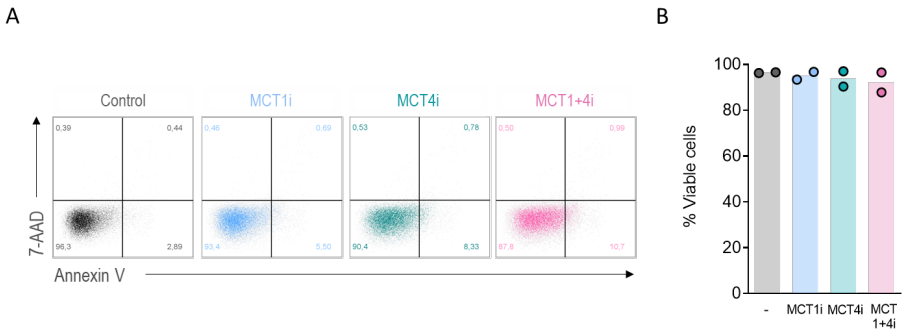

Figure 30. Viability of human granulocytes is not affected by MCT1 and MCT4 inhibition. Granulocytes were freshly isolated from peripheral blood of healthy donors, stimulated with 10 µg/ml fMLP and treated with 0.1 µM Astra Zeneca MCT1 inhibitor (MCT1i) and/or Astra Zeneca MCT4 inhibitor (MCT4i). (B) Viability was assessed after 5 h by Annexin V/7-AAD staining followed by flow cytometric analysis. Viable cells were designated as Annexin V^- $7\text{-}AAD^-$. Representative plots (A) and median values with single data points (B) are shown.

Neutrophils are supposed to be involved in tumor metastasis formation. Once in blood circulation, tumor cells bind to neutrophil CD11b via ICAM-1 and utilize them as a protective shield from immune surveillance. Furthermore, it was shown that binding of neutrophils to tumor cells leads to activation of cellular migration pathways and tumor cell extravasation from the circulating system into a new metastatic tissue bed (146,147).

More precisely, CD66b and CD11b are adhesion molecules, stored in granules and expressed on the surface upon neutrophil activation and degranulation. CD62 (L-selectin) is also an adhesion molecule and mediates the rolling of neutrophils along vascular endothelium. Interestingly, stimulation of neutrophils *in vitro* induces shedding of CD62L, leading to a decreased expression on the surface (148). CD35 (complement receptor type 1), which physiologically mediates the binding and phagocytosis of C3b-coated particles and immune complexes, is moreover considered as an activation marker of neutrophils. However, MCT inhibition did not alter expression of CD66b, CD11b, CD35 or CD62L or ROS production by neutrophils (Figure 31A-E).

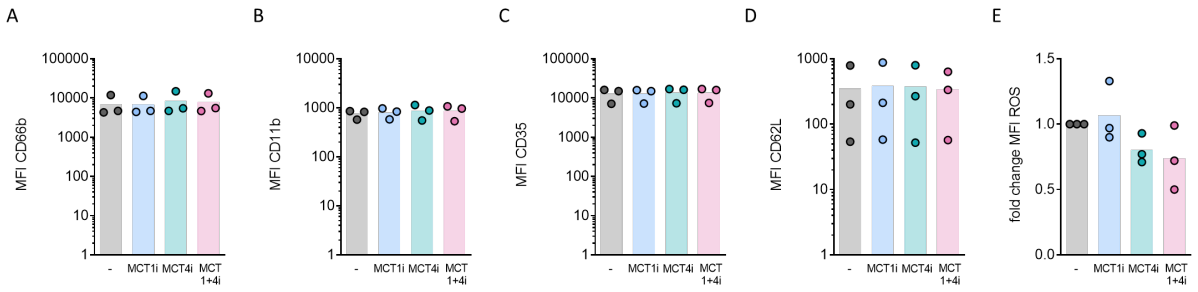

Figure 31. MCT1 and MCT4 inhibition does not affect surface marker expression of human granulocytes. Granulocytes were freshly isolated from peripheral blood of healthy donors, stimulated with 10 µg/ml fMLP and treated with 0.1 µM Astra Zeneca MCT1 inhibitor (MCT1i) and/or Astra Zeneca MCT4 inhibitor (MCT4i). (A-D) CD66b, CD11b, CD35 and CD62L were determined by flow cytometry. (F) Reactive oxygen species (ROS) was determined by DCFDA staining, followed by flow cytometric analysis. Median values with single data points are shown.

Overall, MCT1 and MCT4 inhibitor treatment did not affect neutrophil granulocytes in terms of viability, surface marker expression or ROS production.

Anti-glycolytic inhibition with specific MCT1 and MCT4 inhibitors decreased lactate secretion and extracellular acidification by tumor cells, T cells, and macrophages. Although proliferation of tumor cells and T cells was reduced by dual MCT1 and MCT4 blockade, viability of all cell types studied was not affected. Remarkable, interferon γ production by T cells was preserved, whereas IL-6 expression by macrophages was impaired by MCT blockade. In conclusion, analysis of the effects of lactic acid on immune cells revealed severe immunosuppressive effects and MCT inhibition proved to be a promising strategy to reduce tumor-induced lactic acidosis, did not affect T cell function, and showed positive effects on macrophage phenotype.

4.3 The immunomodulatory role of MCT inhibitors in colorectal carcinoma

The Warburg phenotype is a major feature of tumor cells and is characterized by increased glycolysis. The resulting lactic acidosis of the TME has a detrimental effect on immune cell function and survival (35,36,38,39,112,301,302,305,335). Therefore, genes and proteins related to glycolysis have been implicated as prognostic markers for many cancers (301,302). Colorectal cancer (CRC) is the third most common cancer and even ranks second in mortality according to GLOBCAN (1). Several studies investigated the prognostic value of single proteins related to glycolysis, but the results for CRC were inconsistent (336,337). Offermans et al. recently demonstrated that Warburg subtypes are associated with potentially important differences in CRC survival by analyzing the expression of six proteins associated with the increased glycolytic flux, including MCT4, using immunohistochemistry on tissue microarrays (338). Moreover, others have found a correlation between MCT4 expression and survival of CRC patients (77–79).

Current treatment strategies for CRC are limited. Immune checkpoint blockade (ICB) therapies such as anti-programmed cell death ligand 1 (aPD-L1) have been shown to be effective in various cancers, while preclinical and clinical data for CRC are rare. Immunotherapy for CRC patients is restricted to a specific subset of tumors with mismatch repair deficit (MMRd)/microsatellite instability (MSI). However, the response rate is low (195). Resistance to ICB might be mediated by high tumor glycolysis leading to an immunosuppressive TME. Therefore, investigating combination therapies of MCT inhibitors, attenuating the Warburg effect of tumors, with ICB could help to overcome immunotherapy resistance.

Consequently, we investigated the immunomodulatory roles of AZD3965 MCT1 inhibitor (MCT1i) and MSC-4381 MCT4 inhibitor (MCT4i) in combination with aPD-L1 immune checkpoint blockade *in vitro* and *in vivo*. First, we established a human CRC HCT116 tumor spheroid model to study the infiltration and function of immune cells. We then attempted to transfer the effects seen in human *in vitro* models to a mouse model. For this, we used CRC MC38 cancer tumor spheroids cultured with immune cells, and finally tested the effects of MCT inhibitors and aPD-L1 *in vivo* in C57BL/6 mice with MC38 tumors.

4.3.1 Immunomodulatory role of MCT inhibitors in human colorectal cancer *in vitro*

In vitro models reflecting the complexity of the interaction between tumors cells, the TME and immune cells and are limited. Here, we present a model to study the impact of drugs on tumor-immune cell crosstalk: Co-cultures of tumor spheroids with activated immune cells. 3D tumor spheroids are like

avascular tumor metastases. In contrast to 2D cell culture, spheroids mimic the characteristic features of solid tumors such as spatial architectures with extracellular matrix, establishment of a TME with various soluble mediators such as metabolites, cytokines and chemokines, gene expression patterns, and gradients of hypoxia, nutrients and lactate. Tumor spheroids provide fundamental hallmarks to better understand the effects the effects of immunomodulatory anti-metabolic drugs (339).

4.3.1.1 MCT4 inhibition augments ICB in a HCT116 spheroid co-culture model

To study MCT1 and MCT4 inhibition in a CRC spheroid model, we used HCT116 cells. HCT116 cells form robust tumor spheroids. We tested the effects of MCT1 and MCT4 inhibition in combination with immune checkpoint blockade using aPD-L1 antibodies or a mutated isotype control.

4.3.1.1.1 HCT116 monolayer vs spheroid

2D cell cultures and 3D tumor spheroids may differ profoundly in gene expression (340). In particular, metabolic-related genes may be altered due to factors such as oxygen availability or nutrient restriction. Therefore, we first examined the metabolic differences of HCT116 monolayers in terms of MCT and CD147 expression. Indeed, MCT4 was markedly upregulated in HCT116 spheroids compared to HCT116 monolayers (Figure 32A). The increase of MCT1 in HCT116 spheroids relative to the 2D culture was only moderate. Interestingly, although HCT116 spheroids had more MCT4, the co-factor CD147 tended to be slightly reduced (Figure 32B). HCT116 spheroids were found to be highly glycolytic and produced up to 20 mM lactate within 9 d. However, the most striking difference between monolayer (Figure 20A) and spheroid was that lactate efflux was already reduced by a single MCT4 inhibitor to the same level as when combined with an MCT1 inhibitor (Figure 32C).

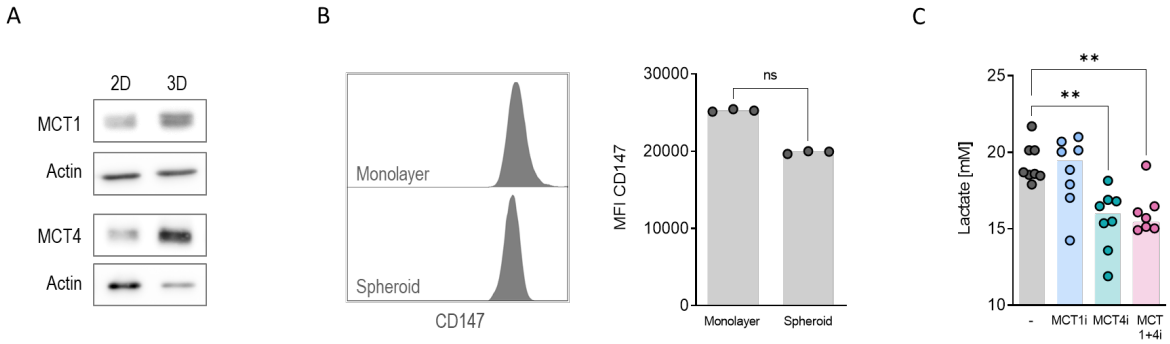

Figure 32. Single MCT4 inhibition decreases lactate secretion of HCT116 spheroids due to MCT4 upregulation. HCT116 were either cultured as monolayer or spheroids. HCT116 monolayers were treated for 24 h and spheroids for 9 d with 0.1 µM MCT1 inhibitor (MCT1i) and/or MCT4 inhibitor (MCT4i). (A) Expression of MCT1 and MCT4 was analyzed in whole-cell lysates of HCT116 monolayers (2D) or HCT116 spheroids (3D) by Western blot analysis. One representative plot out of three independent experiments is shown. (B) CD147 expression was determined by flow cytometry. Representative plots and median values with single data points are shown. (C) Lactate concentrations were measured after 9 d in HCT116 spheroid culture supernatants. Depicted are median values and single data points. Significance was determined using one-way ANOVA and post-hoc Bonferroni multiple comparison test (**$p < 0.01$).

Besides increased MCT4 expression, one more difference between HCT116 monolayers and spheroids is the growth behavior. In terms of oxygen and nutrient availability, spheroids consist of three zones, namely a necrotic core, a hypoxic or quiescent middle zone, and a proliferating rim. However, treatment with MCT1 and MCT4 inhibitors did not result in decreased viability of HCT116 spheroids, changes in size, or disrupted morphology (Figure 33).

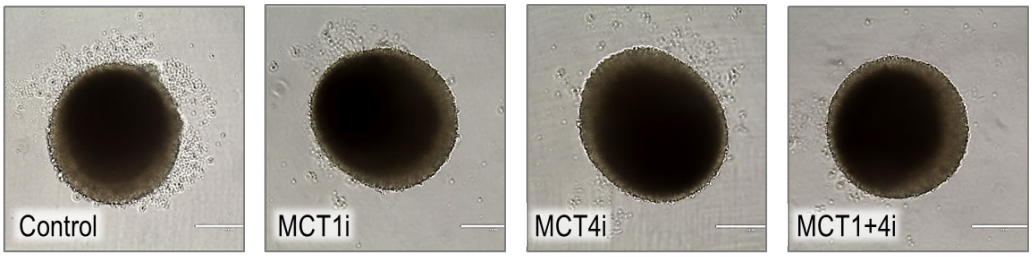

Figure 33. Morphology of HCT116 spheroids is not affected by MCT inhibition. HCT116 cells were either cultured as spheroids. HCT116 spheroids for 9 d with 0.1 µM MCT1 inhibitor (MCT1i) and/or MCT4 inhibitor (MCT4i). The morphology of treated spheroids was assessed after 9 d of treatment and images were recorded using the EVOS system.

In addition to lactic acid, several other factors are involved in immune suppression by tumors. One important mechanism by which tumors escape the immune system is the expression of immune checkpoint ligands such as PD-L1, which binds to the immune checkpoint programmed cell death protein 1 (PD-1) on T cells, thereby limiting the T cell response against the tumor. We detected high PD-L1 expression levels on HCT116 monolayers and spheroids (Figure 34). Therefore, our emphasis has not only been on targeting glycolysis, but also on combining anti-glycolytic treatment with immunotherapy.

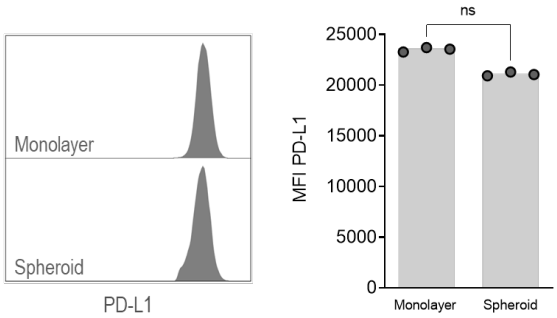

Figure 34. HCT116 tumor cells express high levels of PD-L1. HCT116 were either cultured as monolayer or spheroids. HCT116 monolayers were treated for 24 h and spheroids for 9 d with 0.1 µM MCT1 inhibitor (MCT1i) and/or MCT4 inhibitor (MCT4i). Programmed cell death ligand (PD-L1) expression was determined by flow cytometry. Representative plots and median values with single data points are shown.

Hence, a higher MCT4 to MCT1 ratio in HCT116 spheroids compared to monolayers leads an efficient decrease in lactate secretion by single MCT4 inhibitor treatment. Combination with checkpoint blockade inhibitors is reasonable due to a high PD-L1 expression in HCT116 monolayers and spheroids.

4.3.1.1.2 Immune infiltration

After studying HCT116 tumor spheroids, we were interested in the interplay of tumor cells with immune cells. Therefore, we established a co-culture protocol of HCT116 spheroids with allogeneic immune cells (Figure 35A). HCT116 tumor cells were allowed to form spheroids. After 4 d, spheroids were treated with MCT1 and MCT4 inhibitors alone or in combination for 9 d. Immune cells were freshly isolated from blood of healthy donors. Bulk unstimulated immune cells consisting of mononuclear cells (MNCs) and polymorphonuclear leucocytes (PMNs) were added to tumor spheroids. In parallel, T cells were stimulated for 24 h with αCD3/CD28 beads and IL-2. Next day, pre-activated T cells were added to HCT116 spheroids in co-culture along with aPD-L1 or Isotype control for an additional 24 h. Afterwards, spheroids were harvested, pooled, washed and prepared for subsequent flow cytometry staining. We analyzed immune cell infiltration and function. Immune cell populations were determined as shown in the gating strategy in Figure 35B, staining the following common immune cell marker: CD45 as pan-leukocyte marker, CD14 as marker for tumor-associated monocytes (TAMs), CD66b as marker for tumor-associated neutrophils (TANs) and CD3 as marker for T cells. Dead cells and doublets were excluded from all analyses.

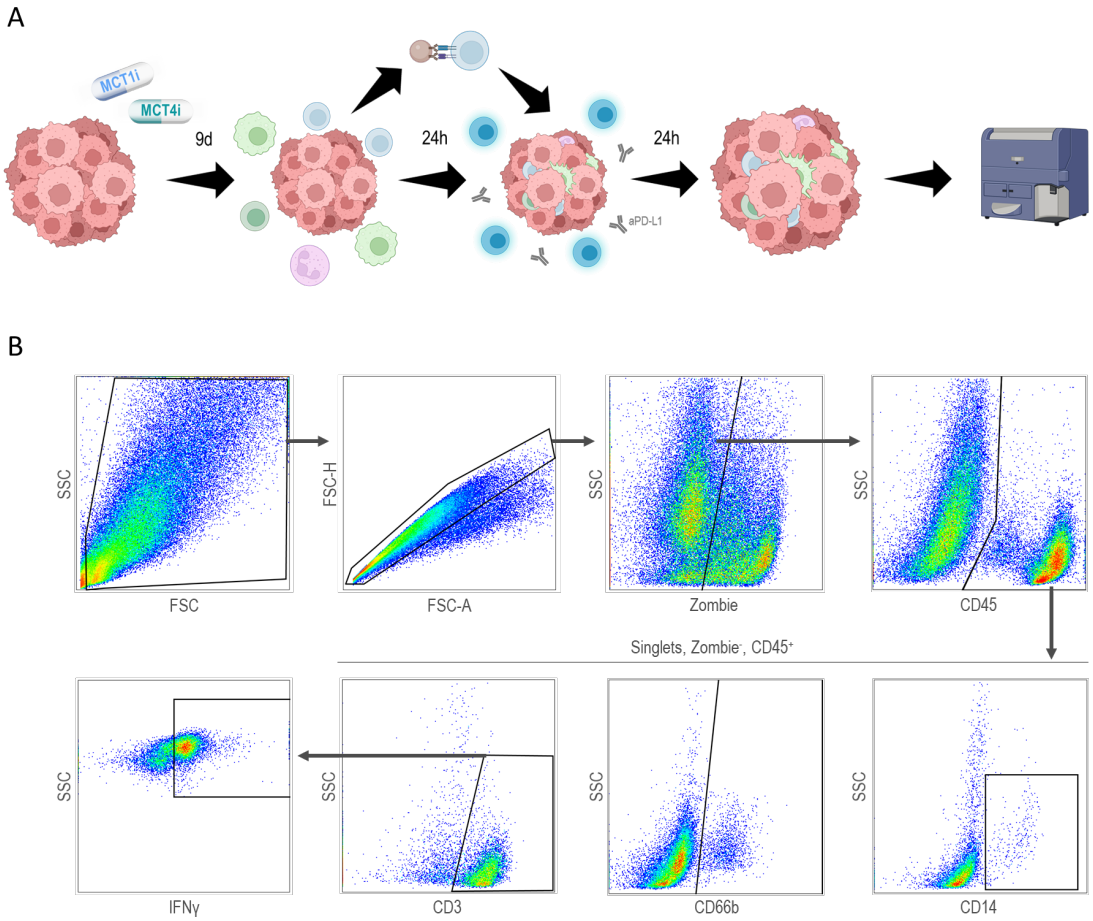

Figure 35. HCT116 spheroid co-culture with immune cells. (A) Co-culture protocol. HCT116 spheroids were treated with inhibitors for 9 d. Immune cells were freshly isolated from peripheral blood of healthy donors and added for 24 h. In parallel, T cells were stimulated for 24 h with αCD3/CD28 beads at a cell-to-bead ratio of 1:1 in the presence of 25 IU/ml IL-2. Next day, pre-activated T cells were added to HCT116 spheroid

co-culture along with aPD-L1 or Isotype control for an additional 24 h. Afterwards, spheroids were harvested, pooled, washed and prepared for subsequent flow cytometry staining. Created with BioRender.com. (B) Gating strategy for leukocytes ($CD45^+$) among total living ($Zombie^-$) singular cells and tumor-associated monocytes (TAMs) ($CD14^+$), tumor-associated neutrophils (TANs) ($CD66b^+$) and T cells ($CD3^+$) among $CD45^+$ cells after 24 h co-culture. Interferon γ positive T cells ($CD3^+$ $IFN\gamma^+$) were determined among $CD3^+$ T cells.

Tumor cell proliferation was determined by Ki67 staining. Ki67 is a nuclear protein, which is increased during cell progression through S phase of the cell cycle. Viability was determined by staining with a live-dead dye (Zombie) that only enters cells with damaged cell membranes. However, even after 48 h of co-culture with immune cells, we did not detect any clear effects of MCT blockade or checkpoint blockade using aPD-L1 on HCT116 tumor cell proliferation or viability (Figure 36).

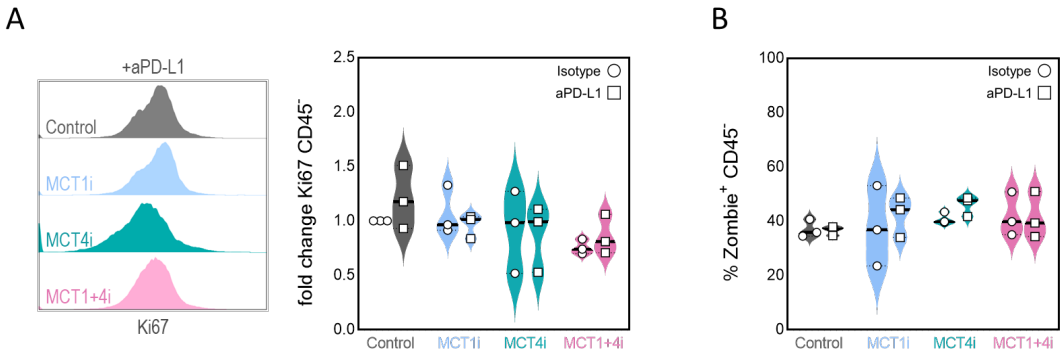

Figure 36. No effects on HCT116 spheroid proliferation and viability after 48 h co-culture with immune cells. HCT116 spheroids were treated with inhibitors for 9 d. Immune cells were freshly isolated from peripheral blood of healthy donors and added for 24 h. In parallel, T cells were stimulated for 24 h with αCD3/CD28 beads at a cell-to-bead ratio of 1:1 in the presence of 25 IU/ml IL-2. Next day, pre-activated T cells were added to HCT116 spheroid co-culture along with aPD-L1 or Isotype control for an additional 24 h. Afterwards, spheroids were harvested, pooled, washed and prepared for subsequent flow cytometry staining. (A) Tumor cell proliferation was determined by Ki67 staining and analysis by flow cytometry. (B) Dead tumor cells were designated as $Zombie^+$ $CD45^-$ and determined by flow cytometry. Representative plots and median values with single data points are shown.

Tumor spheroids produce chemokines that attract immune cells. Indeed, immune cells infiltrated HCT116 spheroids. Consistent with reduced lactate levels upon MCT4 inhibition, total infiltration of $CD45^+$ immune cells was significantly improved by treatment with MCT4 inhibitor (2-fold increase compared to untreated control). Furthermore, combination with aPD-L1 had an additional beneficial effect, resulting in a 3-fold increase in immune cell infiltration. Surprisingly, combination of MCT4 and MCT1 inhibitor treatment was even slightly worse compared to MCT4 blockade alone. Dual MCT1 and MCT4 blockade resulted in higher immune cell infiltrate only by trend, although lactate concentration was reduced to the same level. Additional aPD-L1 together with MCT1 and MCT4 inhibition was not different from MCT1 and MCT4 inhibition alone. Single MCT1 inhibitor or aPD-L1 treatment both had no impact on the immune cell infiltrate in HCT116 spheroids (Figure 37A).

A proportion of T cells was pre-activated for 24 h prior to co-culture with HCT116 spheroids. Consequently, tumor-infiltrating T cells (TILs) characterized by CD3 expression were the most

abundant cell type among all infiltrated leukocytes, accounting for approximately 70 %. Tumor-associated CD14$^+$ TAMs and tumor-associated CD66b$^+$ TANs were poorly represented with an average of 5 % respectively. However, the composition of T cells, TAMs and TANs did not change by MCT inhibition or immune checkpoint blockade (Figure 37B-E).

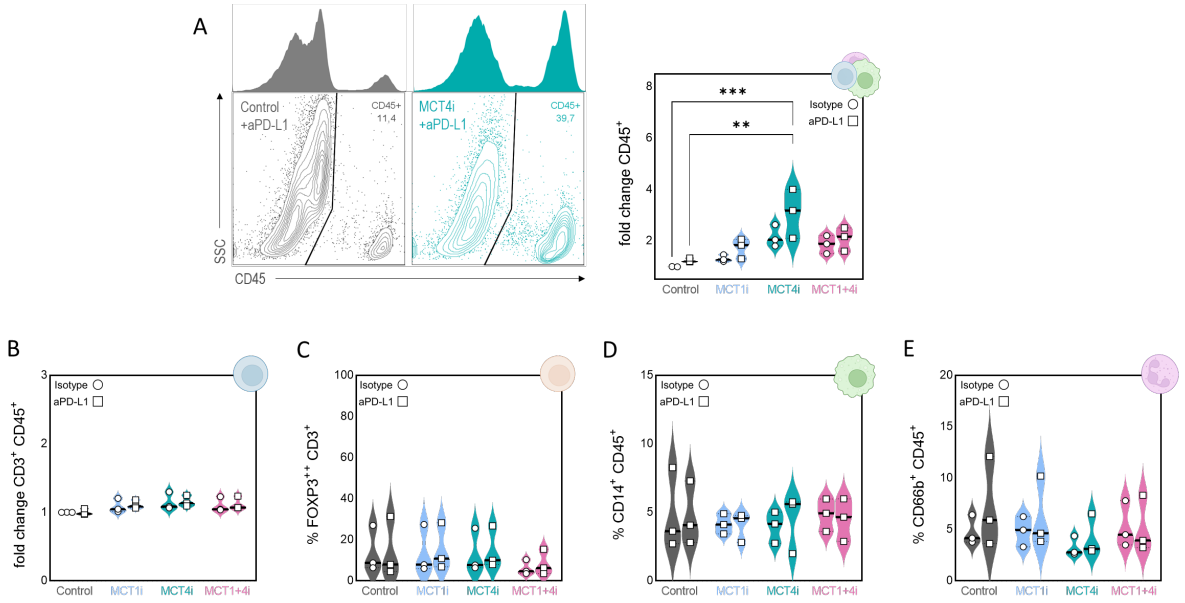

Figure 37. Enhanced infiltration of immune cells in HCT116 spheroids with MCT4 inhibitor treatment. HCT116 spheroids were treated with inhibitors for 9 d. Immune cells were freshly isolated from peripheral blood of healthy donors and added for 24 h. In parallel, T cells were stimulated for 24 h with αCD3/CD28 beads at a cell-to-bead ratio of 1:1 in the presence of 25 IU/ml IL-2. Next day, pre-activated T cells were added to HCT116 spheroid co-culture along with aPD-L1 or Isotype control for an additional 24 h. Afterwards, spheroids were harvested, pooled, washed and prepared for subsequent flow cytometry staining. (A) Gated on single and viable cells. Fold change of CD45$^+$ infiltrated immune cells after 48 h co-culture. Representative plots and median values with single data points are shown. Significance was determined using one-way ANOVA and post-hoc Bonferroni multiple comparison test (**$p < 0.01$; ***$p < 0.001$). (B-E) Gated on single, viable cells and CD45$^+$ cells. (B) Fold change of T cells (% CD3$^+$) among CD45$^+$ cells after 48 h co-culture. (C) Percentage of Forkhead Box P3 (FOXP3) high regulatory T cells (FOXP3^{++}) among CD3$^+$ T cells among CD45$^+$ cells after 48 h co-culture. (D) Percentage of tumor-associated monocytes (TAMs) (CD14$^+$) among CD45$^+$ cells after 48 h co-culture. (E) Percentage of tumor-associated neutrophils (TANs) (CD66b$^+$) among CD45$^+$ cells after 48 h co-culture. Depicted are median values and single data points. Pictures of cells were created with BioRender.com.

Cytotoxic T cells are the key players of anti-tumor immunity, and the number of tumor-infiltrated T lymphocytes (TILs) has been associated with a better prognosis (26,27,129) and prediction of response to chemotherapy in CRC (341,342). Therefore, we investigated T cell effector functions in terms of their expansion, determined by Ki67 staining, and cytokine production. In line with previous T cell experiments, MCT4 inhibition in co-culture with HCT116 spheroids did not impair T cell proliferation, whereas combined treatment with MCT1 and MCT4 inhibitors decreased proliferation compared to untreated control, which might explain the decreased number of immune cells after application of both inhibitors (Figure 37A). Inhibition of MCT1 or PD-L1 alone had no effect on proliferation of TILs in HCT116 spheroids (Figure 38A).

Interferon γ (IFNγ) is a cytokine extensively produced by activated T cells. Moreover, IFNγ signature has been shown to predict response to immunotherapy in various tumor entities (343–346). We found significantly more IFNγ$^+$ TILs upon MCT4 inhibition with and without aPD-L1 treatment, approximately 60 %, compared to 30 % IFNγ$^+$ TILs in untreated control. Interestingly, dual MCT1 and MCT4 inhibition proved to be worse than MCT4 inhibition alone and failed to improve cytokine production by TILs. Single MCT1 or PD-L1 inhibition did not affect frequency of IFNγ$^+$ TILs in HCT116 spheroids (Figure 38B).

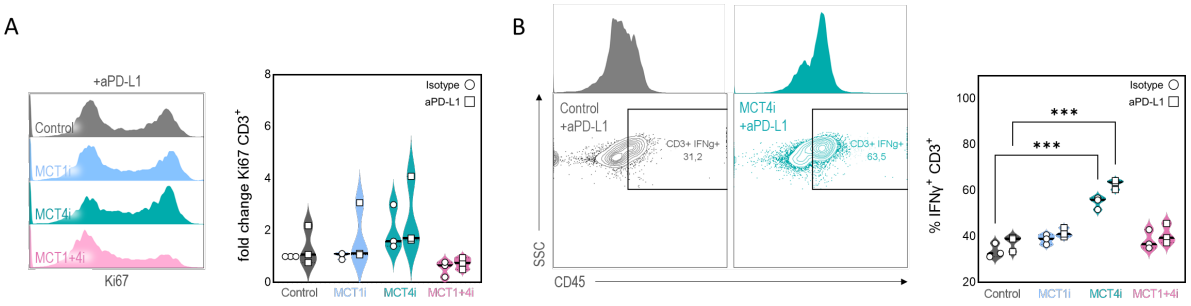

Figure 38. Increased infiltration number of INFγ$^+$ T cells in HCT116 spheroids with MCT4 inhibitor treatment. HCT116 spheroids were treated with inhibitors for 9 d. Immune cells were freshly isolated from peripheral blood of healthy donors and added for 24 h. In parallel, T cells were stimulated for 24 h with αCD3/CD28 beads at a cell-to-bead ratio of 1:1 in the presence of 25 IU/ml IL-2. Next day, pre-activated T cells were added to HCT116 spheroid co-culture along with aPD-L1 or Isotype control for an additional 24 h. Afterwards, spheroids were harvested, pooled, washed and prepared for subsequent flow cytometry staining. Gated on single, viable cells and CD45$^+$ CD3$^+$ T cells. (A) T cell proliferation was determined by Ki67 staining and analysis by flow cytometry after 2 d co-culture. (B) Percentage of interferon γ positive T cells (IFNγ$^+$) after 48 h co-culture. Representative plots and median values with single data points are shown. Significance was determined using one-way ANOVA and post-hoc Bonferroni multiple comparison test (**p < 0.01; ***p < 0.001).

In conclusion, colorectal HCT116 tumor spheroids cultured with immune cells for 48 h provide a suitable model to study the immunomodulatory effects of MCT inhibitors with and without aPD-L1 immune checkpoint blockade. It is noteworthy, that lowered lactate levels reduced by single MCT4 inhibition supported immune cell infiltration and IFNγ production by TILs, but only tended to enhance beneficial effects of immune checkpoint inhibition therapy. However, combined targeting of MCT1 and MCT4 even decreased the efficacy compared to single inhibition of MCT4 in this CRC co-culture model.

4.3.1.1.3 Live cell imaging

Flow cytometry analysis of HCT116 spheroid-associated immune cells revealed an immunoregulatory effect of MCT4 inhibitor treatment. However, direct anti-cancer effects were only moderate in terms of proliferation and death of HCT116 tumor cells. Yet, it is known that T cell response after activation is a dynamic process in which the effective response peaks only after 3 to 5 days. Therefore, we were interested in whether TILs might be able to kill HCT116 spheroids after a prolonged period of time.

Thus, we performed a co-culture experiment as described in Chapter 4.3.1.1.2. But instead of preparing HCT116 spheroids for flow cytometry analysis after 48 h of co-culture, we only washed the spheroids to remove non-infiltrated immune cells, and replaced the medium with all treatments and

added a viability dye (Cyto3D® Live-Dead Assay Kit). We then monitored the fluorescence of the viability dye for another 48 h under cell culture conditions using the Incucyte Live Cell Imaging System. This means that HCT116 tumor spheroids were cultured with TILs for a total of 4 d (Figure 39A). In Figure 39B, representative pictures after 4 d co-culture are shown. The viability dye consists of two components: Arcidine Orange, which penetrates all viable cells and fluoresces in green, and Propidium Iodide, which can only enter cells with damaged cell membrane and stains dead cells with red fluorescence. Although we did not observe increased tumor cell death in short-term co-cultures, HCT116 spheroids were severely affected in terms of viability by MCT4 inhibition in combination with aPD-L1 immune checkpoint blockade. There were many dead cells as indicated by red fluorescence and only a very small remnant of HCT116 tumor spheroid remained. In this regards, dual MCT1 and MCT4 inhibitor treatment with aPD-L1 was also inferior to MCT4i+aPD-L1 therapy. Nevertheless, when MCT1 and MCT4 were inhibited, a rim of dead cells was observed, and in combination with aPD-L1, the necrotic core was more pronounced (Figure 39B). Mean green fluorescence intensity as an estimate for viable cells was quantified after 4 days of co-culture and reflected the eye-evaluated results that HCT116 spheroid killing is induced by MCT4 inhibition in combination with aPD-L1 (Figure 39C).

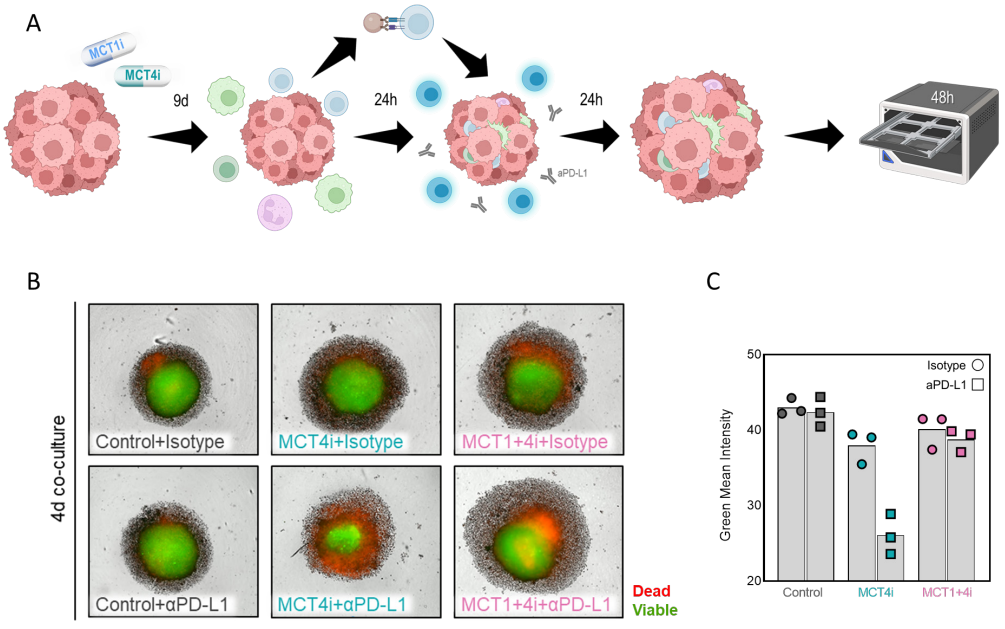

Figure 39. Induction of HCT116 tumor cell kill upon MCT4 inhibitor and aPD-L1 treatment after 4 d co-culture with immune cells. (A) Co-culture protocol. HCT116 spheroids were treated with inhibitors for 9 d. Immune cells were freshly isolated from peripheral blood of healthy donors and added for 24 h. In parallel, T cells were stimulated for 24 h with αCD3/CD28 beads at a cell-to-bead ratio of 1:1 in the presence of 25 IU/ml IL-2. Next day, pre-activated T cells were added to HCT116 spheroid co-culture along with aPD-L1 or Isotype control for an additional 24 h. Spheroids were then washed, fresh medium containing MCT1 and/or MCT4 inhibitors and Cyto3D® Live-Dead Assay Kit was added, and spheroids with infiltrated immune cells were monitored under cell culture conditions for 48 h using the Incucyte Live Cell Imaging System. Created with BioRender.com. (B) Representative pictures out of three independent experiments showing HCT116 spheroids after 4 d co-culture with immune cells. Green Fluorescence = viable cells (Acridine Orange$^+$), red = dead cells (Propidium Iodide$^+$). (C) Quantification of the Green Mean Fluorescence Intensity, which determines viable cells after 4 d co-culture. Median values with single data points are shown.

However, live-dead dyes stain every cell regardless of its origin. Therefore, we ran the co-culture for in total 7 d and then analyzed the remaining live cells for percentage of tumor cells and $CD3^+$ TILs by flow cytometry. Upon treatment with aPD-L1 and MCT4 inhibitor combined, almost all cells were dead after 7 d of co-culture. However, within the 5 % living cells, we found 42 % TILs, whereas almost no TILs were found in HCT116 spheroids treated with aPD-L1 alone (Figure 40).

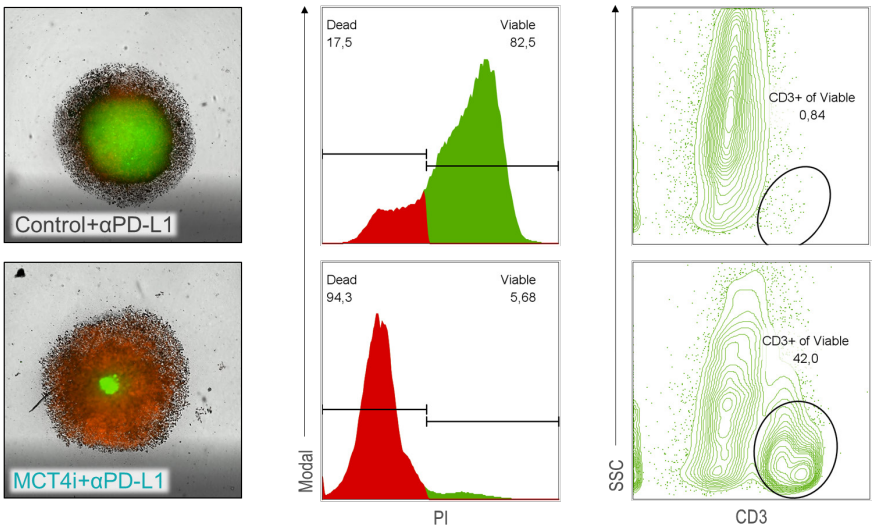

Figure 40. HCT116 tumor cell death upon MCT4 inhibition in combination with aPD-L1 is mediated by T cells. HCT116 spheroids were treated with or without MCT4 inhibitor for 9 d. Immune cells were freshly isolated from peripheral blood of healthy donors and added for 24 h. In parallel, T cells were stimulated for 24 h with αCD3/CD28 beads at a cell-to-bead ratio of 1:1 in the presence of 25 IU/ml IL-2. Next day, pre-activated T cells were added to HCT116 spheroid co-culture along with aPD-L1 for an additional 24 h. Spheroids were then washed, fresh medium containing MCT4 inhibitors and Cyto3D® Live-Dead Assay Kit was added, and spheroids with infiltrated immune cells were monitored under cell culture conditions for 5 d using the Incucyte Live Cell Imaging System. Spheroids were harvested, pooled, washed and prepared for flow cytometry staining. Viable cell number was determined as Propidium Iodide positive (PI^+) cells. Percentage of $CD3^+$ T cells was determined among viable cells.

Live cell imaging of long-term CRC HCT116 tumor spheroid co-cultures with immune cells showed that only inhibition of MCT4 in combination with the immune checkpoint inhibitor aPD-L1 induced tumor cell killing, most likely mediated by TILs.

4.3.1.2 MCT1 inhibition augments ICB in a $HCT116^{MCT4-/-}$ spheroid co-culture model

A single MCT4 inhibitor and combination with an MCT1 inhibitor decreased lactate secretion from CRC HCT116 Wildtype ($HCT116^{WT}$) tumor spheroids. In our co-culture model, more immune cells infiltrated HCT116 spheroids with MCT4 inhibition compared to spheroids with high lactate content. Moreover, tumor cell death was observed when MCT4 and aPD-L1 inhibitors were combined. As a proof of concept and to investigate the effects of MCT4 blockade on immune cells, we repeated the co-cultures of tumor spheroids with immune cells using MCT4 Knock-Out HCT116 ($HCT116^{MCT4-/-}$) spheroids.

4.3.1.2.1 HCT116$^{MCT4-/-}$ monolayer vs spheroid

We confirmed the lack of MCT4 expression by Western blot analysis. HCT116$^{MCT4-/-}$ cells still expressed MCT1, and moreover, MCT1 was slightly upregulated in 3D HCT116$^{MCT4-/-}$ spheroids (Figure 41A). Compared to HCT116^{WT} cells, expression of the co-factor CD147 was much lower in HCT116$^{MCT4-/-}$ cells and slightly less in 3D culture compared to monolayers (Figure 41B). However, although CD147 expression was lower and MCT4 not present, HCT116$^{MCT4-/-}$ tumor cells were as glycolytic as HCT116^{WT} cells and produced up to 20 mM lactate within 9 d. Since HCT116$^{MCT4-/-}$ spheroids were lacking MCT4, application of a single MCT inhibitor was sufficient to reduce lactate accumulation to the same level as when combined with the MCT1 inhibitor. MCT4 inhibition did not affect lactate efflux of HCT116$^{MCT4-/-}$ spheroids (Figure 41C).

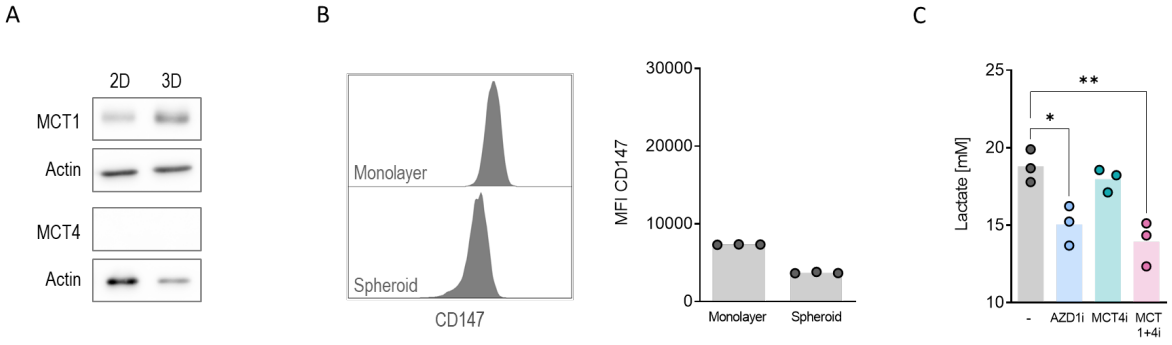

Figure 41. Single MCT1 inhibition decreases lactate secretion of HCT116$^{MCT4-/-}$ spheroids. HCT116$^{MCT4-/-}$ cells were either cultured as monolayer or spheroids. HCT116$^{MCT4-/-}$ monolayers were treated for 24 h and spheroids for 9 d with 0.1 µM MCT1 inhibitor (MCT1i) and/or MCT4 inhibitor (MCT4i). (A) Expression of MCT1 and MCT4 was analyzed in whole-cell lysates of HCT116$^{MCT4-/-}$ monolayers (2D) or HCT116$^{MCT4-/-}$ spheroids (3D) by Western blot analysis. One representative plot out of three independent experiments is shown. (B) CD147 expression was determined by flow cytometry. One representative plot and corresponding median values with single data points are shown. (C) Lactate concentrations were measured after 9 d in HCT116$^{MCT4-/-}$ spheroid culture supernatants. Depicted are median values and single data points. Significance was determined using one-way ANOVA and post-hoc Bonferroni multiple comparison test (*$p < 0.05$; **$p < 0.01$).

However, the immune checkpoint ligand PD-L1 was highly expressed in HCT116 monolayers and spheroids regardless of the presence MCT4 (Figure 42). Therefore, it is reasonable to combine MCT inhibitors with immune checkpoint blockade in co-cultures with T cells.

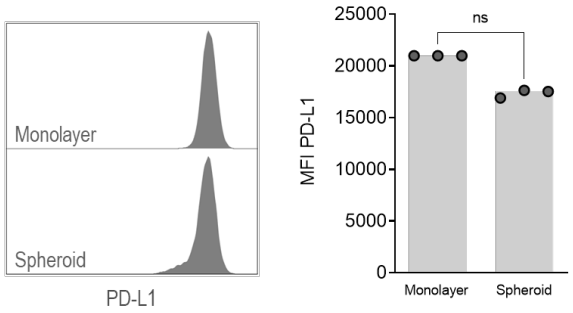

Figure 42. HCT116$^{MCT4-/-}$ tumor cells express high levels of PD-L1. HCT116$^{MCT4-/-}$ cells were either cultured as monolayer or spheroids. HCT116$^{MCT4-/-}$ monolayers were treated for 24 h and spheroids for 9 d with 0.1 µM MCT1 inhibitor (MCT1i) and/or MCT4 inhibitor (MCT4i). Programmed cell death ligand (PD-L1) expression was determined by flow cytometry. Representative plots and median values with single data points are shown.

Similar to HCT116^{WT} spheroids, HCT116$^{MCT4-/-}$ spheroids were not affected by MCT inhibition in spheroid morphology, size or viability (Figure 43).

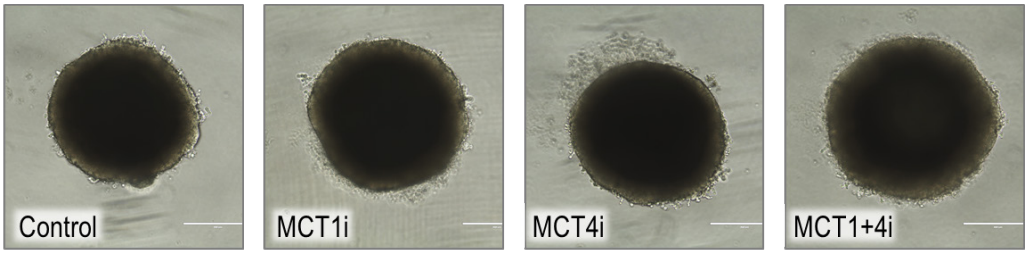

Figure 43. Morphology of HCT116$^{MCT4-/-}$ spheroids is not affected by MCT inhibition. HCT116$^{MCT4-/-}$ cells were cultured as spheroids and treated for 9 d with 0.1 µM MCT1 inhibitor (MCT1i) and/or MCT4 inhibitor (MCT4i). The morphology of treated spheroids was assessed after 9 d of treatment and images were recorded using the EVOS system.

In short, HCT116$^{MCT4-/-}$ spheroids lack MCT4, leading to decreased lactate efflux with single MCT1 inhibition and resistance towards MCT4 inhibition.

4.3.1.2.2 Immune infiltration

Co-culture of HCT116$^{MCT4-/-}$ cells was conducted as described in Chapter 4.3.1.1.2. Briefly, HCT116$^{MCT4-/-}$ spheroids were treated with MCT inhibitors for a duration of 9 d. Then, bulk unstimulated immune cells were added to HCT116$^{MCT4-/-}$ spheroids. Next day, 24 h pre-activated T cells were added for further 24 h. Spheroids were washed, pooled and processed for flow cytometry staining. We analyzed immune cell infiltration and function. Immune cell populations were determined as shown in the gating strategy in Figure 35B by staining the following common immune cell marker: CD45 as pan-leukocyte marker, CD14 as marker for tumor-associated monocytes (TAMs), CD66b as marker for tumor-associated neutrophils (TANs) and CD3 as marker for T cells. Dead cells and doublets were excluded from all analyses.

Tumor cell proliferation was determined by Ki67 staining and viability was determined by staining with a live-dead dye (Zombie) that only enters cells with damaged cell membranes. Similar to 48 h HCT116^{WT} co-culture, we did not find clear effects on HCT116$^{MCT4-/-}$ tumor cell proliferation or viability under MCT1 and MCT4 inhibitory therapy with or without checkpoint blockade with aPD-L1 (Figure 44).

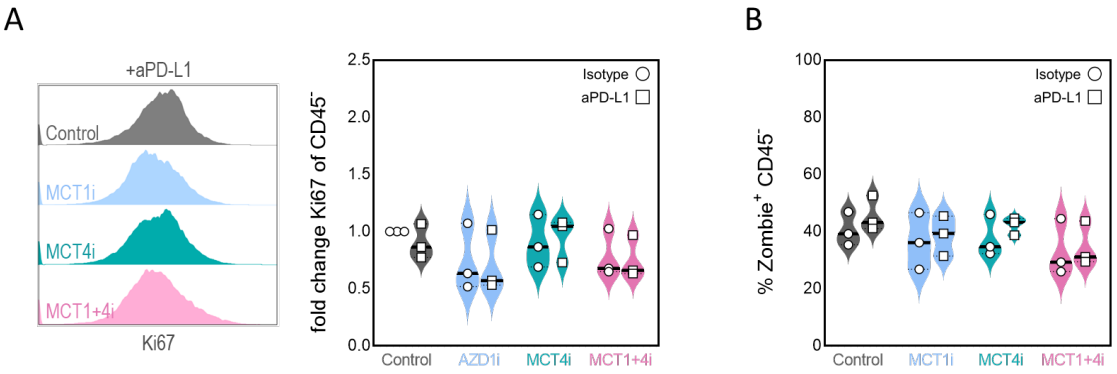

Figure 44. Co-culture with immune cells does not affect viability and proliferation of HCT116$^{MCT4-/-}$ spheroids. HCT116$^{MCT4-/-}$ spheroids were treated with inhibitors for 9 d. Immune cells were freshly isolated from peripheral blood of healthy donors and added for 24 h. In parallel, T cells were stimulated for 24 h with αCD3/CD28 beads at a cell-to-bead ratio of 1:1 in the presence of 25 IU/ml IL-2. Next day, pre-activated T cells were added to HCT116$^{MCT4-/-}$ spheroid co-culture along with aPD-L1 or Isotype control for an additional 24 h. Afterwards, spheroids were harvested, pooled, washed and prepared for subsequent flow cytometry staining. (A) Tumor cell proliferation was determined by Ki67 staining and analysis by flow cytometry. (B) Dead tumor cells were designated as Zombie$^+$ CD45$^-$ and determined by flow cytometry. (A) Representative plots and (A, B) median values with single data points are shown).

From HCT116^{WT} spheroid co-cultures, we knew that MCT4 inhibition supports immune cell infiltration and function. HCT116$^{MCT4-/-}$ cells were more sensitive towards MCT1 inhibition. Therefore, we were interested in whether treatment with MCT1 inhibitors in the HCT116$^{MCT4-/-}$ model can achieve the same effects as MCT4 inhibitors in the HCT116^{WT} model. Consistent with reduced lactate levels upon MCT1 inhibition, total infiltration of CD45$^+$ immune cells was significantly improved by treatment with MCT1 inhibitor (2.8-fold increase compared to untreated control). Furthermore, combination with aPD-L1 had an additional beneficial effect, resulting in a 4-fold increase in immune cell infiltration. As observed in HCT116^{WT} co-cultures, combination of specific MCT1 inhibitor and MCT4 inhibitor treatment was even slightly worse than MCT1 blockade alone, indicating that MCT4 expression on tumor-infiltrating cells might play a role. Dual MCT1 and MCT4 blockade resulted in higher immune cell infiltrate only by trend, although lactate concentration was reduced to the same level. Additional aPD-L1 treatment together with MCT1 and MCT4 inhibition was not different from MCT1. Interestingly, MCT4 inhibition alone or in combination with aPD-L1 treatment tended to increase immune cell infiltrate in HCT116$^{MCT4-/-}$ spheroids (Figure 45A).

TILs characterized by CD3 were the most abundant cell type among all infiltrated leukocytes, accounting for approximately 60-70 % of CD45$^+$ cells. CD14$^+$ TAMs and CD66b$^+$ TANs were poorly

represented with under 10 % respectively. However, composition of T cells, TAMs and TANs did not change upon MCT inhibition or immune checkpoint blockade (Figure 45B-E).

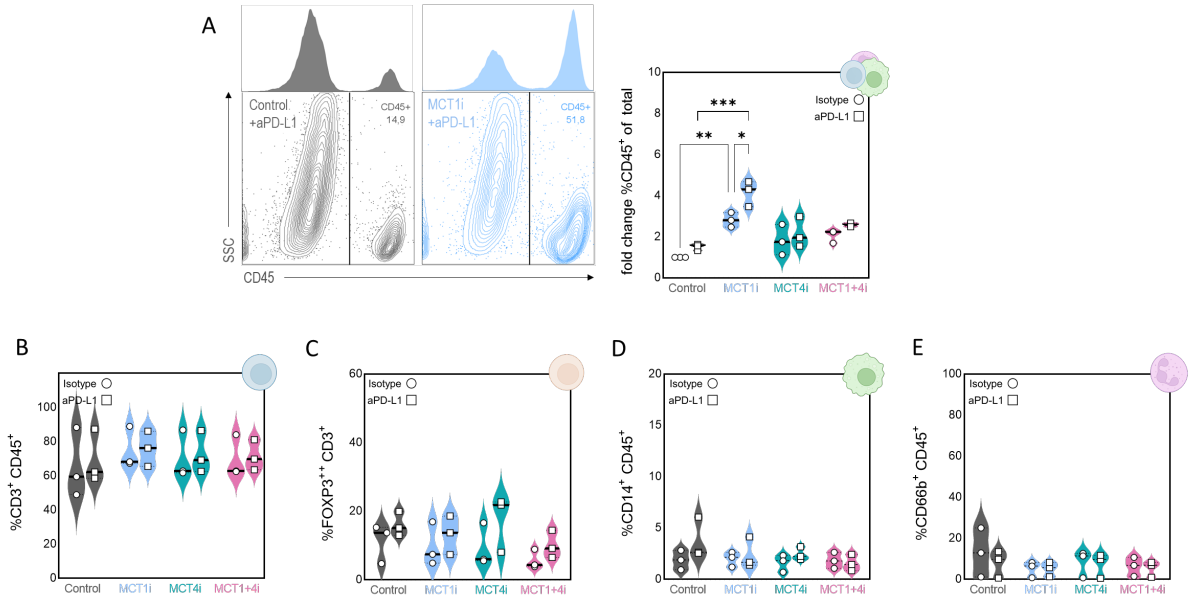

Figure 45. Enhanced infiltration of immune cells in HCT116$^{MCT4-/-}$ spheroids upon MCT1 inhibitor treatment. HCT116$^{MCT4-/-}$ spheroids were treated with inhibitors for 9 d. Immune cells were freshly isolated from peripheral blood of healthy donors and added for 24 h. In parallel, T cells were stimulated for 24 h with αCD3/CD28 beads at a cell-to-bead ratio of 1:1 in the presence of 25 IU/ml IL-2. Next day, pre-activated T cells were added to HCT116$^{MCT4-/-}$ spheroid co-culture along with aPD-L1 or Isotype control for an additional 24 h. Afterwards, spheroids were harvested, pooled, washed and prepared for subsequent flow cytometry staining. (A) Gated on single and viable cells. Fold change of CD45$^+$ infiltrated immune cells after 48 h co-culture. Representative plots and median values with single data points are shown. Significance was determined using one-way ANOVA and post-hoc Bonferroni multiple comparison test (*p < 0.05; **p < 0.01; ***p < 0.001). (B-E) Gated on single, viable cells and CD45$^+$ cells. (B-D) Gated on single, viable cells and CD45$^+$. (B) Fold change of T cells (CD3$^+$) among CD45$^+$ cells after 48 h co-culture. (C) Percentage of Forkhead Box P3 (FOXP3) high regulatory T cells (FOXP3^{++}) among CD3$^+$ T cells among CD45$^+$ cells after 48 h co-culture. (D) Percentage of tumor-associated monocytes (CD14$^+$) among CD45$^+$ cells after 48 h co-culture. (D) Percentage of tumor-associated neutrophils (CD66b$^+$) among CD45$^+$ cells after 48 h co-culture. Depicted are median values and single data points. Pictures of cells were created with BioRender.com.

Comparable to HCT116^{WT} co-culture, we investigated T cell effector functions in terms of their expansion, determined by Ki67 staining, and cytokine production. Complementary to MCT4i treatment in HCT116^{WT} co-culture, single MCT1 inhibition in co-culture with HCT116$^{MCT4-/-}$ spheroids did not impair T cell proliferation, whereas combined treatment with MCT1 and MCT4 inhibitors decreased proliferation compared to untreated control. Inhibition of MCT4 or PD-L1 alone had no effect on the proliferation of TILs in HCT116$^{MCT4-/-}$ spheroids (Figure 46A). However, we found significantly more IFNγ$^+$ TILs upon MCT1 inhibition with and without aPD-L1 treatment compared to untreated control. Like seen before, dual MCT1 and MCT4 inhibition proved to be worse than MCT1 inhibition alone and failed to improve cytokine production in TILs. Single MCT4i in combination with aPD-L1 tended to increase the fraction of IFNγ$^+$ TILs in HCT116$^{MCT4-/-}$ spheroids. Single PD-L1 inhibition had no impact on IFNγ production in TILs (Figure 46B).

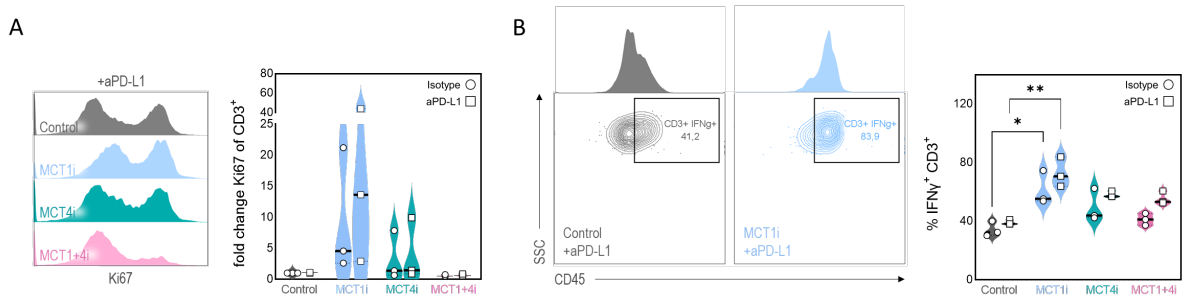

Figure 46. Increased infiltration of INFγ⁺ T cells in HCT116$^{MCT4-/-}$ spheroids with MCT1 inhibitor treatment. HCT116$^{MCT4-/-}$ spheroids were treated with inhibitors for 9 d. Immune cells were freshly isolated from peripheral blood of healthy donors and added for 24 h. In parallel, T cells were stimulated for 24 h with αCD3/CD28 beads at a cell-to-bead ratio of 1:1 in the presence of 25 IU/ml IL-2. Next day, pre-activated T cells were added to HCT116$^{MCT4-/-}$ spheroid co-culture along with aPD-L1 or Isotype control for an additional 24 h. Afterwards, spheroids were harvested, pooled, washed and prepared for subsequent flow cytometry staining. Gated on single, viable cells and CD45⁺ CD3⁺ T cells. (A) T cell proliferation was determined by Ki67 staining and analysis by flow cytometry after 2 d co-culture. (B) Percentage of interferon γ positive T cells (IFNγ⁺) after 48 h co-culture. (A, B) Representative plots and median values with single data points are shown. Significance was determined using one-way ANOVA and post-hoc Bonferroni multiple comparison test (*p < 0.05; **p < 0.01).

Conclusively, in colorectal HCT116$^{MCT4-/-}$ spheroids, single MCT1 inhibition lowered lactate levels, promoted immune cell infiltration and IFNγ production by TILs, and tended to improve immune checkpoint therapy. However, as in HCT116^{WT} spheroid co-cultures, combined inhibition of MCT1 and MCT4 was less successful than inhibition of MCT1 alone in this CRC HCT116$^{MCT4-/-}$ co-culture model. In addition, we observed minor effects of single MCT4 inhibition on immune cell infiltration and IFNγ production in TILs by trend, independent of MCT4 expression in tumor cells.

4.3.2 Immunomodulatory role of MCT inhibitors in murine colorectal cancer

We investigated the effects of selective MCT1 and/or MCT4 inhibitors on tumor and immune cells, but also in a more physiological HCT116 CRC spheroid co-culture model with immune cells, in which we further studied a potential supportive effect on immune checkpoint therapy. These findings revealed an immunomodulatory role of single MCT4 inhibition in CRC based on the reduction of extracellular lactic acid accumulation. Immune cell infiltration and T cell effector functions were augmented in human CRC *in vitro* models. Therefore, we were interested in finally translating these results into an *in vivo* model using the murine CRC cell line MC38, which was inoculated into immunocompetent C57BL/6N wildtype mice. However, as the differences in size and lifespan already indicate, humans and mice have fundamental differences, and what is true for humans is not necessarily true for mice, and vice versa. Although mice mirror the human biology in many aspects, we and others found differences in terms of immunology (347). Therefore, prior to *in vivo* experiments, we confirmed the efficacy of selective MCT4 inhibitor treatment in a murine MC38 tumor spheroid co-culture model.

4.3.2.1 MCT4 inhibition improves T cell mediated killing in MC38 spheroid co-cultures *in vitro*

Tumor spheroids reflect the complexity of the interaction between tumors cells, the TME and immune cells. As shown above, tumor spheroid co-cultures with immune cells represent a model to study the impact of drugs on tumor-immune cell crosstalk. For investigation of MCT1 and MCT4 inhibition in a murine CRC spheroid model, we used MC38 cells. MC38 cells form robust tumor spheroids. We tested the effects of MCT1 and MCT4 inhibition in combination with immune checkpoint blockade using aPD-L1 antibodies or isotype control.

4.3.2.1.1 MC38 monolayer vs spheroid

As seen for human HCT116^{WT} tumor cells, 2D cell cultures and 3D tumor spheroids may differ profoundly in their MCT expression. Indeed, Mct4 was also markedly upregulated in murine MC38 spheroids relative to MC38 monolayers. MC38 monolayers barely express Mct1 but slightly upregulate it in 3D culture (Figure 47A). The co-factor CD147 was not altered in 3D culture compared with monolayers (Figure 47B). Just like HCT116 spheroids, MC38 spheroids were found to be highly glycolytic and produced up to 20 mM lactate within 7 d. As in HCT116^{WT} spheroids, the most striking difference between MC38 monolayers (data not shown) and spheroids was that lactate efflux was already diminished by treatment with a single MCT4 inhibitor, but combination with MCT1 inhibitor tended to show an additive effect on lactate reduction (Figure 47C). Moreover, PD-L1 was highly expressed in MC38 monolayers and spheroids similar to HCT116 spheroids (Figure 47D). Therefore, it is reasonable to combine MCT inhibitors with immune checkpoint blockade in co-cultures with T cells.

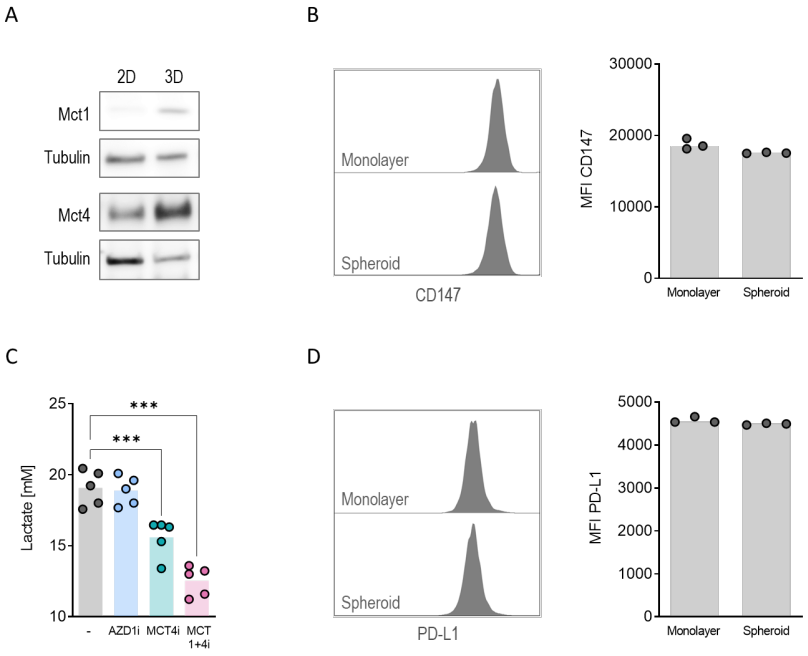

Figure 47. Single MCT4 inhibition decreases lactate secretion of MC38 spheroids. MC38 tumor cells were either cultured as monolayer or spheroids. MC38 monolayers were treated for 24 h and spheroids for 9 d with 0.1 µM MCT1 inhibitor (MCT1i) and/or MCT4 inhibitor (MCT4i).

(A) Expression of Mct1 and Mct4 was analyzed in whole-cell lysates of MC38 monolayers (2D) or MC38 spheroids (3D) by Western blot analysis. One representative plot out of two independent experiments is shown. (B) CD147 expression was determined by flow cytometry (Median Fluorescence Intensity, MFI). Representative plots and median values with single data points are shown. (C) Lactate concentrations were measured after 7 d in MC38 spheroid culture supernatants. Depicted are median values and single data points. Significance was determined using one-way ANOVA and post-hoc Bonferroni multiple comparison test (***$p < 0.001$). (D) PD-L1 expression was determined by flow cytometry (Median Fluorescence Intensity (MFI)). Representative plots and median values with single data points are shown.

In brief, in line with findings for human HCT116 spheroid co-cultures, a higher Mct4 to Mct1 ratio in MC38 spheroids compared to monolayer results in efficient decrease in lactate with single MCT4 inhibitor treatment. Combination with checkpoint blockade inhibitors is reasonable due to high a PD-L1 expression in MC38 monolayers and spheroids.

4.3.2.1.2 MC38 spheroid co-cultures

We performed MC38 spheroid co-culture experiments with Live Cell Imaging to study the effects of MCT4 inhibition on killing capacity of TILs (Figure 48A). MC38 tumor cells were allowed to form spheroids. After 4 d, spheroids were treated with MCT1 and MCT4 inhibitors alone or in combination for 7 d. Immune cells were freshly isolated from spleen of wildtype C57BL/6N mice. The composition of murine splenocytes is very different from human blood, as they consist of 60 % B cells. Thus, we depleted B cells prior to co-culture with MC38 spheroids. Bulk unstimulated B cell depleted splenocytes consisting of mononuclear cells (MNCs) and polymorphonuclear leucocytes (PMNs) were added to tumor spheroids. In parallel, T cells were stimulated for 24 h with αCD3/CD28 beads and IL-2. Next day, pre-activated T cells were added to MC38 spheroids in co-culture along with aPD-L1 or Isotype control for an additional 24 h. Next day, we washed away the non-infiltrated immune cells, replaced the medium with all treatments and added a viability dye (Cyto3D® Live-Dead Assay Kit). We then monitored the fluorescence of the viability dye for another 48 h under cell culture conditions using the Incucyte Live Cell Imaging System. In Figure 48B, representative pictures after 4 d co-culture are shown. The live-dead dye consists of two components: Arcidine Orange, which penetrates all viable cells and fluoresces in green, and Propidium Iodide, which can only enter cells with damaged cell membrane and stains dead cells with red fluorescence. Similar to human HCT116 spheroids (Figure 39), murine MC38 spheroids exhibited a reddish coloring indicating cell death when single MCT4 inhibition was combined with aPD-L1, but in murine MC38 spheroids also without aPD-L1 treatment. However, despite the increase in dead cells, MC38 tumor spheroids were not destroyed and retained their shape after inhibition of MCT4 with and without aPD-L1. Also, in the murine *in vitro* model system, dual MCT1 and MCT4 inhibitor treatment with aPD-L1 was inferior to MCT4i+aPD-L1 therapy. Moreover, single aPD-L1 immune checkpoint blockade did not induce killing of MC38 tumor cells (Figure 48B).

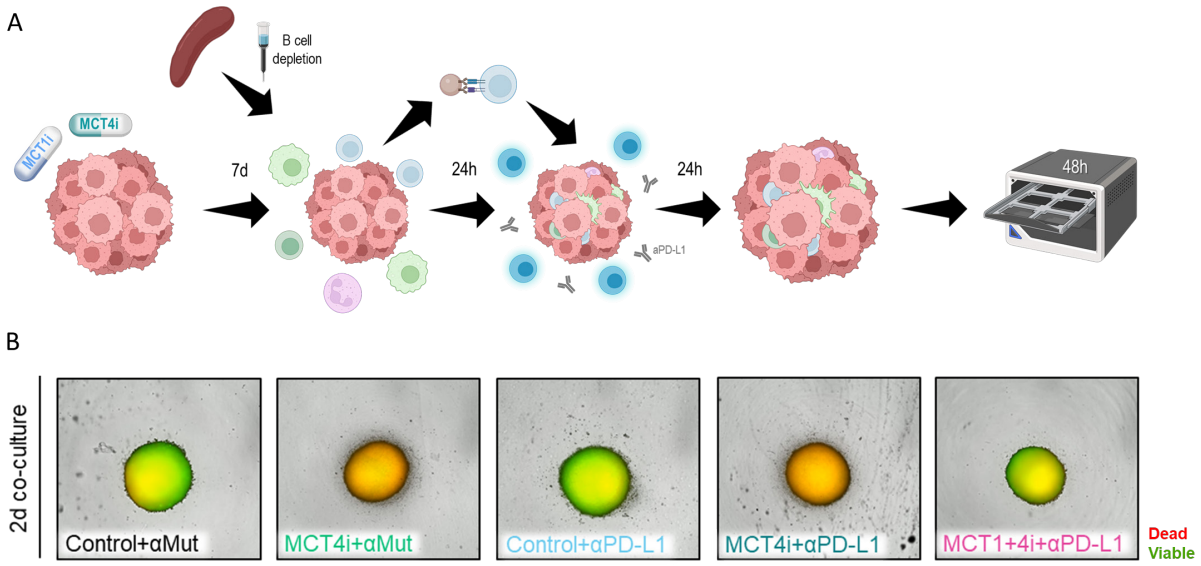

Figure 48. Induction of MC38 tumor cell killing upon MCT4 inhibitor treatment after 4 d co-culture with immune cells. (A) Co-culture protocol. MC38 spheroids were treated with inhibitors for 7 d. Immune cells were freshly isolated from spleen of C57Bl6/N Wildtype mice, B cells were depleted and remaining splenocytes were added for 24 h. In parallel, T cells were stimulated for 24 h with αCD3/CD28 beads at a cell-to-bead ratio of 1:1 in the presence of 50 IU/ml IL-2. Next day, pre-activated T cells were added to MC38 spheroid co-culture along with aPD-L1 or Isotype control (αMut) for an additional 24 h. Spheroids were then washed, fresh medium containing MCT1 and/or MCT4 inhibitors and Cyto3D® Live-Dead Assay Kit was added, and spheroids with infiltrated immune cells were monitored under cell culture conditions for 48 h using the Incucyte Live Cell Imaging System. Created with BioRender.com. (B) Representative pictures of three independent experiments showing MC38 spheroids after 4 d co-culture with immune cells. Green Fluorescence = viable cells (Acridine Orange$^+$), red = dead cells (Propidium Iodide$^+$).

Using MC38 spheroid co-cultures with splenocytes, we confirmed an immunomodulatory effect of selective MCT4 inhibitor treatment in terms of increased tumor cell killing.

4.3.2.1.3 MC38-OVA spheroid co-cultures

MCT4 inhibition induced tumor cell killing in MC38 wildtype co-cultures with immune cells. Nevertheless, MC38 tumor spheroids were not destroyed by immune cells and retained their shape after inhibition of MCT4 with and without aPD-L1. Therefore, we aimed to investigate tumor cell killing by TILs in an antigen-specific spheroid co-culture model. For this purpose, we used genetically modified MC38-OVA cells that constitutively co-express green fluorescent protein (GFP) and ovalbumin. MC38-OVA spheroids were treated with MCT inhibitors and following co-cultured with B cell depleted splenocytes isolated from spleens of OT-I mice as described for MC38 wildtype in Chapter 4.3.2.1.2 and shown in Figure 49A. OT-I T cells express a transgenic T cell receptor that recognizes ovalbumin. We stimulated OT-I T cells in an antigen-specific manner using the SIINFEKL peptide, which consists of a peptide from ovalbumin synthesized as presented by the MHC-I H-2Kb allele. After 24 h, pre-activated T cells were added to MC38 spheroid co-culture. When TILs infiltrate the spheroids, they recognize ovalbumin presented by MHC-I molecules on MC38-OVA cells. GFP fluorescence of MC38-OVA cells was monitored over time to determine MC38-OVA viability.

Even in this antigen-specific model, MC38-OVA spheroids were not affected by OT-I T cells without treatment, underlining the immunosuppressive role of lactic acid. Strikingly, MC38-OVA spheroids were completely destroyed by OT-I T cells upon MCT4 inhibition combined with aPD-L1 immune checkpoint blockade. Also, with the single MCT4 inhibitor and single aPD-L1 treatment MC38-OVA spheroids were clearly attacked, but only the combination of both drugs led to a complete dissolution of the spheroid. Interestingly, as seen for all previous experiments, dual MCT1 and MCT4 inhibition showed no impact on GFP fluorescence relative to untreated control (Figure 49B).

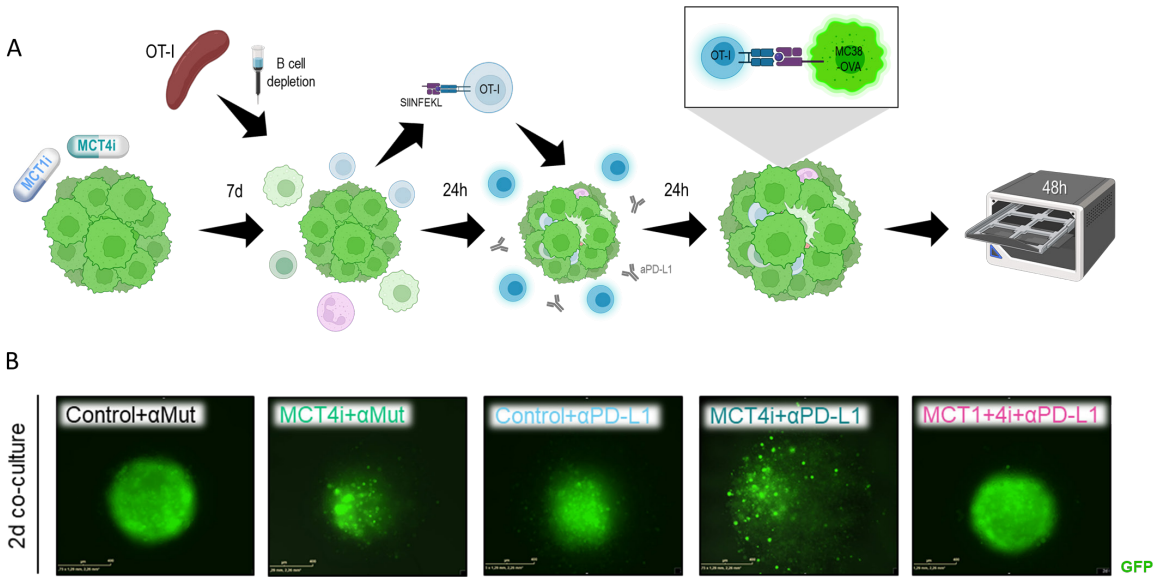

Figure 49. Induction of MC38-OVA tumor cell killing upon MCT4 inhibition with aPD-L1 treatment after 4 d co-culture with immune cells. (A) Co-culture protocol. MC38 spheroids were treated with inhibitors for 7 d. Immune cells were freshly isolated from spleen of OT-I mice, B cells were depleted and remaining of splenocytes were added for 24 h. In parallel, OT-I T cells were stimulated for 24 h with 1 µg/ml SIINFEKL peptide in the presence of 50 IU/ml IL-2. Next day, pre-activated T cells were added to MC38 spheroid co-culture along with aPD-L1 or Isotype control (αMut) for an additional 24 h. Spheroids were then washed, fresh medium containing MCT1 and/or MCT4 inhibitors was added, and Green Fluorescent Protein (GFP) expression of MC38-OVA spheroids with infiltrated immune cells were monitored under cell culture conditions for 48 h using the Incucyte Live Cell Imaging System. Created with BioRender.com. (B) Pictures showing MC38 spheroids after 4 d co-culture with immune cells. Green Fluorescence = viable cells (GFP^+).

Overall, inhibition of MCT4 in combination with the immune checkpoint inhibitor aPD-L1 enabled in complete destruction of MC38-OVA spheroids by OT-I T cells as part of an antigen-specific T cell response.

4.3.2.2 MCT inhibition augments ICB *in vivo*

Impact of MCT1 and MCT4 inhibition with and without immune checkpoint blockade were intensively studied in human and murine *in vitro* models. The results obtained so far evidence selective MCT4 inhibitors have promising potential to reverse lactic acid immunosuppression in CRC and thereby enhance T cell anti-tumor immunity. Furthermore, MCT4 inhibition might augment immunotherapy

such as immune checkpoint blockade. Based on the improved immune cell infiltration and T cell effector functions in tumor spheroids with MCT4 inhibition, MCT inhibitors were finally be tested in an animal model.

Based on our promising results using MC38 cells, we chose this cell line for *in vivo* experiments. $1x10^6$ MC38 cells were injected subcutaneously into the flank of C57BL/6 mice. Treatment was started at day 6 after cell implantation. MCT inhibitors were administered p.o. daily (AZD3965 MCT1 inhibitor (MCT1i) and MSC-4381 MCT4 inhibitor (MCT4i)) and aPD-L1 was administered i.p. every third day. We conducted 3 different types of studies (Figure 50): Survival, immune infiltration and tumor pH measurement. Survival studies were performed to evaluate the efficacy of indicated therapies. For survival studies, all treatments were continued throughout the study period until the endpoint was reached with a maximum tumor volume of 1700 mm^3. Immune infiltration and tumor pH analyses were carried out at an earlier time point. This involved measuring pH in the tumors on day 11, 12, or 13, or removing the tumors and processing them for flow cytometric analysis.

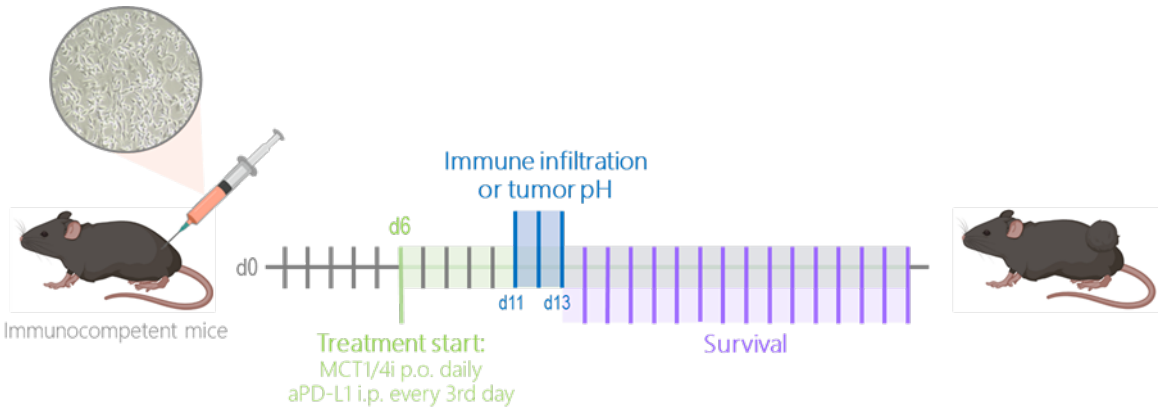

Figure 50. *In vivo* protocol. $1x10^6$ MC38 cells were injected subcutaneously into the flank of C57BL/6 mice. Treatment was started at day 6 after cell implantation. MCT inhibitors were administered p.o. daily (AZD3965 MCT1 inhibitor (MCT1i) 100 mg/kg body weight; MSC-4381 MCT4 inhibitor (MCT4i) 30 mg/kg body weight) and aPD-L1 (10 mg/kg body weight) was administered i.p. every third day. For survival/efficacy studies, all treatments were continued for entire duration of the study, until humane endpoint was reached (max tumor volume 1700 mm^3). For immune infiltration and tumor pH studies, all treatments were continued for the entire duration of the study, until tumors were collected and processed for flow cytometry analysis or pH was measured in tumors on day 11, 12 or 13. Created with BioRender.com.

4.3.2.2.1 $MC38^{wt}$ studies

4.3.2.2.1.1 Survival study

MC38 tumor cells were injected into the flank of syngeneic immunocompetent C57BL/6N mice to investigate the anti-tumor efficacy of MCT4 inhibitor (MCT4i), MCT1 inhibitor (MCT1i) and aPD-L1, as monotherapy or in combination (Table 28). Treatments were started on day 6 and continued throughout the study period until the humane endpoint was reached with a maximum tumor volume of 1700 mm^3. Tumors were measured daily.

Table 28. Treatment group assignment MC38^{WT} survival study

Treatment group	#mice
Isotype+Vehicle	12
Isotype+MCT4i	11
aPD-L1+Vehicle	12
aPD-L1+MCT4i	15
aPD-L1+MCT1i+MCT4i	12

MCT4 inhibitor monotherapy failed to inhibit tumor growth relative to vehicle control (Figure 51A). For aPD-L1 immune checkpoint blockade, we observed a separation into responders and non-responders, with responders showing slightly delayed tumor growth compared to vehicle-treated tumors (Figure 51B). Remarkably, when MCT4 inhibition and aPD-L1 treatment were combined, MC38 tumor growth was significantly delayed (Figure 51C). However, additional administration of MCT1 inhibitor showed no further benefit on tumor growth inhibition, but was also not inferior to MCT4 monotherapy, contrary to the *in vitro* experiments (Figure 51D).

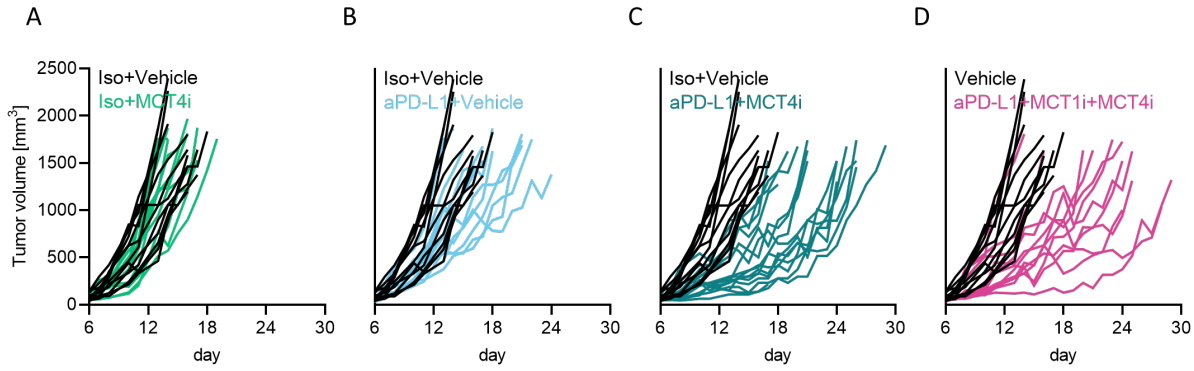

Figure 51. Delayed MC38 tumor growth with combination therapy of MCT4 inhibitor and aPD-L1 in mice bearing MC38 tumors. 1x10^6 MC38 cells were injected subcutaneously into the flank of C57BL/6 mice. Treatment was started at day 6 after cell implantation. MCT inhibitors were administered p.o. daily (AZD3965 MCT1 inhibitor (MCT1i) 100 mg/kg body weight; MSC-4381 MCT4 inhibitor (MCT4i) 30 mg/kg body weight) and aPD-L1 (10 mg/kg body weight) was administered i.p. every third day. All treatments were continued for the entire duration of the study, until humane endpoint was reached (max tumor volume 1700 mm^3). Tumor volume was monitored over time. (A-D) Individual tumor growth curves. Each line represents one mouse.

Inhibition of MC38 tumor growth by the MCT4 inhibitor in combination with aPD-L1 was reflected in significantly improved survival compared with vehicle-treated mice and aPD-L1 monotherapy. Mice treated with vehicle survived to a median of 16 days, whereas mice treated with MCT4i and aPD-L1 survived to a median of day 24. Again, additional MCT1 inhibitor treatment showed no additive effect on survival of MC38 tumor-bearing mice. Immune checkpoint blockade with aPD-L1 resulted in a modest 2-day increase in median survival compared to the vehicle-treated group (Figure 52A). As

shown in Figure 52B, MCT4i alone had no impact on MC38 tumor growth at day 13, and single aPD-L1 therapy reduced tumor volume to approximately 70 % of vehicle-treated MC38 tumors. Nevertheless, MCT4 inhibition significantly augmented immune checkpoint blockade, and tumor growth was inhibited by MCT4 and aPD-L1 therapy with a tumor volume averaging only 30 % of vehicle-treated MC38 tumors.

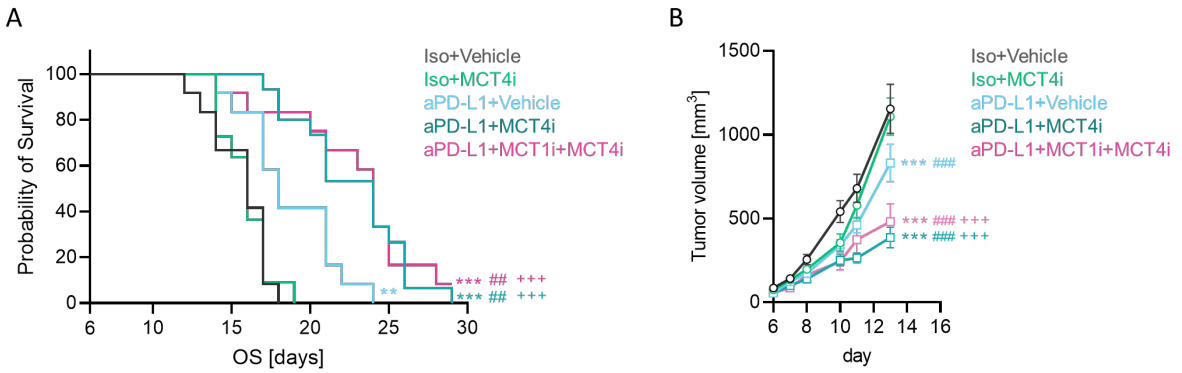

Figure 52. Improved survival with combination of MCT4 inhibitor and aPD-L1 treatment in MC38 tumor bearing mice. 1x10^6 MC38 cells were injected subcutaneously into the flank of C57BL/6 mice. Treatment was started at day 6 after cell implantation. MCT inhibitors were administered p.o. daily (AZD3965 MCT1 inhibitor (MCT1i) 100 mg/kg body weight; MSC-4381 MCT4 inhibitor (MCT4i) 30 mg/kg body weight) and aPD-L1 (10 mg/kg body weight) was administered i.p. every third day. All treatments were continued for the entire duration of the study, until humane endpoint was reached (max tumor volume 1700 mm^3). (A) Survival plotted as Kaplan Meier estimation curve. Significance was calculated applying the log-rank (Mantel-Cox) test with correction for multiple testing (Bonferroni correction of the p value for the number of statistical tests (n = 10) performed (**p < 0.01 compared to vehicle; ***p < 0.001 compared to vehicle; ##p < 0.01 compared to aPD-L1; +++p < 0.001 compared to MCT4i). (B) Tumor volume was monitored over time. Mean + SEM is shown. Significance was determined by 2-way ANOVA and post-hoc Tukey's multiple comparisons (***p < 0.001 compared to Vehicle; ##p < 0.01 compared to aPD-L1; +++p < 0.001 compared to MCT4i).

All treatment groups had comparable tumor weights at the end of the study. Furthermore, we did not observe any toxic effects or changes in liver or body weight upon MCT inhibition or immune checkpoint blockade (Figure 53A,C,D). Interestingly, we detected an increase in spleen weight in all treatment groups receiving aPD-L1, indicating activation of the immune system (Figure 53B).

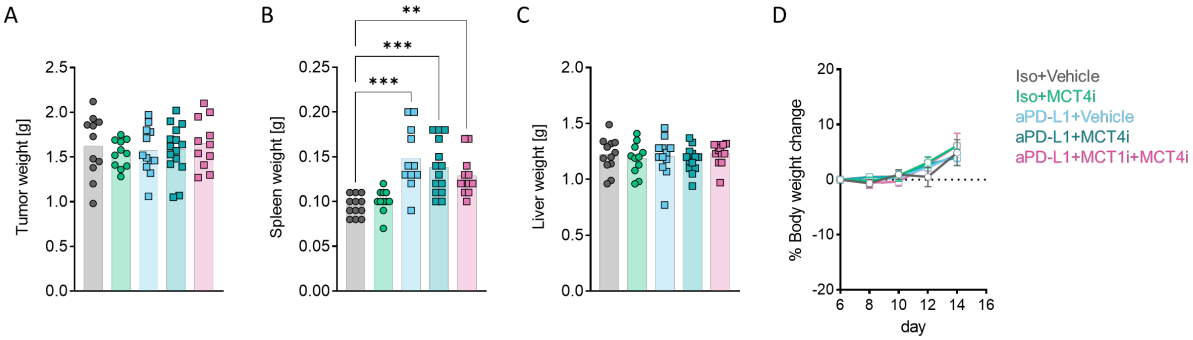

Figure 53. No toxic effects upon MCT4 inhibitor and aPD-L1 combination therapy but increased spleen weight upon immune checkpoint inhibition. 1x10^6 MC38 cells were injected subcutaneously into the flank of C57BL/6 mice. Treatment was started at day 6 after cell implantation. MCT inhibitors were administered p.o. daily (AZD3965 MCT1 inhibitor (MCT1i) 100 mg/kg body weight; MSC-4381 MCT4 inhibitor (MCT4i) 30 mg/kg body weight) and aPD-L1 (10 mg/kg body weight) was administered i.p. every third day. All treatments were continued for the entire

duration of the study, until humane endpoint was reached (max tumor volume 1700 mm^3). (A) Tumor weight. (B) Spleen weight. Significance was determined using one-way ANOVA and post-hoc Bonferroni multiple comparison test (*p < 0.05; ***p < 0.001). (C) Liver weight. Median values with single data points are shown. (D) Body weight was monitored over time and the percentage Body Weight Change (% BWC) was calculated relatively to the individual body weight at treatment start. Mean + SEM is shown.

Overall, monotherapy with the MCT4 inhibitor failed to improve anti-tumor response, but in combination with aPD-L1 immune checkpoint blockade, it acts synergistically to delay tumor growth and prolong survival.

4.3.2.2.1.2 Immune infiltration study

The efficacy study with mice bearing MC38 tumors revealed that the immune checkpoint blockade was significantly improved by treatment with MCT4 inhibitor. However, the additional administration of MCT1 had no further beneficial effect, so in keeping with the 3Rs (Replacement, Reduction, Refinement) as principle of experimental scientific work, we continued with the MCT4 inhibitor and omitted the MCT1 inhibitor. Interestingly, we noticed increased spleen weight in treatment groups with delayed tumor growth, suggesting immune activation. Thus, we were interested in the immune infiltrate of MC38 tumors with and without treatments. For this purpose, MC38 tumor cells were injected into the flank of syngeneic immunocompetent C57BL/6N mice (Table 29). At the time point at which we observed the greatest differences in tumor volume between mice treated with vehicle and mice treated with MCT4i and aPD-L1, namely day 11-13, tumors were harvested and processed for flow cytometry.

Table 29. Treatment group assignment $MC38^{wt}$ immune infiltration study

Treatment group	#mice for tumor growth	#mice for flow cytometry
Isotype+Vehicle	5	5
Isotype+MCT4i	6	6
aPD-L1+Vehicle	7	6
aPD-L1+MCT4i	8	6

Consistent with the survival study, MC38 tumor growth was inhibited upon combination therapy of aPD-L1 with MCT4 inhibitor (Figure 54).

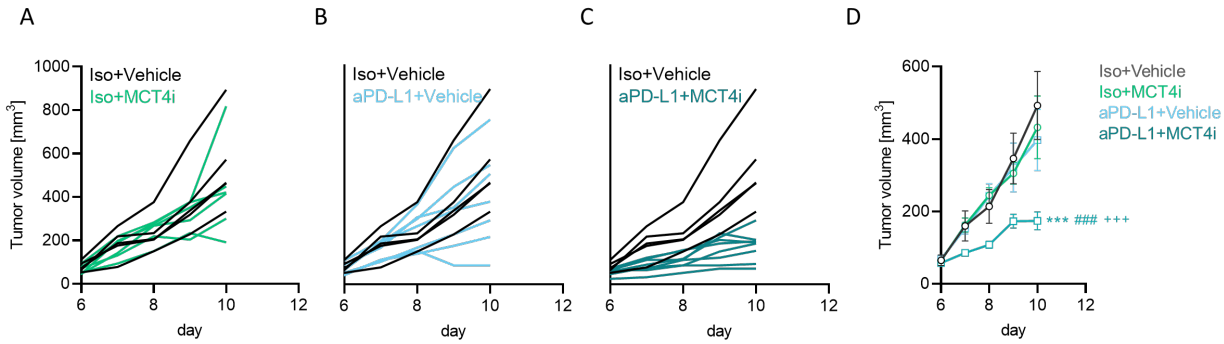

Figure 54. Delayed MC38 tumor growth with combination therapy of MCT4 inhibitor and aPD-L1 in mice bearing MC38 tumors. 1x10^6 MC38 cells were injected subcutaneously into the flank of C57BL/6 mice. Treatment was started at day 6 after cell implantation. MSC-4381 MCT4 inhibitor (MCT4i) (30 mg/kg body weight) was administered p.o. daily and aPD-L1 (10 mg/kg body weight) was administered i.p. every third day. All treatments were continued for the entire duration of the study, until tumors were collected and processed for flow cytometry analysis or pH measurements on day 11, 12 or 13. Tumor volume was monitored over time. (A-C) Individual tumor growth curves. Each line represents one mouse. (D) Mean + SEM of tumor growth is shown. Significance was determined by 2-way ANOVA and post-hoc Tukey's multiple comparisons (***p < 0.001 compared to Vehicle; ###p < 0.001 compared to aPD-L1; +++p < 0.001 compared to MCT4i).

We attempted to match the tumor weights between the groups as much as possible on the day of termination, but due to the growth inhibition under MCT4i and aPD-L1 therapy, the tumors tended to be smaller. However, this difference was not significant (Figure 55A). At this earlier time point, spleen weight of MC38 tumor-bearing mice was not yet increased upon immune checkpoint blockade (Figure 55B). No Toxic effects were observed on livers of mice included in the study (Figure 55C).

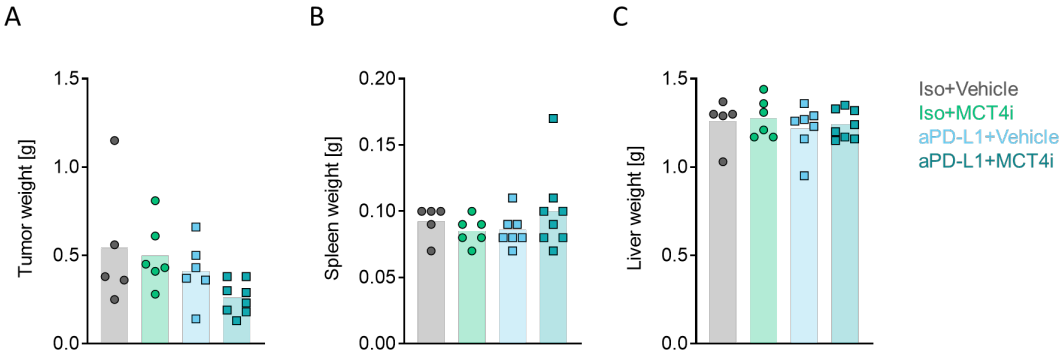

Figure 55. No toxic effects upon MCT4 inhibitor and aPD-L1 combination therapy. 1x10^6 MC38 cells were injected subcutaneously into the flank of C57BL/6 mice. Treatment was started at day 6 after cell implantation. MSC-4381 MCT4 inhibitor (MCT4i) (30 mg/kg body weight) was administered p.o. daily and aPD-L1 (10 mg/kg body weight) was administered i.p. every third day. All treatments were continued for the entire duration of the study until tumors were collected and processed for flow cytometry analysis or pH measurements on day 11, 12 or 13. (A) Tumor weight. (B) Spleen weight. (C) Liver weight. Median values with single data points are shown.

Tumors were harvested and single cell suspensions were prepared as described in Chapter 3.6.4. Immune cell populations were determined as shown in the gating strategy in Figure 56, staining the following common immune cell marker: CD45 as pan-leukocyte marker, CD3, CD4 and CD8 as T cell markers, Foxp3 as marker for regulatory T cells. NK1.1 as marker for Natural Killer cells (NK cells), CD11b as marker for myeloid cells, further characterized as myeloid suppressor cells by Gr-1, and F4/80

as marker for tumor-associated macrophages (TAMs). Dead cells and doublets were excluded from all analyses.

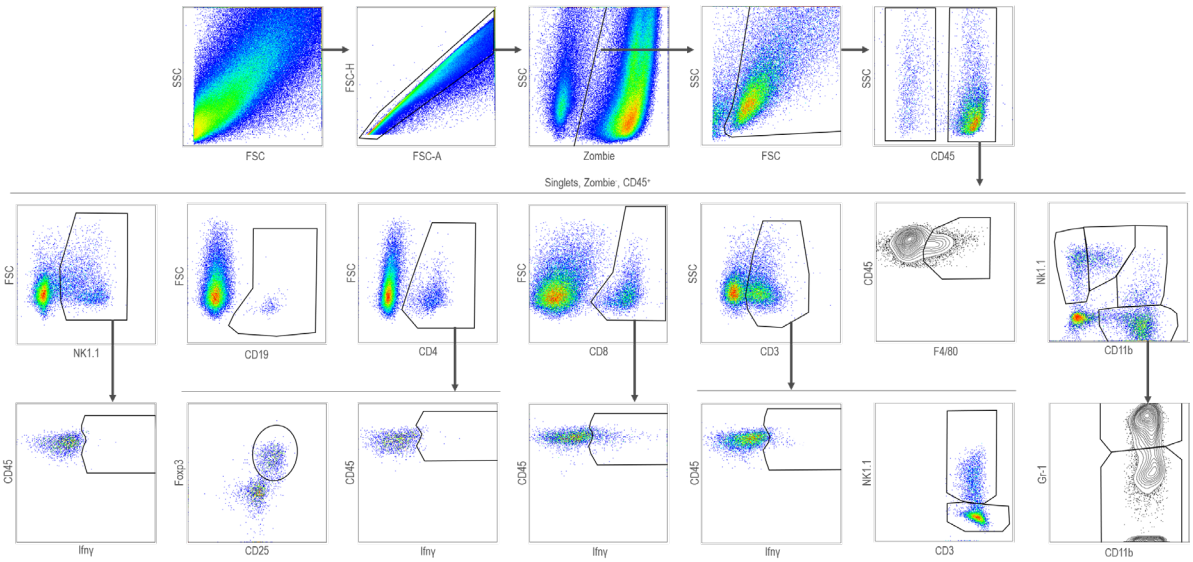

Figure 56. Gating strategy for analysis of MC38 immune infiltrate. 1x10^6 MC38 cells were injected subcutaneously into the flank of C57BL/6 mice. Treatment was started at day 6 after cell implantation. MSC-4381 MCT4 inhibitor (MCT4i) (30 mg/kg body weight) was administered p.o. daily and aPD-L1 (10 mg/kg body weight) was administered i.p. every third day. All treatments were continued for the entire duration of the study, until tumors were collected and processed for flow cytometry analysis or pH measurements on day 11, 12 or 13. Gating strategy for leukocytes (CD45$^+$) among total living (Zombie$^-$) singular cells. T cells were designated as CD3$^+$, CD8$^+$ or CD4$^+$ T cells, Foxp3$^+$ CD4$^+$ regulatory T cells (Treg) and double negative CD4$^-$ CD8$^-$ T cells. Natural Killer cells (NK cells) were determined as NK1.1$^+$ and Natural Killer T cells (NK T cells) as CD3$^+$ NK1.1$^+$. Myeloid cells were determined as CD11b$^+$. Tumor-associated Gr-1$^+$ myeloid suppressor cells (MDSCs), Gr-1$^-$ myeloid cells were determined among CD11b$^+$ cells. Tumor-associated macrophages (TAMs) were determined as F4/80$^+$.

Figure 57 provides an overview of the composition of leucocytes in MC38 tumors. Myeloid cells were most abundant in MC38 tumors with approximately 40 % CD11b$^+$ myeloid cells and 30 % TAMs among CD45$^+$ cells (Figure 57C). Only about 20 % of leucocytes were T cells and 10 % NK cells (Figure 57B,C). Strikingly, aPD-L1 therapy in combination with MCT4 inhibition increased CD8$^+$ T cell infiltration in MC38 tumors relative to the vehicle-treated group. However, no changes were detected in CD4$^+$ T cells, CD4$^+$ Foxp3$^+$ regulatory T cells or NK cells by MCT inhibition or aPD-L1 application (Figure 57A,B). Interestingly, the phenotype of myeloid cells shifted from suppressive Gr-1$^+$ CD11b$^+$ cells to Gr-1$^-$ CD11b$^+$ immunocompetent cells. Infiltration of TAMs was not affected by any therapy (Figure 57C).

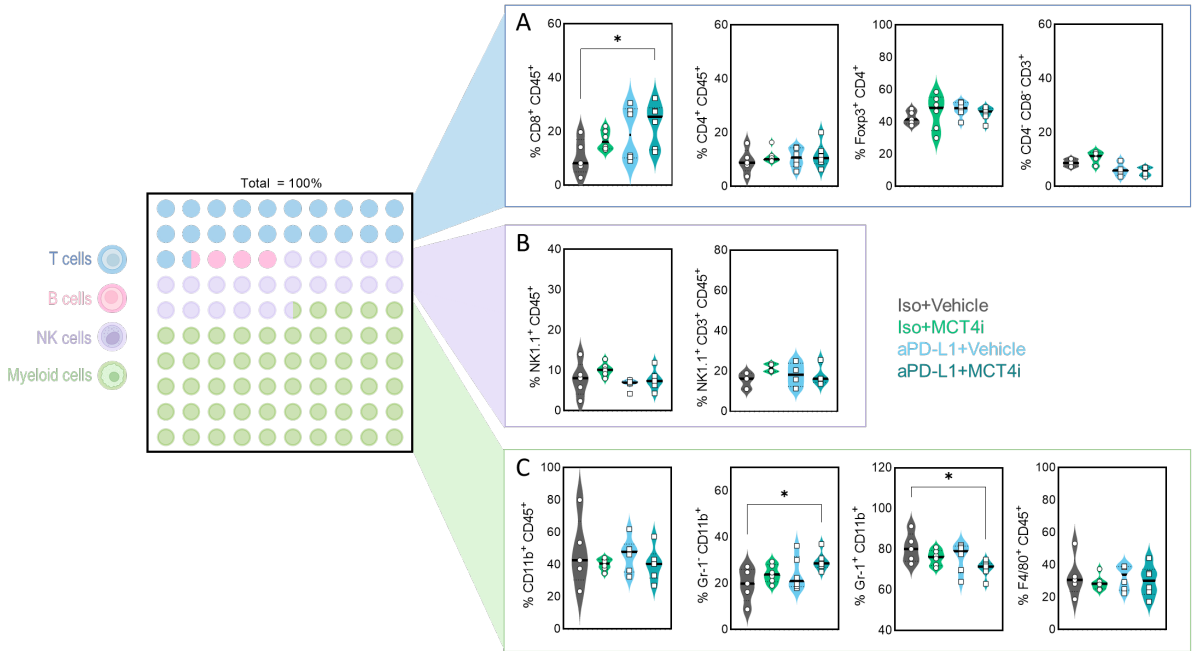

Figure 57. Composition of immune cells in MC38 tumors. 1x10^6 MC38 cells were injected subcutaneously into the flank of C57BL/6 mice. Treatment was started at day 6 after cell implantation. MSC-4381 MCT4 inhibitor (MCT4i) (30 mg/kg body weight) was administered p.o. daily and aPD-L1 (10 mg/kg body weight) was administered i.p. every third day. All treatments were continued for the entire duration of the study, until tumors were collected and processed for flow cytometry analysis or pH measurements on day 11, 12 or 13. Gated on single, viable cells and CD45$^+$ immune cells. (A) Percentage of CD8$^+$ T cells, CD4$^+$ T cells, Foxp3$^+$ CD4$^+$ regulatory T cells (Treg) and double negative CD4$^-$ CD8$^-$ T cells. (B) Percentage of NK1.1$^+$ Natural Killer (NK) cells and CD3$^+$ NK1.1$^+$ Natural Killer T cells (NK T cells). (C) Percentage of tumor-associated Gr-1$^+$ myeloid suppressor cells (MDSCs), Gr-1$^-$ CD11b$^+$ myeloid cells and F4/80$^+$ tumor-associated macrophages (TAMs). Median values with single data points are shown. Significance was determined using one-way ANOVA and post-hoc Bonferroni multiple comparison test (*p < 0.05). Pictures of cells were created with BioRender.com.

Cytotoxic T cells are the major mediators of anti-tumor immunity, moreover the number of TILs has been associated with a better prognosis (26,27,129) in CRC. In line with *in vitro* experiments and *in vivo* tumor growth, T cell infiltration in MC38 tumors was improved by combination of MCT4 inhibitor and aPD-L1, but not by single treatments (Figure 58A). In particular, more CD8$^+$ T cells were found in the immune infiltrate of MC38 tumors, whereas the CD4$^+$ T cell compartment was not altered (Figure 57B,C). Beside the quantity of TILs, IFNγ signature has been shown to predict response to immunotherapy in various tumor entities (343–346). *In vitro* spheroid co-cultures indicated an enhanced interferon production upon MCT4 inhibition. Indeed, we found significantly increased numbers of Ifnγ$^+$ CD8$^+$ T cells in MC38 tumors when mice were treated with aPD-L1 and MCT4i, but aPD-L1 as monotherapy also tended to enhance the abundance CD8$^+$ and moreover Ifnγ$^+$ cells among CD8$^+$ T cells in MC38 tumors of some mice (Figure 58B).

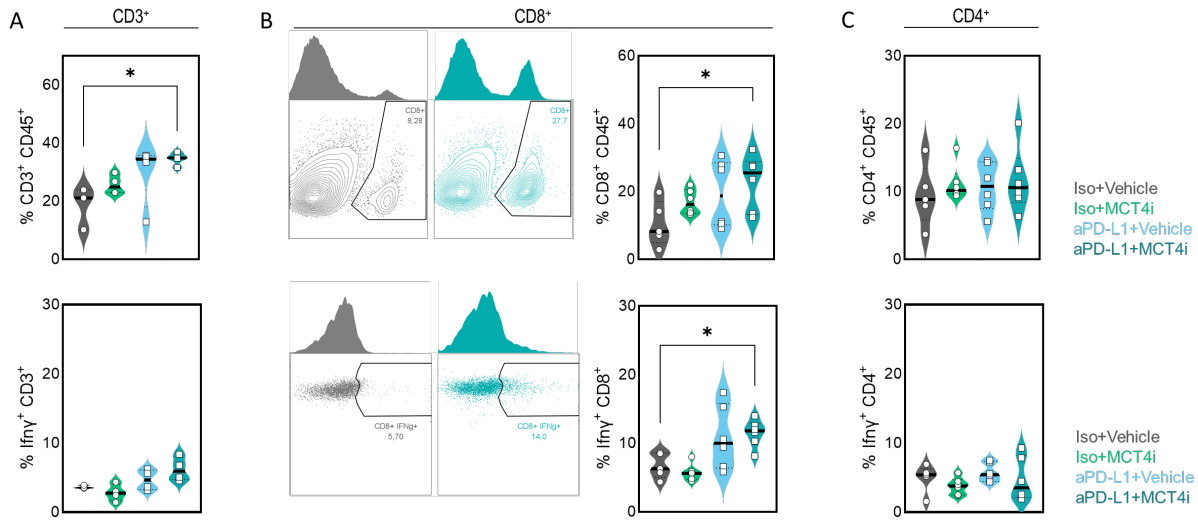

Figure 58. Increased numbers of CD8⁺ Ifnγ⁺ T cells in MC38 tumors with MCT4 inhibitor and aPD-L1 combination therapy. 1x10⁶ MC38 cells were injected subcutaneously into the flank of C57BL/6 mice. Treatment was started at day 6 after cell implantation. MSC-4381 MCT4 inhibitor (MCT4i) (30 mg/kg body weight) was administered p.o. daily and aPD-L1 (10 mg/kg body weight) was administered i.p. every third day. All treatments were continued for the entire duration of the study, until tumors were collected and processed for flow cytometry analysis or pH measurements on day 11, 12 or 13. (A-C) Gated on single, viable cells. (A) Percentage of CD3⁺ T cells among CD45⁺ cells and percentage of interferon γ positive (Ifnγ⁺) cells among CD3⁺ T cells. (B) Percentage of CD8⁺ T cells among CD45⁺ cells and percentage of Ifnγ⁺ cells among CD8⁺ T cells. (C) Percentage of CD4⁺ T cells among CD45⁺ cells and percentage of Ifnγ⁺ cells among CD4⁺ T cells. Representative plots (B) and median values (A-C) with single data points are shown. Significance was determined using one-way ANOVA and post-hoc Bonferroni multiple comparison test (*p < 0.05).

Although T cell infiltration and function were improved by treatment with MCT4 inhibitor and aPD-L1 treatment, neither frequencies of NK and NKT cells were elevated nor their Ifnγ production increased in MC38 tumors upon MCT inhibition and/or immune checkpoint blockade (Figure 59A,B).

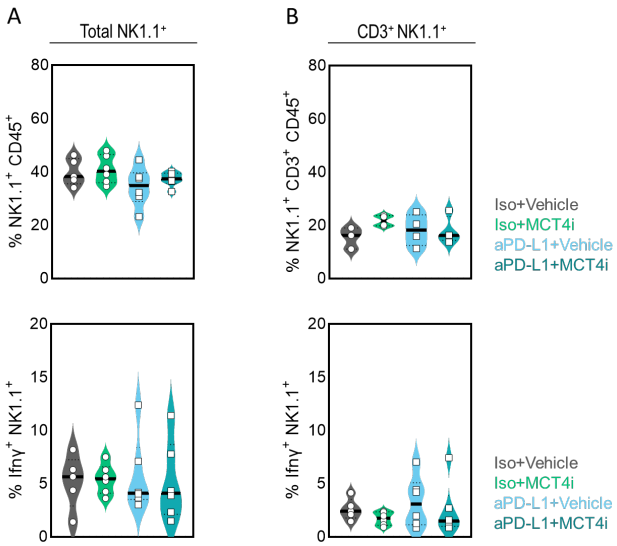

Figure 59. No changes in NK cells in MC38 tumors with MCT4 inhibitor and aPD-L1 combination therapy. 1x10⁶ MC38 cells were injected subcutaneously into the flank of C57BL/6 mice. Treatment was started at day 6 after cell implantation. MSC-4381 MCT4 inhibitor (MCT4i) (30 mg/kg body weight) was administered p.o. daily and aPD-L1 (10 mg/kg body weight) was administered i.p. every third day. All treatments were continued for the entire duration of the study, until tumors were collected and processed for flow cytometry analysis or pH measurements on day

11, 12 or 13. (A-B) Gated on single, viable cells. (A) Percentage of NK1.1$^+$ Natural Killer (NK) cells among CD45$^+$ cells and percentage of interferon γ positive (Ifnγ$^+$) cells among NK cells. (B) Percentage of CD3$^+$ NK1.1$^+$ Natural Killer T cells (NK T cells) among CD45$^+$ cells and percentage of interferon γ positive (Ifnγ$^+$) cells among NK T cells. Median values with single data points are shown.

Consistent with other studies, we found that myeloid cells represent the largest compartment within the immune infiltrate of MC38 tumors grown in immunocompetent mice. However, it has been estimated that 80 % of studies that have attempted to relate tumor-associated macrophage density to prognosis in any type of cancer have found a negative correlation, whereas less than 10 % have found a positive correlation (137,332,333). Lactic acid has been shown to contribute to tumor-promoting polarization of myeloid cells in the TME (38,39).

Indeed, in MC38 tumors with MCT4 inhibitor and aPD-L1 treatment, we found fewer suppressive Gr-1$^+$ myeloid cells among CD11b$^+$ cells compared with vehicle-treated mice (Figure 60B,C). Moreover, MHC-II expression tended to be upregulated in CD11b$^+$ myeloid cells and F4/80$^+$ TAMs by MCT4 inhibition and aPD-L1 immune checkpoint blockade referring to vehicle control (Figure 60A,B). In general, MHC-II was barely found on suppressive Gr-1$^+$ myeloid cells but highly expressed on Gr-1$^-$ tumor-associated myeloid cells. However, the expression of MHC-II even in Gr-1$^+$ cells tended to be induced by the combination of MCT4i and aPD-L1 (Figure 60B,C). No effects on the myeloid cells and MHC-II examined were observed with MCT4 inhibitor or aPD-L1 monotherapy.

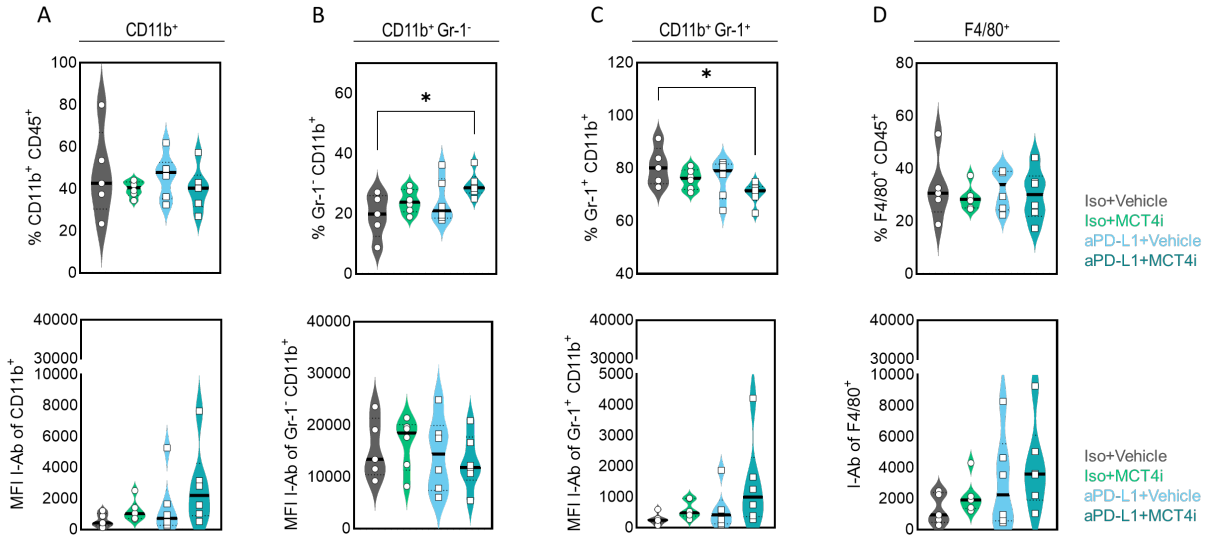

Figure 60. Impact of MCT inhibition on myeloid cells in MC38 tumors. 1x10^6 MC38 cells were injected subcutaneously into the flank of C57BL/6 mice. Treatment was started at day 6 after cell implantation. MSC-4381 MCT4 inhibitor (MCT4i) (30 mg/kg body weight) was administered p.o. daily and aPD-L1 (10 mg/kg body weight) was administered i.p. every third day. All treatments were continued for the entire duration of the study, until tumors were collected and processed for flow cytometry analysis or pH measurements on day 11, 12 or 13. (A-D) Gated on single, viable cells. (A) Percentage of CD11b$^+$ myeloid cells among CD45$^+$ cells and Median Fluorescence Intensity (MFI) of I-Ab (MHC-II) cells among CD11b$^+$ cells. (B) Percentage of Gr-1$^+$ CD11b$^+$ myeloid suppressor cells (MDSCs) among CD45$^+$ cells and MFI of I-Ab (MHC-II) cells among MDSCs cells. (C) Percentage of Gr-1$^-$ CD11b$^+$ myeloid cells among CD45$^+$ cells and MFI of I-Ab (MHC-II) cells among Gr-1$^-$ CD11b$^+$ myeloid cells. (D) Percentage of F4/80$^+$ tumor-associated macrophages (TAMs) cells among CD45$^+$ cells and MFI of I-Ab (MHC-II) cells among TAMs.

Median values with single data points are shown. Significance was determined using one-way ANOVA and post-hoc Bonferroni multiple comparison test (*p < 0.05).

To evaluate whether the effects of MCT4 inhibitors are due to a remodeling of the TME, we investigated leukocytes in the spleen, blood, and draining lymph nodes of MC38 tumor-bearing mice compared with the tumor immune infiltrate. However, we could not detect any of the effects found in the tumor on T cell infiltration, Ifnγ production or density of Gr-1$^+$ suppressive myeloid cells in spleen, blood or lymph nodes with MCT inhibition and/or immune checkpoint blockade (Figure 61). This suggest, MCT4 inhibitor treatment in combination with aPD-L1 acts primarily in the tumor milieu.

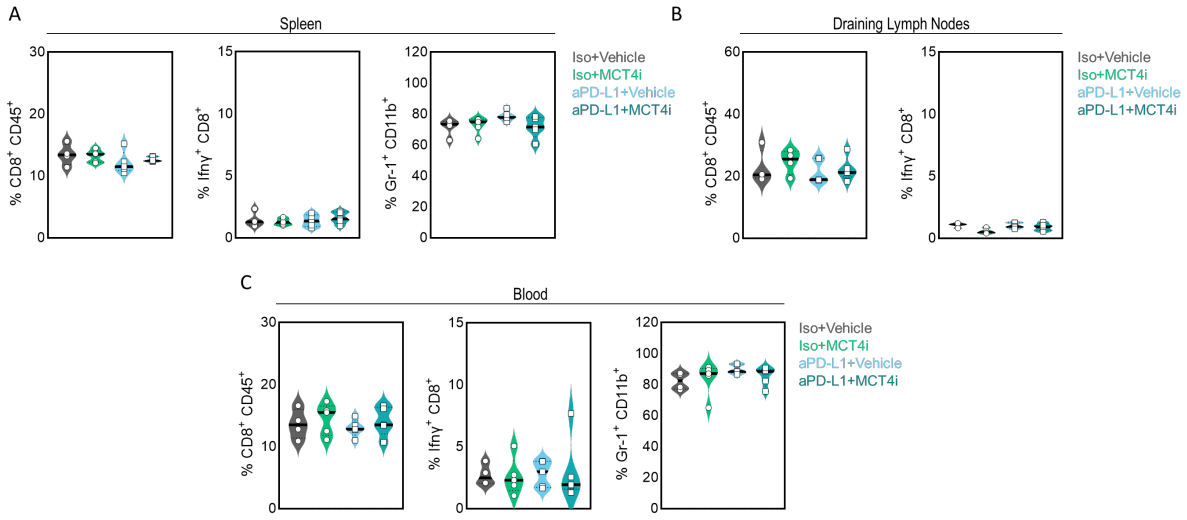

Figure 61. Tumor-specific effect of MCT inhibition on immune cells in mice bearing MC38 tumors. 1x10^6 MC38 cells were injected subcutaneously into the flank of C57BL/6 mice. Treatment was started at day 6 after cell implantation. MSC-4381 MCT4 inhibitor (MCT4i) (30 mg/kg body weight) was administered p.o. daily and aPD-L1 (10 mg/kg body weight) was administered i.p. every third day. All treatments were continued for the entire duration of the study, until tumors were collected and processed for flow cytometry analysis or pH measurements on day 11, 12 or 13. Gated on single, viable cells and CD45$^+$ immune cells. (A) Percentage of CD8$^+$ T cells, interferon γ positive (Ifnγ$^+$) CD8$^+$ T cells and Gr-1$^+$ CD11b$^+$ positive tumor-associated myeloid suppressor cells (MDSCs) in spleens of MC38 tumor bearing mice. (B) Percentage of CD8$^+$ T cells, Ifnγ$^+$) CD8$^+$ T cells in lymph nodes of MC38 tumor bearing mice. (C) Percentage of CD8$^+$ T cells, Ifnγ$^+$ CD8$^+$ T cells and Gr-1$^+$ CD11b$^+$ MDSCs in blood of MC38 tumor bearing mice. Median values with single data points are shown.

In addition to lactic acid, elevated levels of reactive oxygen species (ROS), often found in tumors, have been discussed as an immunosuppressive factor (348,349). Indeed, we found high ROS levels in tumor cells of MC38 tumors (Figure 62A). While tumor cells often develop antioxidant defense mechanisms to prevent damage by ROS, immune cells evolve more susceptible ROS-induced dysfunction and apoptosis (350). Indeed, MC38 tumor-associated CD8$^+$ T cells and NK$^+$ cells tended to increased ROS levels compared to T cells and NK cells in blood of tumor-bearing mice (Figure 62B,C). The same trend of high ROS was observed for Gr-1$^-$ myeloid cells and TAMs compared to those circulating in blood (Figure 62D). Following, ROS might be another cause for immunosuppression in the TME. However, none of the indicated treatments did modulate ROS production in any cell type (Figure 62).

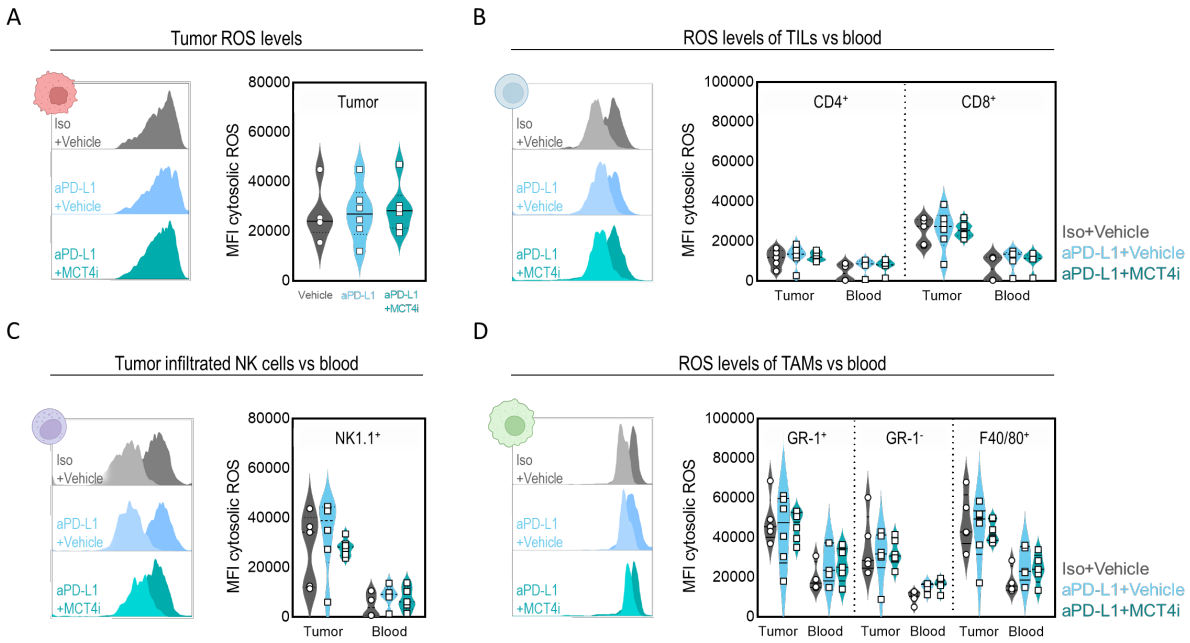

Figure 62. Increased ROS levels in immune cells in a tumor environment. 1x10^6 MC38 cells were injected subcutaneously into the flank of C57BL/6 mice. Treatment was started at day 6 after cell implantation. MSC-4381 MCT4 inhibitor (MCT4i) (30 mg/kg body weight) was administered p.o. daily and aPD-L1 (10 mg/kg body weight) was administered i.p. every third day. All treatments were continued for the entire duration of the study, until tumors were collected and processed for flow cytometry analysis or pH measurements on day 11, 12 or 13. Gated on single, viable cells and CD45$^+$ immune cells. (A-D) Reactive oxygen species (ROS) was determined by 2',7'-Dichlordihydrofluorescein-diacetat (DCFDA) staining and flow cytometry analysis. (A) Median Fluorescence Intensity (MFI) of ROS in MC38 tumor cells. (B) MFI of ROS in tumor-infiltrated CD4$^+$ and CD8$^+$ T cells (TILs) versus blood T cells. (C) MFI of ROS in tumor-infiltrated NK1.1$^+$ Natural Killer (NK) cells versus blood NK cells. (D) MFI of ROS in tumor-associated Gr-1$^+$, Gr-1$^-$ CD11b$^+$ myeloid cells and F4/80$^+$ tumor-associated macrophages (TAMs) versus blood myeloid cells. Representative plots and median values with single data points are shown. (B-D) Brighter histograms display MFI from blood cells darker histograms display MFI from tumor-infiltrated cells. Pictures of cells were created with BioRender.com.

In conclusion, MCT4 monotherapy failed to inhibit tumor progression in an MC38 tumor model compared to vehicle treated control. However, aPD-L1 monotherapy delayed tumor growth in some mice and moderately prolonged median survival of mice bearing MC38 tumors. By contrast, the combination therapy of MCT4 inhibitor and aPD-L1 acted synergistically to inhibit tumor growth and improve survival, which may be due to improved CD8$^+$ T cell performance in terms of infiltration and Ifnγ production. Nevertheless, additional MCT1 inhibition showed no further effect on tumor growth inhibition and survival compared with MCT4i along with aPD-L1, suggesting that in the MC38 tumor model, MCT4 inhibition alone was sufficient to remodel the TME. All treatments were well tolerated by mice bearing MC38 tumors, with no adverse effects observed.

4.3.2.2.1.3 Tumor pH study

MCT1 and MCT4 are the major tumor-associated lactate transporters that maintain the glycolytic phenotype of cancer cells by constantly exporting lactate in co-transport with protons. This leads to lactic acidosis of the TME. In our *in vitro* studies, we confirmed the prevention of tumor-induced lactic

acidosis by inhibiting MCTs. Interestingly, in both human HCT116 and murine MC38 spheroid co-cultures, selective treatment with MCT4 inhibitors was shown to be sufficient to reduce lactate. In an *in vivo* MC38 tumor model, MCT4 inhibition was able to delay tumor progression only in combination with aPD-L1 as immune checkpoint therapy. However, we were interested in the underlying mechanism and whether the improved immune surveillance was due to the reduced lactate acidosis by MCT4 inhibition. Therefore, we aimed to measure pH in tumors. Since metabolism and tissue pH change immediately after death, we measured pH in tumors of anesthetized mice using a special microprobe pH meter.

For this purpose, MC38 tumor cells were injected into the flank of syngeneic immunocompetent C57BL/6N mice (Table 30). At the time point at which we observed the greatest differences in tumor volume between mice treated with vehicle and mice treated with MCT4i and aPD-L1, namely day 11-13, pH was assessed in tumors of anesthetized mice.

Table 30. Treatment group assignment MC38^{wt} tumor pH study

Treatment group	#mice for tumor growth	#mice for pH measurement
Isotype+Vehicle	4	4
Isotype+MCT4i	7	5
aPD-L1+Vehicle	4	3
aPD-L1+MCT4i	6	5

In line with the previous *in vivo* studies, MC38 tumor growth was inhibited by combination therapy of aPD-L1 with MCT4 inhibitor (Figure 63).

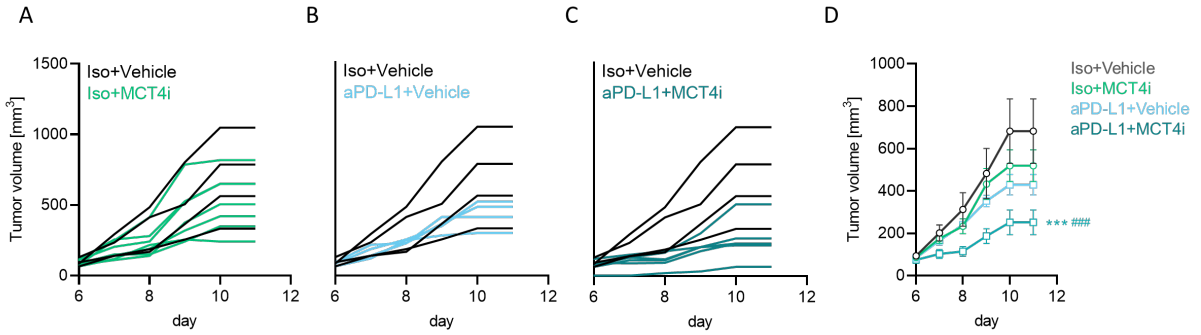

Figure 63. Delayed MC38 tumor growth with combination therapy of MCT4 inhibitor and aPD-L1 in mice bearing MC38 tumors. 1x10^6 MC38 cells were injected subcutaneously into the flank of C57BL/6 mice. Treatment was started at day 6 after cell implantation. MCT inhibitors were administered p.o. daily (AZD3965 MCT1 inhibitor (MCT1i) 100 mg/kg body weight; MSC-4381 MCT4 inhibitor (MCT4i) 30 mg/kg body weight) and aPD-L1 (10 mg/kg body weight) was administered i.p. every third day. All treatments were continued for the entire duration of the study, until tumors were collected and processed for flow cytometry analysis or pH measurements on day 11, 12 or 13. Tumor volume was monitored over time. (A-C) Individual tumor growth curves. Each line represents one mouse. (D) Mean + SEM of tumor growth is shown. Significance was

determined by 2-way ANOVA and post-hoc Tukey's multiple comparisons (***p < 0.001 compared to Vehicle; ###p < 0.001 compared to aPD-L1).

As in immune infiltration study, we attempted to match the tumor weights between the groups as much as possible on the day of pH measurement, but due to the growth inhibition under MCT4i and aPD-L1 therapy, the tumors tended to be smaller in this group (Figure 64A). Again, at this earlier timepoint, spleen weight of MC38 tumor-bearing mice was not yet increased upon immune checkpoint blockade (Figure 64B). No toxic effects were observed on livers of mice included in the study (Figure 64C).

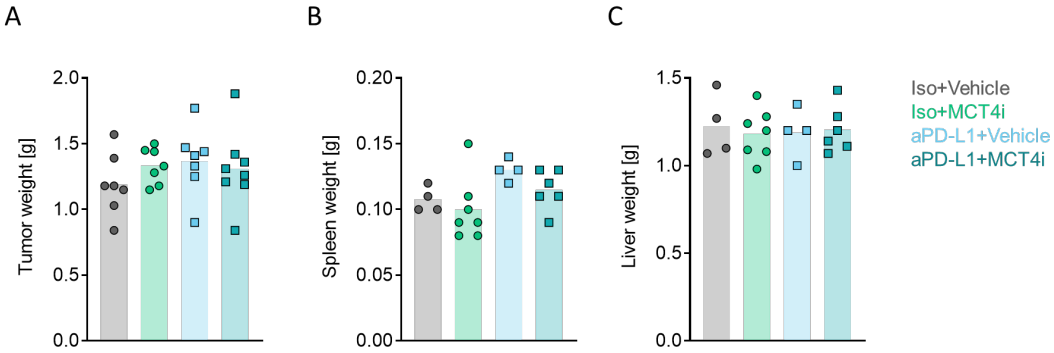

Figure 64. No toxic effects upon MCT4 inhibitor and aPD-L1 combination therapy but increased spleen weight. $1x10^6$ MC38 cells were injected subcutaneously into the flank of C57BL/6 mice. Treatment was started at day 6 after cell implantation. MCT inhibitors were administered p.o. daily (AZD3965 MCT1 inhibitor (MCT1i) 100 mg/kg body weight; MSC-4381 MCT4 inhibitor (MCT4i) 30 mg/kg body weight) and aPD-L1 (10 mg/kg body weight) was administered i.p. every third day. All treatments were continued for the entire duration of the study, until tumors were collected and processed for pH measurements on day 11, 12 or 13. (A) Tumor weight. (B) Spleen weight. (C) Liver weight. Median values with single data points are shown.

Ultimately, blocking MCTs in tumor cells might be associated with a restriction of glycolysis in tumor cells. Therefore, we analyzed glucose uptake using 2-deoxy-2-[(7-nitro-2,1,3-benzoxadiazol-4-yl)amino]-D-glucose (2NBDG). 2NBDG is a fluorescent glucose analogue taken up by GLUT-1 glucose transporters, which are frequently overexpressed in Warburg tumors (37). Indeed, glucose uptake by MC38 tumor cells was reduced by inhibition of MCT4 in conjunction with aPD-L1 compared with vehicle-treated control, suggesting decreased glycolysis (Figure 65A). Complementary, glucose concentrations were measured in the TME of MC38 tumors by the Institute for Functional Genomics at the University of Regensburg. Consistent with decreased glucose uptake by MC38 tumor cells, we found increased glucose levels in the TME of MC38 tumors after MCT4i and aPD-L1 treatment compared with vehicle-treated tumors (Figure 65B). However, none of the immune cell compartments examined were affected in their 2NBDG uptake by anti-glycolytic treatment (Figure 65C).

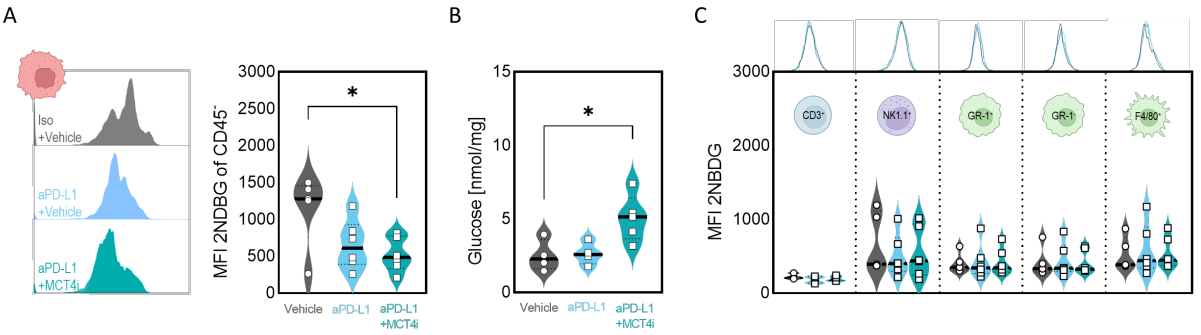

Figure 65. Glucose consumption is restricted in MC38 tumor cells. 1x10^6 MC38 cells were injected subcutaneously into the flank of C57BL/6 mice. Treatment was started at day 6 after cell implantation. MSC-4381 MCT4 inhibitor (MCT4i) (30 mg/kg body weight) was administered p.o. daily and aPD-L1 (10 mg/kg body weight) was administered i.p. every third day. All treatments were continued for the entire duration of the study, until tumors were collected and processed for flow cytometry analysis or pH measurements on day 11, 12 or 13. (A,C) Glucose uptake was determined via 2-deoxy-2-[(7-nitro-2,1,3-benzoxadiazol-4-yl)amino]-D-glucose (2NBDG) staining and analysis by flow cytometry. (A) Median Fluorescence intensity (MFI) of 2NBDG in MC38 tumor cells. (B) D-Glucose concentration in tumors was measured by the Institute for Functional Genomics, University of Regensburg. (C) Median Fluorescence intensity of 2NBDG in immune cells (CD3$^+$ T cells, NK1.1$^+$ Natural Killer (NK) cells, Gr-1$^+$ and Gr-1$^-$ tumor-associated myeloid cells and F4/80$^+$ tumor associated macrophages (TAMs) tumor cells. Median values with single data points are shown. Representative plots and median values with single data points are shown. Significance was determined using one-way ANOVA and post-hoc Bonferroni multiple comparison test (*$p < 0.05$). Pictures of cells were created with BioRender.com.

Glucose is not necessarily the only source for lactate production. Another source can be, for instance, glutamine, which can be metabolized into lactate. Therefore, we were interested in the link between lactate and glucose. In MC38 tumors that were not treated or treated with immune checkpoint blockers and MCT4 inhibitors, we found a significant negative correlation between glucose and lactate, suggesting that tumor-derived lactate might originate from glucose (Figure 66A).

If glycolysis of MC38 tumor cells would be impaired by MCT4i therapy, not only glucose consumption but also TME acidification could be prevented. Interestingly, when we evaluated the pH levels of tumors with aPD-L1 immune checkpoint blockade, we found increased tumor pH values when MCT4 inhibitor was present compared with aPD-L1 as monotherapy. However, aPD-L1 alone decreased the pH of MC38 tumors compared with vehicle-treated control (Figure 66B).

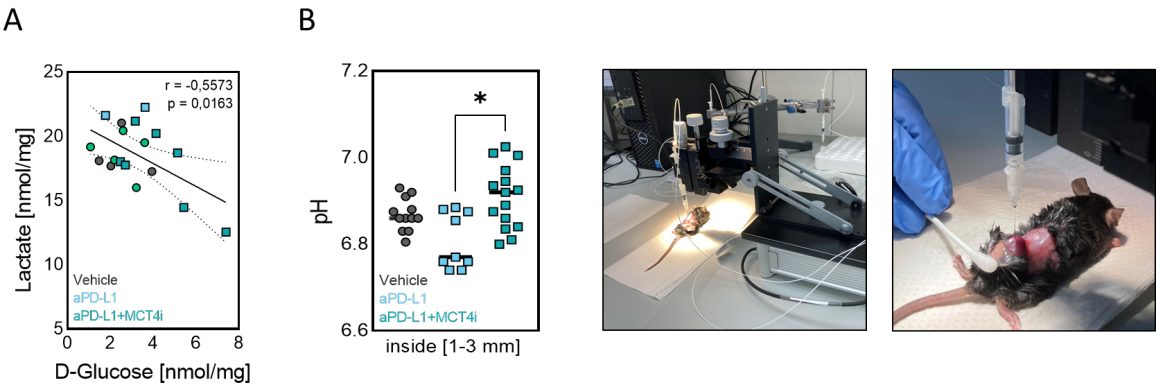

Figure 66. Tumoral pH. 1x10^6 MC38 cells were injected subcutaneously into the flank of C57BL/6 mice. Treatment was started at day 6 after cell implantation. MSC-4381 MCT4 inhibitor (MCT4i) (30 mg/kg body weight) was administered p.o. daily and aPD-L1 (10 mg/kg body weight) was administered i.p. every third day. All treatments were continued for the entire duration of the study, until tumors were collected and processed for pH measurements on day 11, 12 or 13. (A) Lactate and glucose concentration of tumors was measured by the Institute for Functional Genomics, University of Regensburg. D-Glucose was plotted against lactate concentrations in MC38 tumors. Correlation was calculated using Pearson's correlation test. (B) Tumor pH was measured in anesthetized mice using a microprobe pH meter at 1, 2 and 3 mm depth. Individual data points are shown. Significance was determined using one-way ANOVA and post-hoc Bonferroni multiple comparison test (*p < 0.05).

On the whole, impaired glycolysis and thereby prevented lactic acidosis might be the underlying mechanism for improved immunosurveillance in MC38 tumors and prolonged survival of mice treated with combination therapy of MCT4 inhibition and immune checkpoint blockade compared with mice receiving vehicle.

4.3.2.2.2 MC38$^{Mct4-/-}$ study

Combination therapy of MCT4 inhibitor and aPD-L1 acted synergistically to inhibit tumor growth and prolong survival of mice bearing MC38 tumors. This might be due impaired glycolysis and reversing immunosuppression by lactic acid, resulting in an improved CD8$^+$ T cell performance in terms of infiltration and Ifnγ production. Nevertheless, not only tumor cells but also activated T cells and in particular myeloid cells express MCT4. As a proof of concept and to investigate the effects of MCT4 blockade on tumor growth by only targeting immune cells and not tumor cells, we injected MC38 Mct4 Knock-Out cells (MC38$^{Mct4-/-}$) into the flank of syngeneic immunocompetent C57BL/6N mice to investigate the anti-tumor efficacy of MCT4 inhibitor (MCT4i) and aPD-L1, as monotherapy or in combination (Table 31). Treatments were started on day 6 and continued throughout the study period until the humane endpoint was reached with a maximum tumor volume of 1700 mm^3. Tumors were measured daily.

Table 31. Assignment of treatment groups MC38$^{Mct4-/-}$ study

Treatment group	#mice
Isotype+Vehicle	6
Isotype+MCT4i	7
aPD-L1+Vehicle	7
aPD-L1+MCT4i	8

Interestingly, MC38$^{MCT4-/-}$ tumors, although lacking Mct4, grew only slightly slower than MC38^{wt} tumors. This suggests that MC38$^{Mct4-/-}$ tumor cells evolve an escape mechanism compensating for the absence of MCT4. As seen in MC38^{wt} *in vivo* experiments, MC38$^{Mct4-/-}$ tumor growth from mice receiving single MCT4 inhibitor treatment showed no differences in tumor growth compared to mice treated with vehicle (Figure 67A). Similar to MC38^{wt} tumors, some mice responded to aPD-L1 monotherapy with delayed tumor growth, while others did not (Figure 67B). Additional administration of the MCT4 inhibitor only tended to further reduce tumor progression of MC38$^{Mct4-/-}$ tumors (Figure 67C).

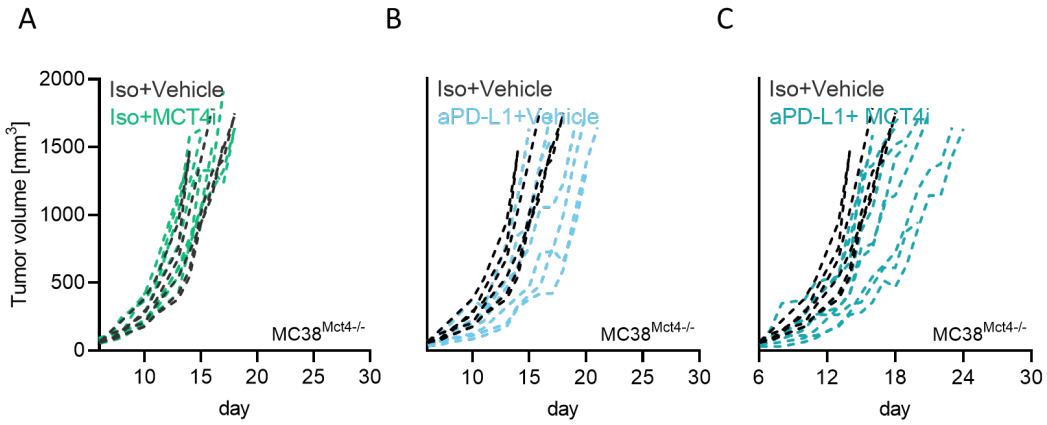

Figure 67. Delayed MC38$^{Mct4-/-}$ tumor growth with combination therapy of MCT4 inhibitor and aPD-L1. 1x10^6 MC38 MCT4 Knock-Out (MC38$^{Mct4-/-}$) cells were injected subcutaneously into the flank of C57BL/6 mice. Treatment was started at day 6 after cell implantation. MSC-4381 MCT4 inhibitor (MCT4i) (30 mg/kg body weight) was administered p.o. daily and aPD-L1 (10 mg/kg body weight) was administered i.p. every third day. All treatments were continued for the entire duration of the study, until humane endpoint was reached (max tumor volume 1700 mm^3). Tumor volume was monitored over time. (A-C) Individual tumor growth curves. Each line represents one mouse.

In line with the absence of MCT4 in MC38$^{Mct4-/-}$ tumors, tumor growth was significantly reduced by aPD-L1 monotherapy to the same level as when combined with an MCT4 inhibitor (Figure 68B). Nevertheless, survival of mice bearing MC38$^{Mct4-/-}$ tumors was significantly prolonged only by combination of aPD-L1 and MCT4 blockade relative to vehicle-treated mice (Figure 68A). These findings suggest that MCT4 blockade not only acts on tumor cells but also may have beneficial effects on immune cells in the TME of MC38$^{Mct4-/-}$ tumors.

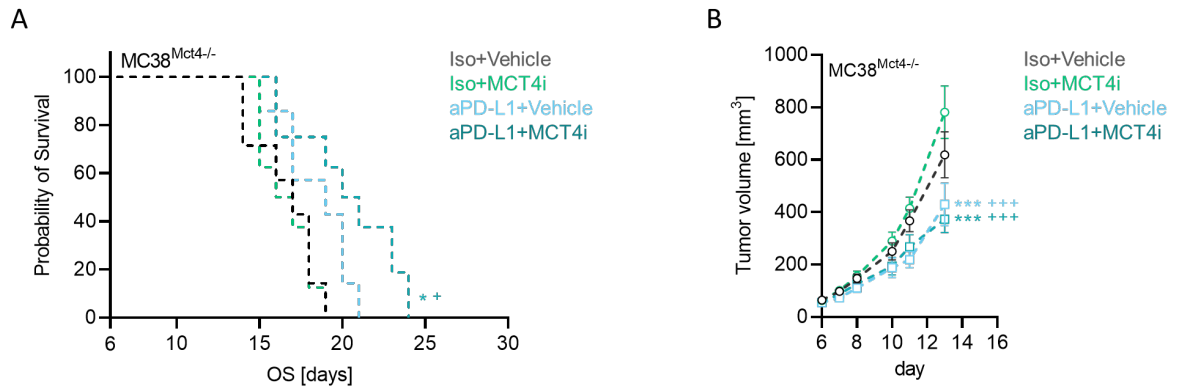

Figure 68. Better survival with combination therapy of MCT4 inhibitor and aPD-L1 in mice bearing MC38$^{Mct4-/-}$. 1x10^6 MC38 Mct4 Knock-Out (MC38$^{Mct4-/-}$) cells were injected subcutaneously into the flank of C57BL/6 mice. Treatment was started at day 6 after cell implantation. MSC-4381 MCT4 inhibitor (MCT4i) (30 mg/kg body weight) was administered p.o. daily and aPD-L1 (10 mg/kg body weight) was administered i.p. every third day. All treatments were continued for the entire duration of the study, until humane endpoint was reached (max tumor volume 1700 mm^3). (A) Survival was plotted as Kaplan Meier estimation curve. Significance was calculated applying the log-rank (Mantel-Cox) test with correction for multiple testing (Bonferroni correction of the p value for the number of statistical tests (n = 8) performed (*p < 0.006 compared to vehicle; +p < 0.006 compared to MCT4i). (B) Tumor volume was monitored over time. Mean + SEM is shown. Significance was determined by 2-way ANOVA and post-hoc Tukey's multiple comparisons (***p < 0.001 compared to Vehicle; +++p < 0.001 compared to MCT4i).

All treatment groups had comparable tumor weights at the end of the study (Figure 69A). Furthermore, all treatments were well tolerated since we did not observe any toxic effects or changes in liver or body weight upon MCT inhibition or immune checkpoint blockade (Figure 69C,D). In contrast to MC38^{wt} tumors, spleen weight was only slightly increased in aPD-L1 treated mice (Figure 69B).

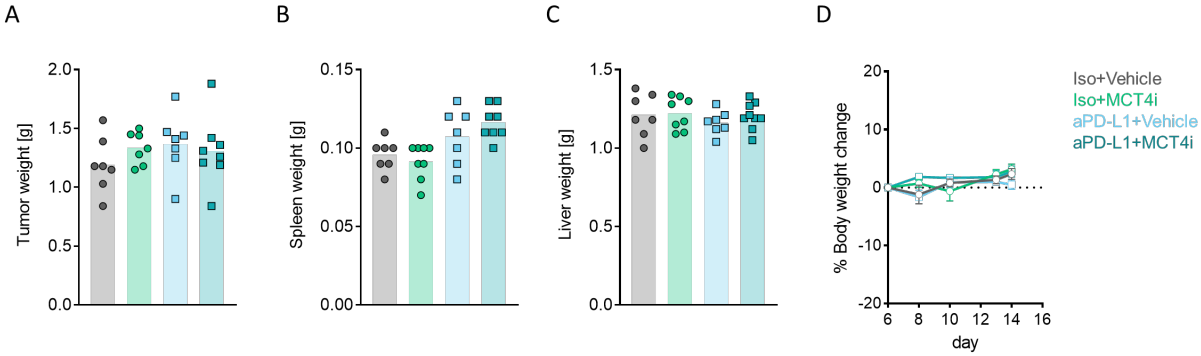

Figure 69. No toxic effects upon MCT4 inhibitor and aPD-L1 combination therapy but slightly increased spleen weight in aPD-L1 treated animals. 1x10^6 MC38 MCT4 Knock-Out (MC38$^{Mct4-/-}$) cells were injected subcutaneously into the flank of C57BL/6 mice. Treatment was started at day 6 after cell implantation. MSC-4381 MCT4 inhibitor (MCT4i) (30 mg/kg body weight) was administered p.o. daily and aPD-L1 (10 mg/kg body weight) was administered i.p. every third day. All treatments were continued for the entire duration of the study, until humane endpoint was reached (max tumor volume 1700 mm^3). (A) Tumor weight. (B) Spleen weight. Significance was determined using one-way ANOVA and post-hoc Bonferroni multiple comparison test (*p < 0.05; ***p < 0.001). (C) Liver weight. Median values with single data points are shown. (D) Body weight was monitored over time and the percentage of body weight change was calculated relatively to the individual body weight at treatment start. Mean + SEM is shown.

Overall, MCT4 inhibition in combination with aPD-L1 was not as efficient in reducing tumor growth in $MC38^{Mct4-/-}$ tumors as in $MC38^{wt}$ tumors. However, although $MC38^{Mct4-/-}$ tumors lack MCT4, MCT4 inhibition improved immune checkpoint blockade in terms of survival compared with mice treated with vehicle. This suggests that inhibition of MCT4 not only targets tumor cells but can also positively affect infiltrated immune cells.

4.4 The immunomodulatory role of MCT inhibitors in renal cell carcinoma

Besides CRC, we were interested in investigating the effect of MCT1 and MCT4 inhibition on a second tumor entity using clear cell renal cell carcinoma (ccRCC). Renal cell carcinoma comprises several subtypes, with ccRCC subtype being responsible for the majority of cancer-related deaths (351,352). Notably, the outcome of ccRCC patients is not defined by T cell infiltration but strongly associated with the number of myeloid inhibitory cells (353). Therefore, RCC is a good model to study the impact of MCT inhibitors with respect to myeloid cells.

When analyzing survival of ccRCC patients using publicly available TCGA data on the r2 platform (http://r2.amc.nl), we could confirm the published results. Survival was not associated with expression of CD8 as marker for $CD8^+$ T cells nor with interferon as effector cytokine (Figure 70A,B). Instead, a low CD14 expression (marker for tumor-associated macrophages (TAMs)) seemed to be beneficial for the outcome of ccRCC patients (Figure 70C). Most notably, IL-6 emerged as highly prognostic factor for survival in ccRCC (Figure 70D). Moreover, MCT1 (SLC16A1) and MCT4 (SLC16A3) expression correlated with a worse prognosis (Figure 70E,F).

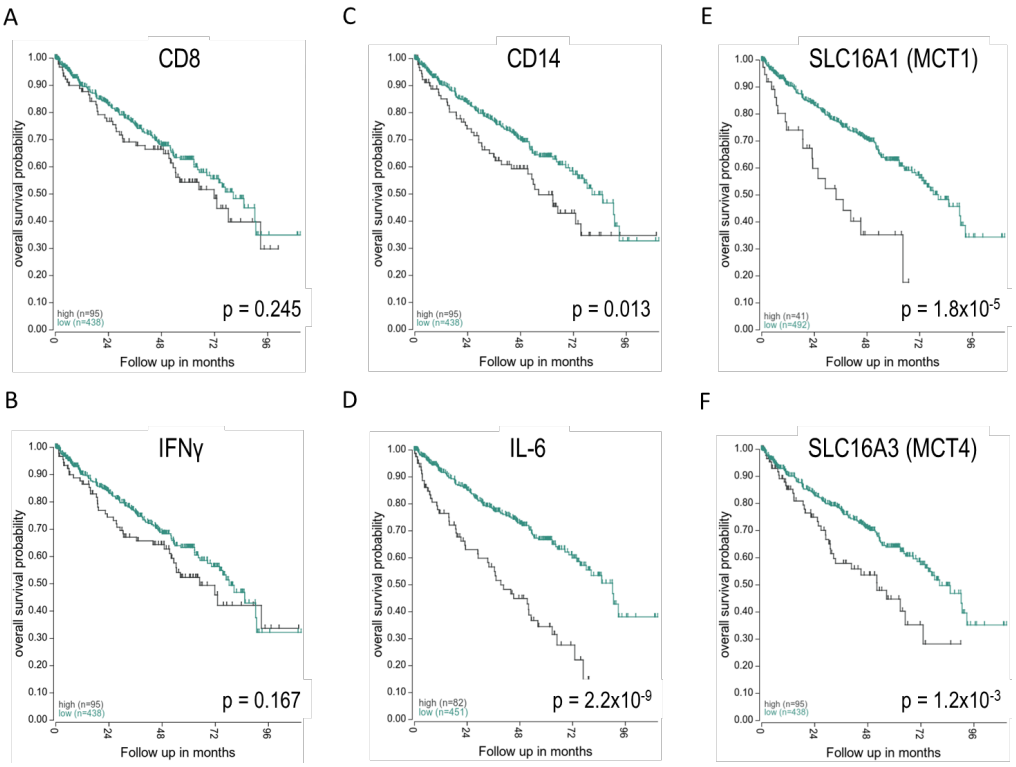

Figure 70. Myeloid cell infiltration, MCT1, MCT4 and IL-6 expression correlate with a poor outcome in ccRCC patients. Overall survival of 533 clear cell renal cell carcinoma (ccRCC) patients with high and low expression levels of indicated genes, calculated with the R2: Tumor Kidney Renal Clear Cell Carcinoma - TCGA - 533 - rsem – tcgars dataset (http://r2.amc.nl). (A) CD8 expression as marker for T cells. (B) Interferon γ (IFNγ) expression as marker for T cell effector functions. (C) CD14 expression as marker for infiltration of tumor-associated macrophages (TAMs). (D) IL-6 cytokine expression. (E) SLC16A1 as marker for MCT1 expression. (F) SLC16A3 as marker for MCT4 expression.

Interestingly, RCCs are generally highly infiltrated by immune cells such as T cells. However, the infiltrating immune cells seem not to be capable of targeting and killing the tumor. It has been reported that besides suppressive myeloid cells, soluble factors in the TME might be involved, particularly tumor-derived IL-6 was shown to play a critical role (354).

We found similar results when analyzing survival of patients using public TCGA data. Furthermore, we found MCT1 and MCT4 to play a role alongside TAMs and IL-6. Therefore, we examined the effects of inhibiting MCT1 and MCT4 in an RCC spheroid co-culture model and in ccRCC tumor biopsies from patients. As MCT inhibitors we used Astra Zeneca as specific MCT1 inhibitor (MCT1i) and MSC-4381 MCT4 inhibitor provided by Merck (MCT4i) but also compared the effect of diclofenac as MCT1/4 (302) and (cyclooxygenase) COX inhibitor. Acetylsalicylic acid (ASA), which is known as a COX inhibitor but does not act on MCT1 or MCT4, was used as control for effects mediated by COX inhibition.

4.4.1 MCT inhibition reduces lactate and IL-6 in RJ494 spheroid co-cultures *in vitro*

To study the impact of MCT1 and MCT4 inhibition in an RCC spheroid co-culture model we used the RJ494 RCC cell line. Spheroids mimic a TME that forms gradients of hypoxia, nutrients and lactate. For experiments, spheroids were preformed and following treated for 10 d. Consistent with previous results, lactate secretion was reduced to 50 % with MCT1 and MCT4 inhibitor, which was comparable to the level reached by diclofenac treatment. ASA alone had no effect on lactate efflux, and the combination of MCT1+4i had no additional effect (Figure 71A). We could not detect any differences in the size of the treated spheroids (Figure 71B).

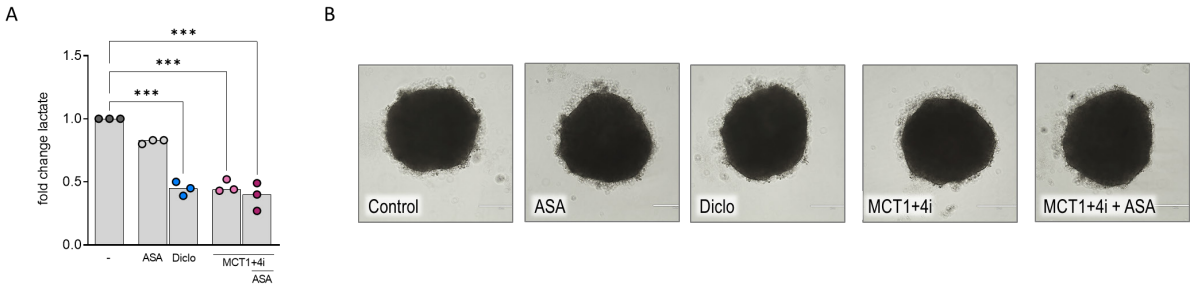

Figure 71. Lactate secretion of RJ494 spheroids is reduced by diclofenac and MCT1 and MCT4 inhibitors. RJ494 tumor spheroids were allowed to grow for 4 d. Spheroids were then treated with either 1 mM acetylsalicylic acid (ASA), 0.2 mM diclofenac (Diclo) or 0.1 µM MCT1 inhibitor (MCT1i) and MCT4 inhibitor (MCT4i) with or without ASA. (A) Lactate concentrations were measured after 10 d in culture supernatants. Depicted are median values and single data points. Significance was determined using one-way ANOVA and post-hoc Bonferroni multiple comparison test (***$p < 0.001$). (B) The morphology of treated spheroids was assessed after 10 d of treatment. Images were recorded using the EVOS system.

We were next interested in the performance of immune cells in co-culture with RJ494 spheroids upon MCT inhibition. Therefore, we co-cultured RJ494 tumor spheroids, which were treated for 10 d, with

immune cells freshly isolated from peripheral blood of healthy donors (Figure 72A). After 24 h, spheroids were washed and we analyzed infiltration of $CD14^+$ TAMs, $CD66b^+$ TANs and $CD3^+$ T cells using the gating strategy shown in Figure 72B.

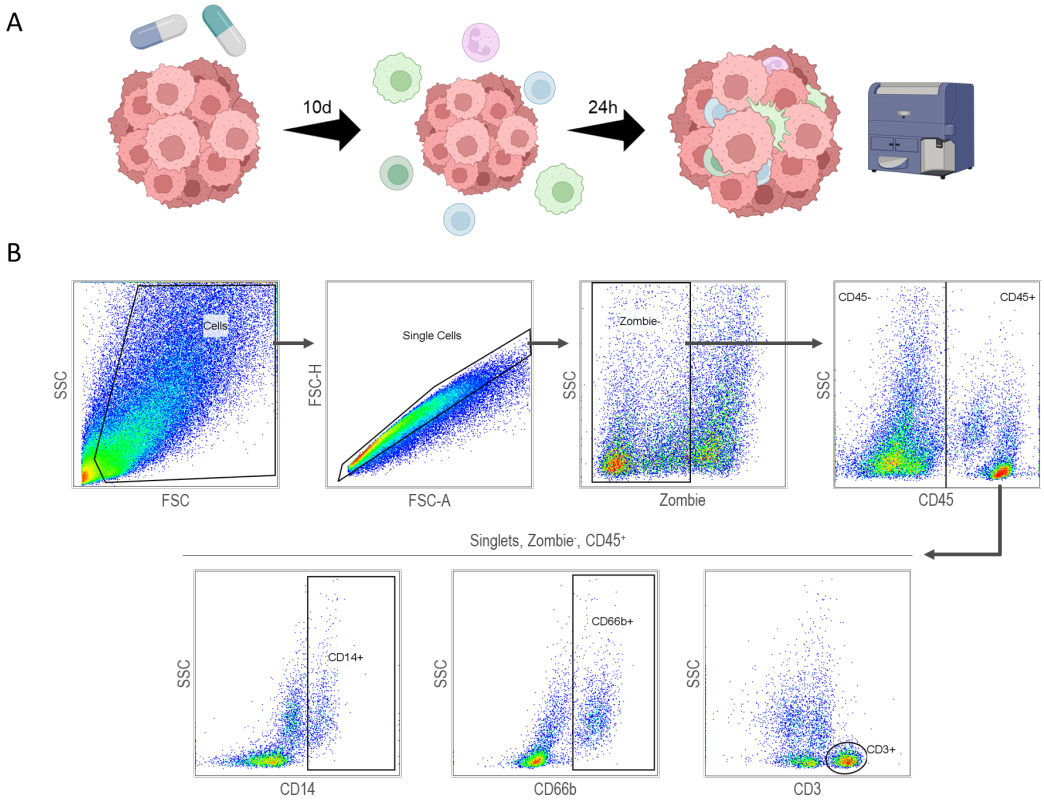

Figure 72. RJ494 spheroid co-culture with immune cells. (A) Co-culture protocol. Spheroids were treated with inhibitors for 10 d. Immune cells were freshly isolated from peripheral blood of healthy donors and added for 24 h. Afterwards, Spheroids were harvested, pooled, washed and prepared for subsequent flow cytometry staining. Created with BioRender.com. (B) Gating strategy for leukocytes ($CD45^+$) among total living ($Zombie^-$) singular cells and tumor-associated monocytes (TAMs) ($CD14^+$), tumor-associated neutrophils (TANs) ($CD66b^+$) and T cells ($CD3^+$) among $CD45^+$ cells after 24 h co-culture.

RJ494 spheroids showed generally high immune infiltration, but displayed high donor-dependent variations from 13 % to 70 % infiltrated $CD45^+$ cells (data not shown). However, in contrast to the HCT116 spheroid model, we did not observe a clearly increased immune cell infiltration neither with MCT1+4 inhibitors nor with diclofenac as MCT inhibitor (Figure 73). Interestingly, similar to RCC patient tumors, T cells represented the largest proportion of infiltrated immune cells at approximately 40 %, compared to approximately 20 % TANs and 15 % TAMs (data not shown). However, the immune composition among the $CD45^+$ infiltrated cells showed no clear trend upon any treatment (Figure 73B-D).

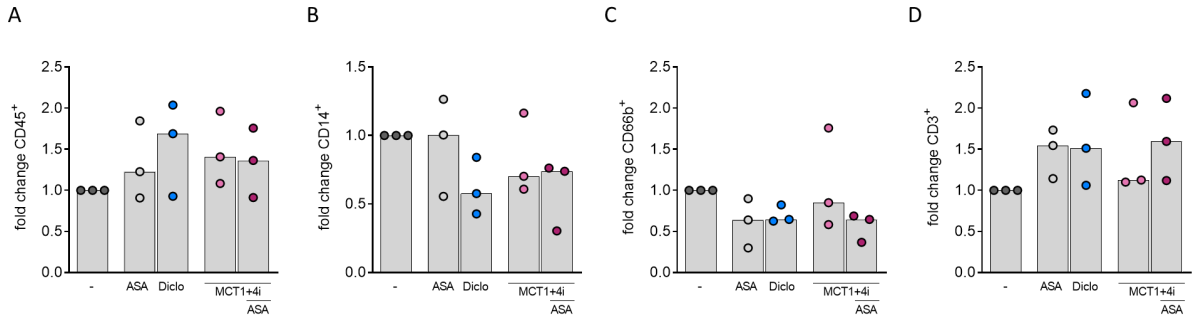

Figure 73. No changes in immune cell infiltration in RJ494 spheroids upon MCT inhibition. RJ494 spheroids were treated for 10 d either with acetylsalicylic acid (ASA), diclofenac (Diclo) or MCT1 and MCT4 inhibitors (MCT1+4i) with or without ASA. Immune cells were freshly isolated from peripheral blood of healthy donors and added for 24 h. Afterwards, Spheroids were harvested, pooled, washed and prepared for subsequent flow cytometry staining. (A) Gated on single and viable cells. Fold change of $CD45^+$ infiltrated immune cells. (B-D) Gated on single, viable cells and $CD45^+$ cells. Fold change of tumor-associated monocytes (TAMs) ($CD14^+$) (B), tumor-associated neutrophils (TANs) ($CD66b^+$) (C) and T cells ($CD3^+$) (D) among $CD45^+$ cells after 24 h co-culture. Depicted are median values and single data points (n = 3).

Since literature and our survival analysis of TCGA data identified IL-6 as prognostic factor, we examined IL-6 expression in spheroid single cell suspensions. TAMs showed the highest IL-6 levels, followed by RJ494 tumor cells. Lowest IL-6 expression was found in T cells (Figure 74A). It should be mentioned that our investigations of primary macrophages treated with MCT1 and MCT4 inhibitors revealed a blockade of IL-6 production. Indeed, we found reduced IL-6 secretion by diclofenac but also a strong trend toward inhibition by MCT1 and MCT4 blockers with and without ASA (Figure 74B).

TAMs emerged as major source for IL-6 secretion in RJ494 co-culture model. Moreover, TAMs predict the outcome of RCC patients. Therefore, we analyzed the function of TAMs more in detail. In contrast to IL-6, TNF expression was not altered (Figure 74C). In addition, in accordance with the previous observations, the antigen presenting molecule MHC-II tended to be upregulated by MCT inhibition, although only combination with ASA led to a significant change in expression. Similarly, the immune checkpoint ligand PD-L1 was downregulated upon MCT inhibition (Figure 74D,E).

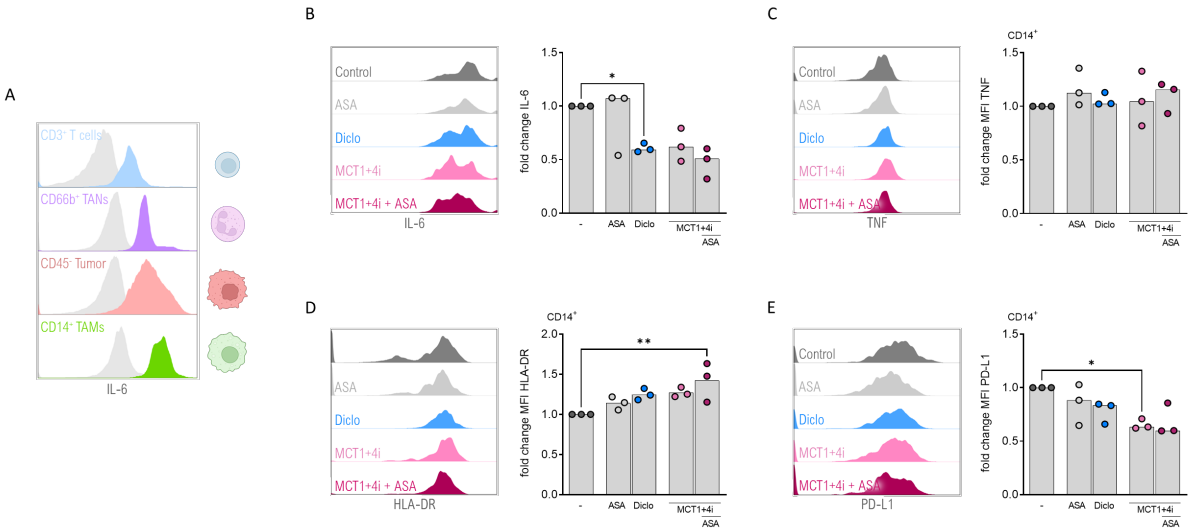

Figure 74. MCT inhibition induces an immunocompetent phenotype of TAMs in RJ494 spheroids. RJ494 spheroids were treated for 10 d either with acetylsalicylic acid (ASA), diclofenac (Diclo) or MCT1 and MCT4 inhibitors (MCT1+4i) with or without ASA. Immune cells were freshly isolated from peripheral blood of healthy donors and added for 24 h. Afterwards, spheroids were harvested, pooled, washed and prepared for subsequent flow cytometry staining. Pictures created with BioRender.com. (A) IL-6 expression of different immune cell populations. Gated on single, viable cells and $CD45^+$ cells. Representative histograms of IL-6 expression of T cells ($CD3^+$), tumor-associated neutrophils (TANs) ($CD66b^+$), tumor cells ($CD45^-$) and tumor-associated monocytes (TAMs) ($CD14^+$) after 24 h co-culture. Grey histograms are corresponding isotype controls. (B) IL-6 levels in culture supernatants were measured by ELISA after 24 h co-culture. (C-E) TNF, HLA-DR and PD-L1 were determined by flow cytometry. Representative plots and median values with single data points are shown (n = 3). Significance was determined using one-way ANOVA and post-hoc Bonferroni multiple comparison test (*$p < 0.05$; **$p < 0.01$).

Overall, MCT inhibition distinctly decreased lactate efflux from RJ494 monolayers and spheroids with diclofenac and specific MCT inhibitors alike. Although MCT1 and MCT4 blockade had no beneficial effect on overall immune infiltration, IL-6 secretion was clearly diminished. In TAMs, we found that TNF expression was preserved, MHC-II upregulated, and PD-L1 downregulated by MCT inhibition indicating a polarization toward increased immunocompetence.

4.4.2 MCT inhibition reduces lactate and IL-6 in ccRCC tumor biopsies *ex vivo*

Finally, to investigate the effects of MCT inhibition on "real" TAMs and M-MDSCs, we used human tumor biopsies of RCC patients. Single cell RNAseq analysis of RCC samples (performed by Dr. Malte Simon, DKFZ) revealed high expression of SLC16A3, encoding MCT4, in RCC tumor cells and TAMs (Figure 75). Therefore, tumor cells and suppressive myeloid cells might be the primary target of MCT inhibition in RCC tumors. Following, we treated single cell suspensions or tumoroids (tumor fragments) derived from ccRCC biopsies for 24 h with the AZD3965 specific MCT1 inhibitor (MCT1i) and MSC-4381 MCT4 inhibitor provided by Merck (MCT4i) or diclofenac as MCT1/4 (302) and COX inhibitor. ASA was used as control for COX inhibition.

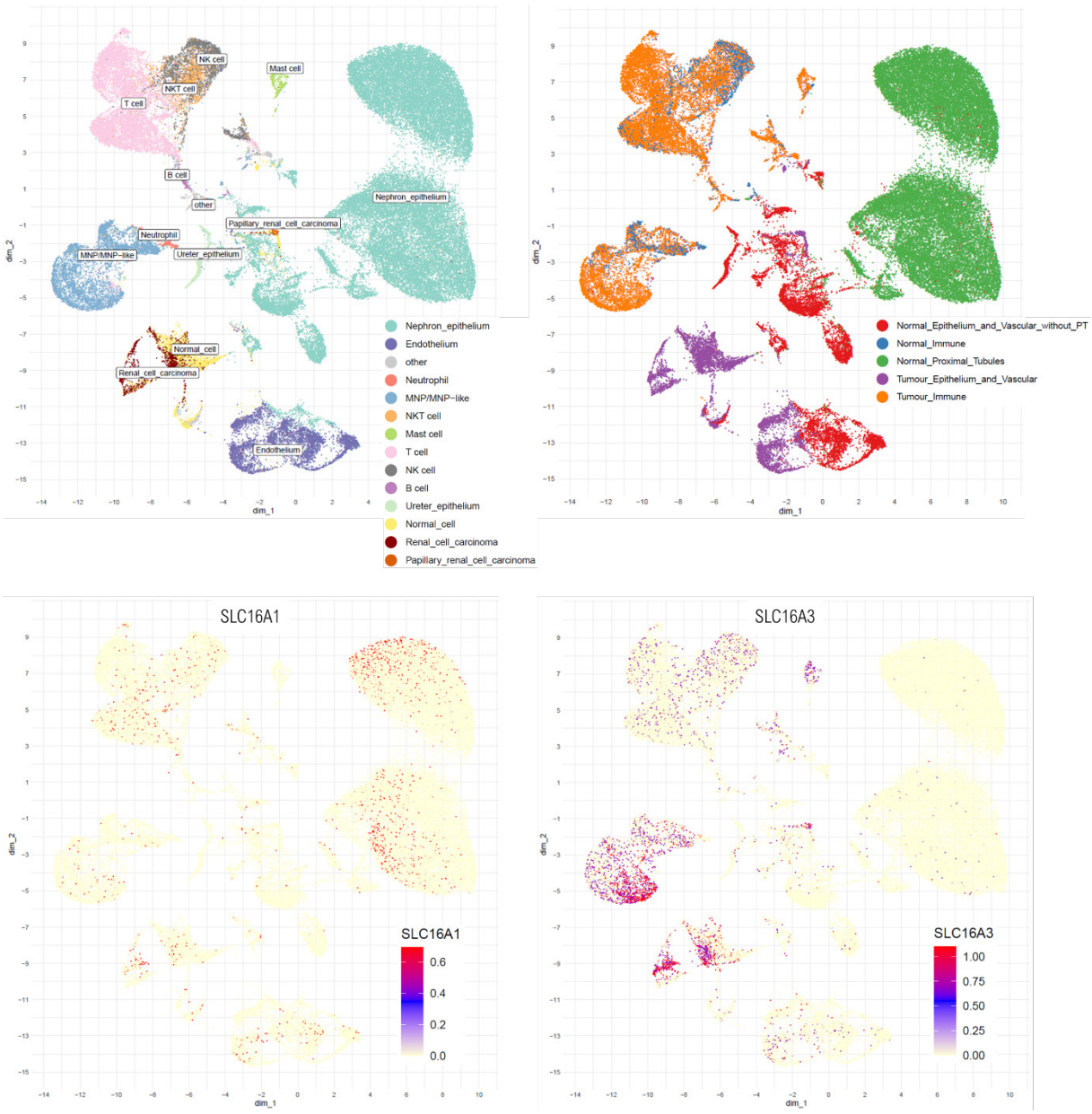

Figure 75. Myeloid cells and RCC show high expression of SLC16A3. Analysis of Young et al. (355) RCC scRNA-seq dataset (Data downloaded from https://science.sciencemag.org/highwire/filestream/713964/field_highwire_adjunct_files/6/aat1699_DataS1.gz.zip. Analysis was performed by Dr. Malte Simon. Cells were filtered by the authors QC criteria and subsetted to 'Tumour Immune Compartment' resulting in 17821 cells. Using the Seurat package (v. 3.2.1) from R data was normalized (NormalizeData(normalization.method = "LogNormalize", scale.factor = 10000)) and scaled (ScaleData). Subsequently, variable features were identified using the function "FindVariableFeatures(selection.method = "vst", nfeatures = 2000)" and used as input for PCA (RunPCA). Finally, an UMAP representation was calculated based on the first 10 principal components (RunUMAP(dims=1:10)). Simplified cell annotation labels were created from the column "Cell_type1" of Table S2.

4.4.2.1 Single cell suspensions

To generate single cell suspensions, patient's ccRCC biopsies were minced and enzymatically and mechanically dissociated as depicted in Figure 76A. The mixture of tumor and immune cells was incubated with the indicated treatments, and after 24 h, the culture supernatants and immune infiltration were examined. Immune cell infiltrate was determined by the number of $CD45^+$ cells. In RJ494 co-culture spheroids, we detected especially polarizing effects on TAM phenotype. Hence, we analyzed T cell frequency ($CD3^+$) and in more specifically TAMs ($CD14^+$) among $CD45^+$ cells after 24 h (Figure 76B).

Besides TAMs, a heterogenous population of immature myeloid cells is found in tumors. Due to their origin from bone marrow derived immature myeloid cells (IMC) and immunosuppressive phenotype these cells are called MDSCs (356). MDSCs are divided into granulocytic $CD14^-$ and monocytic $CD14^+$ subtypes with MHC-II negative or low expression (357). Here, we defined M-MDSCs as $CD14^+$ HLA-DR low cells (Figure 76B).

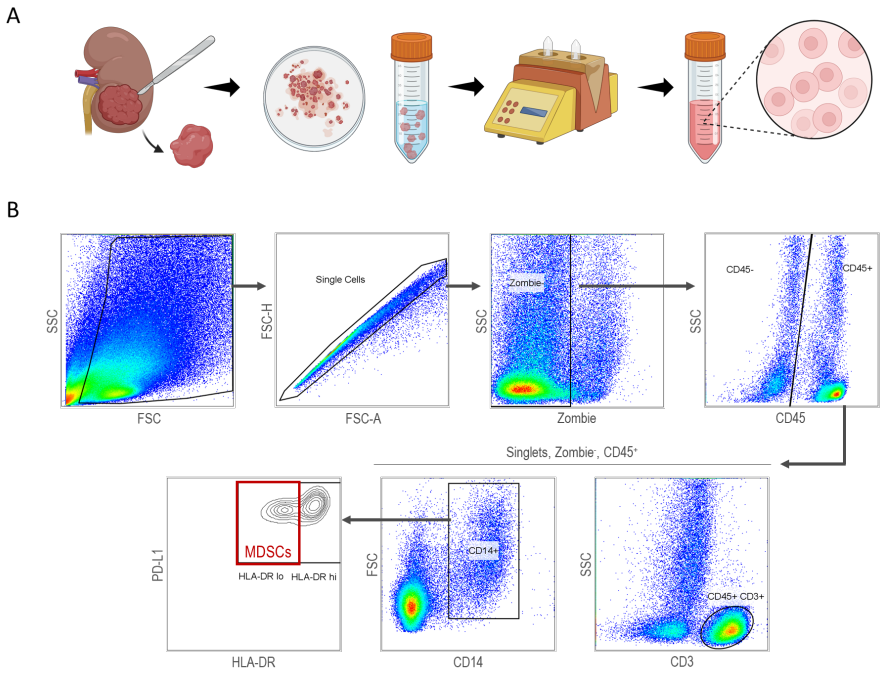

Figure 76. Workflow of RCC patient biopsy cell suspension and gating strategy. (A) Preparation of single cell suspensions from RCC biospies. Tumor biopsies were minced and mechanically and enzymatically dissociated. After 24 h, cells were analyzed by flow cytometry. (B) Gating strategy for leukocytes ($CD45^+$) among total living ($Zombie^-$), single cells and tumor-associated monocytes (TAMs) ($CD14^+$), and T cells ($CD3^+$) among $CD45^+$ cells after 24 h. Myeloid suppressor cells (M-MDSCs) were designated as $CD14^+$ HLA-DR low cells.

First, we analyzed the immune composition in tissue biopsies from the tumor center (central ccRCC) or periphery (peripheral ccRCC) compared to healthy kidney tissue (tumor-free kidney tissue from the same patient). In contrast to healthy kidney, we found high levels of immune cell infiltrates in peripheral but also central ccRCC. However, during tissue digestion, a lot of tumor cells die, while

immune cells are less susceptible. Therefore, the observed frequencies of about 85 % CD45$^+$ immune cells in ccRCC do not accurately reflect the *in vivo* situation. Nevertheless, the frequencies of immune cells in healthy kidney were much lower than in tumor tissue, at only 10 % (Figure 77A). Consistent with the literature, CD3$^+$ T cells were most abundant in ccRCC, with approximately 70 % among CD45$^+$ cells and only an average of 8 % CD14$^+$ tumor-associated myeloid cells were found. However, composition of T cells and myeloid cells was comparable to healthy kidney, although healthy kidney tends to have less T cells and more CD14$^+$ myeloid cells (Figure 77B,C). Interestingly, we found a roughly 10-fold increase in MDSCs in central and peripheral ccRCC biopsies (Figure 77D) compared to healthy kidney tissue. Overall, central and peripheral ccRCC did not show major differences in terms immune infiltration.

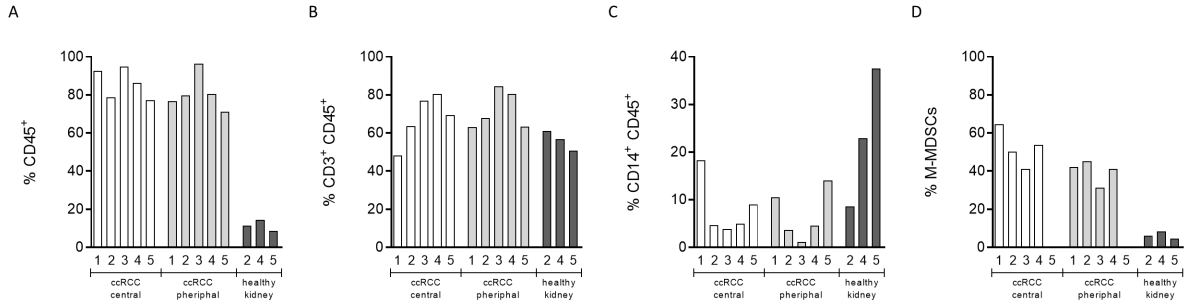

Figure 77. Composition of infiltrated immune cells in central and peripheral ccRCC compared to healthy kidney. Tumor or kidney biopsies were minced and mechanically and enzymatically dissociated. After 24 h, cells were analyzed by flow cytometry. (A) Gated on single and viable cells. Frequencies of CD45$^+$ infiltrated immune cells. (B-D) Gated on single, viable cells and CD45$^+$ cells. Frequencies of (B) tumor-associated T cells (CD3$^+$), (C) tumor-associated myeloid cells (TAMs, CD14$^+$), and (D) myeloid suppressor cells (CD14$^+$ HLA-DR low) among CD45$^+$ cells. Depicted are values for each patient and each number indicates one patient.

In addition to myeloid cells, tumor IL-6 concentration is an important prognostic factor for the outcome of ccRCC patients. Induction of IL-6 has been associated with factors derived from the TME. Therefore, we measured not only baseline IL-6 levels but also lactate levels in supernatants of ccRCC biopsies and healthy kidney. We detected very high amounts of IL-6, up to 50.000 pg/ml, in ccRCC, whereas IL-6 levels in healthy kidney tissue were low (Figure 78A). Strikingly, lactate correlated with IL-6 (Figure 78A,B). It is known that TAMs are one of the main producers of IL-6 in the TME, along with tumor cells. Indeed, we found a correlation between IL-6 levels and the frequency of CD14$^+$ TAMs in central and peripheral ccRCC (Figure 78C).

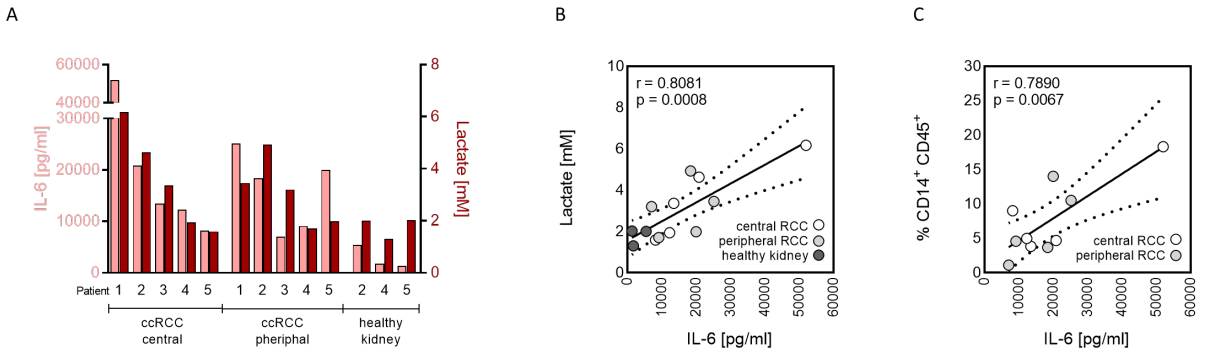

Figure 78. IL-6 levels correlate with lactate levels in central ccRCC. Tumor or kidney biopsies were minced and mechanically and enzymatically dissociated. After 24 h, supernatants were collected. (A,B) Lactate concentrations were measured after 24 h in culture supernatants. IL-6 levels in culture supernatants were measured by ELISA after 24 h. (A) Depicted are values for each patient and each number indicates one patient. (B) IL-6 was plotted against the respective donor-matched lactate secretion. (C) IL-6 was plotted against corresponding $CD14^+$ cells. (B,C) Correlation was calculated using Pearson's correlation test.

Analyzing the effects of MCT1 and MCT4 inhibitors on primary monocyte-derived macrophages, we observed blockade of lactate and IL-6 secretion. In line, diclofenac reduced lactate to the same level as MCT1 and MCT4 inhibitors with or without ASA (Figure 79A). In addition, IL-6 secretion was reduced by both diclofenac and MCT1 and MCT4 inhibition in combination with ASA. In this case, inhibition of MCT1 and MCT4 without ASA only tended to decrease IL-6 secretion (Figure 79B). Moreover, we detected fewer MHC-II-depleted M-MDSCs upon diclofenac treatment, whereas specific MCT inhibitors with or without ASA only had a trend to reduce M-MDSCs (Figure 79C). Consistent with reduced abundance of suppressive MDSCs, PD-L1 expression of TAMs was lowered by diclofenac treatment and also tended to do so with specific MCT1 and MCT4 blockers in combination with ASA (Figure 79D). In contrast to IL-6, TNF expression was not altered by MCT inhibition (Figure 79E). ASA alone had no effects.

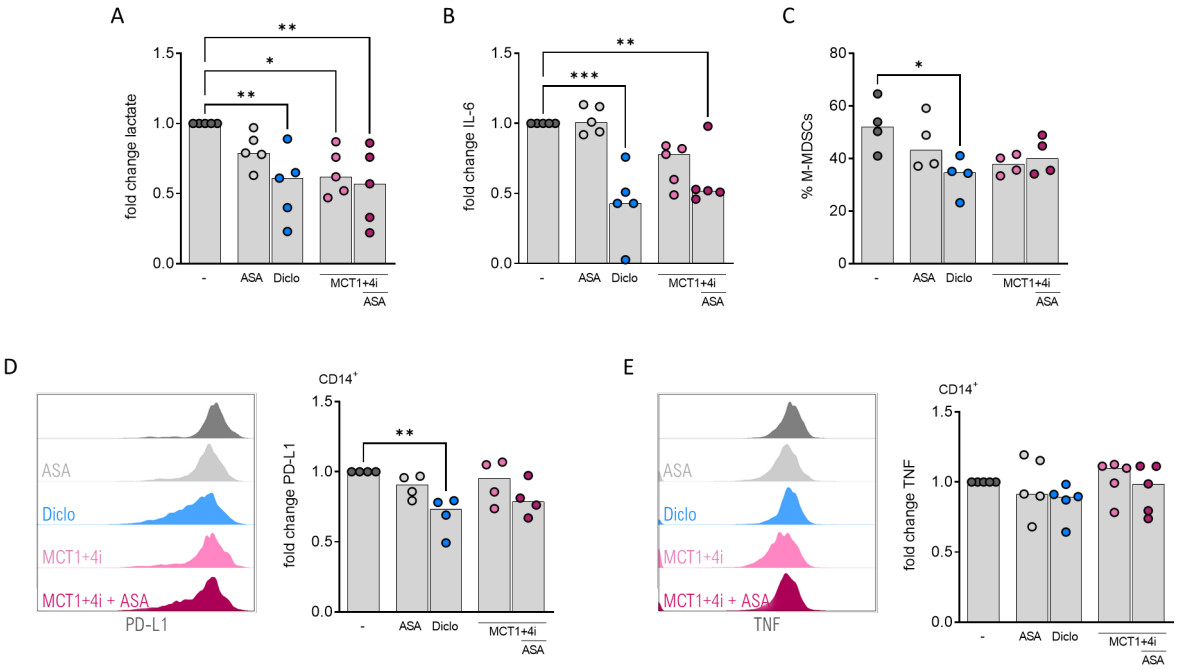

Figure 79. Secretion of lactate and IL-6 is inhibited in RCC biopsies upon MCT1 and MCT4 inhibition. Tumor biopsies were minced and mechanically and enzymatically dissociated. Single cell suspensions were then treated either with acetylsalicylic acid (ASA), diclofenac (Diclo) or MCT1 and MCT4 inhibitors (MCT1+4i) with or without ASA. After 24 h, supernatant was collected and cells were analyzed by flow cytometry. (A) Lactate concentrations were measured after 24 h in culture supernatants. (B) IL-6 levels in culture supernatants were measured by ELISA after 24 h. (C-E) Flow cytometric analysis of infiltrating immune cells. (C) Gated on single, viable cells $CD14^+$ cells and HLA-DR low cells. Frequencies of M-MDSCs under indicated treatments. (D,E) Gated on single, viable cells and $CD45^+$ $CD14^+$ tumor-associated myeloid cells (TAMs). PD-L1 (D) and TNF (E) expression were determined by flow cytometry. Representative plots and median values with single data points are shown. Significance was determined using one-way ANOVA and post-hoc Bonferroni multiple comparison test (*$p < 0.05$; **$p < 0.01$, ***$p < 0.001$).

In brief, in accordance to literature, we found high levels of baseline IL-6 and increased numbers of M-MDSCs in ccRCC tumor biopsies compared to healthy kidney. Although T cells were most abundant, frequencies of TAMs correlated with IL-6 levels and IL-6 with lactate levels, respectively. Strikingly, accumulation of IL-6 and lactate was diminished by diclofenac treatment, possibly leading to fewer M-MDSCs and reduced PD-L1 expression.

4.4.2.2 Patient-derived tumor organoids: Tumoroids

MCT inhibition by diclofenac or MCT inhibitors reduced lactate efflux of single cell suspensions derived from ccRCC tumor biopsies. However, the characteristics of the TME are lost during tumor dissociation. Therefore, we aimed to study the impact of anti-glycolytic drugs on so-called tumoroids.

Tumoroids are patient-derived tumor organoids with intact TME generated by fresh processing of tumor biopsies into equal-sized fragments of about 30 mg without chemical dissociation or reassembly (Figure 80A) and were treated for 48 h with indicated treatments. Indeed, diclofenac and combined MCT1 and MCT4 inhibitor treatment attenuated the Warburg phenotype of ccRCC tumoroids by

decreasing lactate secretion to 50 % of control. We further tested NCI-737 as inhibitor of lactate dehydrogenase (LDHi) as alternative target for glycolysis. In line, LDHi treatment resulted in reduced lactate accumulation.

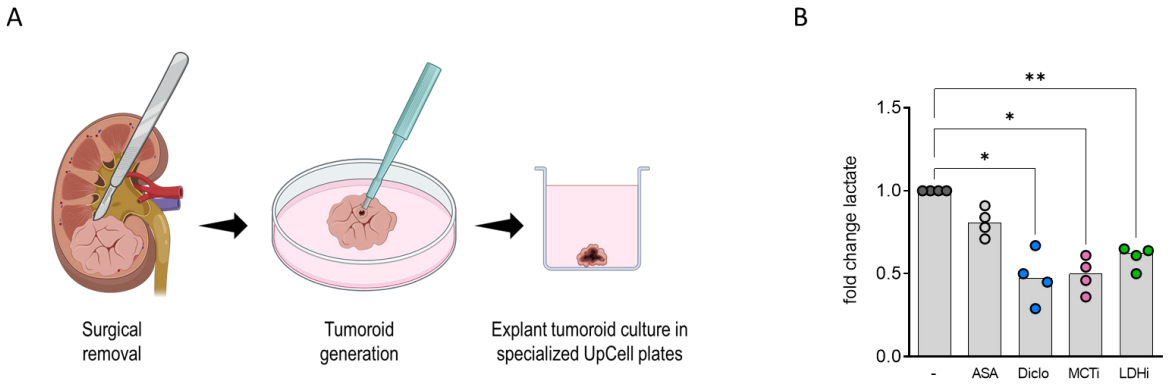

Figure 80. Inhibition of lactate efflux of patient-derived tumoroids by MCT or LDH inhibition. (A) Each fresh tumor was minimally processed into uniformly-sized tumoroids of about 30 mg without chemical dissociation or reassembly. Wet weight was assessed before culture for normalization. Tumoroids were then treated for 48 h either with acetylsalicylic acid (ASA), diclofenac (Diclo), MCT1 and MCT4 inhibitors (MCT1+4i) or NCI-737 LDH inhibitor (LDHi). Created with BioRender.com. (B) Lactate concentrations were measured after 48 h in culture supernatants and normalized to tumoroid wet weight.

In short, tumoroids should be considered a relevant model for drug testing as they maintain an intact TME. Consistent with previous experiments, we confirmed diclofenac and MCT inhibitors as effective treatments counteract glycolysis in ccRCC tumoroids. In addition, the LDH inhibitor NCI-737 represents a promising drug as an alternative target for glycolysis that requires further investigation.

5 Discussion

5.1 Counteracting the Warburg effect with MCT inhibitors

Alterations in the energy metabolism of tumor cells have been introduced as a hallmark of cancer by Hanahan and Weinberg in 2011 (3). Accelerated glucose metabolism and a highly elevated turn-over of pyruvate into lactate even in the presence of oxygen, the Warburg phenotype, is a well-known metabolic feature of tumors of different entities and is linked to limited therapy response and worse patient prognosis (37,50,116,274–280,301,358,359). Maintenance of the glycolytic flux requires continuous export of lactate via proton-coupled monocarboxylate transporters (MCTs), of which MCT1 and MCT4 are the key tumor-associated transporters, resulting in lactic acidosis of the TME. Tumor-derived lactic acid has been suggested as a key factor of tumorigenesis. Acidosis contributes to tumor progression by inducing degradation of the extracellular matrix (ECM), thereby promoting tumor invasiveness (48), and is also known to drive angiogenesis (360–362). Furthermore, lactic acid has been shown to modulate immune cell function. Although the increased glucose metabolism has been used as a diagnostic tool for decades, its implementation as a therapeutic target gained attention only recently.

5.1.1 Consequences of lactic acidosis – Warburg as metabolic immune checkpoint

Lactic acidosis due to the Warburg effect is an intrinsic feature of solid tumors. Levels of up to 40 mM lactate have been detected in TME compared to 1-2 mM in blood. Accordingly, the pH in TME ranges from 5.6 to 7, whereas the interstitial pH of the tissue is normally 7.3 to 7.4 (363). Our own *in vivo* measurements revealed an intratumoral pH of approximately 6.86 in MC38 tumors.

T cells

Nowadays, it is widely established that tumor-derived lactic acid suppresses effector functions of T cells (33,110,121,301,364,365). T cell proliferation has been shown to be blocked by lactic acid or sodium lactate in a concentration-dependent manner (113,328). Haas et al. have reported that T cell migration is impaired by lactic acid in the presence of CXCL10, which was reversed by the application of an MCT1 inhibitor (122). To characterize sensitivity of T cells to lactic acid, viability and intracellular pH changes were studied as a first step. In line with published data (33,364), we observed apoptosis of T cells treated with 20 mM lactic acid. In contradiction to the results of other groups (366), our group has previously demonstrated that only lactic acid, but not HCl or sodium lactate affected T cell viability, IFNγ and IL-2 production (364). Elia and colleagues demonstrated that tumor-derived lactate alters the pyruvate metabolism of $CD8^+$ T cells, resulting in decreased cytotoxicity (367). They postulate that the

cytotoxic function of $CD8^+$ T cells depends on autocrine succinate signaling, which requires the conversion of pyruvate to oxaloactetate by the pyruvate carboxylase to replenish TCA intermediates. Extracellular lactate modulates the entry of pyruvate into the TCA cycle from the pathway via pyruvate carboxylase to preferentially via pyruvate dehydrogenase, which subsequently impairs succinate signaling and thus limits effector functions of $CD8^+$ T cells (367). Interestingly, it has been shown that subcutaneous administration of sodium lactate to mice bearing MC38 tumors resulted in increased stemness of $CD8^+$ T cells and thus enhanced anti-tumor immunity (368). The inhibitory effect of lactic acid does not seem to be limited to a specific T cell subset (33). Remarkably, exposure of T cells to 20 mM lactic acid, which corresponds to a pH of approximately 6.0 (data not shown), resulted in a dramatic decrease in the cytosolic pH of T cells below 4.5, which is similar to what was observed in murine T cells (34).

Lactate is negatively charged and can only cross the plasma membrane when co-transported with protons via MCTs. MCT-mediated transport of "lactic acid" is dependent on concentration gradients of both lactate and protons (369). Indeed, T cells upregulate MCT1 and MCT4 expression after stimulation. As T cells face high lactic acid concentrations in the TME, this drives the import of lactic acid into the cytosol of T cells via MCTs, as it has been demonstrated by ^{13}C-lactate/HCl tracing (33,364). Kumagai et al. demonstrated that Treg cells take up lactic acid via MCT1, leading to increased PD-1 expression (114). Possibly, MCTs facilitate proton entry for lactic acid more readily than for HCl. In addition, high intracellular lactate concentrations lead to blockade and modulation of T cell metabolism, as evidenced by impaired glycolysis, modulated pyruvate utilization and reduced respiration of T cells upon lactic acid exposure (33,370). T cells show a certain metabolic flexibility (371), but metabolism plays an important role in T cell expansion and function (123,372). In addition, for instance, pH sensors such as GPR65 regulate endo-lysosomal function and T cell metabolism to maintain tissue homeostasis (373). Interestingly, reversal of acidosis by neutralizing pH with sodium bicarbonate improved metabolic fitness and T cell expansion (370). In another approach of our group, lactate was shown increase respiration in LDHB overexpressing T cells, but effector functions were only partially restored and T cell death induced by lactic acid was not prevented (33). At the molecular level, lactic acid prevents phosphorylation of JNK, c-Jun, p38, and NFAT activation, which are crucial signaling pathways for IFNγ production (34,39,110). However, the precise mechanisms underlying cell death of T cells after exposure to lactic acid are still unclear.

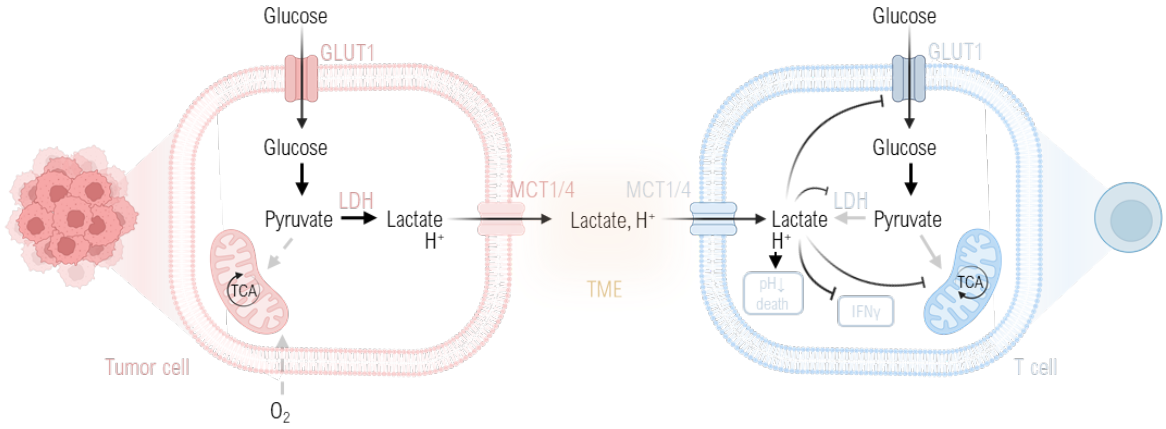

Figure 81. Inhibition of T cells by lactic acid. Tumor cells produce excessive amounts of lactate, which is exported via monocarboxylate transporters (MCT) 1 and 4 in co-transport with protons (H^+). Lactate and H^+ are imported into T cells via MCT1 and MCT4 in a concentration-dependent manner, resulting in intracellular acidosis, metabolic blockade, decreased effector functions, and cell death. GLUT1, glucose transporter 1; LDH, lactate dehydrogenase; IFNγ, interferon γ. Created with BioRender.com.

Macrophages

In contrast to T cells, we found that myeloid cells were much less sensitive to lactic acid. Although monocyte-derived macrophages expressed MCT1 and MCT4, they survived even 20 mM lactic acid exposure. This is consistent with data published for monocytes, the precursor cells of macrophages (36). Interestingly, macrophages showed lower intracellular acidification when treated with lactic acid compared to T cells. This suggests that the differences in sensitivity to lactic acid may be based on differences in the pH regulatory systems of macrophages and T cells.

It is possible that macrophages cope better with an acidic pH due to their original function as first defense against pathogens at sites of inflammation. Local acidosis is typical for inflammatory foci and has been shown to trigger the release of pro-inflammatory cytokines such as IL-1α, IL-6, and tumor necrosis factor (TNF) by macrophages (374). Although macrophages survive acidic conditions, tumor-derived lactic acidosis hijacks tumor-associated macrophages (TAMs) and polarizes them to tumor-promoting state with properties such as secretion of interleukin (IL)-6, IL-10 tumor growth factor (TGF)-β, and vascular endothelial growth factor (VEGF) (38,39,134). Therefore, infiltration by TAMs is associated with poorer outcomes and resistance to immunotherapies in many cancers (38,147).

In addition, it has been recently demonstrated that the resistance of macrophages to apoptosis induction may be due to their ability to buffer their intracellular pH by increasing highly basic polyamines (375). Similarly, administration of difluoromethylornithine (DFMO), a clinically approved inhibitor of polyamine formation, resulted in a decrease in the intracellular pH of TAMs (375). In line, our own data show that L-arginine application restored anti-parasitic leishmanicidal activity of murine macrophages by normalization of intracellular pH in lactic acidotic environment (376).

However, macrophages represent a highly dynamic population, so manipulating the phenotype of TAMs may be a promising strategy toward developing efficient anti-tumor immunity and potentially preventing therapy resistance.

Neutrophils

Similar to macrophages, neutrophils showed resistance to lactic acid treatment and survived exposure to 20 mM lactic acid. Interestingly, it has been described for neutrophils that extracellular acidosis and thereby decreased intracellular pH actually delays apoptosis (317,319). In contrast to macrophages, intracellular acidification due to lactic acid treatment was more pronounced in neutrophils. This argues against the hypothesis that resistance to lactic acid is achieved by improved pH regulation. However, the time frame for analysis of neutrophil apoptosis is very short because neutrophils have a short lifespan of about 6 hours after isolation, which does not allow to study long-term effects (377,378). Remarkably, neutrophils from cancer patients have been shown to exhibit a prolonged half-life of 17 hours (379), which fits into the picture of neutrophil apoptosis being delayed by intracellular acidification (317,319).

Overall, we found large differences in the sensitivity of immune cells to lactic acid, with T cells being very sensitive and myeloid cells being more resistant. In light of these findings, efforts should be taken to develop pharmacological interventions to target tumor glycolysis in order to reverse lactic acid-driven immunosuppression and improve immunosurveillance.

5.1.2 Reduced lactic acidosis and preserved T cell function with MCT inhibitors

A long time elevated glycolytic activity was considered as a unique feature of tumor cells, and the Warburg effect was proposed as a metabolic characteristic of tumor cells (37). Nowadays it is clear that not only tumor cells depend on glycolysis and lactic acid, the end product of glycolysis, is not only a waste product but much more an immune-regulatory molecule that severely impairs T cell and NK cell effector functions (33,34,110,111,364,365) and fosters the differentiation and activity of tumor-promoting immune cell populations, such as Tregs (113,114,335) or myeloid cells (36,38,39,112). Many efforts have been made to therapeutically target the glycolytic metabolism of tumor cells, e.g. with GLUT inhibitors and LDH inhibitors (281,282,380,381). But none of them have made it from the laboratory to the bedside. Over the last years MCTs emerged as an attractive target to restrict glucose metabolism and lactate secretion. In this context, MCT1 and MCT4 are the key tumor-associated lactate transporters and of major importance to maintain the Warburg phenotype of tumor cells.

MCT1 is almost ubiquitously expressed, whereas MCT4, especially responsible for the export of lactate due to its low pyruvate affinity, is mainly found in highly glycolytic cells. This can partially be explained

by the fact that MCT4 expression is triggered by hypoxia-inducible factor 1a (HIF1α), a master regulator of the cellular response to hypoxia (290). Fang et al. recently showed, that single MCT inhibition using VB124 is enough to mitigate lactic acidosis and improve the response to immune checkpoint blockade (ICB) *in vivo* in a hepatocellular carcinoma model system (294).

In this PhD project, we aimed to delineate whether single blockade of MCT1 or MCT4 is sufficient to reduce lactate secretion and assessed the immunomodulatory role of the selective MCT1 inhibitor (MCT1i) AZD3965 and a novel MCT4 inhibitor (MCT4i) (293).

5.1.2.1 MCT inhibition reduces tumor-derived lactic acid

In a first step, we investigated the anti-tumor effect of inhibiting MCT1 and/or MCT4 on the colorectal carcinoma cell line HCT116. HCT116 cells expressed both transporters MCT1 and MCT4. In presence of both lactate transporters, several studies revealed that glycolytic and especially hypoxic tumors may be refractory to MCT1 inhibitor AZD3965 (102,331,382). This suggests that co-expression of MCT4 facilitates an escape mechanism for tumor cells (80). Indeed, monotherapy with MCT1 or MCT4 inhibitors in HCT116 2D cultures had no effect on lactate secretion, while combined treatment diminished lactate efflux and extracellular acidification.

Tumor spheroids provide fundamental hallmarks to improve translation into *in vivo* settings. In contrast to 2D cell culture, spheroids mimic the characteristic features of solid tumors such as spatial architectures with extracellular matrix, establishment of a TME with various soluble mediators such as metabolites, cytokines and chemokines, gene expression patterns, gradients of hypoxia, nutrients and lactate. Tidwell et al. recently compared the metabolism of 2D and 3D cultured colorectal carcinoma (CRC) cell lines HCT116 and SW948 and found increased glycolytic activity and MCT4 expression of tumor spheroids compared with monolayer cultures (383). In line, we observed pronounced upregulation of MCT4 in HCT116 spheroids, resulting in a higher MCT4/MCT1 ratio compared with monolayer cultures. The increase in MCT4 expression might be mediated by HIF1α activation due to hypoxic gradients in tumor spheroids (290). Moreover, it has been shown that HIF1α is activated via ROS/PI3K/Akt signaling pathway in CRC tumors (384). Strikingly, in 3D HCT116 tumor spheroids, single MCT4 inhibition was sufficient to reduce lactate secretion as the MCT4/MCT1 ratio shifted in favor of MCT4. According to the analysis of TCGA data by Bovenzi et al, many cancers have higher MCT4 expression than MCT1 expression (76), suggesting that MCT4 is a superior target than MCT1.

In accordance with other studies, our results reveal that the direct anti-tumor effects even upon dual MCT1 and MCT4 inhibition remain limited (80,323,365). The viability of HCT116 was not affected in both 2D and 3D cultures, and proliferation was reduced only by the combined inhibition of MCT1 and MCT4. One escape mechanism could be the metabolic flexibility of tumor cells, as they might be able

to switch to mitochondrial respiration to meet their energy needs (125). Indeed, HCT116 cells already showed basal respiration, which was slightly increased by inhibition of MCT4. As a result, cells might be sensitized to inhibitors of mitochondrial respiration such as metformin. Benjamin et al demonstrated a lethal effect on HL60 cells by combining the MCT1/4 inhibitor syrosingopine with metformin, an inhibitor of the complex I respiratory chain (323). In this context, hyperpolarized magnetic resonance spectroscopic imaging was used to show that inhibition of LDH drives MIA PaCa-2 and HT29 tumor cells towards mitochondrial respiration. Inhibition of both mitochondrial complex 1 and LDH suppresses metabolic flexibility and leads to inhibition of tumor growth *in vivo* (385). In line, we have previously shown cytotoxic and cytostatic effects on THP-1 and primary AML cells by the combination of diclofenac and metformin (386).

Therefore, combining glycolytic and mitochondrial inhibition might be a promising strategy to increase efficacy of anti-metabolic therapy, however, the adverse effects of such anti-metabolic drugs on T cells need to be carefully studied. Our group has previously shown that T cells exhibit metabolic flexibility and maintain their effector functions under either glucose deprivation or mitochondrial restriction, whereas restriction of either factor severely impairs T cell function (371).

5.1.2.2 Preserved T cell function upon MCT inhibition

Since accelerated glycolysis occurs not only in tumor cells but also in activated T cells, inhibition of MCT1/4 could affect their effector functions and subsequent immune surveillance (307,372,387,388). To our knowledge, there are limited data on the importance of MCT1/4 transporters in T cells, particularly in relation to the human immune system. Being considered not only as anti-tumor agents but also as immunotherapeutic approaches to prevent lactic acidosis of TME, adverse effects of MCT inhibition on T cells should be carefully studied.

Upon activation, $CD3^+$ and $CD8^+$ T cells showed robust MCT1 and MCT4 expression, which was slightly downregulated in $CD8^+$ T cells by inhibition of both transporters. Moreover, the expression of the chaperone CD147 was slightly reduced in $CD3^+$ and $CD8^+$ T cells by combined targeting of MCT1 and MCT4. The kinetics of MCT expression with a delayed MCT4 upregulation upon activation renders T cells more sensitive to inhibition of MCT1 compared to tumor cells (365), resulting in decreased lactate secretion and less acidification with MCT1 inhibitor alone in $CD8^+$ T cells and in combination with MCT4 inhibitor in $CD3^+$ and $CD8^+$ T cells. Viability of $CD3^+$ and $CD8^+$ T cells was not affected by MCT inhibition.

In the past, MCT1 was even considered a target for immunosuppression by Murray and colleagues because treatment with AZD3965 as MCT1 inhibitor decreased lactate secretion and proliferation of human T cells (286). Unfortunately, they did not analyze effector functions under MCT inhibition.

Interestingly, in our hands single MCT1 inhibition and combination with MCT4 inhibitor diminished respiration of T cells. Notably, MCT2 is also inhibited by the MCT1 inhibitor AZD3965 (287). MCT1/2 are potent transporters for pyruvate, and there are controversial reports whether MCT1/2 can also be expressed in the mitochondrial membrane, potentially facilitating pyruvate transport to the tricarboxylic acid cycle (89,96,98–100,389). Consistent with this hypothesis, Jonnalagadda et al. demonstrated cellular uptake of MCT1/4-inhibitory compounds based on the structure of cyanocinnamic acid and found them localized near mitochondrial compartments (284). If MCT1 or MCT2 were responsible for the transport of pyruvate into the mitochondria of T cells besides the transport of lactate, this could be a reason for the impaired respiration in addition to the decreased glycolysis.

We recently demonstrated that treatment with diclofenac as an MCT1/4 inhibitor did not affect cytokine production by T cells (365). Likewise, interferon γ production by $CD3^+$ and $CD8^+$ T cells was preserved with single and combined targeting of MCT1 and MCT4 with selective inhibitors. In addition, $CD4^+$ and $CD8^+$ T cells from mice lacking MCT4 showed sustained interferon γ production (365). Although cytokine production was not affected, proliferation of $CD3^+$ and $CD8^+$ T cells was reduced when MCT1 and MCT4 were simultaneously challenged, as previously shown by Murray et al. (286). The anti-glycolytic drug 2-deoxyglucose is known to impair effector functions of T cells (329,330,371), whereas we and others have shown that T cell function was not impaired under low glucose conditions (371,390)

In summary, consistent with our previous studies (365,371) our data provide evidence that MCTs or glucose metabolism might be of minor importance for effector functions of human T cells, however limit T cell proliferation (123,307,391,392). These results indicate that the use of MCT inhibitors could be further explored for immunotherapies.

5.1.2.3 Immunocompetent phenotype of macrophages upon MCT inhibition

Apart from tumor cells and T cells, tumor-associated myeloid cells contribute to lactate acidosis in the TME (37). In general, macrophages and other myeloid cells are recruited to tumors in large quantities, where they undergo adaptions in their metabolism and phenotype that can promote immunosuppression in turn. Glycolytic tumors such as B16 melanoma and LLC lung carcinomas were demonstrated to foster immunosuppressive macrophage polarization (38,39). Reinfeld et al. demonstrated that microbead isolated $CD11b^+$ myeloid cells from MC38 tumors showed the highest capacity for fluorodeoxyglucose (FDG) uptake and seem to be highly glycolytic (141). Moreover, it has been shown that LDHB in TAMs is downregulated in murine and human breast cancer, thereby increasing aerobic glycolysis (393). In line, TAMs express lactate dehydrogenase A (LDHA), which is considered as the lactate producing subunit of the LDH (394), and myeloid-specific deletion of LDHA

supported T cell anti-tumor response and reduced tumor growth (142). Besides targeting the tumor metabolism, targeting the metabolism of tumor-associated myeloid cells is crucial to convert an immunosuppressive to an immune-supporting TME. Therefore, we aimed to target the immunosuppressive glycolytic character of LPS stimulated monocyte-derived macrophages, yielding mixed phenotypes.

Monocyte-derived macrophages expressed MCT1 and MCT4, and neither MCT nor CD147 levels were affected by MCT inhibition. Surprisingly, macrophages were the most resistant cell type to MCT inhibition, as lactate efflux was reduced by only about 30 % with combined MCT1 and MCT4 inhibition. This suggests that macrophages are capable of exporting lactate via unknown transporters, which are not blocked by selective MCT1/2 and MCT4 inhibitors. In addition to MCT1/2 (targeted by MCT1i) and MCT4 (targeted by MCT4i), MCT3 and SLC5A8/12 are known lactate transporters that may be involved in macrophage metabolism and could mediate lactate transport. To date, nothing is known about the expression levels of proton-linked MCT3 and sodium-coupled SLC5A8/12 in macrophages.

Of note, secretion of IL-6 was strongly reduced by inhibition of MCT1 and MCT4. In this context, Tan et al. demonstrated that blockade of MCTs with CHCA or knockdown of MCT4 in macrophages resulted in decreased IL-6 secretion (395). IL-6 is one of the most important cytokines in the tumor microenvironment (TME). High levels in tumors reflect a strong association with inflammation, where it promotes tumorigenesis through multiple mechanisms and signaling pathways (396) and are associated with poor outcome in many cancers (397,398). Blocking IL-6 and combining it with conventional cancer therapies is considered as a potential therapeutic approach for cancers with predominant IL-6 signaling (396). Huseni and colleagues demonstrated that IL-6-STAT3 signaling inhibits conventional cytotoxic differentiation of cytotoxic T cells *in vitro* and that IL-6 receptor deficiency in T cells improves anti-PD-L1 therapy *in vivo* (399). This suggests that tumor-derived and systemic IL-6 serves as an immune checkpoint that tumors ambush to evade killing by cytotoxic $CD8^+$ T cells activated by ICB treatment. Therefore, there are compelling reasons to target the IL-6 pathway in combination with ICB (400). Recent publications have shown that targeted inhibition of IL-6 increases the efficacy of anti-PD-L1 treatment in hepatocellular carcinoma and pancreatic cancer in murine pancreatic cancer models (401,402). Indeed, several clinical trials are already underway testing the ability of IL-6-targeted agents to improve efficacy of ICB, including an anti-IL-6 receptor antibody Tocilizumab and anti-PD-L1 antibody Atezolizumab in patients with non-small cell lung cancer (NCT04691817) and another anti-IL-6 receptor targeting antibody Sarilumab in combination with anti-CTLA4 inhibitor Ipilimumab, anti-PD-1 Nivolumab, and the anti-LAG-3 antibody Relatlimab in patients with melanoma (NCT05428007) (400).

Therefore, the demonstrated inhibitory effect of MCT inhibition on IL-6 production by macrophages could provide an additional beneficial effect for combination strategies with immune checkpoint blockade (ICB). In addition, PD-L1 expression decreased while MHC-II expression increased with dual MCT inhibition, highlighting the beneficial effects and promotion of an immunocompetent phenotype. Complementary, uptake of lactic acid by Treg cells in a highly glycolytic TME induced PD-1 expression (114).

Feng et al. described the lactate-dependent induction of PD-L1 expression via G protein-coupled receptor 81 (GPR81) signaling in human lung cancer cells (403). The expression of GPR81, a cell-surface receptor for lactate, was recently detected on macrophages (404). MCT inhibition reduces glycolysis and thus lactate, which could counteract lactate-GPR81-PD-L1 signaling. Furthermore, it has been shown that MCH-II is downregulated in lactate-GPR81 dependent manner in DCs (405). Another mechanism could be transcriptional regulation of gene expression through lactylation of histone lysine by T-lactate, a novel epigenetic histone modification discovered by Zhang et al. 2019 (406). They found a correlation between lactylation and expression of M2-associated genes such as arginase 1 (Arg-1). Reduction of lactate production by LDH inhibitors also reduced lactylation and expression of Arg-1 (406).

Although lactate secretion was not completely reduced, MCT inhibition led to a remodeling of macrophages to an immunocompetent phenotype with decreased IL-6 secretion and PD-L1 expression and increased MHC-II expression, which in turn could support response to immunotherapy.

5.1.2.4 No impact on granulocytes by MCT inhibition

TANs correspond to a heterogeneous group of neutrophils and are, similar to macrophages, subclassified into pro-tumoral N2-like or and anti-tumoral N1-like neutrophils, respectively (154). It has been shown that the neutrophil phenotype can be reprogrammed during tumor progression from N1-like towards pro-tumorigenic N2-like (407). TANs often promote tumor progression by numerous implicated pathways, but on the other side N1-like neutrophils can also damage tumor cells by ROS and cytokine secretion (408). However, not only tumor resident TANs are related to cancer but also blood circulating neutrophils. More precisely, blood neutrophils are attributed to tumor metastasis formation. Once in the vascular blood system, tumor cells bind various adhesion molecules of neutrophils. On the one hand, this mechanism shields the tumor membrane from immune surveillance; on the other hand, it activates migratory pathways, leading to increased extravasation and, in turn, promoting access to premetastatic tissue beds (409). This mechanism has been demonstrated to contribute liver metastasis (410,411). Neutrophils contain few mitochondria and cover their energy demands primarily through glycolysis (313). Furthermore, neutrophils are

considered to express MCT1 and MCT (314). However, to our knowledge, nothing is known about the effects of targeting glycolysis in neutrophils.

Several strategies have already been developed to target immunosuppressive neutrophils in cancer based on depletion of existing neutrophils, inhibition of polymorphonuclear myeloid-derived suppressor cells (PMN-MDSCs) development, and attraction of neutrophils or targeting their immunosuppressive mechanisms (412). We observed no changes in viability of neutrophils upon MCT inhibition. Moreover, none of the analyzed surface molecules nor neutrophil ROS production were affected by MCT inhibitor treatment. Our results suggest that MCT inhibition does not harm neutrophils, although interpretation of these results is problematic due to the short lifespan of neutrophils *in vitro*. Nevertheless, further investigations of the complex interaction between neutrophils and tumor cells could provide new insights and pave the way for novel future cancer treatments and moreover metastases prevention.

5.2 MCT inhibition for tumor therapy and immune activation in colorectal carcinoma

Analysis of the impact of lactic acid on immune cells revealed severe immunosuppressive effects. MCT inhibition proved to be a promising strategy to reduce tumor-induced lactic acidosis, did not affect T cell function, and showed positive effects on the macrophage phenotype. However, the study of tumor cells or immune cells is not realistic enough to mimic the complexity of the TME. Tumors consist of numerous cell types, including tumor cells, lymphoid and myeloid immune cells. To elucidate the immunomodulatory role of MCT inhibitors with and without ICB, we established a 3D co-culture model of colorectal carcinoma (CRC) tumor spheroids with human peripheral immune cells and studied the *in vivo* effects in a syngeneic CRC mouse model.

5.2.1 Role of MCTs in colorectal carcinoma

CRC is the third most common cancer and even ranks second in mortality according to GLOBOCAN (1). Several studies investigated the prognostic value of single proteins related to glycolysis, but the results for CRC were inconsistent (336,337). Offermans et al. analyzed the expression of six Warburg-related proteins, including MCT4, and recently demonstrated that CRC patients with a defined high expression of Warburg-related proteins have a worse outcome than patients with low levels of these proteins (338). In addition, others have found a correlation between MCT4 expression analyzed by immunohistochemistry (IHC) and survival of CRC patients (77–79). Nevertheless, when analyzing SLC16A3 encoding MCT4 in TCGA data, we found a correlation with overall survival only in rectal cancer, but not in colon cancer. Consistent with this, Mirnezami et al. found higher lactate levels in rectal cancers than in colon cancers (413). However, all studies reporting a prognostic value of MCT4 and survival of CRC patients rely on IHC staining rather than bulk RNAseq, suggesting that bulk mRNA expression data may not adequately reflect protein expression.

Current treatment strategies for CRC are limited. Immune checkpoint blockade (ICB) therapies such as anti-programmed cell death ligand 1 (aPD-L1) have been shown to be effective in various cancers, while preclinical and clinical data for CRC are rare. Immunotherapy for CRC patients is restricted to a small subset of 15 % of tumors with mismatch repair deficit (MMRd)/microsatellite instability (MSI).

Several studies have shown that $CD8^+$ T cell infiltration is a prognostic factor for overall survival in CRC (26,27,129). In consequence, Galon and colleagues proposed an immunoscore classification of CRC in addition to classical tumor-node-metastasis TNM staging (130,131). In addition, the abundance of cytotoxic T cells has been associated with response to immunotherapy in MSI CRC tumors (195). In line, Vasaikar et al. found a negative correlation between $CD8^+$ T cell count and increased glycolysis in

MSI-high CRC tumors, suggesting that the Warburg effect limits the success of immune checkpoint inhibitors (37,115). Given that tumor-induced lactic acidosis impairs the function of T cells and NK cells, as well as other immune cells, resistance to immunotherapy could be functionally linked to the Warburg phenotype (118,365). Therefore, we tested whether combination therapies of MCT inhibitors, which attenuate the Warburg effect, with ICB could enhance the success of immunotherapies (118,119,143,365).

5.2.2 MCT4 inhibition supports T cell function and potentiates ICB in human 3D HCT116 spheroid co-cultures

HCT116 cells express high levels of the immune checkpoint PD-L1, probably rendering them sensitive to T cell mediated killing in the presence of anti-PD-L1 antibody. However, as HCT116 cells are highly glycolytic, a combined treatment of ICB and MCT blockade, reducing the secretion of immunosuppressive lactic acid, might be superior to ICB alone. To test this hypothesis, we established a 3D co-culture model of HCT116 tumor spheroids with human whole blood immune cells. Spheroid cultures are an old tool to study tumor biology that has recently gained renewed interest (414). More than a decade ago, our group demonstrated the potential of tumor spheroids to study the interaction between tumor and immune cells (415). Nevertheless, spheroid co-culture models are not yet widely used by the scientific community, although they could complement and refine animal experiments. Recent publications have shown the infiltration of immune cells into CRC spheroids and highlight the potential of spheroid co-cultures with immune cells to study immunotherapy approaches (416–418).

As mentioned in Chapter 5.1.2.1, MCT4 was upregulated in HCT116 spheroids. Given that MCT4 monotherapy was sufficient to reduce lactate secretion in 3D spheroids to the same level as the combination with MCT1, MCT4 may play a more important role than MCT1. Strikingly, inhibition of MCT4 with or without anti-PD-L1 antibody resulted in a significant increase in leukocyte infiltration into HCT116 spheroids. The elevated leukocyte levels could not be delineated to a specific impact on a single immune cell population as immune cell composition in terms of T cell, Treg, monocyte, and granulocyte frequency was not altered. Neither ICB nor MCT1i alone elevated overall immune cell infiltration, moreover, double MCT blockade diminished the positive effect of MCT4 inhibition. Since we observed reduced lactate accumulation upon MCT4 inhibition with or without MCT1 inhibitor, we hypothesized that T cell function might be improved in a co-culture system. Indeed, co-cultured spheroid-infiltrated T cells showed enhanced anti-tumor function after MCT4 inhibition, as evidenced by increased proliferation and IFNγ production. Although lactate efflux was blocked to the same extent, additional MCT1 inhibitor application failed to further improve T cell response. Surprisingly, additional blockade of MCT1 using specific inhibitors counteracted the beneficial effect of MCT4

inhibition on T cell response in co-culture with HCT116 spheroids and impaired T cell proliferation. In line, Murray et al. postulated that MCT1 might be important for proliferation and proposed MCT1 as target for suppression of T cells (286). In our previously published study on the impact of diclofenac, we did not detect these adverse effects on T cells *in vitro*. The underlying reason could be that diclofenac blocks MCT4 with much higher potency than MCT1 (365) and probably less effective than a selective MCT1 inhibitor.

Highly glycolytic tumor metabolism and glycolytic gene expression is negatively associated with response to anti-PD-1 ICB, which has been published for renal cell carcinoma (118) and melanoma (365). In our CRC co-culture model, combination therapy of MCT4 inhibitor and anti-PD-L1 immune checkpoint blockade induced T cell-mediated killing of HCT116 tumor spheroids. In line, Fang et al. recently demonstrated that the MCT4 inhibitor VB124 can enhance the response to ICB *in vivo* in a model system of hepatocellular carcinoma. They demonstrated that knockdown of MCT4 reduced tumor cell glycolytic activity and thus extracellular acidification (294). Overall, our findings demonstrate that MCT4 inhibition can reverse the immunological consequences of the Warburg effect, e.g. lactic acid-driven immunosuppression and thereby enhance ICB in a CRC *in vitro* spheroid co-culture model with predominant MCT4 expression.

To prove the specificity of the observed effects in the presence of the MCT4 inhibitor, we knocked-out the respective transporter in HCT116 cells. As previously shown single MCT4 knock-out did not alter lactate secretion (102,327), but rendered tumor cells sensitive to MCT1 blockade and as expected insensitive to MCT4 inhibition. In line with its impact on lactate secretion, monotherapy with MCT1 inhibitor increased the number of infiltrating leukocytes in an $HCT116^{MCT4-/-}$ model. T cell proliferation was not affected but IFNγ expression was elevated in the presence of aPD-L1 antibody and MCT1 inhibition. Improved T cell function with MCT1 inhibitor and aPD-L1 in $HCT116^{MCT4-/-}$ spheroids proved that prevention of lactic acidosis is the underlying mechanism. Surprisingly, there was still an effect of the MCT4 inhibitor, indicating a tumor cell independent impact of the inhibitor on infiltrating immune cells. Similar to wildtype HCT116 spheroids the combined administration of both inhibitors had no positive impact leukocyte infiltration or IFNγ expression.

Taken together, our results demonstrate that selective MCT4 inhibition synergizes with ICB *in vitro*. The improved leukocyte infiltration and T cell function is based on reduced lactic acidosis by MCT4 inhibition and T cell-mediated killing by additional unleashing of the T cell response with anti-PD-L1 therapy.

5.2.3 MCT4 blockade improves the efficacy of immune checkpoint blockade *in vivo*

We investigated the effects of selective MCT1 and MCT4 inhibitors on tumor or immune cells alone, but also in a human CRC HCT116 spheroid co-culture model with tumor and immune cells. These results demonstrated an immunomodulatory role of single MCT4 inhibition based on the reduction of lactic acid accumulation. Attenuation of the immunological consequences of lactic acid by MCT4 inhibition enhanced the efficacy of ICB in HCT116 spheroids in co-culture with whole blood leukocytes. Therefore, we were interested in finally translating these results into an *in vivo* model in which the murine CRC cell line MC38 was inoculated into immunocompetent C57BL/6N wildtype mice. Although mice mirror human biology in most respects, we and other researchers have found differences in terms of immunology (347). In humans, for instance, neutrophils are the most common immune cell type in the blood with about 60 %, whereas blood of mice contains hardly any neutrophils but large amounts of B cells of about 60 %. In addition, blood glucose and lactate levels differ fundamentally. While in humans the blood levels are about 5 mM for glucose and 1-2 mM for lactate, in mice levels are much higher with concentrations of about 10 mM for both (419). Therefore, prior to *in vivo* experiments, we confirmed the efficacy of selective MCT4 inhibitor treatment in a murine MC38 tumor spheroid co-culture model.

5.2.3.1 MC38 spheroid co-culture

To confirm the supportive effect of MCT inhibition in the murine system *in vitro*, we performed live cell imaging of murine CRC MC38 spheroids co-cultured with B cell-depleted and pre-activated splenocytes to investigate the effects of MCT4 inhibition on the killing capacity of MC38 tumor cells by tumor-infiltrated T cells (TILs). In general, MC38 cells showed very low expression of MCT1 and high expression of MCT4. Consistent with the shift in MCT pattern in HCT116 cells, MCT4 was strongly upregulated in MC38 spheroids compared with monolayers, resulting in decreased lactate efflux upon selective MCT inhibitor treatment, suggesting that MC38 is an MCT4-driven tumor model.

Indeed, we observed enhanced killing of MC38 tumor cells by MCT4 inhibition, which might be due to lower levels of immunosuppressive lactic acid. However, in contrast to human HCT116 co-culture, the killing was already observed with monotherapy with the MCT4 inhibitor and was not supported by combination with aPD-L1, although we found PD-L1 expressed on MC38 tumor cells. Jenkins et al. observed immune cell-mediated killing with aPD-1 therapy in *ex vivo* MC38 spheroids prepared from single-cell preparations of MC38 tumors (420). A major difference between human and mouse spheroid model is that T cells in HCT116 co-cultures are not HLA-matched and therefore alloreactive, whereas mouse MC38 co-cultures use syngeneic splenocytes. In an alloreactive setting, T cells already

recognize foreign peptide-MHC complexes, resulting in an alloreactive, non-antigen-specific response, which could explain the stronger immune response in human HCT116 co-cultures.

Finally, we wanted to test the treatment in an antigen-specific model. Therefore, we used genetically modified MC38-OVA cells that constitutively co-express green fluorescent protein (GFP) and ovalbumin. MC38-OVA spheroids were treated with MCT inhibitors and ICB and following co-cultured with B cell depleted splenocytes isolated from spleens of OT-I mice. OT-I $CD8^+$ cytotoxic T cells recognize the ovalbumin presented via MHC-I molecules from MC38 tumor cells. Strikingly, MC38-OVA spheroids were completely destroyed by OT-I T cells upon MCT4 inhibition combined with aPD-L1 immune checkpoint blockade. Also, with the single MCT4 inhibitor and single aPD-L1 treatment MC38-OVA spheroids were clearly attacked, but only combination of both drugs led to a complete dissolution of the spheroid. Interestingly, the addition of MCT1 reversed the beneficial effect of the selective MCT4 inhibitor, as also observed in the HCT116 co-culture experiment, suggesting that MCT4 inhibition is efficient as an immunostimulatory treatment and even superior to dual MCT1 and MCT4 blockade.

In summary, we could prove that MCT4 inhibition enhances anti-tumor response of T cells not only in human but also murine *in vitro* experiments and possibly acts synergistically with ICB.

5.2.3.2 Combined MCT4 inhibition and ICB improves $CD8^+$ T cell infiltration and skews myeloid cell phenotype in MC38 tumors

Finally, we aimed to translate our findings to the *in vivo* situation and inoculated the CRC cell line MC38 into syngeneic C57BL/6 mice. In our previous study, diclofenac as MCT1/4 inhibitor supported checkpoint therapy using anti-PD-1 and anti-CTLA-4 in a 4T1 breast cancer mouse models (365). Huang et al. showed that MCT1 inhibitor (AZD3965) loaded inside to ultra-pH-sensitive nanoparticles increased anti-PD-1 efficacy in B16 and TC-1 tumor models (308). Our data revealed that dual MCT1 and MCT4 blockade using selective inhibitors improved ICB in MC38 tumors. Strikingly, MCT4 monotherapy with ICB showed similar efficacy as in combination MCT1 inhibition, which might be due to high MCT4 and low MCT1 expression of MC38 tumor cells. However, the additional use of MCT1 was not inferior to MCT4i therapy with ICB, as observed in *in vitro* cultures. This suggests that T cells are more metabolically flexible *in vivo* than under *in vitro* conditions with artificial stimulation.

Interestingly, spleen weights were increased in all treatment groups receiving aPD-L1 antibody, suggesting immune activation. Of note, in a recent study, an increased mean spleen volume was observed in stage III and IV cancer patients treated with anti-CTLA-4 and anti-CTLA-4/anti-PD-1 ICB (421). Control of MC38 tumor growth upon MCT4 inhibitor along with aPD-L1 might be mediated by increased abundance of IFNγ-producing cytotoxic $CD8^+$ T cells. In line, Fang et al. recently demonstrated that VB124 is capable to improve the response to ICB *in vivo* in a hepatocellular

carcinoma model system by increasing $CD8^+$ T cell infiltration and function (294). Furthermore, they showed that the increased $CD8^+$ T cell infiltration was due to increased secretion of the chemokines CXCL9 and CXCL10, which attracts T cells. They hypothesized that blockade of MCT4 leads to intracellular accumulation of lactate, which is then introduced into the TCA cycle, resulting in increased ROS levels. The increase in ROS then triggers transcription of CXCL9 and CXCL10 via NF-kB signaling. In fact, recent studies have linked CXCL9 and CXCL10 to the response to ICB (422–424). Whether the expression of CXCL9 and CXCL10 was also regulated in our experiments and responsible for the increased $CD8^+$ T cell infiltration requires further investigation.

Besides improved $CD8^+$ T cell infiltration and function, we found less $Gr\text{-}1^+$ myeloid-derived suppressor cells (MDSCs) upon combination therapy with MCT4 inhibitor and ICB and the remaining MDSCs expressed higher levels of MHC-II. Compared to $Gr\text{-}1^-$ cells, MDSCs expressed extremely low levels of MHC-II, indicating their immunosuppressive function. Increase in MHC-II expression might further support immunosurveillance due to increased antigen-presentation to $CD4^+$ T cells. Similar, MHC-II levels on tumor-associated macrophages (TAMs) were elevated. These findings are consistent with the induction of an immunocompetent phenotype in monocyte-derived macrophages by MCT inhibition. Zhang et al. found high histone lactylation in TAMs compared with peritoneal macrophages and a correlation between lactylation and transcription of M2-related genes such as Arg-1. Interestingly, exogenous lactate activates M2-related gene expression through histone lactylation, and reduction of lactate by LDH inhibition decreased lactylation and M2-like polarization (406). Others showed that MHC-II expression in DCs is lowered by lactate via GPR81 signaling (405).

To determine the specificity of the effects of MCT4 inhibition and ICB, we analyzed immune cells from blood, spleen, and lymph nodes. MCT4 inhibition appears to be tumor-specific, as no effects on T cells or myeloid cells were observed outside the tumor.

Tasdogan et al. observed little effect on tumor growth upon selective MCT1 inhibition, but a reduction in metastasis in patient-derived xenografts and in mouse melanomas (425). Likewise, selective MCT4 inhibition failed to prevent tumor progression, which is consistent with results from Heinrich et al. (293). One reason might be that MC38 cells are metabolically flexible and can switch to oxidative phosphorylation while glycolysis is restricted.

However, although we see improved anti-tumor immunity of $CD8^+$ T cells upon MCT4 inhibition and anti-PD-L1 *in vitro* and *in vivo*, MC38 tumors were not completely rejected. This indicates that tumors develop escape mechanisms, which need to be further investigated. Our *in vitro* tumor spheroid co-cultures with immune cells indicate that complete rejection of MC38 tumors *in vivo* may require an antigen-specific system such as ovalbumine expressing MC38-OVA cells and OVA-specific OT-I T cells.

Only in this antigen-specific system we observed a complete destruction of MC38 OVA spheroids by OT-T cells. We observed excessive high levels of reactive oxygen species (ROS) in tumors and found increased cytosolic ROS levels in all types of immune cells, especially $CD8^+$ T cells and NK cells. On the one hand, ROS is an important signaling molecule, on the other hand, excessive ROS levels impair T cell function and viability (348,426,427). The exact mechanisms are still unclear, but targeting ROS could be a potential strategy to further counteract immune suppression. In our study related to the global COVID-19 pandemic, we found accumulation of ROS in T cells from patients with severe COVID-19 associated with impaired mitochondrial structure and metabolic quiescence (428). In addition, Pilipow and colleagues showed that scavenging ROS with N-acetylcysteine in activated naïve $CD8^+$ T cells blocks terminal differentiation but promotes long-lived memory T cells with stem cell-like properties, which enhances adoptive CD19-specific CAR T cell therapy in a xenogeneic model (429).

To elucidate the main MCT4i target, tumor or stromal cells, we performed *in vivo* tumor experiments using MC38 lacking MCT4. Mct4 knock-out did not affect tumor growth kinetics. This suggests that $MC38^{Mct4-/-}$ cells may have adapted to MCT4 limitation and upregulated MCT1 as a compensatory mechanism, allowing them to sustain their continuous proliferation. However, in $MC38^{Mct4-/-}$ ICB alone reduced tumor growth to a level comparable to $MC38^{wt}$ tumors treated with ICB and MCT4 inhibitor. This early effect of ICB was transient and prolonged survival only by trend, whereas only $MC38^{Mct4-/-}$ tumor bearing animals receiving both, aPD-L1 and MCT4i, showed better survival probability compared to controls. These data indicate, that early on the MCT4 inhibitor acts mainly on tumor cells, but hereafter impacts also stromal cells. Apart from tumor cells and T cells, tumor-associated myeloid cells are important producers of lactate (37). Reinfeld et al. demonstrated that microbead isolated $CD11b^+$ myeloid cells from MC38 tumors showed the highest capacity for FDG uptake and seem to be highly glycolytic (141). Moreover, it has been shown that TAMs express lactate dehydrogenase A (LDHA) and myeloid-specific deletion of LDHA supported T cell anti-tumor response and reduced tumor growth (142). This suggests that MCT4 inhibitors later on target infiltrating immune cells as macrophages. In line, Tan et al. recently reported MCT4 expression in human and mouse bone marrow-derived macrophages and found that knockdown of MCT4 decreased IL-6 secretion (395). IL-6 is associated with poor outcome in many cancers (397,398).

This suggests that MCT4i not only acts on tumor cell lactate metabolism, but also promotes an immune-stimulatory environment and polarization of tumor-infiltrating immune cells.

5.2.3.3 MCT4 inhibition mitigates the Warburg phenotype *in vivo*

Combined treatment with MCT4 inhibitor and ICB improved T cell infiltration and function *in vitro* and *in vivo* and prolonged survival of mice bearing MC38 tumors. *In vitro* experiments revealed decreased lactic acid efflux from tumor and immune cells upon MCT4 inhibition. Therefore, we hypothesized that

MCT4 inhibition would attenuate the Warburg effect *in vivo* and thereby counteract the immunological consequences.

Indeed, we were able to show that blockade of the predominant proton-coupled lactate transporter MCT4 in MC38 tumors prevented intratumoral acidification compared with anti-PD-L1 monotherapy. As previously reported, inhibition of T cell function was due to concomitant acidification by lactic acid, as buffering reversed the effect (364). In this context, Uhl et al. recently showed that lactic acid produced by acute myeloid leukemia cells inhibited T cell effector functions, which could be reverted by buffering with sodium bicarbonate (370). However, it is unclear whether systemic administration of sodium bicarbonate is feasible for cancer patients and whether it can neutralize the acidic pH in the TME at all. Another strategy against tumor acidosis is to inhibit the proton pumps with proton pump inhibitors (PPIs). It has been shown that blockade the of H^+/K^+ ATPase counteracted acidification of the TME, reverses anergry and improved effector function of T cells leading to delayed tumor growth of B16-OVA tumors *in vivo* (303). Furthermore, this treatment skewed macrophages into an immune-stimulatory phenotype (430) and induced tumor cell death due to intracellular acidification (431). However, retrospective studies have indicated that concomitant treatment of patients with PPIs and ICB may have a positive effect on the response and survival of melanoma patients, but a negative effect on patients with non-small cell lung cancer (432–434). Cappellesso et al. recently identified SLC4A4 as the most highly expressed bicarbonate transporter in pancreatic ductal adenocarcinomas. Targeting SLC4A4 decreased TME acidosis due to bicarbonate accumulation and enhanced T-cell-mediated anti-tumor response, resulting in improved response to immunotherapy (435).

MCT4 blockade leads to intracellular accumulation of lactate, which in turn hinders further metabolization of pyruvate to lactate. Consequently, glycolysis is impaired, as evidenced by increased glucose concentrations in tumors and complementary decreased glucose uptake of MC38 tumor cells. Moreover, we found a correlation between tumoral glucose and lactate concentrations. The importance of interstitial fluid analysis was recently emphasized by Apostolova and Pearce (436). In our studies we were able to confirm that the immune cells in the interstitial fluid are exposed to even higher concentrations of lactate and furthermore the same effects on glucose levels were observed (data not shown).

In agreement with Vasaikar et al., these results suggest that attenuation of the Warburg effect by MCT4 inhibitor treatment improves ICB through enhanced $CD8^+$ T cell infiltration and cytotoxicity (115). In line, Fang et al. reported that inhibition of MCT4 using VB124 as inhibitor compromises lactate accumulation in the TME (294). The absence of any effects on T cells in spleen, blood and draining lymph nodes as well as unaffected glucose uptake of tumor-associated immune cells emphasizes the specific targeting of tumor glycolysis by MCT4 inhibitors.

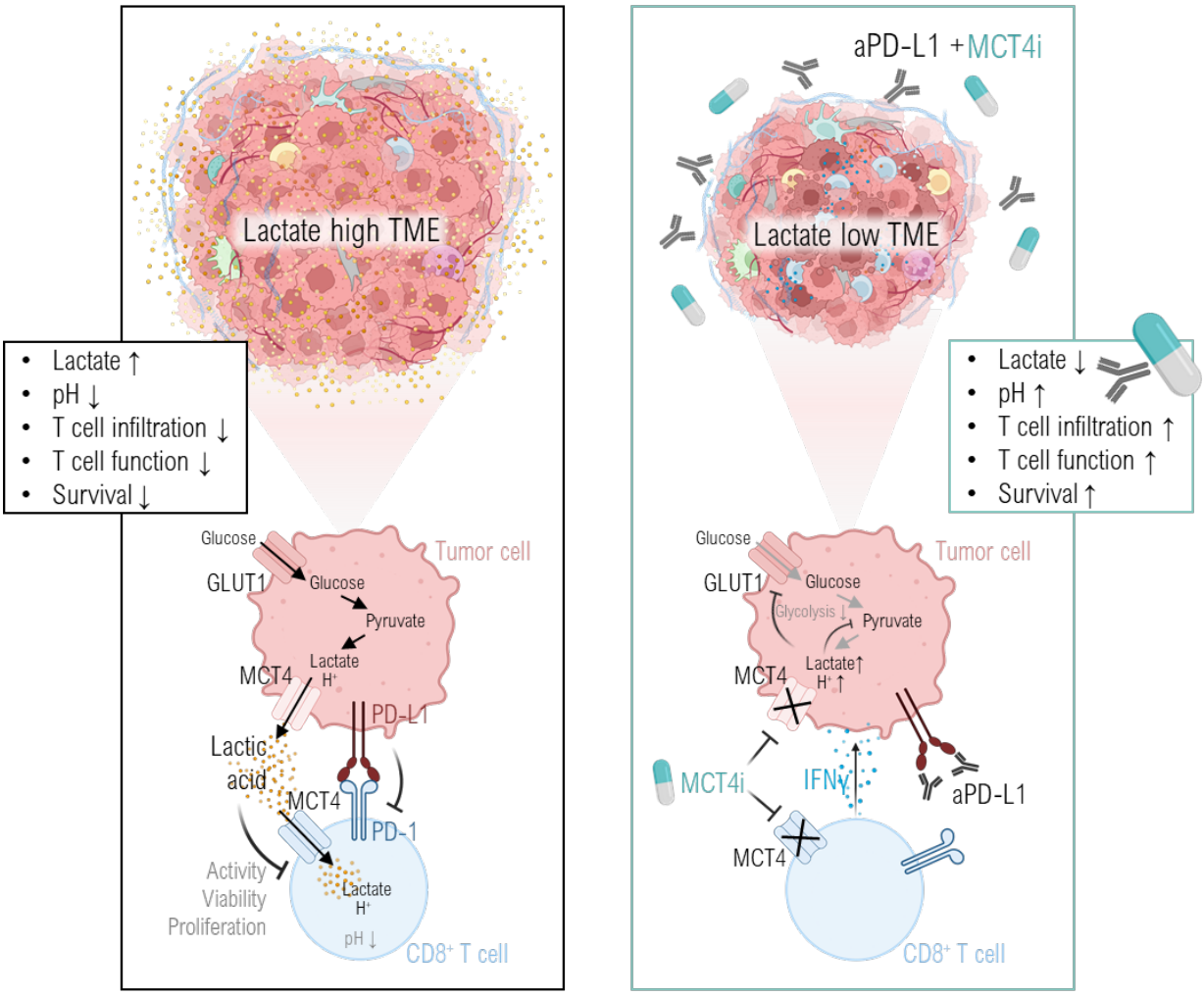

Figure 82. MCT4 blockade reverses lactic acid-driven immunosuppression and increases the efficacy of immune checkpoint blockade. LEFT: Intratumoral lactate accumulation and acidification, the result of the Warburg phenotype, adversely affect T cell function, thereby limiting anti-tumor immune response and the response to immunotherapeutic approaches. RIGHT: Therefore, targeting the predominant monocarboxylate transporter 4 (MCT4), a proton-coupled lactate symporter, is a promising strategy to overcome glycolysis-related therapy resistance. Co-administration of a MCT4 inhibitor to immune checkpoint blockade (ICB) using aPD-L1 augmented T cell infiltration and function *in vivo* and increased intratumoral pH, and prolonged survival compared to ICB only treatment in the MC38 colorectal carcinoma model. Hence, MCT4 inhibition might be a suitable treatment approach to improve ICB efficacy.

5.3 Immunomodulatory role of MCT inhibition in clear cell renal cell carcinoma

5.3.1 Expression of MCT1 and MCT4 determines the outcome of patients with ccRCC

Besides CRC, we were interested in testing the effect of MCT1 and MCT4 inhibition in a second tumor entity. For this purpose, we chose clear cell renal cell carcinoma (ccRCC). Renal cell carcinoma accounts for 2-3 % of solid tumors in adults and comprises several subtypes, with ccRCC subtype being responsible for the majority of cancer-related deaths (351,352,437,438).

ccRCC originates from the proximal tubule and the cell cytoplasm is mostly clear, which stores glycogen. It is characterized by various genetic abnormalities, which lead to loss-of function of the tumor suppressor gene von Hippel-Lindau (VHL). The HIFα subunits are hydroxylated in an oxygen dependent reaction, allowing the recognition by the VHL, a ubiquitin ligase, and subsequent proteasomal degradation. Inactivation of VHL stabilizes HIF1, which binds to regulatory hypoxia-responsive elements (HRE) in DNA (58). Subsequently, expression of more than 70 genes is induced, including VEGF, GLUT1, most glycolytic enzymes, LDHA, and lactate transporter MCT4 (55,59). This molecular tumorigenesis emphasizes the highly glycolytic phenotype of this tumor entity.

Overexpression of MCT4 has been described in several cancers and analysis of TCGA data revealed a correlation of high MCT1 and MCT4 expression with poorer outcome in ccRCC. In line, Kim et al. described overexpression of MCT1, MCT4 and the chaperone CD147 as predictors of tumor progression (439). Enriched glycolysis-related signature is associated with poorer RCC prognosis, progression and immune microenvironment (440). Moreover, our group previously demonstrated that high GLUT1 expression negatively correlated with $CD8^+$ T cell infiltration in ccRCC (438). Notably, T cell infiltration has been described as prognostic factor for several malignancies such as CRC (26). Surprisingly, neither CD8 nor IFNγ expression showed a correlation with survival, but CD14 and IL-6 expression were associated with a poor outcome of ccRCC patients. Consistent with this, Shen et al. reported an association between elevated $CD68^+$ TAMs and poor overall survival and progression-free survival (441), suggesting that TME-polarized pro-tumorigenic myeloid cells are the major determinants for patient outcome in ccRCC.

Therefore, TAMs, MCT1 and MCT4 emerge as potential targets for tumor therapy and selective MCT1 and MCT4 inhibitors, diclofenac as dual MCT1 and MCT4 inhibitor but also cyclooxygenase (COX) 1/2 inhibitor and acetylsalicylic acid (ASA) as COX1/2 inhibitor (442) have been investigated for their anticancer effects.

5.3.2 MCT inhibition reduces lactate and IL-6 secretion in human 3D RJ494 spheroid co-cultures

We first examined the effects of MCT1+4 inhibitors, diclofenac, ASA, and a combination of MCT inhibitors with ASA mimicking the combined MCT and COX inhibitory effects of diclofenac on RCC RJ494 tumor spheroids. RJ494 expresses lactate transporters MCT1 and MCT4, and lactate efflux was reduced by inhibition of both MCTs with selective inhibitors and diclofenac but not ASA. This is consistent with our previous study showing that diclofenac, but not ASA, inhibits MCT1 and MCT4 (365). As previously observed with CRC HCT116 and MC38 spheroids, treatment itself had no effect on morphology or viability of RJ494 spheroids lacking immune cells, indicating metabolic flexibility of tumor cells.

To analyze the effects of MCT inhibition in an "RCC tumor environment", we established a co-culture model with immune cells migrating into 3D RJ494 tumor spheroids, similar to previous CRC co-cultures. However, none of the treatments resulted in clear changes in immune cell infiltration or composition. As TAMs but not T cells correlate with patient prognosis in ccRCC, we focused on infiltrated TAMs. IL-6 can be produced by various cell types in the tumor (443), but TAMs showed the highest levels of IL-6 expression compared to tumor cells, neutrophils and T cells in our RJ494 co-culture model. Analyses of macrophages without tumor contact showed a strong reduction in IL-6 secretion with MCT1+4 inhibition. Similarly, IL-6 levels were significantly reduced by selective MCT inhibitors and diclofenac, but not by ASA, whereas TNF was not affected. In this context, Tan et al demonstrated that blockade of MCTs with CHCA or knockdown of MCT4 in macrophages resulted in decreased IL-6 secretion (395).

The expression of IL-6 is regulated at multiple stages, including chromatin remodeling, transcription, mRNA export, post-transcriptional, and translational levels. A variety of transcription factors have been shown to regulate IL-6 gene activation. IL-6 expression is promoted by NF-kB (nuclear factor kappa B), NF-IL6 (nuclear factor of IL-6), SP1 (specificity protein 1), CREB (cyclic AMP response element-binding protein), IRF-1 (interferon regulatory factor 1), AP-1 (activation protein 1), HSF1 (heat shock transcription factor 1), Fli-1 (Friend leukemia virus integration 1), Tax (transactivator protein), TAT (transactivator of the transcription), and loss of p53 (444). Repressors of IL-6 expression are Ahr (aryl hydrocarbon receptor), GR (glucocorticoid receptor), ER (estrogen receptor), Rb (retinoblastoma), PPAR-α (peroxisome proliferator-activated receptor-α), and several miRNAs (444). Our experiments suggest that glycolysis or lactate may be involved in the regulation of IL-6 expression, because selective MCT inhibitors and diclofenac but not ASA decreased IL-6 secretion. Grivennikov et al. showed that IL-6 expression is triggered by phosphorylated STAT3 (445), and diclofenac has been shown to decrease phosphorylation of STAT3 (446). Other NSAIDs such as celecoxib and sulindac have been demonstrated

to inhibit IL-6/IL-6R induced JAK2/STAT3 phosphorylation (447,448). However, the exact mechanism of MCT inhibition in IL-6 regulation requires further investigation.

Nevertheless, high concentrations of IL-6 in the TME and blood of RCC patients are correlated with worse survival (449–451). Classically, IL-6 initially binds to the α-chain of the non-signaling membrane-bound IL-6 receptor (IL-6R, gp80). Subsequently, this complex binds to two molecules of gp130 and induces signal transduction. JAK/STAT3 and SHP2/Gab/MAPK are the two main pathways involved in gp130 signaling (452–454). Besides the membrane-bound IL-6R, a soluble form sIL-6R has been identified in blood and urine (455). In a process called trans-signaling, the complex of IL-6 and sIL-6R can activate gp130, which is ubiquitously expressed (456–458). IL-6 has been described as key player in regulation of MDSC activity (459,460). Moreover, studies have reported that targeting IL-6 improves differentiation of $CD4^+$ T cells into IFNγ producing Th1 cells (461,462) and augments ICB in murine models of hepatocellular carcinoma and pancreatic cancer (401,402,463). Therefore, there is growing evidence that targeting high levels of IL-6 in RCC patients might be a promising therapy.

In addition, we found a trend toward increased MHC-II expression of TAMs with all MCT-inhibiting treatments, which was significant only when applying a combination of MCT1+4 inhibitor with ASA. PD-L1 expression of TAMs was decreased by selective MCT inhibitors. Likewise, MCT inhibition in macrophages without tumor contact resulted in an immunocompetent phenotype. Increased MHC-II expression promotes antigen presentation, and decreased PD-L1 expression means less binding to PD-1 on T cells, which normally suppresses T cell activation.

Consistent with the results obtained in co-cultures with CRC models, co-culture of leukocytes with RJ494 spheroids showed that both lactate and IL-6 levels were reduced by inhibition of MCT1+4 with selective inhibitors and diclofenac, but not with ASA.

5.3.3 MCT inhibition skews TAMs and MDSCs in RCC biopsies to an immunocompetent phenotype via targeting lactate and IL-6 secretion

Single-cell RNAseq analysis of RCC samples from the dataset of Young et al. (355) revealed a high expression of MCT1 and MCT4 in ccRCC and TAMs and RCC tumor cells showed the highest expression levels of MCT4. Given that MCT1, MCT4 and TAMs strongly correlate with poorer outcome of RCC patients, they emerge as promising target. Therefore, we investigated the effects of MCT inhibitors, diclofenac and ASA on 'real' TAMs in single cell preparations of tumor biopsies from RCC patients.

RCC tumors were heavily infiltrated by immune cells compared to healthy kidney tissue, with T cells being the most common immune cell type. Although fewer TAMs were present, we found high levels of IL-6 in the supernatant of RCC biopsy cultures. Interestingly, IL-6 levels correlated directly with

lactate levels in the supernatants. In RJ494 cultures, we identified TAMs as the major source of IL-6, and in RCC tumor biopsies, the number of TAMs and IL-6 concentration showed a positive correlation indicating a link between glycolytic activity of TAMs and IL-6 expression. In line, high exogenous lactic acid exposure, which blocks glycolysis, limits IL-6 secretion by macrophages (464,465). Import of lactate via MCT1 and MCT4 requires co-transport of protons, which explains why sodium lactate has not been shown to have the same immunosuppressive effect as lactic acid (364).

Consistent with previous experiments, selective MCT inhibitors and treatment with diclofenac, but not treatment with ASA, reduced lactate and IL-6 levels in overnight cultures of ccRCC biopsies. This indicates that glycolysis and lactate may be involved in the induction of IL-6 expression and that restriction of glycolysis impairs IL-6 expression. In accordance, Tan et al demonstrated that blockade of MCTs with CHCA or knockdown of MCT4 in macrophages resulted in decreased IL-6 secretion (395). The role of glycolysis in IL-6 regulation needs to be further clarified by treatment with other anti-glycolytic drugs such as LDH inhibitors. We confirmed decreased lactate efflux also in so called "tumoroids", which are patient-derived tumor-organoids with intact TME consisting uniformly sized fragments of freshly processed tumor biopsies without chemical dissociation or reassembly.

Interestingly, the proportion of immunosuppressive MDSCs was reduced by diclofenac and tended to be reduced by selective MCT inhibitors. Weber et al. described IL-6 as a master regulator of MDSCs (459), and tumor-derived lactate was found to mediate activation of MDSCs via the GPR81/mTOR/HIF1α/STAT3 pathway (466). MDSCs have been established as one of the most effective immunosuppressive cells in TME, inhibiting anti-tumor immunity of T cells and NK cells (172). In mouse melanoma, only MDSCs with IL-6 expression suppressed $CD8^+$ T cell function compared to MDSCs without IL-6 and upregulated CCR5 and Arg-1 in a STAT3-dependent manner (459,460). Therefore, simultaneous lowering of IL-6 and lactate by selective MCT inhibitors or diclofenac may synergistically support immune surveillance.

Several agents targeting either IL-6 or the IL-6R have been developed. Siltuximab has been investigated in preclinical and clinical trials. However, patients with multiple myeloma did not benefit regarding overall or progression-free survival (467–469). Another phase II trial has been testing Siltuximab as second-line therapy for men with castration-resistant prostate cancer and resulted in a PSA response rate of 3.8 % and a RECIST stable disease rate of 23 % (470). Tocilizumab blocks both membrane-bound and soluble IL-6 receptors. It has been approved for therapy of Castleman's disease, rheumatoid arthitis, systemic-onset, and polyarticular-course juvenile idiopathic arthritis (469,471–473). In addition to autoimmune diseases, promising effects on ovarian cancer, oral cancer, glioma, multiple myeloma, and mesothelioma have been observed (469,474). Clinical trials with Tocilizumab in cancer patients are ongoing.

In line with analysis of macrophages and TAMs in RJ494 spheroids, PD-L1 expression tended to be decreased upon MCT inhibition.

Taken together, our results suggest that selective MCT inhibitors and diclofenac act on lactate and proton co-transporting MCT1 and MCT4 in TAMs/MDSCs and tumor cells and decrease IL-6 secretion. Given that high MCT1, MCT4, and IL-6 levels strongly determine the outcome of ccRCC patients, the use of MCT inhibitors may be a promising strategy for immunomodulatory treatment. The role of MCT1/4 inhibition and subsequent reduction in lactate secretion for IL-6 suppression needs to be confirmed in further experiments with other glycolytic inhibitors such as LDH inhibitors.

5.4 Perspectives

The harsh immunosuppressive TME in solid tumors poses a major obstacle to successful therapeutic outcomes. Hypoxia, nutrient competition, and accumulation of waste products such as lactic acid contribute to the suppression of immune cells and limit anti-tumor activity. Immunotherapies including ICB have become pivotal for cancer treatment and have increased the number of patients with a realistic chance of complete remission. However, ICB has been shown to be ineffective in a range of patients and cancers. By now, it has become an established paradigm that tumor-derived lactic acid acts as immune-regulatory molecule (301,364,365) and is a substantial factor contributing to ICB resistance (118,119,294,365). In the last decades, targeting tumor metabolism and modulating the TME became an important therapeutic strategy to mitigate metabolism-related immunosuppression. This PhD project demonstrates that MCT4 inhibition can partially reverse the immunological consequences of the Warburg effect, e.g. lactic acid-driven immunosuppression, and thereby enhance ICB response in CRC *in vitro* and *in vivo* models with predominant MCT4 expression. In ccRCC, a second myeloid-driven tumor model, MCT inhibition acts as an immunomodulatory treatment by reducing lactate and IL-6 and inducing an immune-stimulatory phenotype in myeloid cells.

Accumulation of lactic acid is one of the major consequences of the Warburg effect. It requires the continuous export mediated by MCTs, of which MCT1 and MCT4 are the key tumor-associated transporters. Lactic acidosis of the TME acts pro-tumorigenic, induces angiogenesis, metastasis and dramatically affects anti-tumor immune response (34,50,52,475). Such a milieu contributes to immune escape as it impairs effector functions of T cells and NK cells (33,110,111,301,364,365) and fosters the differentiation and activity of tumor-promoting immune cell populations, such as Tregs (113,114,335) and suppressive myeloid cells (36,38,39,415). Similar to immune checkpoint such as PD-1, the Warburg phenotype represents a metabolic immune checkpoint and has been linked to limited efficacy of ICB in melanoma (119,365) and renal cell carcinoma (118) and also to resistance to adoptive T cell transfer (476). Given this central role for tumor progression, a number of strategies have been developed to target glucose and lactate metabolism to overcome therapy resistance. More recently, the role of lactate metabolism in immune cells has received increasing attention, leading to the conclusion that immune cells rely on similar metabolic programs as tumor cells. Because of these similarities, agents that target lactate metabolism may have adverse effects limiting immune cell metabolism and function and therefore need to be carefully studied on both the tumor and immune cell sides.

Restriction of glucose uptake by specific inhibitors of GLUT1, the major glucose transporter in tumor and immune cells, is currently being investigated for its direct anti-tumor effect but needs to be tested in combination with ICB in the future (477–479). The hexokinase inhibitors 2-DG and Lonidamine have only been studied as monotherapy in clinical trials (NCT00096707, NCT00435448). LDH inhibition with

oxamate enhanced efficacy of anti-PD-1 therapy in a humanized mouse model of non-small cell lung cancer (480) and Cascone and colleagues demonstrated a synergistic effect of ACT in combination with inhibition of LDHA using GSK2837808A (476). Administration of the highly specific LDH inhibitor NCI-006 delayed tumor growth and improved survival in mice bearing pancreatic xenografts (385), but has not yet been tested in combination with ICB.

Several approaches targeting TME acidification have been explored. Administration of PPIs has been shown to counteract TME acidification, improve effector function of T cells, and reduce tumor growth of B16 OVA tumors *in vivo* (303). Furthermore, sodium bicarbonate infusions have been investigated, although their feasibility in humans is questionable (370,436,481,482). Buffering pH with sodium bicarbonate prolonged survival of mice in a graft-versus-host disease model (370) and enhanced ICB and ACT in a B16 melanoma model (481). A novel approach is the inhibition of the bicarbonate transporter SLC4A4, which is highly expressed in pancreatic ductal adenocarcinomas, and improved T cell function and ICB efficacy (435).

MCT inhibitors targeting lactate metabolism and concomitant acidification emerged as treatment to reverse lactic acid-derived immunosuppression. Diclofenac as MCT1/4 inhibitor augmented ICB efficacy in a 4T1 model (365), and Huang et al. showed that MCT1 inhibitor (AZD3965) loaded inside to ultra-pH-sensitive nanoparticles increased anti-PD-1 efficacy in B16 and TC-1 tumor models (308). Consistent with our data, Fang et al. recently demonstrated that the selective MCT4 inhibitor VB124 is capable to improve the response to ICB *in vivo* in a hepatocellular carcinoma model system by increasing $CD8^+$ T cell infiltration and function (294). This suggests that a single MCT4 blockade may be sufficient to counteract the immunological consequences of the Warburg phenotype, implying that selective MCT4 inhibitors may have an advantage in target selectivity over MCT1 inhibitors and LDH inhibitors because MCT4 is expressed only in highly glycolytic cells.

Together with the results of this dissertation, these observations suggest that targeting lactate metabolism is promising for modulation of both tumor and immune cells and to further augment the efficacy of ICB. These strategies should be further explored in the future for selective targeting, including the investigation of the scope of single MCT4i in other tumor entities, fine-tuning, and finding a balance between reversing lactic acid-induced immunosuppression and avoiding immune cell damage.

6 Summary

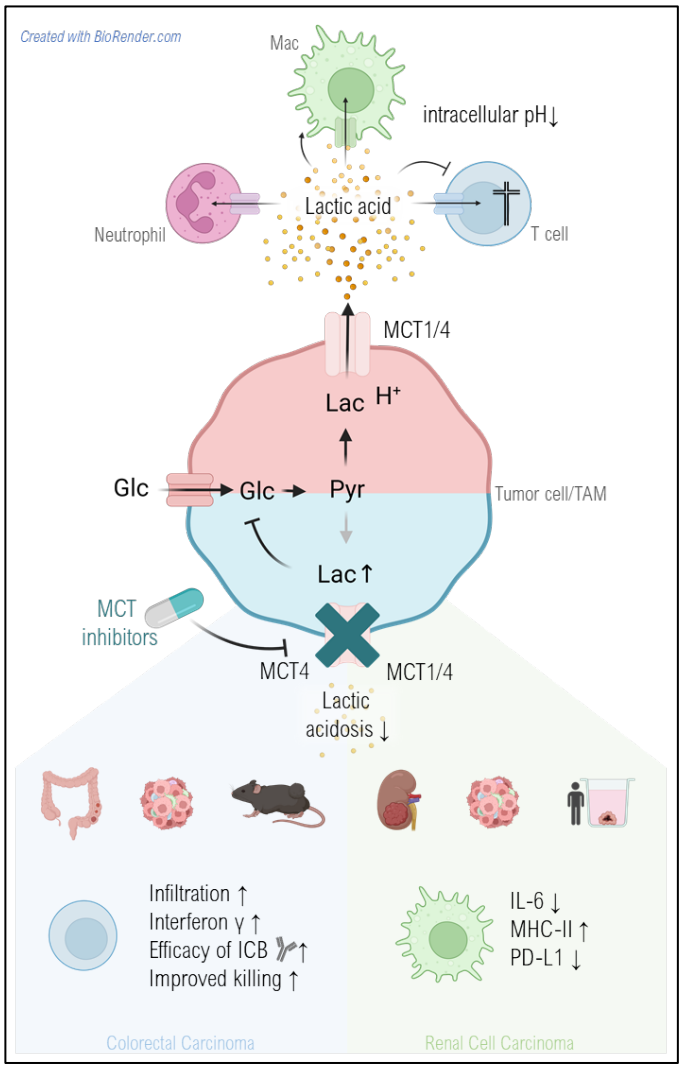

In the 21st century, cancer is one of the leading causes of death worldwide, accounting for approximately 10 million deaths in 2020. The development of advanced immunotherapeutic approaches that do not directly target the cancer, but instead unleash the immune system to attack tumor cells, has broadened the range of cancer treatments available. One of these revolutionizing immunotherapies was the immune checkpoint blockade (ICB). A famous example from 2015 is the former U.S. President Jimmy Carter, who was treated with the immune checkpoint inhibitor pembrolizumab (anti-PD-1 inhibitor, Keytruda), leading to immediate recovery from his advanced melanoma, a previously fatal diagnosis. Meanwhile, it has become clear that only a small number of patients respond to ICB, highlighting the importance of studying the underlying mechanisms of resistance.

Tumors are more and more considered as 'organs' that consist of tumor cells, soluble factors and in addition of a whole recruitment of different cell types creating the intricate tumor microenvironment (TME). It is characterized by low nutrient levels and high levels of lactic acid, which negatively affects infiltrating immune cells. Tumor cells exhibit an accelerated glycolytic flux, termed "Warburg phenotype", that requires continuous export of lactate and protons via monocarboxylate transporters (MCTs), of which MCT1 and MCT4 are frequently overexpressed in tumors. We hypothesize a direct link between tumor-derived lactic acid and the failure of immunotherapies: regardless of how unleashed or specific the T cell is, it cannot mediate an anti-tumor response due to suppression by lactic acidosis. In addition, other cell types such as myeloid cells are co-opted by lactic acid to promote tumor growth. Reducing lactate secretion by genetic interference or pharmacological inhibition of lactate transport with unspecific inhibitors of lactate transporters has been shown to boost anti-tumor

immunity. Therefore, this work investigated the effect of targeting MCTs with specific MCT1 and MCT4 inhibitors on lactic acid-induced immunosuppression in colorectal carcinoma (CRC) and clear cell renal cell carcinoma (ccRCC).

Exposure of T cells to lactic acid resulted in intracellular acidification, followed by cell death. Although viability of macrophages and neutrophils turned out insensitive to lactic acid, it was proven that lactic acid skews myeloid cells into a tumor-promoting phenotype. In brief, lactic acid is not only a waste product of tumor metabolism, but rather an immunoregulatory molecule negatively influencing the anti-tumor immune response. Accordingly, one strategy to improve immunosurveillance might be to avoid lactic acidosis by blockade of lactate transporters MCT1 and MCT4. However, highly proliferating effector T cells, macrophages, and neutrophil granulocytes also rely on glycolysis to meet their energetic demands and express MCT1 and MCT4. Thus, we carefully studied the effect of MCT inhibitors on both tumor and immune cells. Anti-glycolytic inhibition with specific MCT1 and MCT4 inhibitors decreased lactate secretion and extracellular acidification by tumor cells, T cells, and macrophages. Although proliferation of tumor cells and T cells was reduced by dual MCT1 and MCT4 blockade, viability of all cell types studied was not affected. Remarkably, interferon γ production by T cells was preserved, whereas IL-6 expression by macrophages was impaired by MCT blockade.

MCT inhibition proved to be a promising strategy to reduce tumor-induced lactic acidosis. However, the study of tumor cells or immune cells is not realistic enough to mimic the complexity of the TME. Here, we established a model to study the impact of drugs on tumor-immune cell crosstalk: Co-cultures of tumor spheroids with activated whole blood leucocytes. 3D tumor spheroids are like avascular tumor metastases and resemble the characteristic features of solid tumors. Of note, lactate transporter MCT4 was strongly upregulated in 3D CRC HCT116 tumor spheroids compared to monolayers. In this setting, exclusive MCT4 inhibition was sufficient to reduce lactate secretion to the same level as the combination with MCT1. This suggests MCT4 may play a more important role than MCT1. Since resistance to ICB might be mediated by high tumor glycolysis, we investigated whether combination therapies of MCT inhibitors, mitigating “Warburg”, with ICB could help to overcome therapy resistance. Strikingly, inhibition of MCT4 with or without anti-PD-L1 antibody resulted in improved leukocyte infiltration into tumor spheroids and augmented T cell function, whereas additional MCT1 inhibitor application was even counterproductive in the CRC HCT116 co-culture model. Finally, selective MCT4 inhibition synergized with ICB as T cell-mediated killing of tumor spheroids was only observed upon combinational treatment.

The *in vitro* results could be translated to an *in vivo* MC38 CRC tumor model, where MCT4i and anti-PD-L1 co-administration prolonged survival, significantly improved T cell tumor infiltration and function and reduced the frequency of suppressive myeloid cells. It is known that intracellular lactate

accumulation can exert a feedback inhibition on cellular glucose metabolism. Indeed, MCT4 inhibitor in combination with aPD-L1 increased intra-tumoral glucose concentrations and concomitantly, decreased glucose uptake by MC38 tumor cells. Mechanistically, MCT4 inhibitor treatment and ICB reduced intra-tumoral acidification. These results demonstrate that selective MCT4 inhibition is sufficient to improve the response to ICB in MCT4-driven tumors by reversing lactic acid-driven immunosuppression.

Besides CRC, we were interested in testing the effect of MCT1 and MCT4 inhibition in ccRCC as a second tumor entity. Analysis of TCGA data revealed a correlation of high MCT1 and MCT4 expression with poorer outcome in ccRCC. Surprisingly, neither CD8 nor IFNγ expression showed any correlation with survival, but rather CD14 expression of tumor-associated myeloid cells (TAMs) and IL-6, which were associated with poor outcome of ccRCC patients.

We analyzed the effect of MCT inhibition in an "*in vitro* RCC tumor environment" using a co-culture model with immune cells migrating into 3D RCC RJ494 tumor spheroids, similar to previous CRC co-cultures. MCT inhibition resulted in sufficient reduction of lactate secretion by RJ494 tumor spheroids. As TAMs and IL-6 but not T cells correlate with patient prognosis in ccRCC, we focused on infiltrated TAMs in this tumor entity. TAMs showed the highest levels of IL-6 expression compared to tumor cells, neutrophils and T cells in our RJ494 co-culture model. Analyses of macrophages without tumor contact showed a strong reduction in IL-6 secretion with MCT1+4 inhibition. Similarly, IL-6 levels were strongly reduced by MCT inhibitors. In addition, MCT inhibition skewed TAMs into a more immunocompetent phenotype as evidenced by increased MHC-II expression and lowered PD-L1 expression. Increased MHC-II expression promotes antigen presentation, and decreased PD-L1 expression means less binding to PD-1 on T cells, which normally suppresses T cell activation.

Finally, to investigate the effects of MCT inhibition *ex vivo* on "real" TAMs, we used human tumor biopsies of RCC patients. Single-cell RNAseq analysis of a publicly available RCC dataset revealed the highest expression of MCT4 in TAMs, followed by ccRCC tumor cells. Interestingly, IL-6 levels correlated directly with lactate levels in supernatants of overnight cultures of ccRCC biopsies. In RJ494 cultures, we identified TAMs as the major source of IL-6, and in RCC tumor biopsies, the number of TAMs and IL-6 concentration showed a positive correlation indicating a link between glycolytic activity of TAMs and IL-6 expression. Consistent with previous experiments, MCT inhibition reduced lactate and IL-6 levels in overnight cultures of ccRCC biopsies. This indicates that glycolysis and lactate may be involved in the induction of IL-6 expression and that restriction of glycolysis impairs IL-6 expression. We confirmed decreased lactate efflux also in so called “tumoroids”, which are patient-derived tumor-organoids with intact TME consisting of uniformly sized fragments of freshly processed tumor biopsies without chemical dissociation or reassembly.

Overall, this thesis demonstrated that MCT4 inhibition can counteract the immunological consequences of the Warburg effect and thereby enhance T cell function and ICB response in CRC *in vitro* and *in vivo* models with predominant MCT4 expression. Furthermore, MCT inhibitors emerged as promising strategy to reduce lactate and IL-6 levels in ccRCC *in vitro* and *ex vivo* models, resulting in an immunocompetent phenotype in TAMs in ccRCC.

7 Zusammenfassung

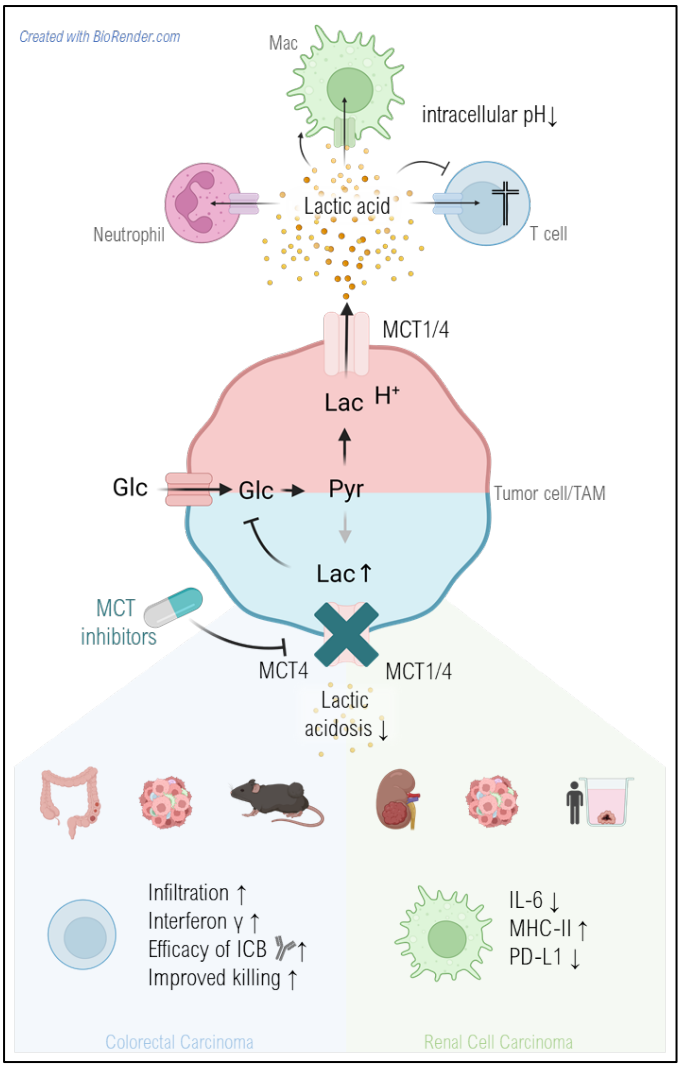

Im 21. Jahrhundert ist Krebs eine der häufigsten Todesursachen weltweit und war im Jahr 2020 für etwa 10 Millionen Todesfälle verantwortlich. Die Entwicklung fortschrittlicher immuntherapeutischer Ansätze, die nicht direkt auf den Krebs abzielen, sondern das Immunsystem für den Angriff auf die Tumorzellen entfesseln, hat das Spektrum der verfügbaren Krebsbehandlungen erweitert. Eine dieser revolutionären Immuntherapien war die Immun-Checkpoint-Blockade (ICB). Ein berühmtes Beispiel aus dem Jahr 2015 ist der ehemalige Präsident der Vereinigten Staaten, Jimmy Carter, dem der Immun-Checkpoint-Inhibitor Pembrolizumab (Anti-PD-1-Inhibitor, Keytruda) verabreicht wurde, was zur Remission seines fortgeschrittenen Melanom führte, einer eigentlich tödlichen Diagnose. Inzwischen ist deutlich geworden, dass nur eine kleine Zahl von Patienten auf ICB anspricht, was zeigt, wie wichtig es ist, die zugrundeliegenden Resistenzmechanismen zu untersuchen.

Tumore werden mehr und mehr als "Organe" betrachtet, die aus Tumorzellen, löslichen Faktoren und einer ganzen Reihe verschiedener Zelltypen bestehen, welche ein komplexes Tumor-Mikromilieu (TME) bilden. Dieses ist durch einen niedrigen Nährstoffgehalt und einen hohen Gehalt an Milchsäure gekennzeichnet, was sich negativ auf infiltrierende Immunzellen auswirkt. Tumorzellen zeichnen sich durch eine erhöhte Glykolyse aus, dem sog. „Warburg-Phänotyp“, welche den kontinuierlichen Export von Laktat und Protonen über Monocarboxylat-Transporter (MCTs) erfordert. Davon sind MCT1 und MCT4 häufig in Tumoren überexprimiert. Wir stellen die Hypothese auf, dass ein direkter Zusammenhang zwischen der vom Tumor stammenden Milchsäure und dem nicht-Ansprechen von Immuntherapien besteht: Unabhängig davon, wie entfesselt oder spezifisch die T Zellen sind, können sie auf-

grund der Hemmung durch die Laktatazidose keine Antitumorreaktion ausführen. Darüber hinaus werden andere Zelltypen wie myeloische Zellen von der Milchsäure umprogrammiert, so dass sie das Tumorwachstum fördern. Die Reduzierung der Laktatsekretion durch genetische Interferenz oder pharmakologische Hemmung des Laktattransports mithilfe unspezifischer Inhibitoren für Laktattransporter kann nachweislich die Anti-Tumor-Immunität stärken. Daher wurde in dieser Arbeit untersucht, wie sich die gezielte Hemmung von MCTs mit spezifischen MCT1- und MCT4-Inhibitoren auf die durch Milchsäure induzierte Immunsuppression bei Modellen des kolorektalen Karzinoms (CRC) und klarzelligen Nierenzellkarzinoms (ccRCC) auswirkt.

Die Behandlung von T Zellen mit Milchsäure führte zur intrazellulären Ansäuerung, gefolgt vom Zelltod. Obwohl sich die Viabilität von Makrophagen und Neutrophilen als unempfindlich gegenüber Milchsäure erwies, wurde bereits gezeigt, dass Milchsäure einen tumorfördernden Phänotyp in myeloischen Zellen induziert. Kurz gesagt, Milchsäure ist nicht nur ein Abfallprodukt des Tumorstoffwechsels, sondern vielmehr ein immunregulatorisches Molekül, das die Anti-Tumor-Immunantwort negativ beeinflusst. Eine Strategie zur Verbesserung der immunologischen Kontrolle des Tumors könnte daher darin bestehen, die Laktatazidose durch Blockade der Laktattransporter MCT1 und MCT4 zu vermeiden. Doch auch stark proliferierende Effektor-T Zellen, Makrophagen und neutrophile Granulozyten sind auf die Glykolyse angewiesen, um ihren Energiebedarf zu decken, und exprimieren MCT1 und MCT4. Daher haben wir die Wirkung von MCT-Inhibitoren sowohl auf Tumor- als auch auf Immunzellen sorgfältig untersucht. Die antiglykolytische Hemmung mit spezifischen MCT1- und MCT4-Inhibitoren verringerte die Laktatsekretion sowie die extrazelluläre Ansäuerung von Tumorzellen, T Zellen und Makrophagen. Obwohl die Proliferation von Tumorzellen und T Zellen durch die duale MCT1- und MCT4-Blockade reduziert wurde, war die Viabilität aller untersuchten Zelltypen nicht beeinträchtigt. Bemerkenswerterweise blieb die Produktion von Interferon γ durch T Zellen erhalten, während die IL-6-Expression durch Makrophagen durch die MCT-Blockade verringert wurde.

Die MCT-Blockade erwies sich als vielversprechende Strategie, um der tumorinduzierten Laktatazidose entgegenzuwirken. Die separate Untersuchung von Tumorzellen oder Immunzellen ist jedoch nicht realistisch genug, um die Komplexität des TME nachzuahmen. Deshalb haben wir ein Modell zur Untersuchung der Auswirkungen von Arzneimitteln auf den Tumor-Immunzell-Crosstalk entwickelt: Ko-Kulturen von Tumor-Sphäroiden mit aktivierten Vollblut-Leukozyten. 3D-Tumor-Sphäroide sind wie avaskuläre Tumormetastasen und ähneln den charakteristischen Merkmalen solider Tumore. Bemerkenswert ist, dass der Laktattransporter MCT4 in 3D-CRC HCT116-Tumorsphäroiden im Vergleich zu Monolayern stark hochreguliert war. In dieser Situation reichte die ausschließliche Hemmung von MCT4 aus, um die Laktatsekretion auf das gleiche Niveau zu reduzieren wie in Kombination mit MCT1. Dies deutet darauf hin, dass MCT4 eine wichtigere Rolle als MCT1 spielen

könnte. Da eine verstärkte Glykolyse in Tumoren zur Resistenz gegen ICB führen könnte, untersuchten wir zudem, ob Kombinationstherapien von MCT-Inhibitoren, die den "Warburg-Phänotyp" abschwächen, mit ICB zu einem verbesserten Therapiereansprechen beitragen könnten. Bemerkenswerterweise führte die Hemmung von MCT4 mit oder ohne Anti-PD-L1-Antikörper zu einer verbesserten Infiltration von Leukozyten in Tumor-Sphäroide sowie einer gesteigerten T Zell-Funktion, während die zusätzliche Anwendung eines MCT1-Inhibitors im CRC HCT116-Kokulturmodell sogar kontraproduktiv war. Schließlich wirkte die selektive MCT4-Inhibition synergistisch mit ICB, da die T Zell-vermittelte Abtötung von Tumorspheroiden nur bei kombinierter Behandlung beobachtet wurde.

Die *in vitro* Ergebnisse konnten auf ein *in vivo* Modell des CRC-Tumors MC38 übertragen werden, in dem die gleichzeitige Verabreichung von MCT4i und Anti-PD-L1 das Überleben verlängerte, die T Zell-Infiltration und -Funktion signifikant verbesserte sowie die Anzahl suppressiver myeloischer Zellen reduzierte. Es ist bekannt, dass die intrazelluläre Laktatakkumulation eine Rückkopplungshemmung auf den zellulären Glukosestoffwechsel ausüben kann. In der Tat erhöhte der MCT4-Inhibitor in Kombination mit aPD-L1 die intra-tumoralen Glukosekonzentrationen und verringerte gleichzeitig die Glukoseaufnahme durch MC38-Tumorzellen. Mechanistisch gesehen reduzierte die Behandlung mit MCT4-Inhibitor und ICB die intra-tumorale Ansäuerung. Diese Ergebnisse zeigen, dass eine selektive MCT4-Hemmung ausreicht, um das Ansprechen auf ICB bei MCT4-hoch-exprimierenden Tumoren zu verbessern, indem der durch Milchsäure hervorgerufene Immunsuppression entgegengewirkt wird.

Neben dem CRC waren wir daran interessiert, die Wirkung der MCT1- und MCT4-Hemmung im ccRCC als einer zweiten Tumorentität zu testen. Die Analyse von TCGA-Daten ergab eine Korrelation zwischen einer hohen MCT1- und MCT4-Expression und einem schlechteren Überleben bei ccRCC. Überraschenderweise zeigte weder die CD8- noch die IFNγ-Expression eine Korrelation mit dem Überleben, sondern vielmehr die CD14-Expression von tumorassoziierten myeloischen Zellen (TAMs) sowie IL-6, die mit einem schlechteren Überleben von ccRCC-Patienten in Verbindung gebracht wurden.

Wir analysierten die Wirkung der MCT-Hemmung in einer "*in vitro* RCC-Tumorumgebung" unter Verwendung eines Ko-Kulturmodells mit Immunzellen, die in 3D RCC RJ494-Tumorsphäroide einwandern. Die MCT-Hemmung führte zu einer deutlichen Verringerung der Laktatsekretion durch RJ494-Tumor-Sphäroide. Da TAMs und IL-6, nicht aber T-Zellen, mit der Patientenprognose in ccRCC korrelieren, konzentrierten wir uns auf infiltrierte TAMs in dieser Tumorentität. Im Vergleich zu Tumorzellen, Neutrophilen und T-Zellen wiesen TAMs in unserem RJ494-Kokulturmodell die höchste IL-6-Expression auf. Analysen von Makrophagen ohne Tumorkontakt zeigten eine starke Verringerung der IL-6-Sekretion bei MCT1+4-Hemmung. Analog wurden die IL-6-Spiegel durch MCT Inhibition stark

reduziert. Darüber hinaus führte die MCT-Hemmung dazu, dass die TAMs sich in Richtung eines immunkompetenteren Phänotyps veränderten, was sich in einer erhöhten MHC-II-Expression und einer verringerten PD-L1-Expression zeigte. Eine erhöhte MHC-II-Expression fördert die Antigenpräsentation, und eine verringerte PD-L1-Expression bedeutet eine geringere Bindung an PD-1 auf T-Zellen, welche normalerweise die Aktivierung von T-Zellen unterdrückt.

Um schließlich die Auswirkungen der MCT-Hemmung *ex vivo* auf "echte" TAMs zu untersuchen, verwendeten wir humane Tumorbiopsien von RCC-Patienten. Die Einzelzell-RNAseq-Analyse eines öffentlich zugänglichen RCC-Datensatzes ergab die höchste Expression von MCT4 in TAMs, gefolgt von ccRCC-Tumorzellen. Interessanterweise korrelierten die IL-6-Werte direkt mit den Laktatwerten im Überstand von Übernacht-Kulturen von ccRCC-Biopsien. In RJ494-Kulturen identifizierten wir TAMs als Hauptquelle von IL-6, und passend dazu zeigten die Anzahl der TAMs und die IL-6-Konzentration in RCC-Tumorbiopsien eine positive Korrelation, was auf einen Zusammenhang zwischen der glykolytischen Aktivität von TAMs und der IL-6-Expression hinweist. In Übereinstimmung mit vorherigen Experimenten reduzierte die MCT-Hemmung die Laktat- und IL-6-Konzentration in Übernachtkulturen von ccRCC-Biopsien. Dies deutet darauf hin, dass Glykolyse und Laktat an der Induktion der IL-6-Expression beteiligt sein könnten und dass eine Hemmung der Glykolyse die IL-6-Expression beeinträchtigt. Wir konnten einen verminderten Laktat-Efflux mit MCT Inhibitoren auch in so genannten "Tumoroiden" bestätigen, d.h. in von Patienten stammenden Tumor-Organoiden mit intaktem TME, die aus gleich großen Fragmenten frisch verarbeiteter Tumorbiopsien ohne chemische Dissoziation bestehen.

Insgesamt konnte in dieser Dissertation gezeigt werden, dass die Hemmung von MCT4 den immunologischen Folgen des Warburg-Effekts entgegenwirken und dadurch die T Zell-Funktion und das ICB-Ansprechen in CRC *in vitro* und *in vivo* Modellen mit dominierender MCT4-Expression verbessern kann. Darüber hinaus erwiesen sich MCT-Inhibitoren als vielversprechende Strategie zur Senkung des Laktat- und IL-6-Spiegels in ccRCC *in vitro* und *ex vivo* Modellen, was zu einem immunkompetenten Phänotyp von TAMs führte.

References

1. Sung H, Ferlay J, Siegel RL, Laversanne M, Soerjomataram I, Jemal A, et al. Global Cancer Statistics 2020: GLOBOCAN Estimates of Incidence and Mortality Worldwide for 36 Cancers in 185 Countries. CA Cancer J Clin 2021;71(3):209–49. PubMed PMID: 33538338.
2. Hanahan D, Weinberg RA. The Hallmarks of Cancer. Cell 2000;100(1):57–70.
3. Hanahan D, Weinberg RA. Hallmarks of cancer: the next generation. Cell 2011;144(5):646–74. PubMed PMID: 21376230.
4. Hanahan D. Hallmarks of Cancer: New Dimensions. Cancer Discov 2022;12(1):31–46. PubMed PMID: 35022204.
5. Jiang B-H, Liu L-Z. Chapter 2 PI3K/PTEN Signaling in Angiogenesis and Tumorigenesis. In: Woude GFV, Klein G, editors. Advances in cancer research. Advances in Cancer Research. Oxford: Elsevier Science & Technology; 2009. p. 19–65.
6. Yuan TL, Cantley LC. PI3K pathway alterations in cancer: variations on a theme. Oncogene 2008;27(41):5497–510. PubMed PMID: 18794884; PubMed Central PMCID: PMC3398461.
7. Blasco MA. Telomeres and human disease: ageing, cancer and beyond. Nat Rev Genet 2005;6(8):611–22. PubMed PMID: 16136653.
8. Oeseburg H, Boer RA de, van Gilst WH, van der Harst P. Telomere biology in healthy aging and disease. Pflugers Arch 2010;459(2):259–68. PubMed PMID: 19756717; PubMed Central PMCID: PMC2801851.
9. Junttila MR, Evan GI. p53--a Jack of all trades but master of none. Nature Reviews Cancer 2009;9(11):821–9. PubMed PMID: 19776747.
10. Qian B-Z, Pollard JW. Macrophage diversity enhances tumor progression and metastasis. Cell 2010;141(1):39–51. PubMed PMID: 20371344; PubMed Central PMCID: PMC4994190.
11. Zumsteg A, Christofori G. Corrupt policemen: inflammatory cells promote tumor angiogenesis. Curr Opin Oncol 2009;21(1):60–70. PubMed PMID: 19125020.
12. Murdoch C, Muthana M, Coffelt SB, Lewis CE. The role of myeloid cells in the promotion of tumour angiogenesis. Nature Reviews Cancer 2008;8(8):618–31. PubMed PMID: 18633355.
13. Dvorak HF. Tumors: wounds that do not heal. Similarities between tumor stroma generation and wound healing. N Engl J Med 1986;315(26):1650–9. PubMed PMID: 3537791.
14. Dvorak HF. Tumors: wounds that do not heal-redux. Cancer Immunology Research 2015;3(1):1–11. PubMed PMID: 25568067; PubMed Central PMCID: PMC4288010.
15. Mantovani A, Allavena P, Sica A, Balkwill F. Cancer-related inflammation. Nature 2008;454(7203):436–44. PubMed PMID: 18650914.
16. Balkwill F, Mantovani A. Inflammation and cancer: back to Virchow? Lancet 2001;357(9255):539–45. PubMed PMID: 11229684.
17. Klymkowsky MW, Savagner P. Epithelial-mesenchymal transition: a cancer researcher's conceptual friend and foe. Am J Pathol 2009;174(5):1588–93. PubMed PMID: 19342369; PubMed Central PMCID: PMC2671246.
18. Polyak K, Weinberg RA. Transitions between epithelial and mesenchymal states: acquisition of malignant and stem cell traits. Nature Reviews Cancer 2009;9(4):265–73. PubMed PMID: 19262571.
19. Thiery JP, Acloque H, Huang RYJ, Nieto MA. Epithelial-mesenchymal transitions in development and disease. Cell 2009;139(5):871–90. PubMed PMID: 19945376.
20. Kessenbrock K, Plaks V, Werb Z. Matrix metalloproteinases: regulators of the tumor microenvironment. Cell 2010;141(1):52–67. PubMed PMID: 20371345; PubMed Central PMCID: PMC2862057.

21. Joyce JA, Pollard JW. Microenvironmental regulation of metastasis. Nature Reviews Cancer 2009;9(4):239–52. PubMed PMID: 19279573; PubMed Central PMCID: PMC3251309.
22. WARBURG O, Wind F, Negelein E. THE METABOLISM OF TUMORS IN THE BODY. J Gen Physiol 1927;8(6):519–30. PubMed PMID: 19872213; PubMed Central PMCID: PMC2140820.
23. Fu X-L, Duan W, Su C-Y, Mao F-Y, Lv Y-P, Teng Y-S, et al. Interleukin 6 induces M2 macrophage differentiation by STAT3 activation that correlates with gastric cancer progression. Cancer Immunology, Immunotherapy 2017;66(12):1597–608. PubMed PMID: 28828629.
24. Coffelt SB, Lewis CE, Naldini L, Brown JM, Ferrara N, Palma M de. Elusive identities and overlapping phenotypes of proangiogenic myeloid cells in tumors. Am J Pathol 2010;176(4):1564–76. PubMed PMID: 20167863; PubMed Central PMCID: PMC2843445.
25. Gajewski TF, Schreiber H, Fu Y-X. Innate and adaptive immune cells in the tumor microenvironment. Nature Immunology 2013;14(10):1014–22. PubMed PMID: 24048123; PubMed Central PMCID: PMC4118725.
26. Galon J, Costes A, Sanchez-Cabo F, Kirilovsky A, Mlecnik B, Lagorce-Pagès C, et al. Type, density, and location of immune cells within human colorectal tumors predict clinical outcome. Science 2006;313(5795):1960–4. PubMed PMID: 17008531.
27. Mlecnik B, Bindea G, Angell HK, Maby P, Angelova M, Tougeron D, et al. Integrative Analyses of Colorectal Cancer Show Immunoscore Is a Stronger Predictor of Patient Survival Than Microsatellite Instability. Immunity 2016;44(3):698–711. PubMed PMID: 26982367.
28. Pagès F, Berger A, Camus M, Sanchez-Cabo F, Costes A, Molidor R, et al. Effector memory T cells, early metastasis, and survival in colorectal cancer. N Engl J Med 2005;353(25):2654–66. PubMed PMID: 16371631.
29. Egeblad M, Nakasone ES, Werb Z. Tumors as organs: complex tissues that interface with the entire organism. Dev Cell 2010;18(6):884–901. PubMed PMID: 20627072; PubMed Central PMCID: PMC2905377.
30. Heuser C, Renner K, Kreutz M, Gattinoni L. Targeting lactate metabolism for cancer immunotherapy - a matter of precision. Semin Cancer Biol 2022;88:32–45. PubMed PMID: 36496155.
31. Renner K, Singer K, Koehl GE, Geissler EK, Peter K, Siska PJ, et al. Metabolic Hallmarks of Tumor and Immune Cells in the Tumor Microenvironment. Frontiers in Immunology 2017;8:248. PubMed PMID: 28337200; PubMed Central PMCID: PMC5340776.
32. Renner K, Bruss C, Schnell A, Koehl G, Becker HM, Fante M, et al. Restricting Glycolysis Preserves T Cell Effector Functions and Augments Checkpoint Therapy. Cell Rep 2019;29(1):135-150.e9. PubMed PMID: 31577944.
33. Decking S-M, Bruss C, Babl N, Bittner S, Klobuch S, Thomas S, et al. LDHB Overexpression Can Partially Overcome T Cell Inhibition by Lactic Acid. Int J Mol Sci 2022;23(11). PubMed PMID: 35682650; PubMed Central PMCID: PMC9180663.
34. Brand A, Singer K, Koehl GE, Kolitzus M, Schoenhammer G, Thiel A, et al. LDHA-Associated Lactic Acid Production Blunts Tumor Immunosurveillance by T and NK Cells. Cell Metabolism 2016;24(5):657–71. PubMed PMID: 27641098.
35. Fischer K, Hoffmann P, Voelkl S, Meidenbauer N, Ammer J, Edinger M, et al. Inhibitory effect of tumor cell-derived lactic acid on human T cells. Blood 2007;109(9):3812–9. PubMed PMID: 17255361.
36. Dietl K, Renner K, Dettmer K, Timischl B, Eberhart K, Dorn C, et al. Lactic acid and acidification inhibit TNF secretion and glycolysis of human monocytes. The Journal of Immunology 2010;184(3):1200–9. PubMed PMID: 20026743.

37. Siska PJ, Singer K, Evert K, Renner K, Kreutz M. The immunological Warburg effect: Can a metabolic-tumor-stroma score (MeTS) guide cancer immunotherapy? Immunological Reviews 2020;295(1):187–202. PubMed PMID: 32157706.
38. Colegio OR. Lactic acid polarizes macrophages to a tumor-promoting state. Oncoimmunology 2016;5(3):e1014774. PubMed PMID: 27141329; PubMed Central PMCID: PMC4839384.
39. Colegio OR, Chu N-Q, Szabo AL, Chu T, Rhebergen AM, Jairam V, et al. Functional polarization of tumour-associated macrophages by tumour-derived lactic acid. Nature 2014;513(7519):559–63. PubMed PMID: 25043024; PubMed Central PMCID: PMC4301845.
40. WARBURG O. On the origin of cancer cells. Science 1956;123(3191):309–14. PubMed PMID: 13298683.
41. Hensley CT, Faubert B, Yuan Q, Lev-Cohain N, Jin E, Kim J, et al. Metabolic Heterogeneity in Human Lung Tumors. Cell 2016;164(4):681–94. PubMed PMID: 26853473; PubMed Central PMCID: PMC4752889.
42. DeBerardinis RJ, Chandel NS. We need to talk about the Warburg effect. Nature Metabolism 2020;2(2):127–9. PubMed PMID: 32694689.
43. Fan TWM, Lane AN, Higashi RM, Farag MA, Gao H, Bousamra M, et al. Altered regulation of metabolic pathways in human lung cancer discerned by (13)C stable isotope-resolved metabolomics (SIRM). Mol Cancer 2009;8:41. PubMed PMID: 19558692; PubMed Central PMCID: PMC2717907.
44. Lunt SY, Vander Heiden MG. Aerobic glycolysis: meeting the metabolic requirements of cell proliferation. Annu Rev Cell Dev Biol 2011;27:441–64. PubMed PMID: 21985671.
45. Vander Heiden MG, Cantley LC, Thompson CB. Understanding the Warburg effect: the metabolic requirements of cell proliferation. Science 2009;324(5930):1029–33. PubMed PMID: 19460998; PubMed Central PMCID: PMC2849637.
46. Hosios AM, Hecht VC, Danai LV, Johnson MO, Rathmell JC, Steinhauser ML, et al. Amino Acids Rather than Glucose Account for the Majority of Cell Mass in Proliferating Mammalian Cells. Dev Cell 2016;36(5):540–9. PubMed PMID: 26954548; PubMed Central PMCID: PMC4766004.
47. Luengo A, Li Z, Gui DY, Sullivan LB, Zagorulya M, Do BT, et al. Increased demand for NAD+ relative to ATP drives aerobic glycolysis. Mol Cell 2021;81(4):691-707.e6. PubMed PMID: 33382985; PubMed Central PMCID: PMC8315838.
48. Gatenby RA, Gillies RJ. Why do cancers have high aerobic glycolysis? Nat Rev Cancer 2004;4(11):891–9. PubMed PMID: 15516961.
49. Robey IF, Baggett BK, Kirkpatrick ND, Roe DJ, Dosescu J, Sloane BF, et al. Bicarbonate increases tumor pH and inhibits spontaneous metastases. Cancer Research 2009;69(6):2260–8. PubMed PMID: 19276390; PubMed Central PMCID: PMC2834485.
50. Walenta. High lactate levels predict likelihood of metastases, tumor recurrence, and restricted patient survival in human cervical cancers. Cancer Res 2000;60:916.
51. Brizel DM, Schroeder T, Scher RL, Walenta S, Clough RW, Dewhirst MW, et al. Elevated tumor lactate concentrations predict for an increased risk of metastases in head-and-neck cancer. International Journal of Radiation Oncology*Biology*Physics 2001;51(2):349–53.
52. Beckert S, Farrahi F, Aslam RS, Scheuenstuhl H, Königsrainer A, Hussain MZ, et al. Lactate stimulates endothelial cell migration. Wound Repair Regen 2006;14(3):321–4. PubMed PMID: 16808811.
53. Altenberg B, Greulich KO. Genes of glycolysis are ubiquitously overexpressed in 24 cancer classes. Genomics 2004;84(6):1014–20. PubMed PMID: 15533718.
54. Levine AJ, Puzio-Kuter AM. The control of the metabolic switch in cancers by oncogenes and tumor suppressor genes. Science 2010;330(6009):1340–4. PubMed PMID: 21127244.

55. Cairns RA, Harris IS, Mak TW. Regulation of cancer cell metabolism. Nat Rev Cancer 2011;11(2):85–95. PubMed PMID: 21258394.
56. Elstrom RL, Bauer DE, Buzzai M, Karnauskas R, Harris MH, Plas DR, et al. Akt stimulates aerobic glycolysis in cancer cells. Cancer Res 2004;64(11):3892–9. PubMed PMID: 15172999.
57. Robey RB, Hay N. Is Akt the "Warburg kinase"?-Akt-energy metabolism interactions and oncogenesis. Semin Cancer Biol 2009;19(1):25–31. PubMed PMID: 19130886; PubMed Central PMCID: PMC2814453.
58. Semenza GL. HIF-1: upstream and downstream of cancer metabolism. Curr Opin Genet Dev 2010;20(1):51–6. PubMed PMID: 19942427; PubMed Central PMCID: PMC2822127.
59. Bensinger SJ, Christofk HR. New aspects of the Warburg effect in cancer cell biology. Semin Cell Dev Biol 2012;23(4):352–61. PubMed PMID: 22406683.
60. Semenza GL. HIF-1 and tumor progression: pathophysiology and therapeutics. Trends Mol Med 2002;8(4):S62-S67. PubMed PMID: 11927290.
61. Wang Q, Hu D, Rui Y, Jiang A, Liu Z, Huang L. Prognosis value of HIF-1α expression in patients with non-small cell lung cancer. Gene 2014;541(2):69–74. PubMed PMID: 24631267.
62. Trastour C, Benizri E, Ettore F, Ramaioli A, Chamorey E, Pouysségur J, et al. HIF-1alpha and CA IX staining in invasive breast carcinomas: prognosis and treatment outcome. International Journal of Cancer 2007;120(7):1451–8. PubMed PMID: 17245699.
63. Rohwer N, Dame C, Haugstetter A, Wiedenmann B, Detjen K, Schmitt CA, et al. Hypoxia-inducible factor 1alpha determines gastric cancer chemosensitivity via modulation of p53 and NF-kappaB. PLOS ONE 2010;5(8):e12038. PubMed PMID: 20706634; PubMed Central PMCID: PMC2919384.
64. Papandreou I, Cairns RA, Fontana L, Lim AL, Denko NC. HIF-1 mediates adaptation to hypoxia by actively downregulating mitochondrial oxygen consumption. Cell Metabolism 2006;3(3):187–97. PubMed PMID: 16517406.
65. Kim J, Tchernyshyov I, Semenza GL, Dang CV. HIF-1-mediated expression of pyruvate dehydrogenase kinase: a metabolic switch required for cellular adaptation to hypoxia. Cell Metabolism 2006;3(3):177–85. PubMed PMID: 16517405.
66. Lu C-W, Lin S-C, Chen K-F, Lai Y-Y, Tsai S-J. Induction of pyruvate dehydrogenase kinase-3 by hypoxia-inducible factor-1 promotes metabolic switch and drug resistance. Journal of Biological Chemistry 2008;283(42):28106–14. PubMed PMID: 18718909; PubMed Central PMCID: PMC2661383.
67. Shim H, Dolde C, Lewis BC, Wu CS, Dang G, Jungmann RA, et al. c-Myc transactivation of LDH-A: implications for tumor metabolism and growth. Proc Natl Acad Sci U S A 1997;94(13):6658–63. PubMed PMID: 9192621; PubMed Central PMCID: PMC21214.
68. Dang CV, Le A, Gao P. MYC-induced cancer cell energy metabolism and therapeutic opportunities. Clin Cancer Res 2009;15(21):6479–83. PubMed PMID: 19861459; PubMed Central PMCID: PMC2783410.
69. Kim J, Gao P, Liu Y-C, Semenza GL, Dang CV. Hypoxia-inducible factor 1 and dysregulated c-Myc cooperatively induce vascular endothelial growth factor and metabolic switches hexokinase 2 and pyruvate dehydrogenase kinase 1. Mol Cell Biol 2007;27(21):7381–93. PubMed PMID: 17785433; PubMed Central PMCID: PMC2169056.
70. Dang CV, Kim J, Gao P, Yustein J. The interplay between MYC and HIF in cancer. Nature Reviews Cancer 2008;8(1):51–6. PubMed PMID: 18046334.
71. Shackelford DB, Shaw RJ. The LKB1-AMPK pathway: metabolism and growth control in tumour suppression. Nature Reviews Cancer 2009;9(8):563–75. PubMed PMID: 19629071; PubMed Central PMCID: PMC2756045.

72. Jenne DE, Reimann H, Nezu J, Friedel W, Loff S, Jeschke R, et al. Peutz-Jeghers syndrome is caused by mutations in a novel serine threonine kinase. Nat Genet 1998;18(1):38–43. PubMed PMID: 9425897.
73. Shakya A, Cooksey R, Cox JE, Wang V, McClain DA, Tantin D. Oct1 loss of function induces a coordinate metabolic shift that opposes tumorigenicity. Nature Cell Biology 2009;11(3):320–7. PubMed PMID: 19219035.
74. Bredella MA, Steinbach L, Caputo G, Segall G, Hawkins R. Value of FDG PET in the assessment of patients with multiple myeloma. AJR Am J Roentgenol 2005;184(4):1199–204. PubMed PMID: 15788594.
75. Reske SN, Kotzerke J. FDG-PET for clinical use. Results of the 3rd German Interdisciplinary Consensus Conference, "Onko-PET III", 21 July and 19 September 2000. Eur J Nucl Med 2001;28(11):1707–23. PubMed PMID: 11702115.
76. Bovenzi CD, Hamilton J, Tassone P, Johnson J, Cognetti DM, Luginbuhl A, et al. Prognostic Indications of Elevated MCT4 and CD147 across Cancer Types: A Meta-Analysis. Biomed Res Int 2015;2015:242437. PubMed PMID: 26779534; PubMed Central PMCID: PMC4686628.
77. Abe Y, Nakayama Y, Katsuki T, Inoue Y, Minagawa N, Torigoe T, et al. The prognostic significance of the expression of monocarboxylate transporter 4 in patients with right- or left-sided colorectal cancer. Asia Pac J Clin Oncol 2019;15(2):e49-e55. PubMed PMID: 30270512.
78. Petrides C, Neofytou K, Agrogiannis G, Petrou A, Angelou A, Kavantzas N, et al. Monocarboxylate transporter 4 as a prognostic biomarker in patients with colorectal cancer and liver metastases. International Journal of Surgery Open 2016;5:37–43.
79. Nakayama Y, Torigoe T, Inoue Y, Minagawa N, Izumi H, Kohno K, et al. Prognostic significance of monocarboxylate transporter 4 expression in patients with colorectal cancer. Exp Ther Med 2012;3(1):25–30. PubMed PMID: 22969839; PubMed Central PMCID: PMC3438655.
80. Marchiq I, Pouysségur J. Hypoxia, cancer metabolism and the therapeutic benefit of targeting lactate/H(+) symporters. Journal of Molecular Medicine 2016;94(2):155–71. PubMed PMID: 26099350; PubMed Central PMCID: PMC4762928.
81. Deora AA, Philp N, Hu J, Bok D, Rodriguez-Boulan E. Mechanisms regulating tissue-specific polarity of monocarboxylate transporters and their chaperone CD147 in kidney and retinal epithelia. Proc Natl Acad Sci U S A 2005;102(45):16245–50. PubMed PMID: 16260747; PubMed Central PMCID: PMC1283422.
82. Kirk P, Wilson MC, Heddle C, Brown MH, Barclay AN, Halestrap AP. CD147 is tightly associated with lactate transporters MCT1 and MCT4 and facilitates their cell surface expression. EMBO J 2000;19(15):3896–904. PubMed PMID: 10921872; PubMed Central PMCID: PMC306613.
83. Wilson MC, Meredith D, Fox JEM, Manoharan C, Davies AJ, HALESTRAP AP. Basigin (CD147) is the target for organomercurial inhibition of monocarboxylate transporter isoforms 1 and 4: the ancillary protein for the insensitive MCT2 is EMBIGIN (gp70). Journal of Biological Chemistry 2005;280(29):27213–21. PubMed PMID: 15917240.
84. Ganapathy V, Thangaraju M, Gopal E, Martin PM, Itagaki S, Miyauchi S, et al. Sodium-coupled monocarboxylate transporters in normal tissues and in cancer. AAPS J 2008;10(1):193–9. PubMed PMID: 18446519; PubMed Central PMCID: PMC2751467.
85. Pinheiro C, Longatto-Filho A, Azevedo-Silva J, Casal M, Schmitt FC, Baltazar F. Role of monocarboxylate transporters in human cancers: state of the art. Journal of Bioenergetics and Biomembranes 2012;44(1):127–39. PubMed PMID: 22407107.
86. Pinheiro C, Longatto-Filho A, Ferreira L, Pereira SMM, Etlinger D, Moreira MAR, et al. Increasing expression of monocarboxylate transporters 1 and 4 along progression to invasive cervical carcinoma. Int J Gynecol Pathol 2008;27(4):568–74. PubMed PMID: 18753962.

87. Stanley WC, Gertz EW, Wisneski JA, Neese RA, Morris DL, Brooks GA. Lactate extraction during net lactate release in legs of humans during exercise. J Appl Physiol (1985) 1986;60(4):1116–20. PubMed PMID: 3084443.
88. McCullagh KJ, Poole RC, Halestrap AP, O'Brien M, Bonen A. Role of the lactate transporter (MCT1) in skeletal muscles. Am J Physiol 1996;271(1 Pt 1):E143-50. PubMed PMID: 8760092.
89. Brooks GA. Cell-cell and intracellular lactate shuttles. J Physiol 2009;587(Pt 23):5591–600. PubMed PMID: 19805739; PubMed Central PMCID: PMC2805372.
90. Juel C, Halestrap AP. Lactate transport in skeletal muscle - role and regulation of the monocarboxylate transporter. J Physiol 1999;517 (Pt 3):633–42. PubMed PMID: 10358105; PubMed Central PMCID: PMC2269375.
91. Bonen A. The expression of lactate transporters (MCT1 and MCT4) in heart and muscle. Eur J Appl Physiol 2001;86(1):6–11. PubMed PMID: 11820324.
92. Garcia CK, Goldstein JL, Pathak RK, Anderson RG, Brown MS. Molecular characterization of a membrane transporter for lactate, pyruvate, and other monocarboxylates: Implications for the Cori cycle. Cell 1994;76(5):865–73.
93. Pierre K, Pellerin L. Monocarboxylate transporters in the central nervous system: distribution, regulation and function. J Neurochem 2005;94(1):1–14. PubMed PMID: 15953344.
94. HALESTRAP AP. The monocarboxylate transporter family--Structure and functional characterization. IUBMB Life 2012;64(1):1–9. PubMed PMID: 22131303.
95. HALESTRAP AP, Meredith D. The SLC16 gene family-from monocarboxylate transporters (MCTs) to aromatic amino acid transporters and beyond. Pflugers Arch 2004;447(5):619–28. PubMed PMID: 12739169.
96. HALESTRAP AP, Wilson MC. The monocarboxylate transporter family--role and regulation. IUBMB Life 2012;64(2):109–19. PubMed PMID: 22162139.
97. Zhao C, Wilson MC, Schuit F, Halestrap AP, Rutter GA. Expression and distribution of lactate/monocarboxylate transporter isoforms in pancreatic islets and the exocrine pancreas. Diabetes 2001;50(2):361–6. PubMed PMID: 11272148.
98. Sahlin K, Fernström M, Svensson M, Tonkonogi M. No evidence of an intracellular lactate shuttle in rat skeletal muscle. J Physiol 2002;541(Pt 2):569–74. PubMed PMID: 12042360; PubMed Central PMCID: PMC2290342.
99. Brooks GA. Lactate shuttle -- between but not within cells? J Physiol 2002;541(Pt 2):333–4. PubMed PMID: 12042341; PubMed Central PMCID: PMC2290336.
100. Dhar-Chowdhury P, Malester B, Rajacic P, Coetzee WA. The regulation of ion channels and transporters by glycolytically derived ATP. Cell Mol Life Sci 2007;64(23):3069–83. PubMed PMID: 17882378.
101. Asada K, Miyamoto K, Fukutomi T, Tsuda H, Yagi Y, Wakazono K, et al. Reduced expression of GNA11 and silencing of MCT1 in human breast cancers. Oncology 2003;64(4):380–8. PubMed PMID: 12759536.
102. Doherty JR, Yang C, Scott KEN, Cameron MD, Fallahi M, Li W, et al. Blocking lactate export by inhibiting the Myc target MCT1 Disables glycolysis and glutathione synthesis. Cancer Research 2014;74(3):908–20. PubMed PMID: 24285728; PubMed Central PMCID: PMC3946415.
103. Gan L, Xiu R, Ren P, Yue M, Su H, Guo G, et al. Metabolic targeting of oncogene MYC by selective activation of the proton-coupled monocarboxylate family of transporters. Oncogene 2016;35(23):3037–48. PubMed PMID: 26434591.
104. Boidot R, Végran F, Meulle A, Le Breton A, Dessy C, Sonveaux P, et al. Regulation of monocarboxylate transporter MCT1 expression by p53 mediates inward and outward lactate fluxes in tumors. Cancer Research 2012;72(4):939–48. PubMed PMID: 22184616.

105. Corbet C, Draoui N, Polet F, Pinto A, Drozak X, Riant O, et al. The SIRT1/HIF2α axis drives reductive glutamine metabolism under chronic acidosis and alters tumor response to therapy. Cancer Research 2014;74(19):5507–19. PubMed PMID: 25085245.
106. Corbet C, Pinto A, Martherus R, Santiago de Jesus JP, Polet F, Feron O. Acidosis Drives the Reprogramming of Fatty Acid Metabolism in Cancer Cells through Changes in Mitochondrial and Histone Acetylation. Cell Metabolism 2016;24(2):311–23. PubMed PMID: 27508876.
107. Thomas C, Bishop D, Moore-Morris T, Mercier J. Effects of high-intensity training on MCT1, MCT4, and NBC expressions in rat skeletal muscles: influence of chronic metabolic alkalosis. Am J Physiol Endocrinol Metab 2007;293(4):E916-22. PubMed PMID: 17609257.
108. Befani C, Mylonis I, Gkotinakou I-M, Georgoulias P, Hu C-J, Simos G, et al. Cobalt stimulates HIF-1-dependent but inhibits HIF-2-dependent gene expression in liver cancer cells. Int J Biochem Cell Biol 2013;45(11):2359–68. PubMed PMID: 23958427; PubMed Central PMCID: PMC3855297.
109. Walenta S, Mueller-Klieser WF. Lactate: mirror and motor of tumor malignancy. Seminars in Radiation Oncology 2004;14(3):267–74. PubMed PMID: 15254870.
110. Mendler AN, Hu B, Prinz PU, Kreutz M, Gottfried E, Noessner E. Tumor lactic acidosis suppresses CTL function by inhibition of p38 and JNK/c-Jun activation. International Journal of Cancer 2012;131(3):633–40. PubMed PMID: 21898391.
111. Long Y, Gao Z, Hu X, Xiang F, Wu Z, Zhang J, et al. Downregulation of MCT4 for lactate exchange promotes the cytotoxicity of NK cells in breast carcinoma. Cancer Medicine 2018;7(9):4690–700. PubMed PMID: 30051648; PubMed Central PMCID: PMC6143925.
112. Gottfried E, Kunz-Schughart LA, Ebner S, Mueller-Klieser W, Hoves S, Andreesen R, et al. Tumor-derived lactic acid modulates dendritic cell activation and antigen expression. Blood 2006;107(5):2013–21. PubMed PMID: 16278308.
113. Angelin A, Gil-de-Gómez L, Dahiya S, Jiao J, Guo L, Levine MH, et al. Foxp3 Reprograms T Cell Metabolism to Function in Low-Glucose, High-Lactate Environments. Cell Metabolism 2017;25(6):1282-1293.e7. PubMed PMID: 28416194; PubMed Central PMCID: PMC5462872.
114. Kumagai S, Koyama S, Itahashi K, Tanegashima T, Lin Y-T, Togashi Y, et al. Lactic acid promotes PD-1 expression in regulatory T cells in highly glycolytic tumor microenvironments. Cancer Cell 2022;40(2):201-218.e9. PubMed PMID: 35090594.
115. Vasaikar S, Huang C, Wang X, Petyuk VA, Savage SR, Wen B, et al. Proteogenomic Analysis of Human Colon Cancer Reveals New Therapeutic Opportunities. Cell 2019;177(4):1035-1049.e19. PubMed PMID: 31031003; PubMed Central PMCID: PMC6768830.
116. Icard P, Shulman S, Farhat D, Steyaert J-M, Alifano M, Lincet H. How the Warburg effect supports aggressiveness and drug resistance of cancer cells? Drug Resist Updat 2018;38:1–11. PubMed PMID: 29857814.
117. Zhang Y-X, Zhao Y-Y, Shen J, Sun X, Liu Y, Liu H, et al. Nanoenabled Modulation of Acidic Tumor Microenvironment Reverses Anergy of Infiltrating T Cells and Potentiates Anti-PD-1 Therapy. Nano Letters 2019;19(5):2774–83. PubMed PMID: 30943039.
118. Ascierto ML, McMiller TL, Berger AE, Danilova L, Anders RA, Netto GJ, et al. The Intratumoral Balance between Metabolic and Immunologic Gene Expression Is Associated with Anti-PD-1 Response in Patients with Renal Cell Carcinoma. Cancer Immunology Research 2016;4(9):726–33. PubMed PMID: 27491898; PubMed Central PMCID: PMC5584610.
119. Daneshmandi S, Wegiel B, Seth P. Blockade of Lactate Dehydrogenase-A (LDH-A) Improves Efficacy of Anti-Programmed Cell Death-1 (PD-1) Therapy in Melanoma. Cancers 2019;11(4):450. PubMed PMID: 30934955; PubMed Central PMCID: PMC6521327.
120. Cascone T, McKenzie JA, Mbofung RM, Punt S, Wang Z, Xu C, et al. Increased Tumor Glycolysis Characterizes Immune Resistance to Adoptive T Cell Therapy. Cell Metabolism 2018;27(5):977-987.e4. PubMed PMID: 29628419; PubMed Central PMCID: PMC5932208.

121. Husain Z, Huang Y, Seth P, Sukhatme VP. Tumor-derived lactate modifies antitumor immune response: effect on myeloid-derived suppressor cells and NK cells. The Journal of Immunology 2013;191(3):1486–95. PubMed PMID: 23817426.
122. Haas R, Smith J, Rocher-Ros V, Nadkarni S, Montero-Melendez T, D'Acquisto F, et al. Lactate Regulates Metabolic and Pro-inflammatory Circuits in Control of T Cell Migration and Effector Functions. PLoS Biol 2015;13(7):e1002202. PubMed PMID: 26181372; PubMed Central PMCID: PMC4504715.
123. Chang C-H, Curtis JD, Maggi LB, Faubert B, Villarino AV, O'Sullivan D, et al. Posttranscriptional control of T cell effector function by aerobic glycolysis. Cell 2013;153(6):1239–51. PubMed PMID: 23746840; PubMed Central PMCID: PMC3804311.
124. Ho P-C, Bihuniak JD, Macintyre AN, Staron M, Liu X, Amezquita R, et al. Phosphoenolpyruvate Is a Metabolic Checkpoint of Anti-tumor T Cell Responses. Cell 2015;162(6):1217–28. PubMed PMID: 26321681; PubMed Central PMCID: PMC4567953.
125. Bohn T, Rapp S, Luther N, Klein M, Bruehl T-J, Kojima N, et al. Tumor immunoevasion via acidosis-dependent induction of regulatory tumor-associated macrophages. Nature Immunology 2018;19(12):1319–29. PubMed PMID: 30397348.
126. Ohashi T, Aoki M, Tomita H, Akazawa T, Sato K, Kuze B, et al. M2-like macrophage polarization in high lactic acid-producing head and neck cancer. Cancer Sci 2017;108(6):1128–34. PubMed PMID: 28370718; PubMed Central PMCID: PMC5480089.
127. Shime H, Yabu M, Akazawa T, Kodama K, Matsumoto M, Seya T, et al. Tumor-secreted lactic acid promotes IL-23/IL-17 proinflammatory pathway. J Immunol 2008;180(11):7175–83. PubMed PMID: 18490716.
128. Melvold RW, Sticca RP. Basic and tumor immunology: a review. Surg Oncol Clin N Am 2007;16(4):711-35, vii. PubMed PMID: 18022541.
129. Mlecnik B, Bindea G, Kirilovsky A, Angell HK, Obenauf AC, Tosolini M, et al. The tumor microenvironment and Immunoscore are critical determinants of dissemination to distant metastasis. Science Translational Medicine 2016;8(327):327ra26. PubMed PMID: 26912905.
130. Galon J, Lanzi A. Immunoscore and its introduction in clinical practice. Q J Nucl Med Mol Imaging 2020;64(2):152–61. PubMed PMID: 32107902.
131. Angell HK, Bruni D, Barrett JC, Herbst R, Galon J. The Immunoscore: Colon Cancer and Beyond. Clin Cancer Res 2020;26(2):332–9. PubMed PMID: 31413009.
132. Tsai C-S, Chen F-H, Wang C-C, Huang H-L, Jung S-M, Wu C-J, et al. Macrophages from irradiated tumors express higher levels of iNOS, arginase-I and COX-2, and promote tumor growth. International Journal of Radiation Oncology*Biology*Physics 2007;68(2):499–507. PubMed PMID: 17398016.
133. van Ravenswaay Claasen HH, Kluin PM, Fleuren GJ. Tumor infiltrating cells in human cancer. On the possible role of CD16+ macrophages in antitumor cytotoxicity. Lab Invest 1992;67(2):166–74. PubMed PMID: 1501443.
134. Noy R, Pollard JW. Tumor-associated macrophages: from mechanisms to therapy. Immunity 2014;41(1):49–61. PubMed PMID: 25035953; PubMed Central PMCID: PMC4137410.
135. Allavena P, Sica A, Garlanda C, Mantovani A. The Yin-Yang of tumor-associated macrophages in neoplastic progression and immune surveillance. Immunological Reviews 2008;222:155–61. PubMed PMID: 18364000.
136. Kim J, Bae J-S. Tumor-Associated Macrophages and Neutrophils in Tumor Microenvironment. Mediators Inflamm 2016;2016:6058147. PubMed PMID: 26966341; PubMed Central PMCID: PMC4757693.

137. Bingle L, Brown NJ, Lewis CE. The role of tumour-associated macrophages in tumour progression: implications for new anticancer therapies. The Journal of Pathology 2002;196(3):254–65. PubMed PMID: 11857487.
138. Gordon S, Taylor PR. Monocyte and macrophage heterogeneity. Nat Rev Immunol 2005;5(12):953–64. PubMed PMID: 16322748.
139. Hu W, Li X, Zhang C, Yang Y, Jiang J, Wu C. Tumor-associated macrophages in cancers. Clin Transl Oncol 2016;18(3):251–8. PubMed PMID: 26264497.
140. Zamarron BF, Chen W. Dual roles of immune cells and their factors in cancer development and progression. Int J Biol Sci 2011;7(5):651–8. PubMed PMID: 21647333; PubMed Central PMCID: PMC3107473.
141. Reinfeld BI, Madden MZ, Wolf MM, Chytil A, Bader JE, Patterson AR, et al. Cell-programmed nutrient partitioning in the tumour microenvironment. Nature 2021;593(7858):282–8. PubMed PMID: 33828302; PubMed Central PMCID: PMC8122068.
142. Seth P, Csizmadia E, Hedblom A, Vuerich M, Xie H, Li M, et al. Deletion of Lactate Dehydrogenase-A in Myeloid Cells Triggers Antitumor Immunity. Cancer Research 2017;77(13):3632–43. PubMed PMID: 28446465; PubMed Central PMCID: PMC5505499.
143. Zhang Q, He Y, Luo N, Patel SJ, Han Y, Gao R, et al. Landscape and Dynamics of Single Immune Cells in Hepatocellular Carcinoma. Cell 2019;179(4):829-845.e20. PubMed PMID: 31675496.
144. Gubin MM, Esaulova E, Ward JP, Malkova ON, Runci D, Wong P, et al. High-Dimensional Analysis Delineates Myeloid and Lymphoid Compartment Remodeling during Successful Immune-Checkpoint Cancer Therapy. Cell 2018;175(4):1014-1030.e19. PubMed PMID: 30343900; PubMed Central PMCID: PMC6501221.
145. Molgora M, Esaulova E, Vermi W, Hou J, Chen Y, Luo J, et al. TREM2 Modulation Remodels the Tumor Myeloid Landscape Enhancing Anti-PD-1 Immunotherapy. Cell 2020;182(4):886-900.e17. PubMed PMID: 32783918; PubMed Central PMCID: PMC7485282.
146. Xiong H, Mittman S, Rodriguez R, Moskalenko M, Pacheco-Sanchez P, Yang Y, et al. Anti-PD-L1 Treatment Results in Functional Remodeling of the Macrophage Compartment. Cancer Research 2019;79(7):1493–506. PubMed PMID: 30679180.
147. Xiang X, Wang J, Di Lu, Xu X. Targeting tumor-associated macrophages to synergize tumor immunotherapy. Signal Transduction and Targeted Therapy 2021;6(1):75. PubMed PMID: 33619259; PubMed Central PMCID: PMC7900181.
148. Mantovani A, Allavena P. The interaction of anticancer therapies with tumor-associated macrophages. J Exp Med 2015;212(4):435–45. PubMed PMID: 25753580; PubMed Central PMCID: PMC4387285.
149. Genard G, Lucas S, Michiels C. Reprogramming of Tumor-Associated Macrophages with Anticancer Therapies: Radiotherapy versus Chemo- and Immunotherapies. Frontiers in Immunology 2017;8:828. PubMed PMID: 28769933; PubMed Central PMCID: PMC5509958.
150. Komohara Y, Fujiwara Y, Ohnishi K, Takeya M. Tumor-associated macrophages: Potential therapeutic targets for anti-cancer therapy. Adv Drug Deliv Rev 2016;99(Pt B):180–5. PubMed PMID: 26621196.
151. Zhang Q, Liu L, Gong C, Shi H, Zeng Y, Wang X, et al. Prognostic significance of tumor-associated macrophages in solid tumor: a meta-analysis of the literature. PLOS ONE 2012;7(12):e50946. PubMed PMID: 23284651; PubMed Central PMCID: PMC3532403.
152. Wu L, Saxena S, Awaji M, Singh RK. Tumor-Associated Neutrophils in Cancer: Going Pro. Cancers 2019;11(4). PubMed PMID: 31010242; PubMed Central PMCID: PMC6520693.
153. Coffelt SB, Wellenstein MD, Visser KE de. Neutrophils in cancer: neutral no more. Nature Reviews Cancer 2016;16(7):431–46. PubMed PMID: 27282249.

154. Fridlender ZG, Sun J, Kim S, Kapoor V, Cheng G, Ling L, et al. Polarization of tumor-associated neutrophil phenotype by TGF-beta: "N1" versus "N2" TAN. Cancer Cell 2009;16(3):183–94. PubMed PMID: 19732719; PubMed Central PMCID: PMC2754404.
155. Sharma P, Hu-Lieskovan S, Wargo JA, Ribas A. Primary, Adaptive, and Acquired Resistance to Cancer Immunotherapy. Cell 2017;168(4):707–23. PubMed PMID: 28187290; PubMed Central PMCID: PMC5391692.
156. Chan T-S, Hsu C-C, Pai VC, Liao W-Y, Huang S-S, Tan K-T, et al. Metronomic chemotherapy prevents therapy-induced stromal activation and induction of tumor-initiating cells. J Exp Med 2016;213(13):2967–88. PubMed PMID: 27881732; PubMed Central PMCID: PMC5154935.
157. Fridlender ZG, Albelda SM. Tumor-associated neutrophils: friend or foe? Carcinogenesis 2012;33(5):949–55. PubMed PMID: 22425643.
158. Wu Y, Wang S, Farooq SM, Castelvetere MP, Hou Y, Gao J-L, et al. A chemokine receptor CXCR2 macromolecular complex regulates neutrophil functions in inflammatory diseases. J Biol Chem 2012;287(8):5744–55. PubMed PMID: 22203670; PubMed Central PMCID: PMC3285346.
159. Gentles AJ, Newman AM, Liu CL, Bratman SV, Feng W, Kim D, et al. The prognostic landscape of genes and infiltrating immune cells across human cancers. Nature Medicine 2015;21(8):938–45. PubMed PMID: 26193342; PubMed Central PMCID: PMC4852857.
160. Tohme S, Yazdani HO, Al-Khafaji AB, Chidi AP, Loughran P, Mowen K, et al. Neutrophil Extracellular Traps Promote the Development and Progression of Liver Metastases after Surgical Stress. Cancer Research 2016;76(6):1367–80. PubMed PMID: 26759232; PubMed Central PMCID: PMC4794393.
161. Masucci MT, Minopoli M, Carriero MV. Tumor Associated Neutrophils. Their Role in Tumorigenesis, Metastasis, Prognosis and Therapy. Frontiers in Oncology 2019;9:1146. PubMed PMID: 31799175; PubMed Central PMCID: PMC6874146.
162. Wculek SK, Malanchi I. Neutrophils support lung colonization of metastasis-initiating breast cancer cells. Nature 2015;528(7582):413–7. PubMed PMID: 26649828; PubMed Central PMCID: PMC4700594.
163. Zhao L, Li T, Yang Y, Zhang Y, Li W, Han L, et al. Clinical value of neutrophil-to-lymphocyte ratio as a predictor of prognosis of RetroNectin®-activated cytokine-induced killer cell therapy in advanced non-small-cell lung cancer. Immunotherapy 2019;11(4):273–82. PubMed PMID: 30547699.
164. Suzuki R, Takagi T, Hikichi T, Konno N, Sugimoto M, Watanabe KO, et al. Derived neutrophil/lymphocyte ratio predicts gemcitabine therapy outcome in unresectable pancreatic cancer. Oncol Lett 2016;11(5):3441–5. PubMed PMID: 27123132; PubMed Central PMCID: PMC4840986.
165. Gonda K, Shibata M, Sato Y, Washio M, Takeshita H, Shigeta H, et al. Elevated neutrophil-to-lymphocyte ratio is associated with nutritional impairment, immune suppression, resistance to S-1 plus cisplatin, and poor prognosis in patients with stage IV gastric cancer. Mol Clin Oncol 2017;7(6):1073–8. PubMed PMID: 29285377; PubMed Central PMCID: PMC5740823.
166. Graziano V, Grassadonia A, Iezzi L, Vici P, Pizzuti L, Barba M, et al. Combination of peripheral neutrophil-to-lymphocyte ratio and platelet-to-lymphocyte ratio is predictive of pathological complete response after neoadjuvant chemotherapy in breast cancer patients. Breast 2019;44:33–8. PubMed PMID: 30611095.
167. Ethier J-L, Desautels D, Templeton A, Shah PS, Amir E. Prognostic role of neutrophil-to-lymphocyte ratio in breast cancer: a systematic review and meta-analysis. Breast Cancer Res 2017;19(1):2. PubMed PMID: 28057046; PubMed Central PMCID: PMC5217326.
168. Granot Z, Henke E, Comen EA, King TA, Norton L, Benezra R. Tumor entrained neutrophils inhibit seeding in the premetastatic lung. Cancer Cell 2011;20(3):300–14. PubMed PMID: 21907922; PubMed Central PMCID: PMC3172582.

169. Finisguerra V, Di Conza G, Di Matteo M, Serneels J, Costa S, Thompson AAR, et al. MET is required for the recruitment of anti-tumoural neutrophils. Nature 2015;522(7556):349–53. PubMed PMID: 25985180; PubMed Central PMCID: PMC4594765.
170. Gershkovitz M, Fainsod-Levi T, Zelter T, Sionov RV, Granot Z. TRPM2 modulates neutrophil attraction to murine tumor cells by regulating CXCL2 expression. Cancer Immunology, Immunotherapy 2019;68(1):33–43. PubMed PMID: 30251149.
171. Sun B, Qin W, Song M, Liu L, Yu Y, Qi X, et al. Neutrophil Suppresses Tumor Cell Proliferation via Fas /Fas Ligand Pathway Mediated Cell Cycle Arrested. Int J Biol Sci 2018;14(14):2103–13. PubMed PMID: 30585273; PubMed Central PMCID: PMC6299367.
172. Umansky V, Blattner C, Gebhardt C, Utikal J. The Role of Myeloid-Derived Suppressor Cells (MDSC) in Cancer Progression. Vaccines (Basel) 2016;4(4). PubMed PMID: 27827871; PubMed Central PMCID: PMC5192356.
173. Bronte V, Brandau S, Chen S-H, Colombo MP, Frey AB, Greten TF, et al. Recommendations for myeloid-derived suppressor cell nomenclature and characterization standards. Nature Communications 2016;7:12150. PubMed PMID: 27381735; PubMed Central PMCID: PMC4935811.
174. Gabrilovich DI, Ostrand-Rosenberg S, Bronte V. Coordinated regulation of myeloid cells by tumours. Nat Rev Immunol 2012;12(4):253–68. PubMed PMID: 22437938; PubMed Central PMCID: PMC3587148.
175. Kumar V, Patel S, Tcyganov E, Gabrilovich DI. The Nature of Myeloid-Derived Suppressor Cells in the Tumor Microenvironment. Trends Immunol 2016;37(3):208–20. PubMed PMID: 26858199; PubMed Central PMCID: PMC4775398.
176. Parker KH, Beury DW, Ostrand-Rosenberg S. Myeloid-Derived Suppressor Cells: Critical Cells Driving Immune Suppression in the Tumor Microenvironment. Adv Cancer Res 2015;128:95–139. PubMed PMID: 26216631; PubMed Central PMCID: PMC4662416.
177. Meirow Y, Kanterman J, Baniyash M. Paving the Road to Tumor Development and Spreading: Myeloid-Derived Suppressor Cells are Ruling the Fate. Frontiers in Immunology 2015;6:523. PubMed PMID: 26528286; PubMed Central PMCID: PMC4601280.
178. Solito S, Marigo I, Pinton L, Damuzzo V, Mandruzzato S, Bronte V. Myeloid-derived suppressor cell heterogeneity in human cancers. Ann N Y Acad Sci 2014;1319:47–65. PubMed PMID: 24965257.
179. Marvel D, Gabrilovich DI. Myeloid-derived suppressor cells in the tumor microenvironment: expect the unexpected. J Clin Invest 2015;125(9):3356–64. PubMed PMID: 26168215; PubMed Central PMCID: PMC4588239.
180. Molon B, Ugel S, Del Pozzo F, Soldani C, Zilio S, Avella D, et al. Chemokine nitration prevents intratumoral infiltration of antigen-specific T cells. J Exp Med 2011;208(10):1949–62. PubMed PMID: 21930770; PubMed Central PMCID: PMC3182051.
181. Bogdan C. Nitric oxide and the immune response. Nature Immunology 2001;2(10):907–16. PubMed PMID: 11577346.
182. Rosenberg SA, Restifo NP. Adoptive cell transfer as personalized immunotherapy for human cancer. Science 2015;348(6230):62–8. PubMed PMID: 25838374; PubMed Central PMCID: PMC6295668.
183. Raber P, Ochoa AC, Rodríguez PC. Metabolism of L-arginine by myeloid-derived suppressor cells in cancer: mechanisms of T cell suppression and therapeutic perspectives. Immunol Invest 2012;41(6-7):614–34. PubMed PMID: 23017138; PubMed Central PMCID: PMC3519282.
184. Gajewski TF, Woo S-R, Zha Y, Spaapen R, Zheng Y, Corrales L, et al. Cancer immunotherapy strategies based on overcoming barriers within the tumor microenvironment. Curr Opin Immunol 2013;25(2):268–76. PubMed PMID: 23579075.

185. Tartour E, Pere H, Maillere B, Terme M, Merillon N, Taieb J, et al. Angiogenesis and immunity: a bidirectional link potentially relevant for the monitoring of antiangiogenic therapy and the development of novel therapeutic combination with immunotherapy. Cancer Metastasis Rev 2011;30(1):83–95. PubMed PMID: 21249423.
186. Qu P, Yan C, Du H. Matrix metalloproteinase 12 overexpression in myeloid lineage cells plays a key role in modulating myelopoiesis, immune suppression, and lung tumorigenesis. Blood 2011;117(17):4476–89. PubMed PMID: 21378275; PubMed Central PMCID: PMC3099569.
187. Pan P-Y, Ma G, Weber KJ, Ozao-Choy J, Wang G, Yin B, et al. Immune stimulatory receptor CD40 is required for T-cell suppression and T regulatory cell activation mediated by myeloid-derived suppressor cells in cancer. Cancer Research 2010;70(1):99–108. PubMed PMID: 19996287; PubMed Central PMCID: PMC2805053.
188. Chen J, Ye Y, Liu P, Yu W, Wei F, Li H, et al. Suppression of T cells by myeloid-derived suppressor cells in cancer. Human Immunology 2017;78(2):113–9. PubMed PMID: 27939507.
189. Tel J, Anguille S, Waterborg CEJ, Smits EL, Figdor CG, Vries IJM de. Tumoricidal activity of human dendritic cells. Trends Immunol 2014;35(1):38–46. PubMed PMID: 24262387; PubMed Central PMCID: PMC7106406.
190. Chan CW, Crafton E, Fan H-N, Flook J, Yoshimura K, Skarica M, et al. Interferon-producing killer dendritic cells provide a link between innate and adaptive immunity. Nature Medicine 2006;12(2):207–13. PubMed PMID: 16444266.
191. Pillarisetty VG, Katz SC, Bleier JI, Shah AB, Dematteo RP. Natural killer dendritic cells have both antigen presenting and lytic function and in response to CpG produce IFN-gamma via autocrine IL-12. J Immunol 2005;174(5):2612–8. PubMed PMID: 15728467.
192. Taieb J, Chaput N, Ménard C, Apetoh L, Ullrich E, Bonmort M, et al. A novel dendritic cell subset involved in tumor immunosurveillance. Nature Medicine 2006;12(2):214–9. PubMed PMID: 16444265.
193. Benencia F, Muccioli M, Alnaeeli M. Perspectives on reprograming cancer-associated dendritic cells for anti-tumor therapies. Frontiers in Oncology 2014;4:72. PubMed PMID: 24778991; PubMed Central PMCID: PMC3984996.
194. Cluntun AA, Badolia R, Lettlova S, Parnell KM, Shankar TS, Diakos NA, et al. The pyruvate-lactate axis modulates cardiac hypertrophy and heart failure. Cell Metabolism 2021;33(3):629-648.e10. PubMed PMID: 33333007; PubMed Central PMCID: PMC7933116.
195. Kather JN, Halama N, Jaeger D. Genomics and emerging biomarkers for immunotherapy of colorectal cancer. Semin Cancer Biol 2018;52(Pt 2):189–97. PubMed PMID: 29501787.
196. Chen DS, Mellman I. Elements of cancer immunity and the cancer-immune set point. Nature 2017;541(7637):321–30. PubMed PMID: 28102259.
197. Ruffell B, DeNardo DG, Affara NI, Coussens LM. Lymphocytes in cancer development: polarization towards pro-tumor immunity. Cytokine Growth Factor Rev 2010;21(1):3–10. PubMed PMID: 20005150; PubMed Central PMCID: PMC2834837.
198. Lafferty KJ, Cunningham AJ. A new analysis of allogeneic interactions. Aust J Exp Biol Med Sci 1975;53(1):27–42. PubMed PMID: 238498.
199. Linsley PS, Brady W, Urnes M, Grosmaire LS, Damle NK, Ledbetter JA. CTLA-4 is a second receptor for the B cell activation antigen B7. J Exp Med 1991;174(3):561–9. PubMed PMID: 1714933; PubMed Central PMCID: PMC2118936.
200. Rudd CE, Taylor A, Schneider H. CD28 and CTLA-4 coreceptor expression and signal transduction. Immunological Reviews 2009;229(1):12–26. PubMed PMID: 19426212; PubMed Central PMCID: PMC4186963.
201. Azuma M, Ito D, Yagita H, Okumura K, Phillips JH, Lanier LL, et al. B70 antigen is a second ligand for CTLA-4 and CD28. Nature 1993;366(6450):76–9. PubMed PMID: 7694153.

202. Wendel M, Galani IE, Suri-Payer E, Cerwenka A. Natural killer cell accumulation in tumors is dependent on IFN-gamma and CXCR3 ligands. Cancer Research 2008;68(20):8437–45. PubMed PMID: 18922917.
203. Martín-Fontecha A, Thomsen LL, Brett S, Gerard C, Lipp M, Lanzavecchia A, et al. Induced recruitment of NK cells to lymph nodes provides IFN-gamma for T(H)1 priming. Nature Immunology 2004;5(12):1260–5. PubMed PMID: 15531883.
204. Kohli K, Pillarisetty VG, Kim TS. Key chemokines direct migration of immune cells in solid tumors. Cancer Gene Ther 2022;29(1):10–21. PubMed PMID: 33603130; PubMed Central PMCID: PMC8761573.
205. Muenst S, Läubli H, Soysal SD, Zippelius A, Tzankov A, Hoeller S. The immune system and cancer evasion strategies: therapeutic concepts. Journal of internal medicine 2016;279(6):541–62. PubMed PMID: 26748421.
206. Chávez-Galán L, Arenas-Del Angel MC, Zenteno E, Chávez R, Lascurain R. Cell death mechanisms induced by cytotoxic lymphocytes. Cell Mol Immunol 2009;6(1):15–25. PubMed PMID: 19254476; PubMed Central PMCID: PMC4002546.
207. Wilson CB, Rowell E, Sekimata M. Epigenetic control of T-helper-cell differentiation. Nat Rev Immunol 2009;9(2):91–105. PubMed PMID: 19151746.
208. Bennett CL, Christie J, Ramsdell F, Brunkow ME, Ferguson PJ, Whitesell L, et al. The immune dysregulation, polyendocrinopathy, enteropathy, X-linked syndrome (IPEX) is caused by mutations of FOXP3. Nat Genet 2001;27(1):20–1. PubMed PMID: 11137993.
209. Brunkow ME, Jeffery EW, Hjerrild KA, Paeper B, Clark LB, Yasayko SA, et al. Disruption of a new forkhead/winged-helix protein, scurfin, results in the fatal lymphoproliferative disorder of the scurfy mouse. Nat Genet 2001;27(1):68–73. PubMed PMID: 11138001.
210. Kim JM, Rasmussen JP, Rudensky AY. Regulatory T cells prevent catastrophic autoimmunity throughout the lifespan of mice. Nature Immunology 2007;8(2):191–7. PubMed PMID: 17136045.
211. Vesely MD, Kershaw MH, Schreiber RD, Smyth MJ. Natural innate and adaptive immunity to cancer. Annu Rev Immunol 2011;29:235–71. PubMed PMID: 21219185.
212. Algarra I, Garca-Lora A, Cabrera T, Ruiz-Cabello F, Garrido F. The selection of tumor variants with altered expression of classical and nonclassical MHC class I molecules: implications for tumor immune escape. Cancer Immunology, Immunotherapy 2004;53(10):904–10. PubMed PMID: 15069585.
213. Teng MWL, Galon J, Fridman W-H, Smyth MJ. From mice to humans: developments in cancer immunoediting. J Clin Invest 2015;125(9):3338–46. PubMed PMID: 26241053; PubMed Central PMCID: PMC4588291.
214. Melaiu O, Lucarini V, Cifaldi L, Fruci D. Influence of the Tumor Microenvironment on NK Cell Function in Solid Tumors. Frontiers in Immunology 2019;10:3038. PubMed PMID: 32038612; PubMed Central PMCID: PMC6985149.
215. Susek KH, Karvouni M, Alici E, Lundqvist A. The Role of CXC Chemokine Receptors 1-4 on Immune Cells in the Tumor Microenvironment. Frontiers in Immunology 2018;9:2159. PubMed PMID: 30319622; PubMed Central PMCID: PMC6167945.
216. Bruno A, Ferlazzo G, Albini A, Noonan DM. A think tank of TINK/TANKs: tumor-infiltrating/tumor-associated natural killer cells in tumor progression and angiogenesis. J Natl Cancer Inst 2014;106(8):dju200. PubMed PMID: 25178695; PubMed Central PMCID: PMC4344546.
217. Moretta L, Montaldo E, Vacca P, Del Zotto G, Moretta F, Merli P, et al. Human natural killer cells: origin, receptors, function, and clinical applications. Int Arch Allergy Immunol 2014;164(4):253–64. PubMed PMID: 25323661.

218. Matta J, Baratin M, Chiche L, Forel J-M, Cognet C, Thomas G, et al. Induction of B7-H6, a ligand for the natural killer cell–activating receptor NKp30, in inflammatory conditions. Blood 2013;122(3):394–404. PubMed PMID: 23687088.
219. Diefenbach A, Jensen ER, Jamieson AM, Raulet DH. Rae1 and H60 ligands of the NKG2D receptor stimulate tumour immunity. Nature 2001;413(6852):165–71. PubMed PMID: 11557981; PubMed Central PMCID: PMC3900321.
220. Malladi S, Macalinao DG, Jin X, He L, Basnet H, Zou Y, et al. Metastatic Latency and Immune Evasion through Autocrine Inhibition of WNT. Cell 2016;165(1):45–60. PubMed PMID: 27015306; PubMed Central PMCID: PMC4808520.
221. Spiegel A, Brooks MW, Houshyar S, Reinhardt F, Ardolino M, Fessler E, et al. Neutrophils Suppress Intraluminal NK Cell-Mediated Tumor Cell Clearance and Enhance Extravasation of Disseminated Carcinoma Cells. Cancer Discov 2016;6(6):630–49. PubMed PMID: 27072748; PubMed Central PMCID: PMC4918202.
222. Pernot S, Terme M, Radosevic-Robin N, Castan F, Badoual C, Marcheteau E, et al. Infiltrating and peripheral immune cell analysis in advanced gastric cancer according to the Lauren classification and its prognostic significance. Gastric Cancer 2020;23(1):73–81. PubMed PMID: 31267360.
223. Ménard C, Blay J-Y, Borg C, Michiels S, Ghiringhelli F, Robert C, et al. Natural killer cell IFN-gamma levels predict long-term survival with imatinib mesylate therapy in gastrointestinal stromal tumor-bearing patients. Cancer Research 2009;69(8):3563–9. PubMed PMID: 19351841.
224. Delahaye NF, Rusakiewicz S, Martins I, Ménard C, Roux S, Lyonnet L, et al. Alternatively spliced NKp30 isoforms affect the prognosis of gastrointestinal stromal tumors. Nature Medicine 2011;17(6):700–7. PubMed PMID: 21552268.
225. Pasero C, Gravis G, Guerin M, Granjeaud S, Thomassin-Piana J, Rocchi P, et al. Inherent and Tumor-Driven Immune Tolerance in the Prostate Microenvironment Impairs Natural Killer Cell Antitumor Activity. Cancer Research 2016;76(8):2153–65. PubMed PMID: 27197252.
226. Habif G, Crinier A, André P, Vivier E, Narni-Mancinelli E. Targeting natural killer cells in solid tumors. Cell Mol Immunol 2019;16(5):415–22. PubMed PMID: 30911118; PubMed Central PMCID: PMC6474204.
227. Beldi-Ferchiou A, Caillat-Zucman S. Control of NK Cell Activation by Immune Checkpoint Molecules. Int J Mol Sci 2017;18(10):2129. PubMed PMID: 29023417; PubMed Central PMCID: PMC5666811.
228. Kim N, Kim HS. Targeting Checkpoint Receptors and Molecules for Therapeutic Modulation of Natural Killer Cells. Frontiers in Immunology 2018;9:2041. PubMed PMID: 30250471; PubMed Central PMCID: PMC6139314.
229. Berzins SP, Uldrich AP, Pellicci DG, McNab F, Hayakawa Y, Smyth MJ, et al. Parallels and distinctions between T and NKT cell development in the thymus. Immunol Cell Biol 2004;82(3):269–75. PubMed PMID: 15186258.
230. Godfrey DI, Uldrich AP, McCluskey J, Rossjohn J, Moody DB. The burgeoning family of unconventional T cells. Nature Immunology 2015;16(11):1114–23. PubMed PMID: 26482978.
231. Cohen NR, Brennan PJ, Shay T, Watts GF, Brigl M, Kang J, et al. Shared and distinct transcriptional programs underlie the hybrid nature of iNKT cells. Nature Immunology 2013;14(1):90–9. PubMed PMID: 23202270; PubMed Central PMCID: PMC3764492.
232. Bindea G, Mlecnik B, Tosolini M, Kirilovsky A, Waldner M, Obenauf AC, et al. Spatiotemporal dynamics of intratumoral immune cells reveal the immune landscape in human cancer. Immunity 2013;39(4):782–95. PubMed PMID: 24138885.
233. Sharonov GV, Serebrovskaya EO, Yuzhakova DV, Britanova OV, Chudakov DM. B cells, plasma cells and antibody repertoires in the tumour microenvironment. Nat Rev Immunol 2020;20(5):294–307. PubMed PMID: 31988391.

234. Lund FE, Randall TD. Effector and regulatory B cells: modulators of CD4+ T cell immunity. Nat Rev Immunol 2010;10(4):236–47. PubMed PMID: 20224569; PubMed Central PMCID: PMC3038334.
235. Castino GF, Cortese N, Capretti G, Serio S, Di Caro G, Mineri R, et al. Spatial distribution of B cells predicts prognosis in human pancreatic adenocarcinoma. Oncoimmunology 2016;5(4):e1085147. PubMed PMID: 27141376; PubMed Central PMCID: PMC4839336.
236. Ladányi A, Kiss J, Mohos A, Somlai B, Liszkay G, Gilde K, et al. Prognostic impact of B-cell density in cutaneous melanoma. Cancer Immunology, Immunotherapy 2011;60(12):1729–38. PubMed PMID: 21779876.
237. Germain C, Gnjatic S, Tamzalit F, Knockaert S, Remark R, Goc J, et al. Presence of B cells in tertiary lymphoid structures is associated with a protective immunity in patients with lung cancer. Am J Respir Crit Care Med 2014;189(7):832–44. PubMed PMID: 24484236.
238. Gilbert AE, Karagiannis P, Dodev T, Koers A, Lacy K, Josephs DH, et al. Monitoring the systemic human memory B cell compartment of melanoma patients for anti-tumor IgG antibodies. PLOS ONE 2011;6(4):e19330. PubMed PMID: 21559411; PubMed Central PMCID: PMC3084832.
239. Kurai J, Chikumi H, Hashimoto K, Yamaguchi K, Yamasaki A, Sako T, et al. Antibody-dependent cellular cytotoxicity mediated by cetuximab against lung cancer cell lines. Clin Cancer Res 2007;13(5):1552–61. PubMed PMID: 17332301.
240. Carmi Y, Spitzer MH, Linde IL, Burt BM, Prestwood TR, Perlman N, et al. Allogeneic IgG combined with dendritic cell stimuli induce antitumour T-cell immunity. Nature 2015;521(7550):99–104. PubMed PMID: 25924063; PubMed Central PMCID: PMC4877172.
241. van Dang D, Hilgenberg E, Ries S, Shen P, Fillatreau S. From the regulatory functions of B cells to the identification of cytokine-producing plasma cell subsets. Curr Opin Immunol 2014;28:77–83. PubMed PMID: 24637161.
242. Ou Z, Wang Y, Liu L, Li L, Yeh S, Qi L, et al. Tumor microenvironment B cells increase bladder cancer metastasis via modulation of the IL-8/androgen receptor (AR)/MMPs signals. Oncotarget 2015;6(28):26065–78. PubMed PMID: 26305549; PubMed Central PMCID: PMC4694886.
243. Woo JR, Liss MA, Muldong MT, Palazzi K, Strasner A, Ammirante M, et al. Tumor infiltrating B-cells are increased in prostate cancer tissue. J Transl Med 2014;12:30. PubMed PMID: 24475900; PubMed Central PMCID: PMC3914187.
244. Charoentong P, Finotello F, Angelova M, Mayer C, Efremova M, Rieder D, et al. Pan-cancer Immunogenomic Analyses Reveal Genotype-Immunophenotype Relationships and Predictors of Response to Checkpoint Blockade. Cell Rep 2017;18(1):248–62. PubMed PMID: 28052254.
245. Iglesia MD, Parker JS, Hoadley KA, Serody JS, Perou CM, Vincent BG. Genomic Analysis of Immune Cell Infiltrates Across 11 Tumor Types. J Natl Cancer Inst 2016;108(11). PubMed PMID: 27335052; PubMed Central PMCID: PMC5241901.
246. Schwartz M, Zhang Y, Rosenblatt JD. B cell regulation of the anti-tumor response and role in carcinogenesis. J Immunother Cancer 2016;4:40. PubMed PMID: 27437104; PubMed Central PMCID: PMC4950763.
247. Sarvaria A, Madrigal JA, Saudemont A. B cell regulation in cancer and anti-tumor immunity. Cell Mol Immunol 2017;14(8):662–74. PubMed PMID: 28626234; PubMed Central PMCID: PMC5549607.
248. Ammirante M, Luo J-L, Grivennikov S, Nedospasov S, Karin M. B-cell-derived lymphotoxin promotes castration-resistant prostate cancer. Nature 2010;464(7286):302–5. PubMed PMID: 20220849; PubMed Central PMCID: PMC2866639.
249. Balkwill F, Montfort A, Capasso M. B regulatory cells in cancer. Trends Immunol 2013;34(4):169–73. PubMed PMID: 23206438.
250. Arina A, Idel C, Hyjek EM, Alegre M-L, Wang Y, Bindokas VP, et al. Tumor-associated fibroblasts predominantly come from local and not circulating precursors. Proceedings of the National

Academy of Sciences 2016;113(27):7551–6. PubMed PMID: 27317748; PubMed Central PMCID: PMC4941507.

251. Kretzschmar K, Weber C, Driskell RR, Calonje E, Watt FM. Compartmentalized Epidermal Activation of β-Catenin Differentially Affects Lineage Reprogramming and Underlies Tumor Heterogeneity. Cell Rep 2016;14(2):269–81. PubMed PMID: 26771241; PubMed Central PMCID: PMC4713864.
252. Hawinkels LJAC, Paauwe M, Verspaget HW, Wiercinska E, van der Zon JM, van der Ploeg K, et al. Interaction with colon cancer cells hyperactivates TGF-β signaling in cancer-associated fibroblasts. Oncogene 2014;33(1):97–107. PubMed PMID: 23208491.
253. Elenbaas B, Weinberg RA. Heterotypic signaling between epithelial tumor cells and fibroblasts in carcinoma formation. Exp Cell Res 2001;264(1):169–84. PubMed PMID: 11237532.
254. Kojima Y, Acar A, Eaton EN, Mellody KT, Scheel C, Ben-Porath I, et al. Autocrine TGF-beta and stromal cell-derived factor-1 (SDF-1) signaling drives the evolution of tumor-promoting mammary stromal myofibroblasts. Proceedings of the National Academy of Sciences 2010;107(46):20009–14. PubMed PMID: 21041659; PubMed Central PMCID: PMC2993333.
255. Costa A, Scholer-Dahirel A, Mechta-Grigoriou F. The role of reactive oxygen species and metabolism on cancer cells and their microenvironment. Semin Cancer Biol 2014;25:23–32. PubMed PMID: 24406211.
256. Arcucci A, Ruocco MR, Granato G, Sacco AM, Montagnani S. Cancer: An Oxidative Crosstalk between Solid Tumor Cells and Cancer Associated Fibroblasts. Biomed Res Int 2016;2016:4502846. PubMed PMID: 27595103; PubMed Central PMCID: PMC4993917.
257. Quante M, Tu SP, Tomita H, Gonda T, Wang SSW, Takashi S, et al. Bone marrow-derived myofibroblasts contribute to the mesenchymal stem cell niche and promote tumor growth. Cancer Cell 2011;19(2):257–72. PubMed PMID: 21316604; PubMed Central PMCID: PMC3060401.
258. Zhang Y, Daquinag A, Traktuev DO, Amaya-Manzanares F, Simmons PJ, March KL, et al. White adipose tissue cells are recruited by experimental tumors and promote cancer progression in mouse models. Cancer Research 2009;69(12):5259–66. PubMed PMID: 19491274; PubMed Central PMCID: PMC3857703.
259. Coffman LG, Pearson AT, Frisbie LG, Freeman Z, Christie E, Bowtell DD, et al. Ovarian Carcinoma-Associated Mesenchymal Stem Cells Arise from Tissue-Specific Normal Stroma. Stem Cells 2019;37(2):257–69. PubMed PMID: 30353617; PubMed Central PMCID: PMC6392140.
260. Mao X, Xu J, Wang W, Liang C, Hua J, Liu J, et al. Crosstalk between cancer-associated fibroblasts and immune cells in the tumor microenvironment: new findings and future perspectives. Mol Cancer 2021;20(1):131. PubMed PMID: 34635121; PubMed Central PMCID: PMC8504100.
261. Liu T, Han C, Wang S, Fang P, Ma Z, Xu L, et al. Cancer-associated fibroblasts: an emerging target of anti-cancer immunotherapy. J Hematol Oncol 2019;12(1):86. PubMed PMID: 31462327; PubMed Central PMCID: PMC6714445.
262. Harper J, Sainson RCA. Regulation of the anti-tumour immune response by cancer-associated fibroblasts. Semin Cancer Biol 2014;25:69–77. PubMed PMID: 24406209.
263. Ziani L, Chouaib S, Thiery J. Alteration of the Antitumor Immune Response by Cancer-Associated Fibroblasts. Frontiers in Immunology 2018;9:414. PubMed PMID: 29545811; PubMed Central PMCID: PMC5837994.
264. Kim R, Emi M, Tanabe K. Cancer immunosuppression and autoimmune disease: beyond immunosuppressive networks for tumour immunity. Immunology 2006;119(2):254–64. PubMed PMID: 17005005; PubMed Central PMCID: PMC1782355.

265. Bhagat TD, Ahrens D von, Dawlaty M, Zou Y, Baddour J, Achreja A, et al. Lactate-mediated epigenetic reprogramming regulates formation of human pancreatic cancer-associated fibroblasts. eLife 2019;8. PubMed PMID: 31663852; PubMed Central PMCID: PMC6874475.
266. Comito G, Iscaro A, Bacci M, Morandi A, Ippolito L, Parri M, et al. Lactate modulates CD4+ T-cell polarization and induces an immunosuppressive environment, which sustains prostate carcinoma progression via TLR8/miR21 axis. Oncogene 2019;38(19):3681–95. PubMed PMID: 30664688.
267. Shangguan C, Gan G, Zhang J, Wu J, Miao Y, Zhang M, et al. Cancer-associated fibroblasts enhance tumor 18F-FDG uptake and contribute to the intratumor heterogeneity of PET-CT. Theranostics 2018;8(5):1376–88. PubMed PMID: 29507627; PubMed Central PMCID: PMC5835943.
268. Pasqualini R, Arap W, McDonald DM. Probing the structural and molecular diversity of tumor vasculature. Trends Mol Med 2002;8(12):563–71.
269. Maishi N, Hida K. Tumor endothelial cells accelerate tumor metastasis. Cancer Sci 2017;108(10):1921–6. PubMed PMID: 28763139; PubMed Central PMCID: PMC5623747.
270. Chang YS, Di Tomaso E, McDonald DM, Jones R, Jain RK, Munn LL. Mosaic blood vessels in tumors: frequency of cancer cells in contact with flowing blood. Proc Natl Acad Sci U S A 2000;97(26):14608–13. PubMed PMID: 11121063; PubMed Central PMCID: PMC18966.
271. McDonald DM, Choyke PL. Imaging of angiogenesis: from microscope to clinic. Nature Medicine 2003;9(6):713–25. PubMed PMID: 12778170.
272. Maishi N, Ohba Y, Akiyama K, Ohga N, Hamada J, Nagao-Kitamoto H, et al. Tumour endothelial cells in high metastatic tumours promote metastasis via epigenetic dysregulation of biglycan. Scientific Reports 2016;6:28039. PubMed PMID: 27295191; PubMed Central PMCID: PMC4904795.
273. Anderson NM, Simon MC. The tumor microenvironment. Curr Biol 2020;30(16):R921-R925. PubMed PMID: 32810447; PubMed Central PMCID: PMC8194051.
274. Ottensmeier CH, Perry KL, Harden EL, Stasakova J, Jenei V, Fleming J, et al. Upregulated Glucose Metabolism Correlates Inversely with CD8+ T-cell Infiltration and Survival in Squamous Cell Carcinoma. Cancer Research 2016;76(14):4136–48. PubMed PMID: 27206847.
275. Pinheiro C, Miranda-Gonçalves V, Longatto-Filho A, Vicente, Anna L. S. A., Berardinelli GN, Scapulatempo-Neto C, et al. The metabolic microenvironment of melanomas: Prognostic value of MCT1 and MCT4. Cell Cycle 2016;15(11):1462–70. PubMed PMID: 27105345; PubMed Central PMCID: PMC4934068.
276. Sun H, Zhu A, Zhou X, Wang F. Suppression of pyruvate dehydrogenase kinase-2 re-sensitizes paclitaxel-resistant human lung cancer cells to paclitaxel. Oncotarget 2017;8(32):52642–50. PubMed PMID: 28881758; PubMed Central PMCID: PMC5581057.
277. Zhao Y, Liu H, Liu Z, Ding Y, LeDoux SP, Wilson GL, et al. Overcoming trastuzumab resistance in breast cancer by targeting dysregulated glucose metabolism. Cancer Research 2011;71(13):4585–97. PubMed PMID: 21498634; PubMed Central PMCID: PMC3129363.
278. Vlachostergios PJ, Oikonomou KG, Gibilaro E, Apergis G. Elevated lactic acid is a negative prognostic factor in metastatic lung cancer. Cancer Biomark 2015;15(6):725–34. PubMed PMID: 26406401.
279. Isidoro A, Casado E, Redondo A, Acebo P, Espinosa E, Alonso AM, et al. Breast carcinomas fulfill the Warburg hypothesis and provide metabolic markers of cancer prognosis. Carcinogenesis 2005;26(12):2095–104. PubMed PMID: 16033770.
280. Choi J-W, Kim Y, Lee J-H, Kim Y-S. Prognostic significance of lactate/proton symporters MCT1, MCT4, and their chaperone CD147 expressions in urothelial carcinoma of the bladder. Urology 2014;84(1):245.e9-15. PubMed PMID: 24857275.

281. Reckzeh ES, Waldmann H. Small-Molecule Inhibition of Glucose Transporters GLUT-1-4. Chembiochem 2020;21(1-2):45–52. PubMed PMID: 31553512; PubMed Central PMCID: PMC7004114.
282. Abdel-Wahab AF, Mahmoud W, Al-Harizy RM. Targeting glucose metabolism to suppress cancer progression: prospective of anti-glycolytic cancer therapy. Pharmacol Res 2019;150:104511. PubMed PMID: 31678210.
283. Gurrapu S, Jonnalagadda SK, Alam MA, Nelson GL, Sneve MG, Drewes LR, et al. Monocarboxylate transporter 1 inhibitors as potential anticancer agents. ACS Medicinal Chemistry Letters 2015;6(5):558–61. PubMed PMID: 26005533; PubMed Central PMCID: PMC4434469.
284. Jonnalagadda S, Jonnalagadda SK, Ronayne CT, Nelson GL, Solano LN, Rumbley J, et al. Novel N,N-dialkyl cyanocinnamic acids as monocarboxylate transporter 1 and 4 inhibitors. Oncotarget 2019;10(24):2355–68. PubMed PMID: 31040927; PubMed Central PMCID: PMC6481325.
285. Benjamin D, Robay D, Hindupur SK, Pohlmann J, Colombi M, El-Shemerly MY, et al. Dual Inhibition of the Lactate Transporters MCT1 and MCT4 Is Synthetic Lethal with Metformin due to NAD+ Depletion in Cancer Cells. Cell Rep 2018;25(11):3047-3058.e4. PubMed PMID: 30540938; PubMed Central PMCID: PMC6302548.
286. Murray CM, Hutchinson R, Bantick JR, Belfield GP, Benjamin AD, Brazma D, et al. Monocarboxylate transporter MCT1 is a target for immunosuppression. Nature Chemical Biology 2005;1(7):371–6. PubMed PMID: 16370372.
287. Curtis NJ, Mooney L, Hopcroft L, Michopoulos F, Whalley N, Zhong H, et al. Pre-clinical pharmacology of AZD3965, a selective inhibitor of MCT1: DLBCL, NHL and Burkitt's lymphoma anti-tumor activity. Oncotarget 2017;8(41):69219–36. PubMed PMID: 29050199; PubMed Central PMCID: PMC5642474.
288. Puri S, Juvale K. Monocarboxylate transporter 1 and 4 inhibitors as potential therapeutics for treating solid tumours: A review with structure-activity relationship insights. European Journal of Medicinal Chemistry 2020;199:112393. PubMed PMID: 32388280.
289. Quanz M, Bender E, Kopitz C, Grünewald S, Schlicker A, Schwede W, et al. Preclinical Efficacy of the Novel Monocarboxylate Transporter 1 Inhibitor BAY-8002 and Associated Markers of Resistance. Molecular Cancer Therapeutics 2018;17(11):2285–96. PubMed PMID: 30115664.
290. Ullah MS, Davies AJ, HALESTRAP AP. The plasma membrane lactate transporter MCT4, but not MCT1, is up-regulated by hypoxia through a HIF-1alpha-dependent mechanism. Journal of Biological Chemistry 2006;281(14):9030–7. PubMed PMID: 16452478.
291. Critchlow, S. E. New Developments in Targeting Lactate Transporters; AACR: Chicago, 2018; 2018.
292. Goldberg FW, Kettle JG, Lamont GM, Buttar D, Ting AKT, McGuire TM, et al. Discovery of Clinical Candidate AZD0095, a Selective Inhibitor of Monocarboxylate Transporter 4 (MCT4) for Oncology. J Med Chem 2023;66(1):384–97. PubMed PMID: 36525250.
293. Heinrich T, Sala-Hojman A, Ferretti R, Petersson C, Minguzzi S, Gondela A, et al. Discovery of 5-{2-5-Chloro-2-(5-ethoxyquinoline-8-sulfonamido)phenylethynyl}-4-methoxypyridine-2-carboxylic Acid, a Highly Selective in Vivo Useable Chemical Probe to Dissect MCT4 Biology. J Med Chem 2021;64(16):11904–33. PubMed PMID: 34382802.
294. Fang Y, Liu W, Tang Z, Ji X, Zhou Y, Song S, et al. Monocarboxylate transporter 4 inhibition potentiates hepatocellular carcinoma immunotherapy through enhancing T cell infiltration and immune attack. Hepatology 2022. PubMed PMID: 35043976.
295. Akinleye A, Rasool Z. Immune checkpoint inhibitors of PD-L1 as cancer therapeutics. J Hematol Oncol 2019;12(1):92. PubMed PMID: 31488176; PubMed Central PMCID: PMC6729004.
296. Doroshow DB, Bhalla S, Beasley MB, Sholl LM, Kerr KM, Gnjatic S, et al. PD-L1 as a biomarker of response to immune-checkpoint inhibitors. Nat Rev Clin Oncol 2021;18(6):345–62. PubMed PMID: 33580222.

297. Redeker A, Welten SPM, Baert MRM, Vloemans SA, Tiemessen MM, Staal FJT, et al. The Quantity of Autocrine IL-2 Governs the Expansion Potential of CD8+ T Cells. The Journal of Immunology 2015;195(10):4792–801. PubMed PMID: 26453748.
298. WARBURG O. On the facultative anaerobiosis of cancer cells and its use in chemotherapy. Munch Med Wochenschr 1961;103:2504–6. PubMed PMID: 14004908.
299. Payen VL, Mina E, van Hée VF, Porporato PE, Sonveaux P. Monocarboxylate transporters in cancer. Molecular Metabolism 2020;33:48–66. PubMed PMID: 31395464; PubMed Central PMCID: PMC7056923.
300. Wu P, Zhou Y, Guo Y, Zhang S-L, Tam KY. Recent developments of human monocarboxylate transporter (hMCT) inhibitors as anticancer agents. Drug Discovery Today 2021;26(3):836–44. PubMed PMID: 33450176.
301. Brand A, Singer K, Koehl GE, Kolitzus M, Schoenhammer G, Thiel A, et al. LDHA-Associated Lactic Acid Production Blunts Tumor Immunosurveillance by T and NK Cells. Cell Metabolism 2016;24(5):657–71. PubMed PMID: 27641098.
302. Renner K, Bruss C, Schnell A, Koehl G, Becker HM, Fante M, et al. Restricting Glycolysis Preserves T Cell Effector Functions and Augments Checkpoint Therapy. Cell Rep 2019;29(1):135-150.e9. PubMed PMID: 31577944.
303. Calcinotto A, Filipazzi P, Grioni M, Iero M, Milito A de, Ricupito A, et al. Modulation of microenvironment acidity reverses anergy in human and murine tumor-infiltrating T lymphocytes. Cancer Research 2012;72(11):2746–56. PubMed PMID: 22593198.
304. El-Kenawi A, Gatenbee C, Robertson-Tessi M, Bravo R, Dhillon J, Balagurunathan Y, et al. Acidity promotes tumour progression by altering macrophage phenotype in prostate cancer. British Journal of Cancer 2019;121(7):556–66. PubMed PMID: 31417189; PubMed Central PMCID: PMC6889319.
305. Wang JX, Choi SYC, Niu X, Kang N, Xue H, Killam J, et al. Lactic Acid and an Acidic Tumor Microenvironment suppress Anticancer Immunity. Int J Mol Sci 2020;21(21). PubMed PMID: 33171818; PubMed Central PMCID: PMC7664620.
306. Anderson KG, Stromnes IM, Greenberg PD. Obstacles Posed by the Tumor Microenvironment to T cell Activity: A Case for Synergistic Therapies. Cancer Cell 2017;31(3):311–25. PubMed PMID: 28292435; PubMed Central PMCID: PMC5423788.
307. Chang C-H, Qiu J, O'Sullivan D, Buck MD, Noguchi T, Curtis JD, et al. Metabolic Competition in the Tumor Microenvironment Is a Driver of Cancer Progression. Cell 2015;162(6):1229–41. PubMed PMID: 26321679; PubMed Central PMCID: PMC4864363.
308. Huang T, Feng Q, Wang Z, Li W, Sun Z, Wilhelm J, et al. Tumor-Targeted Inhibition of Monocarboxylate Transporter 1 Improves T-Cell Immunotherapy of Solid Tumors. Adv Healthc Mater 2021;10(4):e2000549. PubMed PMID: 32431046; PubMed Central PMCID: PMC7674253.
309. Reeh PW, Steen KH. Chapter 8. Tissue acidosis in nociception and pain. In: Kumazawa T, editor. The polymodal receptor-a gateway to pathological plain. Progress in Brain Research. Vol. 113. Amsterdam: Elsevier; 1996. p. 143–51.
310. Michaeli J, Shaul ME, Mishalian I, Hovav A-H, Levy L, Zolotriov L, et al. Tumor-associated neutrophils induce apoptosis of non-activated CD8 T-cells in a TNFα and NO-dependent mechanism, promoting a tumor-supportive environment. Oncoimmunology 2017;6(11):e1356965. PubMed PMID: 29147615; PubMed Central PMCID: PMC5674962.
311. Mishalian I, Bayuh R, Eruslanov E, Michaeli J, Levy L, Zolotarov L, et al. Neutrophils recruit regulatory T-cells into tumors via secretion of CCL17--a new mechanism of impaired antitumor immunity. International Journal of Cancer 2014;135(5):1178–86. PubMed PMID: 24501019.

312. Coffelt SB, Kersten K, Doornebal CW, Weiden J, Vrijland K, Hau C-S, et al. IL-17-producing γδ T cells and neutrophils conspire to promote breast cancer metastasis. Nature 2015;522(7556):345–8. PubMed PMID: 25822788; PubMed Central PMCID: PMC4475637.
313. Rodríguez-Espinosa O, Rojas-Espinosa O, Moreno-Altamirano MMB, López-Villegas EO, Sánchez-García FJ. Metabolic requirements for neutrophil extracellular traps formation. Immunology 2015;145(2):213–24. PubMed PMID: 25545227; PubMed Central PMCID: PMC4427386.
314. Merezhinskaya N, Ogunwuyi SA, Mullick FG, Fishbein WN. Presence and localization of three lactic acid transporters (MCT1, -2, and -4) in separated human granulocytes, lymphocytes, and monocytes. J Histochem Cytochem 2004;52(11):1483–93. PubMed PMID: 15505343; PubMed Central PMCID: PMC3957819.
315. Lahoz-Beneytez J, Elemans M, Zhang Y, Ahmed R, Salam A, Block M, et al. Human neutrophil kinetics: modeling of stable isotope labeling data supports short blood neutrophil half-lives. Blood 2016;127(26):3431–8. PubMed PMID: 27136946; PubMed Central PMCID: PMC4929930.
316. Patel AA, Ginhoux F, Yona S. Monocytes, macrophages, dendritic cells and neutrophils: an update on lifespan kinetics in health and disease. Immunology 2021;163(3):250–61. PubMed PMID: 33555612; PubMed Central PMCID: PMC8207393.
317. Trevani AS, Andonegui G, Giordano M, López DH, Gamberale R, Minucci F, et al. Extracellular acidification induces human neutrophil activation. J Immunol 1999;162(8):4849–57. PubMed PMID: 10202029.
318. Damgaci S, Ibrahim-Hashim A, Enriquez-Navas PM, Pilon-Thomas S, Guvenis A, Gillies RJ. Hypoxia and acidosis: immune suppressors and therapeutic targets. Immunology 2018;154(3):354–62. PubMed PMID: 29485185; PubMed Central PMCID: PMC6002221.
319. Cao S, Liu P, Zhu H, Gong H, Yao J, Sun Y, et al. Extracellular Acidification Acts as a Key Modulator of Neutrophil Apoptosis and Functions. PLOS ONE 2015;10(9):e0137221. PubMed PMID: 26340269; PubMed Central PMCID: PMC4560393.
320. Gonzalez H, Hagerling C, Werb Z. Roles of the immune system in cancer: from tumor initiation to metastatic progression. Genes Dev 2018;32(19-20):1267–84. PubMed PMID: 30275043; PubMed Central PMCID: PMC6169832.
321. Baek G, Tse YF, Hu Z, Cox D, Buboltz N, McCue P, et al. MCT4 defines a glycolytic subtype of pancreatic cancer with poor prognosis and unique metabolic dependencies. Cell Rep 2014;9(6):2233–49. PubMed PMID: 25497091.
322. Baenke F, Dubuis S, Brault C, Weigelt B, Dankworth B, Griffiths B, et al. Functional screening identifies MCT4 as a key regulator of breast cancer cell metabolism and survival. The Journal of Pathology 2015;237(2):152–65. PubMed PMID: 25965974.
323. Benjamin D, Robay D, Hindupur SK, Pohlmann J, Colombi M, El-Shemerly MY, et al. Dual Inhibition of the Lactate Transporters MCT1 and MCT4 Is Synthetic Lethal with Metformin due to NAD+ Depletion in Cancer Cells. Cell Rep 2018;25(11):3047-3058.e4. PubMed PMID: 30540938; PubMed Central PMCID: PMC6302548.
324. Bola BM, Chadwick AL, Michopoulos F, Blount KG, Telfer BA, Williams KJ, et al. Inhibition of monocarboxylate transporter-1 (MCT1) by AZD3965 enhances radiosensitivity by reducing lactate transport. Molecular Cancer Therapeutics 2014;13(12):2805–16. PubMed PMID: 25281618; PubMed Central PMCID: PMC4258406.
325. Critchlow SE, Hopcroft L, Mooney L, Curtis N, Whalley N, Zhong H, et al. Abstract 3224: Pre-clinical targeting of the metabolic phenotype of lymphoma by AZD3965, a selective inhibitor of monocarboxylate transporter 1 (MCT1). Cancer Research 2012;72(8_Supplement):3224.
326. Hambruch N, Herkert B, Gege C, Mallinger A, Fabian J, Kinzel O, et al. Abstract 3588: Identification of a potent, orally bioavailable and selective MCT4 Inhibitor for the treatment of solid Warburg tumors. Cancer Research 2019;79(13_Supplement):3588.

327. Marchiq I, Le Floch R, Roux D, Simon M-P, Pouyssegur J. Genetic disruption of lactate/H+ symporters (MCTs) and their subunit CD147/BASIGIN sensitizes glycolytic tumor cells to phenformin. Cancer Research 2015;75(1):171–80. PubMed PMID: 25403912.
328. Quinn WJ, Jiao J, TeSlaa T, Stadanlick J, Wang Z, Wang L, et al. Lactate Limits T Cell Proliferation via the NAD(H) Redox State. Cell Rep 2020;33(11):108500. PubMed PMID: 33326785; PubMed Central PMCID: PMC7830708.
329. Cham CM, Driessens G, O'Keefe JP, Gajewski TF. Glucose deprivation inhibits multiple key gene expression events and effector functions in CD8+ T cells. European Journal of Immunology 2008;38(9):2438–50. PubMed PMID: 18792400; PubMed Central PMCID: PMC3008428.
330. Cham CM, Gajewski TF. Glucose availability regulates IFN-gamma production and p70S6 kinase activation in CD8+ effector T cells. J Immunol 2005;174(8):4670–7. PubMed PMID: 15814691.
331. Le Floch R, Chiche J, Marchiq I, Naiken T, Naïken T, Ilc K, et al. CD147 subunit of lactate/H+ symporters MCT1 and hypoxia-inducible MCT4 is critical for energetics and growth of glycolytic tumors. Proceedings of the National Academy of Sciences 2011;108(40):16663–8. PubMed PMID: 21930917; PubMed Central PMCID: PMC3189052.
332. Lewis CE, Pollard JW. Distinct role of macrophages in different tumor microenvironments. Cancer Res 2006;66(2):605–12. PubMed PMID: 16423985.
333. Quatromoni JG, Eruslanov E. Tumor-associated macrophages: function, phenotype, and link to prognosis in human lung cancer. Am J Transl Res 2012;4(4):376–89. PubMed PMID: 23145206; PubMed Central PMCID: PMC3493031.
334. Pathria P, Louis TL, Varner JA. Targeting Tumor-Associated Macrophages in Cancer. Trends Immunol 2019;40(4):310–27. PubMed PMID: 30890304.
335. Watson MJ, Vignali PDA, Mullett SJ, Overacre-Delgoffe AE, Peralta RM, Grebinoski S, et al. Metabolic support of tumour-infiltrating regulatory T cells by lactic acid. Nature 2021;591(7851):645–51. PubMed PMID: 33589820; PubMed Central PMCID: PMC7990682.
336. Martins SF, Amorim R, Viana-Pereira M, Pinheiro C, Costa RFA, Silva P, et al. Significance of glycolytic metabolism-related protein expression in colorectal cancer, lymph node and hepatic metastasis. BMC Cancer 2016;16:535. PubMed PMID: 27460659; PubMed Central PMCID: PMC4962413.
337. Javaeed A, Ghauri SK. MCT4 has a potential to be used as a prognostic biomarker - a systematic review and meta-analysis. Oncol Rev 2019;13(2):403. PubMed PMID: 31410246; PubMed Central PMCID: PMC6661531.
338. Offermans K, Jenniskens JC, Simons CC, Samarska I, Fazzi GE, Smits KM, et al. Expression of proteins associated with the Warburg-effect and survival in colorectal cancer. J Pathol Clin Res 2022;8(2):169–80. PubMed PMID: 34791830; PubMed Central PMCID: PMC8822385.
339. Roy M, Finley SD. Metabolic reprogramming dynamics in tumor spheroids: Insights from a multicellular, multiscale model. PLoS Comput Biol 2019;15(6):e1007053. PubMed PMID: 31185009; PubMed Central PMCID: PMC6588258.
340. Takahashi Y, Hori Y, Yamamoto T, Urashima T, Ohara Y, Tanaka H. 3D spheroid cultures improve the metabolic gene expression profiles of HepaRG cells. Biosci Rep 2015;35(3). PubMed PMID: 26182370; PubMed Central PMCID: PMC4613666.
341. Halama N, Braun M, Kahlert C, Spille A, Quack C, Rahbari N, et al. Natural killer cells are scarce in colorectal carcinoma tissue despite high levels of chemokines and cytokines. Clin Cancer Res 2011;17(4):678–89. PubMed PMID: 21325295.
342. Tanis E, Julié C, Emile J-F, Mauer M, Nordlinger B, Aust D, et al. Prognostic impact of immune response in resectable colorectal liver metastases treated by surgery alone or surgery with perioperative FOLFOX in the randomised EORTC study 40983. Eur J Cancer 2015;51(17):2708–17. PubMed PMID: 26342674.

343. Cui C, Xu C, Yang W, Chi Z, Sheng X, Si L, et al. Ratio of the interferon-γ signature to the immunosuppression signature predicts anti-PD-1 therapy response in melanoma. NPJ Genom Med 2021;6(1):7. PubMed PMID: 33542239; PubMed Central PMCID: PMC7862369.
344. Rozeman EA, Hoefsmit EP, Reijers ILM, Saw RPM, Versluis JM, Krijgsman O, et al. Survival and biomarker analyses from the OpACIN-neo and OpACIN neoadjuvant immunotherapy trials in stage III melanoma. Nature Medicine 2021;27(2):256–63. PubMed PMID: 33558721.
345. Ding G, Shen T, Yan C, Zhang M, Wu Z, Cao L. IFN-γ down-regulates the PD-1 expression and assist nivolumab in PD-1-blockade effect on CD8+ T-lymphocytes in pancreatic cancer. BMC Cancer 2019;19(1):1053. PubMed PMID: 31694582; PubMed Central PMCID: PMC6836337.
346. Hänze J, Wegner M, Noessner E, Hofmann R, Hegele A. Co-Regulation of Immune Checkpoint PD-L1 with Interferon-Gamma Signaling is Associated with a Survival Benefit in Renal Cell Cancer. Target Oncol 2020;15(3):377–90. PubMed PMID: 32495158; PubMed Central PMCID: PMC7283197.
347. Mestas J, Hughes CCW. Of mice and not men: differences between mouse and human immunology. J Immunol 2004;172(5):2731–8. PubMed PMID: 14978070.
348. Wang L, Kuang Z, Zhang D, Gao Y, Ying M, Wang T. Reactive oxygen species in immune cells: A new antitumor target. Biomed Pharmacother 2021;133:110978. PubMed PMID: 33176269.
349. Yarosz EL, Chang C-H. The Role of Reactive Oxygen Species in Regulating T Cell-mediated Immunity and Disease. Immune Netw 2018;18(1):e14. PubMed PMID: 29503744; PubMed Central PMCID: PMC5833121.
350. Kesarwani P, Thyagarajan K, Chatterjee S, Palanisamy V, Mehrotra S. Anti-oxidant capacity and anti-tumor T cell function: A direct correlation. Oncoimmunology 2015;4(1):e985942. PubMed PMID: 25949871; PubMed Central PMCID: PMC4368125.
351. Hsieh JJ, Purdue MP, Signoretti S, Swanton C, Albiges L, Schmidinger M, et al. Renal cell carcinoma. Nat Rev Dis Primers 2017;3:17009. PubMed PMID: 28276433; PubMed Central PMCID: PMC5936048.
352. Vera-Badillo FE, Templeton AJ, Duran I, Ocana A, Gouveia P de, Aneja P, et al. Systemic therapy for non-clear cell renal cell carcinomas: a systematic review and meta-analysis. Eur Urol 2015;67(4):740–9. PubMed PMID: 24882670.
353. Santoni M, Massari F, Amantini C, Nabissi M, Maines F, Burattini L, et al. Emerging role of tumor-associated macrophages as therapeutic targets in patients with metastatic renal cell carcinoma. Cancer Immunology, Immunotherapy 2013;62(12):1757–68. PubMed PMID: 24132754.
354. Figel A-M, Brech D, Prinz PU, Lettenmeyer UK, Eckl J, Turqueti-Neves A, et al. Human renal cell carcinoma induces a dendritic cell subset that uses T-cell crosstalk for tumor-permissive milieu alterations. Am J Pathol 2011;179(1):436–51. PubMed PMID: 21703422; PubMed Central PMCID: PMC3123875.
355. Young MD, Mitchell TJ, Vieira Braga FA, Tran MGB, Stewart BJ, Ferdinand JR, et al. Single-cell transcriptomes from human kidneys reveal the cellular identity of renal tumors. Science 2018;361(6402):594–9. PubMed PMID: 30093597; PubMed Central PMCID: PMC6104812.
356. Groth C, Hu X, Weber R, Fleming V, Altevogt P, Utikal J, et al. Immunosuppression mediated by myeloid-derived suppressor cells (MDSCs) during tumour progression. British Journal of Cancer 2019;120(1):16–25. PubMed PMID: 30413826; PubMed Central PMCID: PMC6325125.
357. Greten TF, Manns MP, Korangy F. Myeloid derived suppressor cells in human diseases. Int Immunopharmacol 2011;11(7):802–7. PubMed PMID: 21237299; PubMed Central PMCID: PMC3478130.
358. Lotz C, Kelleher DK, Gassner B, Gekle M, Vaupel P, Thews O. Role of the tumor microenvironment in the activity and expression of the p-glycoprotein in human colon carcinoma cells. Oncol Rep 2007;17(1):239–44. PubMed PMID: 17143504.

359. Kunkel M, Förster GJ, Reichert TE, Jeong J-H, Benz P, Bartenstein P, et al. Detection of recurrent oral squamous cell carcinoma by 18F-2-fluorodeoxyglucose-positron emission tomography: implications for prognosis and patient management. Cancer 2003;98(10):2257–65. PubMed PMID: 14601097.
360. Roland CL, Arumugam T, Deng D, Liu SH, Philip B, Gomez S, et al. Cell surface lactate receptor GPR81 is crucial for cancer cell survival. Cancer Research 2014;74(18):5301–10. PubMed PMID: 24928781; PubMed Central PMCID: PMC4167222.
361. Dhup S, Dadhich RK, Porporato PE, Sonveaux P. Multiple biological activities of lactic acid in cancer: influences on tumor growth, angiogenesis and metastasis. Curr Pharm Des 2012;18(10):1319–30. PubMed PMID: 22360558.
362. Végran F, Boidot R, Michiels C, Sonveaux P, Feron O. Lactate influx through the endothelial cell monocarboxylate transporter MCT1 supports an NF-κB/IL-8 pathway that drives tumor angiogenesis. Cancer Research 2011;71(7):2550–60. PubMed PMID: 21300765.
363. Boedtkjer E, Pedersen SF. The Acidic Tumor Microenvironment as a Driver of Cancer. Annu Rev Physiol 2020;82:103–26. PubMed PMID: 31730395.
364. Fischer K, Hoffmann P, Voelkl S, Meidenbauer N, Ammer J, Edinger M, et al. Inhibitory effect of tumor cell-derived lactic acid on human T cells. Blood 2007;109(9):3812–9. PubMed PMID: 17255361.
365. Renner K, Bruss C, Schnell A, Koehl G, Becker HM, Fante M, et al. Restricting Glycolysis Preserves T Cell Effector Functions and Augments Checkpoint Therapy. Cell Rep 2019;29(1):135-150.e9. PubMed PMID: 31577944.
366. Pucino V, Certo M, Bulusu V, Cucchi D, Goldmann K, Pontarini E, et al. Lactate Buildup at the Site of Chronic Inflammation Promotes Disease by Inducing CD4+ T Cell Metabolic Rewiring. Cell Metabolism 2019;30(6):1055-1074.e8. PubMed PMID: 31708446; PubMed Central PMCID: PMC6899510.
367. Elia I, Rowe JH, Johnson S, Joshi S, Notarangelo G, Kurmi K, et al. Tumor cells dictate anti-tumor immune responses by altering pyruvate utilization and succinate signaling in CD8+ T cells. Cell Metabolism 2022;34(8):1137-1150.e6. PubMed PMID: 35820416; PubMed Central PMCID: PMC9357162.
368. Feng Q, Liu Z, Yu X, Huang T, Chen J, Wang J, et al. Lactate increases stemness of CD8 + T cells to augment anti-tumor immunity. Nature Communications 2022;13(1):4981. PubMed PMID: 36068198; PubMed Central PMCID: PMC9448806.
369. Brooks GA. The Science and Translation of Lactate Shuttle Theory. Cell Metabolism 2018;27(4):757–85. PubMed PMID: 29617642.
370. Uhl FM, Chen S, O'Sullivan D, Edwards-Hicks J, Richter G, Haring E, et al. Metabolic reprogramming of donor T cells enhances graft-versus-leukemia effects in mice and humans. Science Translational Medicine 2020;12(567). PubMed PMID: 33115954; PubMed Central PMCID: PMC8529950.
371. Renner K, Geiselhöringer A-L, Fante M, Bruss C, Färber S, Schönhammer G, et al. Metabolic plasticity of human T cells: Preserved cytokine production under glucose deprivation or mitochondrial restriction, but 2-deoxy-glucose affects effector functions. European Journal of Immunology 2015;45(9):2504–16. PubMed PMID: 26114249.
372. Macintyre AN, Gerriets VA, Nichols AG, Michalek RD, Rudolph MC, Deoliveira D, et al. The glucose transporter Glut1 is selectively essential for CD4 T cell activation and effector function. Cell Metabolism 2014;20(1):61–72. PubMed PMID: 24930970; PubMed Central PMCID: PMC4079750.
373. Chen X, Jaiswal A, Costliow Z, Herbst P, Creasey EA, Oshiro-Rapley N, et al. pH sensing controls tissue inflammation by modulating cellular metabolism and endo-lysosomal function of immune cells. Nature Immunology 2022;23(7):1063–75. PubMed PMID: 35668320; PubMed Central PMCID: PMC9720675.

374. Rajamäki K, Nordström T, Nurmi K, Åkerman KEO, Kovanen PT, Öörni K, et al. Extracellular acidosis is a novel danger signal alerting innate immunity via the NLRP3 inflammasome. J Biol Chem 2013;288(19):13410–9. PubMed PMID: 23530046; PubMed Central PMCID: PMC3650379.
375. Miska J, Rashidi A, Lee-Chang C, Gao P, Lopez-Rosas A, Zhang P, et al. Polyamines drive myeloid cell survival by buffering intracellular pH to promote immunosuppression in glioblastoma. Sci Adv 2021;7(8). PubMed PMID: 33597238; PubMed Central PMCID: PMC7888943.
376. Frick L, Hinterland L, Renner K, Vogl M, Babl N, Heckscher S, et al. Acidic Microenvironments Found in Cutaneous Leishmania Lesions Curtail NO-Dependent Antiparasitic Macrophage Activity. Frontiers in Immunology 2022;13:789366. PubMed PMID: 35493523; PubMed Central PMCID: PMC9047701.
377. Dancey JT, Deubelbeiss KA, Harker LA, Finch CA. Neutrophil kinetics in man. Journal of Clinical Investigation 1976;58(3):705–15. PubMed PMID: 956397; PubMed Central PMCID: PMC333229.
378. Saverymuttu SH, Peters AM, Keshavarzian A, Reavy HJ, Lavender JP. The kinetics of 111indium distribution following injection of 111indium labelled autologous granulocytes in man. Br J Haematol 1985;61(4):675–85. PubMed PMID: 4084457.
379. Steinbach KH, Schick P, Trepel F, Raffler H, Döhrmann J, Heilgeist G, et al. Estimation of kinetic parameters of neutrophilic, eosinophilic, and basophilic granulocytes in human blood. Blut 1979;39(1):27–38. PubMed PMID: 223692.
380. Feichtinger RG, Lang R. Targeting L-Lactate Metabolism to Overcome Resistance to Immune Therapy of Melanoma and Other Tumor Entities. J Oncol 2019;2019:2084195. PubMed PMID: 31781212; PubMed Central PMCID: PMC6875281.
381. Granchi C, Paterni I, Rani R, Minutolo F. Small-molecule inhibitors of human LDH5. Future Med Chem 2013;5(16):1967–91. PubMed PMID: 24175747; PubMed Central PMCID: PMC3952072.
382. Polański R, Hodgkinson CL, Fusi A, Nonaka D, Priest L, Kelly P, et al. Activity of the monocarboxylate transporter 1 inhibitor AZD3965 in small cell lung cancer. Clin Cancer Res 2014;20(4):926–37. PubMed PMID: 24277449; PubMed Central PMCID: PMC3929348.
383. Tidwell TR, Røsland GV, Tronstad KJ, Søreide K, Hagland HR. Metabolic flux analysis of 3D spheroids reveals significant differences in glucose metabolism from matched 2D cultures of colorectal cancer and pancreatic ductal adenocarcinoma cell lines. Cancer Metab 2022;10(1):9. PubMed PMID: 35578327; PubMed Central PMCID: PMC9109327.
384. Dong S, Liang S, Cheng Z, Zhang X, Luo L, Li L, et al. ROS/PI3K/Akt and Wnt/β-catenin signalings activate HIF-1α-induced metabolic reprogramming to impart 5-fluorouracil resistance in colorectal cancer. J Exp Clin Cancer Res 2022;41(1):15. PubMed PMID: 34998404; PubMed Central PMCID: PMC8742403.
385. Oshima N, Ishida R, Kishimoto S, Beebe K, Brender JR, Yamamoto K, et al. Dynamic Imaging of LDH Inhibition in Tumors Reveals Rapid In Vivo Metabolic Rewiring and Vulnerability to Combination Therapy. Cell Rep 2020;30(6):1798-1810.e4. PubMed PMID: 32049011; PubMed Central PMCID: PMC7039685.
386. Renner K, Seilbeck A, Kauer N, Ugele I, Siska PJ, Brummer C, et al. Combined Metabolic Targeting With Metformin and the NSAIDs Diflunisal and Diclofenac Induces Apoptosis in Acute Myeloid Leukemia Cells. Front Pharmacol 2018;9:1258. PubMed PMID: 30450049; PubMed Central PMCID: PMC6224440.
387. van der Windt GJW, Pearce EL. Metabolic switching and fuel choice during T-cell differentiation and memory development. Immunological Reviews 2012;249(1):27–42. PubMed PMID: 22889213; PubMed Central PMCID: PMC3645891.
388. Gubser PM, Bantug GR, Razik L, Fischer M, Dimeloe S, Hoenger G, et al. Rapid effector function of memory CD8+ T cells requires an immediate-early glycolytic switch. Nature Immunology 2013;14(10):1064–72. PubMed PMID: 23955661.

389. Hussien R, Brooks GA. Mitochondrial and plasma membrane lactate transporter and lactate dehydrogenase isoform expression in breast cancer cell lines. Physiol Genomics 2011;43(5):255–64. PubMed PMID: 21177384; PubMed Central PMCID: PMC3068517.
390. Dziurla R, Gaber T, Fangradt M, Hahne M, Tripmacher R, Kolar P, et al. Effects of hypoxia and/or lack of glucose on cellular energy metabolism and cytokine production in stimulated human CD4+ T lymphocytes. Immunology Letters 2010;131(1):97–105. PubMed PMID: 20206208.
391. Pearce EL, Poffenberger MC, Chang C-H, Jones RG. Fueling immunity: insights into metabolism and lymphocyte function. Science 2013;342(6155):1242454. PubMed PMID: 24115444; PubMed Central PMCID: PMC4486656.
392. Buck MD, Sowell RT, Kaech SM, Pearce EL. Metabolic Instruction of Immunity. Cell 2017;169(4):570–86. PubMed PMID: 28475890; PubMed Central PMCID: PMC5648021.
393. Frank A-C, Raue R, Fuhrmann DC, Sirait-Fischer E, Reuse C, Weigert A, et al. Lactate dehydrogenase B regulates macrophage metabolism in the tumor microenvironment. Theranostics 2021;11(15):7570–88. PubMed PMID: 34158867; PubMed Central PMCID: PMC8210612.
394. Markert CL, Shaklee JB, Whitt GS. Evolution of a gene. Multiple genes for LDH isozymes provide a model of the evolution of gene structure, function and regulation. Science 1975;189(4197):102–14. PubMed PMID: 1138367.
395. Tan Z, Xie N, Banerjee S, Cui H, Fu M, Thannickal VJ, et al. The monocarboxylate transporter 4 is required for glycolytic reprogramming and inflammatory response in macrophages. J Biol Chem 2015;290(1):46–55. PubMed PMID: 25406319; PubMed Central PMCID: PMC4281748.
396. Kumari N, Dwarakanath BS, Das A, Bhatt AN. Role of interleukin-6 in cancer progression and therapeutic resistance. Tumour Biol 2016;37(9):11553–72. PubMed PMID: 27260630.
397. Lippitz BE, Harris RA. Cytokine patterns in cancer patients: A review of the correlation between interleukin 6 and prognosis. Oncoimmunology 2016;5(5):e1093722. PubMed PMID: 27467926; PubMed Central PMCID: PMC4910721.
398. Xu J, Ye Y, Zhang H, Szmitkowski M, Mäkinen MJ, Li P, et al. Diagnostic and Prognostic Value of Serum Interleukin-6 in Colorectal Cancer. Medicine (Baltimore) 2016;95(2):e2502. PubMed PMID: 26765465; PubMed Central PMCID: PMC4718291.
399. Huseni MA, Wang L, Klementowicz JE, Yuen K, Breart B, Orr C, et al. CD8+ T cell-intrinsic IL-6 signaling promotes resistance to anti-PD-L1 immunotherapy. Cell Rep Med 2023;4(1):100878. PubMed PMID: 36599350; PubMed Central PMCID: PMC9873827.
400. Vilgelm AE. Illuminating the mechanism of IL-6-mediated immunotherapy resistance. Cell Rep Med 2023;4(1):100901. PubMed PMID: 36652910; PubMed Central PMCID: PMC9873941.
401. Mace TA, Shakya R, Pitarresi JR, Swanson B, McQuinn CW, Loftus S, et al. IL-6 and PD-L1 antibody blockade combination therapy reduces tumour progression in murine models of pancreatic cancer. Gut 2018;67(2):320–32. PubMed PMID: 27797936; PubMed Central PMCID: PMC5406266.
402. Liu H, Shen J, Lu K. IL-6 and PD-L1 blockade combination inhibits hepatocellular carcinoma cancer development in mouse model. Biochem Biophys Res Commun 2017;486(2):239–44. PubMed PMID: 28254435.
403. Feng J, Yang H, Zhang Y, Wei H, Zhu Z, Zhu B, et al. Tumor cell-derived lactate induces TAZ-dependent upregulation of PD-L1 through GPR81 in human lung cancer cells. Oncogene 2017;36(42):5829–39. PubMed PMID: 28604752.
404. Ranganathan P, Shanmugam A, Swafford D, Suryawanshi A, Bhattacharjee P, Hussein MS, et al. GPR81, a Cell-Surface Receptor for Lactate, Regulates Intestinal Homeostasis and Protects Mice from Experimental Colitis. The Journal of Immunology 2018;200(5):1781–9. PubMed PMID: 29386257; PubMed Central PMCID: PMC5858928.

405. Brown TP, Bhattacharjee P, Ramachandran S, Sivaprakasam S, Ristic B, Sikder MOF, et al. The lactate receptor GPR81 promotes breast cancer growth via a paracrine mechanism involving antigen-presenting cells in the tumor microenvironment. Oncogene 2020;39(16):3292–304. PubMed PMID: 32071396.
406. Di Zhang, Tang Z, Huang H, Zhou G, Cui C, Weng Y, et al. Metabolic regulation of gene expression by histone lactylation. Nature 2019;574(7779):575–80. PubMed PMID: 31645732; PubMed Central PMCID: PMC6818755.
407. Mishalian I, Bayuh R, Levy L, Zolotarov L, Michaeli J, Fridlender ZG. Tumor-associated neutrophils (TAN) develop pro-tumorigenic properties during tumor progression. Cancer Immunology, Immunotherapy 2013;62(11):1745–56. PubMed PMID: 24092389.
408. Uribe-Querol E, Rosales C. Neutrophils in Cancer: Two Sides of the Same Coin. J Immunol Res 2015;2015:983698. PubMed PMID: 26819959; PubMed Central PMCID: PMC4706937.
409. Hurt B, Schulick R, Edil B, El Kasmi KC, Barnett C. Cancer-promoting mechanisms of tumor-associated neutrophils. Am J Surg 2017;214(5):938–44. PubMed PMID: 28830617.
410. Spicer JD, McDonald B, Cools-Lartigue JJ, Chow SC, Giannias B, Kubes P, et al. Neutrophils promote liver metastasis via Mac-1-mediated interactions with circulating tumor cells. Cancer Research 2012;72(16):3919–27. PubMed PMID: 22751466.
411. Howard K, Lo KK, Ao L, Gamboni F, Edil BH, Schulick R, et al. Intercellular adhesion molecule-1 mediates murine colon adenocarcinoma invasion. J Surg Res 2014;187(1):19–23. PubMed PMID: 24360118; PubMed Central PMCID: PMC4844553.
412. Subhan MA, Torchilin VP. Neutrophils as an emerging therapeutic target and tool for cancer therapy. Life Sci 2021;285:119952. PubMed PMID: 34520766.
413. Mirnezami R, Jiménez B, Li JV, Kinross JM, Veselkov K, Goldin RD, et al. Rapid diagnosis and staging of colorectal cancer via high-resolution magic angle spinning nuclear magnetic resonance (HR-MAS NMR) spectroscopy of intact tissue biopsies. Ann Surg 2014;259(6):1138–49. PubMed PMID: 23860197.
414. Sutherland RM. Cell and environment interactions in tumor microregions: the multicell spheroid model. Science 1988;240(4849):177–84. PubMed PMID: 2451290.
415. Gottfried E, Kunz-Schughart LA, Andreesen R, Kreutz M. Brave little world: spheroids as an in vitro model to study tumor-immune-cell interactions. Cell Cycle 2006;5(7):691–5. PubMed PMID: 16582627.
416. Herter S, Morra L, Schlenker R, Sulcova J, Fahrni L, Waldhauer I, et al. A novel three-dimensional heterotypic spheroid model for the assessment of the activity of cancer immunotherapy agents. Cancer Immunology, Immunotherapy 2017;66(1):129–40. PubMed PMID: 27858101; PubMed Central PMCID: PMC5222939.
417. Courau T, Bonnereau J, Chicoteau J, Bottois H, Remark R, Assante Miranda L, et al. Cocultures of human colorectal tumor spheroids with immune cells reveal the therapeutic potential of MICA/B and NKG2A targeting for cancer treatment. J Immunother Cancer 2019;7(1):74. PubMed PMID: 30871626; PubMed Central PMCID: PMC6417026.
418. Zboralski D, Hoehlig K, Eulberg D, Frömming A, Vater A. Increasing Tumor-Infiltrating T Cells through Inhibition of CXCL12 with NOX-A12 Synergizes with PD-1 Blockade. Cancer Immunology Research 2017;5(11):950–6. PubMed PMID: 28963140.
419. Haugen ØP, Vallenari EM, Belhaj I, Småstuen MC, Storm-Mathisen J, Bergersen LH, et al. Blood lactate dynamics in awake and anaesthetized mice after intraperitoneal and subcutaneous injections of lactate-sex matters. PeerJ 2020;8:e8328. PubMed PMID: 31934509; PubMed Central PMCID: PMC6951280.

420. Jenkins RW, Aref AR, Lizotte PH, Ivanova E, Stinson S, Zhou CW, et al. Ex Vivo Profiling of PD-1 Blockade Using Organotypic Tumor Spheroids. Cancer Discov 2018;8(2):196–215. PubMed PMID: 29101162; PubMed Central PMCID: PMC5809290.
421. Susok L, Reinert D, Lukas C, Stockfleth E, Gambichler T. Volume increase of spleen in melanoma patients undergoing immune checkpoint blockade. Immunotherapy 2021;13(11):885–91. PubMed PMID: 34229447.
422. Reschke R, Gajewski TF. CXCL9 and CXCL10 bring the heat to tumors. Sci Immunol 2022;7(73):eabq6509. PubMed PMID: 35867802.
423. Reschke R, Yu J, Flood B, Higgs EF, Hatogai K, Gajewski TF. Immune cell and tumor cell-derived CXCL10 is indicative of immunotherapy response in metastatic melanoma. J Immunother Cancer 2021;9(9). PubMed PMID: 34593622; PubMed Central PMCID: PMC8487215.
424. House IG, Savas P, Lai J, Chen AXY, Oliver AJ, Teo ZL, et al. Macrophage-Derived CXCL9 and CXCL10 Are Required for Antitumor Immune Responses Following Immune Checkpoint Blockade. Clin Cancer Res 2020;26(2):487–504. PubMed PMID: 31636098.
425. Tasdogan A, Faubert B, Ramesh V, Ubellacker JM, Shen B, Solmonson A, et al. Metabolic heterogeneity confers differences in melanoma metastatic potential. Nature 2020;577(7788):115–20. PubMed PMID: 31853067; PubMed Central PMCID: PMC6930341.
426. Wang T, Xu H. Multi-faced roles of reactive oxygen species in anti-tumor T cell immune responses and combination immunotherapy. Exploration of Medicine 2022:77–98.
427. Chen X, Song M, Zhang B, Zhang Y. Reactive Oxygen Species Regulate T Cell Immune Response in the Tumor Microenvironment. Oxid Med Cell Longev 2016;2016:1580967. PubMed PMID: 27547291; PubMed Central PMCID: PMC4980531.
428. Siska PJ, Decking S-M, Babl N, Matos C, Bruss C, Singer K, et al. Metabolic imbalance of T cells in COVID-19 is hallmarked by basigin and mitigated by dexamethasone. J Clin Invest 2021;131(22). PubMed PMID: 34779418; PubMed Central PMCID: PMC8592546.
429. Pilipow K, Scamardella E, Puccio S, Gautam S, Paoli F de, Mazza EM, et al. Antioxidant metabolism regulates CD8+ T memory stem cell formation and antitumor immunity. JCI Insight 2018;3(18). PubMed PMID: 30232291; PubMed Central PMCID: PMC6237218.
430. Vishvakarma NK, Singh SM. Immunopotentiating effect of proton pump inhibitor pantoprazole in a lymphoma-bearing murine host: Implication in antitumor activation of tumor-associated macrophages. Immunology Letters 2010;134(1):83–92. PubMed PMID: 20837061.
431. Milito A de, Canese R, Marino ML, Borghi M, Iero M, Villa A, et al. pH-dependent antitumor activity of proton pump inhibitors against human melanoma is mediated by inhibition of tumor acidity. International Journal of Cancer 2010;127(1):207–19. PubMed PMID: 19876915.
432. Li M, Zeng C, Yao J, Ge Y, An G. The association between proton pump inhibitors use and clinical outcome of patients receiving immune checkpoint inhibitors therapy. Int Immunopharmacol 2020;88:106972. PubMed PMID: 33182025.
433. Dar S, Merza N, Qatani A, Rahim M, Varughese T, Mohammad A, et al. Impact of proton-pump inhibitors on the efficacy of immune checkpoint inhibitors in non-small cell lung cancer: A systematic review and meta-analysis. Ann Med Surg (Lond) 2022;78:103752. PubMed PMID: 35600176; PubMed Central PMCID: PMC9119820.
434. Qin B-D, Jiao X-D, Zhou X-C, Shi B, Wang J, Liu K, et al. Effects of concomitant proton pump inhibitor use on immune checkpoint inhibitor efficacy among patients with advanced cancer. Oncoimmunology 2021;10(1):1929727. PubMed PMID: 34350061; PubMed Central PMCID: PMC8296970.
435. Cappellesso F, Orban M-P, Shirgaonkar N, Berardi E, Serneels J, Neveu M-A, et al. Targeting the bicarbonate transporter SLC4A4 overcomes immunosuppression and immunotherapy resistance

in pancreatic cancer. Nat Cancer 2022;3(12):1464–83. PubMed PMID: 36522548; PubMed Central PMCID: PMC9767871.
436. Apostolova P, Pearce EL. Lactic acid and lactate: revisiting the physiological roles in the tumor microenvironment. Trends Immunol 2022;43(12):969–77. PubMed PMID: 36319537.
437. Ambrosetti D, Dufies M, Dadone B, Durand M, Borchiellini D, Amiel J, et al. The two glycolytic markers GLUT1 and MCT1 correlate with tumor grade and survival in clear-cell renal cell carcinoma. PLOS ONE 2018;13(2):e0193477. PubMed PMID: 29481555; PubMed Central PMCID: PMC5826688.
438. Singer K, Kastenberger M, Gottfried E, Hammerschmied CG, Büttner M, Aigner M, et al. Warburg phenotype in renal cell carcinoma: high expression of glucose-transporter 1 (GLUT-1) correlates with low CD8(+) T-cell infiltration in the tumor. International Journal of Cancer 2011;128(9):2085–95. PubMed PMID: 20607826.
439. Kim Y, Choi J-W, Lee J-H, Kim Y-S. Expression of lactate/H^+ symporters MCT1 and MCT4 and their chaperone CD147 predicts tumor progression in clear cell renal cell carcinoma: immunohistochemical and The Cancer Genome Atlas data analyses. Hum Pathol 2015;46(1):104–12. PubMed PMID: 25456395.
440. Xu F, Guan Y, Xue L, Huang S, Gao K, Yang Z, et al. The effect of a novel glycolysis-related gene signature on progression, prognosis and immune microenvironment of renal cell carcinoma. BMC Cancer 2020;20(1):1207. PubMed PMID: 33287763; PubMed Central PMCID: PMC7720455.
441. Shen H, Liu J, Chen S, Ma X, Ying Y, Li J, et al. Prognostic Value of Tumor-Associated Macrophages in Clear Cell Renal Cell Carcinoma: A Systematic Review and Meta-Analysis. Frontiers in Oncology 2021;11:657318. PubMed PMID: 34026635; PubMed Central PMCID: PMC8136289.
442. Zelenay S, van der Veen AG, Böttcher JP, Snelgrove KJ, Rogers N, Acton SE, et al. Cyclooxygenase-Dependent Tumor Growth through Evasion of Immunity. Cell 2015;162(6):1257–70. PubMed PMID: 26343581; PubMed Central PMCID: PMC4597191.
443. Kamińska K, Czarnecka AM, Escudier B, Lian F, Szczylik C. Interleukin-6 as an emerging regulator of renal cell cancer. Urol Oncol 2015;33(11):476–85. PubMed PMID: 26296264.
444. Tanaka T, Narazaki M, Masuda K, Kishimoto T. Regulation of IL-6 in Immunity and Diseases. Adv Exp Med Biol 2016;941:79–88. PubMed PMID: 27734409.
445. Grivennikov SI, Greten FR, Karin M. Immunity, inflammation, and cancer. Cell 2010;140(6):883–99. PubMed PMID: 20303878; PubMed Central PMCID: PMC2866629.
446. Leidgens V, Seliger C, Jachnik B, Welz T, Leukel P, Vollmann-Zwerenz A, et al. Ibuprofen and Diclofenac Restrict Migration and Proliferation of Human Glioma Cells by Distinct Molecular Mechanisms. PLOS ONE 2015;10(10):e0140613. PubMed PMID: 26485029; PubMed Central PMCID: PMC4617646.
447. Liu Y, Liu A, Li H, Li C, Lin J. Celecoxib inhibits interleukin-6/interleukin-6 receptor-induced JAK2/STAT3 phosphorylation in human hepatocellular carcinoma cells. Cancer Prev Res (Phila) 2011;4(8):1296–305. PubMed PMID: 21490132.
448. Nikitakis NG, Hamburger AW, Sauk JJ. The nonsteroidal anti-inflammatory drug sulindac causes down-regulation of signal transducer and activator of transcription 3 in human oral squamous cell carcinoma cells. Cancer Res 2002;62(4):1004–7. PubMed PMID: 11861373.
449. Gudbrandsdottir G, Aarstad HH, Bostad L, Hjelle KM, Aarstad HJ, Bruserud Ø, et al. Serum levels of the IL-6 family of cytokines predict prognosis in renal cell carcinoma (RCC). Cancer Immunology, Immunotherapy 2021;70(1):19–30. PubMed PMID: 32621022; PubMed Central PMCID: PMC7838134.
450. Pilskog M, Nilsen GH, Beisland C, Straume O. Elevated plasma interleukin 6 predicts poor response in patients treated with sunitinib for metastatic clear cell renal cell carcinoma. Cancer Treatment and Research Communications 2019;19:100127. PubMed PMID: 30913495.

451. Wang Y, Zhang Y. Prognostic role of interleukin-6 in renal cell carcinoma: a meta-analysis. Clin Transl Oncol 2020;22(6):835–43. PubMed PMID: 31410730.
452. Fukada T, Hibi M, Yamanaka Y, Takahashi-Tezuka M, Fujitani Y, Yamaguchi T, et al. Two signals are necessary for cell proliferation induced by a cytokine receptor gp130: involvement of STAT3 in anti-apoptosis. Immunity 1996;5(5):449–60. PubMed PMID: 8934572.
453. Kamimura D, Ishihara K, Hirano T. IL-6 signal transduction and its physiological roles: the signal orchestration model. In: Reviews of Physiology, Biochemistry and Pharmacology: Springer, Berlin, Heidelberg; 2003. p. 1–38.
454. Su H, Lei C-T, Zhang C. Interleukin-6 Signaling Pathway and Its Role in Kidney Disease: An Update. Frontiers in Immunology 2017;8:405. PubMed PMID: 28484449; PubMed Central PMCID: PMC5399081.
455. Novick D, Engelmann H, Wallach D, Rubinstein M. Soluble cytokine receptors are present in normal human urine. J Exp Med 1989;170(4):1409–14. PubMed PMID: 2529343; PubMed Central PMCID: PMC2189483.
456. Scheller J, Rose-John S. Interleukin-6 and its receptor: from bench to bedside. Med Microbiol Immunol 2006;195(4):173–83. PubMed PMID: 16741736.
457. Rose-John S, Waetzig GH, Scheller J, Grötzinger J, Seegert D. The IL-6/sIL-6R complex as a novel target for therapeutic approaches. Expert Opin Ther Targets 2007;11(5):613–24. PubMed PMID: 17465721.
458. Zhuang P-Y, Wang J-D, Tang Z-H, Zhou X-P, Quan Z-W, Liu Y-B, et al. Higher proliferation of peritumoral endothelial cells to IL-6/sIL-6R than tumoral endothelial cells in hepatocellular carcinoma. BMC Cancer 2015;15:830. PubMed PMID: 26525581; PubMed Central PMCID: PMC4629315.
459. Weber R, Groth C, Lasser S, Arkhypov I, Petrova V, Altevogt P, et al. IL-6 as a major regulator of MDSC activity and possible target for cancer immunotherapy. Cell Immunol 2021;359:104254. PubMed PMID: 33296753.
460. Weber R, Riester Z, Hüser L, Sticht C, Siebenmorgen A, Groth C, et al. IL-6 regulates CCR5 expression and immunosuppressive capacity of MDSC in murine melanoma. J Immunother Cancer 2020;8(2). PubMed PMID: 32788238; PubMed Central PMCID: PMC7422659.
461. Tsukamoto H, Fujieda K, Hirayama M, Ikeda T, Yuno A, Matsumura K, et al. Soluble IL6R Expressed by Myeloid Cells Reduces Tumor-Specific Th1 Differentiation and Drives Tumor Progression. Cancer Research 2017;77(9):2279–91. PubMed PMID: 28235765.
462. Tsukamoto H, Fujieda K, Senju S, Ikeda T, Oshiumi H, Nishimura Y. Immune-suppressive effects of interleukin-6 on T-cell-mediated anti-tumor immunity. Cancer Sci 2018;109(3):523–30. PubMed PMID: 29090850; PubMed Central PMCID: PMC5834784.
463. Ohno Y, Toyoshima Y, Yurino H, Monma N, Xiang H, Sumida K, et al. Lack of interleukin-6 in the tumor microenvironment augments type-1 immunity and increases the efficacy of cancer immunotherapy. Cancer Sci 2017;108(10):1959–66. PubMed PMID: 28746799; PubMed Central PMCID: PMC5623732.
464. Yang K, Xu J, Fan M, Tu F, Wang X, Ha T, et al. Lactate Suppresses Macrophage Pro-Inflammatory Response to LPS Stimulation by Inhibition of YAP and NF-κB Activation via GPR81-Mediated Signaling. Frontiers in Immunology 2020;11:587913. PubMed PMID: 33123172; PubMed Central PMCID: PMC7573489.
465. Zhou H-C, Yu W-W, Yan X-Y, Liang X-Q, Ma X-F, Long J-P, et al. Lactate-driven macrophage polarization in the inflammatory microenvironment alleviates intestinal inflammation. Frontiers in Immunology 2022;13:1013686. PubMed PMID: 36330516; PubMed Central PMCID: PMC9623299.

466. Yang X, Lu Y, Hang J, Zhang J, Zhang T, Huo Y, et al. Lactate-Modulated Immunosuppression of Myeloid-Derived Suppressor Cells Contributes to the Radioresistance of Pancreatic Cancer. Cancer Immunology Research 2020;8(11):1440–51. PubMed PMID: 32917658.
467. San-Miguel J, Bladé J, Shpilberg O, Grosicki S, Maloisel F, Min C-K, et al. Phase 2 randomized study of bortezomib-melphalan-prednisone with or without siltuximab (anti-IL-6) in multiple myeloma. Blood 2014;123(26):4136–42. PubMed PMID: 24833354; PubMed Central PMCID: PMC4123433.
468. Orlowski RZ, Gercheva L, Williams C, Sutherland H, Robak T, Masszi T, et al. A phase 2, randomized, double-blind, placebo-controlled study of siltuximab (anti-IL-6 mAb) and bortezomib versus bortezomib alone in patients with relapsed or refractory multiple myeloma. Am J Hematol 2015;90(1):42–9. PubMed PMID: 25294016; PubMed Central PMCID: PMC4737504.
469. Liu Q, Yu S, Li A, Xu H, Han X, Wu K. Targeting interlukin-6 to relieve immunosuppression in tumor microenvironment. Tumour Biol 2017;39(6):1010428317712445. PubMed PMID: 28639898.
470. Dorff TB, Goldman B, Pinski JK, Mack PC, Lara PN, van Veldhuizen PJ, et al. Clinical and correlative results of SWOG S0354: a phase II trial of CNTO328 (siltuximab), a monoclonal antibody against interleukin-6, in chemotherapy-pretreated patients with castration-resistant prostate cancer. Clin Cancer Res 2010;16(11):3028–34. PubMed PMID: 20484019; PubMed Central PMCID: PMC2898710.
471. Venkiteshwaran A. Tocilizumab. MAbs 2009;1(5):432–8. PubMed PMID: 20065633; PubMed Central PMCID: PMC2759492.
472. Nagao A, Nakazawa S, Hanabusa H. Short-term efficacy of the IL6 receptor antibody tocilizumab in patients with HIV-associated multicentric Castleman disease: report of two cases. J Hematol Oncol 2014;7:10. PubMed PMID: 24438824; PubMed Central PMCID: PMC3896700.
473. Makol A, Gibson LE, Michet CJ. Successful use of interleukin 6 antagonist tocilizumab in a patient with refractory cutaneous lupus and urticarial vasculitis. J Clin Rheumatol 2012;18(2):92–5. PubMed PMID: 22334272.
474. Uemura M, van Trinh A, Haymaker C, Jackson N, Kim DW, Allison JP, et al. Selective inhibition of autoimmune exacerbation while preserving the anti-tumor clinical benefit using IL-6 blockade in a patient with advanced melanoma and Crohn's disease: a case report. J Hematol Oncol 2016;9(1):81. PubMed PMID: 27595932; PubMed Central PMCID: PMC5011857.
475. Voelxen NF, Blatt S, Knopf P, Henkel M, Appelhans C, Righesso LAR, et al. Comparative metabolic analysis in head and neck cancer and the normal gingiva. Clinical Oral Investigations 2018;22(2):1033–43. PubMed PMID: 28735466.
476. Cascone T, McKenzie JA, Mbofung RM, Punt S, Wang Z, Xu C, et al. Increased Tumor Glycolysis Characterizes Immune Resistance to Adoptive T Cell Therapy. Cell Metabolism 2018;27(5):977-987.e4. PubMed PMID: 29628419; PubMed Central PMCID: PMC5932208.
477. Siebeneicher H, Cleve A, Rehwinkel H, Neuhaus R, Heisler I, Müller T, et al. Identification and Optimization of the First Highly Selective GLUT1 Inhibitor BAY-876. ChemMedChem 2016;11(20):2261–71. PubMed PMID: 27552707; PubMed Central PMCID: PMC5095872.
478. Chan DA, Sutphin PD, Nguyen P, Turcotte S, Lai EW, Banh A, et al. Targeting GLUT1 and the Warburg effect in renal cell carcinoma by chemical synthetic lethality. Science Translational Medicine 2011;3(94):94ra70. PubMed PMID: 21813754; PubMed Central PMCID: PMC3683134.
479. Wu Q, Ba-Alawi W, Deblois G, Cruickshank J, Duan S, Lima-Fernandes E, et al. GLUT1 inhibition blocks growth of RB1-positive triple negative breast cancer. Nature Communications 2020;11(1):4205. PubMed PMID: 32826891; PubMed Central PMCID: PMC7442809.
480. Qiao T, Xiong Y, Feng Y, Guo W, Zhou Y, Zhao J, et al. Inhibition of LDH-A by Oxamate Enhances the Efficacy of Anti-PD-1 Treatment in an NSCLC Humanized Mouse Model. Frontiers in Oncology 2021;11:632364. PubMed PMID: 33859941; PubMed Central PMCID: PMC8042335.

481. Pilon-Thomas S, Kodumudi KN, El-Kenawi AE, Russell S, Weber AM, Luddy K, et al. Neutralization of Tumor Acidity Improves Antitumor Responses to Immunotherapy. Cancer Research 2016;76(6):1381–90. PubMed PMID: 26719539; PubMed Central PMCID: PMC4829106.
482. Yuan YH, Zhou CF, Yuan J, Liu L, Guo XR, Wang XL, et al. NaHCO3 enhances the antitumor activities of cytokine-induced killer cells against hepatocellular carcinoma HepG2 cells. Oncol Lett 2016;12(5):3167–74. PubMed PMID: 27899977; PubMed Central PMCID: PMC5103916.

Publications

Babl N, Sala-Hojman A, Ferretti R, Decking SM, Matos C, Koehl G, Siska PJ, Bruss C, Kellermeier F, Dettmer K, Oefner PJ, Althammer M, Voll F, Wichland M, Ugele I, Gild I, Ramaswamy S, Heinrich T, Herhaus C, Kreutz M, Renner K. MCT4 Blockade Increases the Efficacy of Immune Checkpoint Blockade. Cell Reports. 2023; under review

Babl N, Hofbauer J, Matos C, Voll F, Menevse AN, Rechenmacher M, Mair R, Beckhove P, Herr W, Siska PJ, Renner K, Kreutz M, Schnell A. Low-density lipoprotein balances T cell metabolism and enhances response to anti-PD-1 blockade in a HCT116 spheroid model. Front Oncol. 2023 Jan 27;13:1107484. doi: 10.3389/fonc.2023.1107484

Schoeppe R*, **Babl N***, Decking SM, Schönhammer G, Siegmund A, Bruss C, Dettmer K, Oefner PJ, Frick L, Weigert A, Jantsch J, Herr W, Rehli M, Renner K, Kreutz M. Glutamine synthetase expression rescues human dendritic cell survival in a glutamine-deprived environment. Front Oncol. 2023 Jan 19;13:1120194. doi: 10.3389/fonc.2023.1120194

Decking SM, Bruss C, **Babl N**, Bittner S, Klobuch S, Thomas S, Feuerer M, Hoffmann P, Dettmer K, Oefner PJ, Renner K, Kreutz M. LDHB Overexpression Can Partially Overcome T Cell Inhibition by Lactic Acid. Int J Mol Sci. 2022 May 26;23(11):5970. doi: 10.3390/ijms23115970

Hofbauer J, Hauck A, Matos C, **Babl N**, Decking SM, Rechenmacher M, Schulz C, Regotta S, Mickler M, Haferkamp S, Siska PJ, Herr W, Renner K, Kreutz M, Schnell A. Immunometabolic Markers in a Small Patient Cohort Undergoing Immunotherapy. Biomolecules. 2022 May 18;12(5):716. doi: 10.3390/biom12050716

Frick L, Hinterland L, Renner K, Vogl M, **Babl N**, Heckscher S, Weigert A, Weiß S, Gläsner J, Berger R, Oefner PJ, Dettmer K, Kreutz M, Schatz V, Jantsch J. Acidic Microenvironments Found in Cutaneous Leishmania Lesions Curtail NO-Dependent Antiparasitic Macrophage Activity. Front Immunol. 2022 Apr 14;13:789366. doi: 10.3389/fimmu.2022.789366

Matos C, Peter K, Weich L, Peuker A, Schoenhammer G, Roider T, Ghimire S, **Babl N**, Decking S, Güllstorf M, Kröger N, Hammon K, Herr W, Stark K, Heid IM, Renner K, Holler E, Kreutz M. Anti-Thymocyte Globulin Treatment Augments 1,25-Dihydroxyvitamin D3 Serum Levels in Patients Undergoing Hematopoietic Stem Cell Transplantation. Front Immunol. 2022 Jan 4;12:803726. doi: 10.3389/fimmu.2021.803726.

Siska PJ, Decking SM*, **Babl N***, Matos C*, Bruss C*, Singer K, Klitzke J, Schön M, Simeth J, Köstler J, Siegmund H, Ugele I, Paulus M, Dietl A, Kolodova K, Steines L, Freitag K, Peuker A, Schönhammer G,

Raithel J, Graf B, Geismann F, Lubnow M, Mack M, Hau P, Bohr C, Burkhardt R, Gessner A, Salzberger B, Wagner R, Hanses F, Hitzenbichler F, Heudobler D, Lüke F, Pukrop T, Herr W, Wolff D, Spang R, Poeck H, Hoffmann P, Jantsch J, Brochhausen C, Lunz D, Rehli M, Kreutz M, Renner K. Metabolic imbalance of T cells in COVID-19 is hallmarked by basigin and mitigated by dexamethasone. J Clin Invest. 2021 Nov 15;131(22):e148225. doi: 10.1172/JCI148225

Renner K, Bruss C, Schnell A, Koehl G, Becker HM, Fante M, Menevse AN, **Kauer N**, Blazquez R, Hacker L, Decking SM, Bohn T, Faerber S, Evert K, Aigle L, Amslinger S, Landa M, Krijgsman O, Rozeman EA, Brummer C, Siska PJ, Singer K, Pektor S, Miederer M, Peter K, Gottfried E, Herr W, Marchiq I, Pouyssegur J, Roush WR, Ong S, Warren S, Pukrop T, Beckhove P, Lang SA, Bopp T, Blank CU, Cleveland JL, Oefner PJ, Dettmer K, Selby M, Kreutz M. Restricting Glycolysis Preserves T Cell Effector Functions and Augments Checkpoint Therapy. Cell Rep. 2019 Oct 1;29(1):135-150.e9. doi: 10.1016/j.celrep.2019.08.068

Renner K, Seilbeck A, **Kauer N**, Ugele I, Siska PJ, Brummer C, Bruss C, Decking SM, Fante M, Schmidt A, Hammon K, Singer K, Klobuch S, Thomas S, Gottfried E, Peter K, Kreutz M. Combined Metabolic Targeting With Metformin and the NSAIDs Diflunisal and Diclofenac Induces Apoptosis in Acute Myeloid Leukemia Cells. Front Pharmacol. 2018 Nov 2;9:1258. doi: 10.3389/fphar.2018.01258

Acknowledgement

An dieser Stelle möchte ich mich von ganzem Herzen bei allen Menschen bedanken, die mich während dieser unglaublichen Zeit meiner Promotion begleitet und unterstützt haben!

Mein ganz besonderer Dank gilt an erster Stelle meiner Mentorin und Doktormutter **Prof. Dr. Marina Kreutz**. Schon während meiner Masterarbeit habe ich mich sehr wohl, unterstützt und gefördert gefühlt. Du hast mich von Anfang an inspiriert und mir wurde schnell klar, genau hier möchte ich die nächsten 4 Jahre auch meine Doktorarbeit machen. Ich danke Dir für diese Chance, für das stetige Coaching, die herausragende Betreuung, die fachlichen Diskussionen, deinen ansteckenden Enthusiasmus, das vertrauensvolle Arbeitsverhältnis, den Rückhalt, das spannende Projekt, Deinen Glauben an mich und Deine Unterstützung in jeder Hinsicht! Ich bin stolz sagen zu können, dass ich wirklich viel Spaß hatte und glücklich darüber bin die Doktorarbeit bei Dir gestartet zu haben – es war eine wundervolle Zeit!

Außerdem möchte mich von ganzem Herzen bei (meiner inoffiziell 2. Doktormutter) **Prof. Dr. Kathrin Renner** bedanken. Vielen Dank auch an Dich für die ausgezeichnete Betreuung, für die enorme Unterstützung und dafür, dass ich so unglaublich viel von Dir lernen durfte! Gerade bei den für mich extrem herausfordernden Tierexperimenten warst Du für mich ein Fels in der Brandung, ich danke Dir für den im wahrsten Sinne des Wortes tatkräftigen Beistand, ohne Dich hätte ich diese Herausforderungen nicht so leicht überstanden. Danke, dass Du mir selbst jetzt noch alle möglichen Fragen beantwortest!

Meinen beiden Mentoren **Prof. Dr. Richard Warth** und **Prof. Dr. Viktor Umansky** möchte ich auch meinen besonderen Dank aussprechen. Vielen Dank für die Übernahme des Mentorats sowie für die konstruktiven Diskussionen und Ratschläge im Rahmen meiner Progress Reports. Herr **Prof. Dr. Warth** hat bereits zu Beginn meines Studiums den Grundstein für meine Laufbahn gelegt und meine Begeisterung für Wissenschaft, für das Studium der Molekularen Medizin und die Forschung entfacht – vielen herzlichen Dank dafür!

Vielen Dank an **Prof. Dr. Wolfgang Herr**, der mir ermöglicht hat meine Dissertation am Lehrstuhl der Inneren Medizin III anzufertigen.

A very big THANK YOU also goes to all of the Merck's collaboration partners. Many thanks to **Dr. Christian Herhaus**, **Dr. Ada Sala-Hojman** and **Dr. Roberta Ferretti** for the wonderful and pleasant collaboration. Thank you for the chance to work on this exciting project, thank you for the numerous meetings and professional discussions, for the close teamwork and the always great atmosphere. Many thanks also for your intensive work on our joint manuscript and all your constructive helpful

suggestions. I have learned a lot during our 3-year (and beyond) collaboration and I am incredibly grateful that I could get this insight and I think I am very lucky to be part of this journey. I enjoyed it very much! In this context, I would also like to thank everyone else involved at Merck, thanks to **Dr. Stephan Gürtler** for the incredibly fast review of all my abstracts/presentations and my PhD thesis. Thanks to **Dr. Timo Heinrich** for providing the substances without complications and thanks to **Dr. Shivapriya Ramaswamy** for her expertise and discussions at several meetings.

Außerdem möchte ich **Dr. Gudrun Köhl** für Ihre Unterstützung bei allen Mausexperimenten danken, ohne Dein fachliches Können wäre das so nicht möglich gewesen. Vielen Dank für alles! Vielen Dank an **Fabian Kellermeier**, **Dr. Katja Dettmer**, **Prof. Dr. Peter Öfner** für die Messung, Auswertung und Hilfestellung bei der Interpretation der Metabolomics-Experimente. Des Weiteren möchte ich mich herzlich bei **Dr. Malte Simon** bedanken, der mich immer tatkräftig in allen bioinformatischen Fragestellungen und Auswertungen unterstützt hat.

Danke an **Prof. Dr. Michael Rehli** für die konstruktiven Vorschläge in den Laborseminaren und an die gesamte AG Rehli für die freundschaftliche Zusammenarbeit. Vor allem ein großes Dankeschön an **Johanna** für alle unsere Parkplatzgespräche und dass man immer auf Dich zählen kann. Und auch an alle anderen AG Mitglieder **Hanna**, **Margit**, **Ute**, **Jan** und **Alex** – es war immer schön mit Euch zusammenzuarbeiten!

Ganz besonders möchte ich mich auch noch bei **meiner allertollsten AG Kreutz** bedanken, dank Euch bin ich immer gerne in die Arbeit gegangen:

Mein größter Dank gilt **Dr. Sonja Decking** und **Dr. Carina Matos**.

Ich möchte Dir von ganzem Herzen danken, liebe **Sonja**. DANKE für die unzähligen Stunden, die wir gemeinsam im Labor (und auch außerhalb) verbracht haben. Danke für alles was ich von Dir lernen durfte, danke für all deine Unterstützung. Ich konnte einfach immer auf Dich zählen, selbst an den unzähligen Wochenenden, die Du wegen mir im Tierstall verbracht hast, um mir zu helfen. Ich bin dankbar, dass wir dieses tiefe Vertrauensverhältnis entwickeln konnten und wir uns immer zu 100 % aufeinander verlassen können, wir waren einfach ein Dream Team ;-). Zusammen gab es eigentlich keine Herausforderung, die wir nicht meistern konnten. Danke auch, dass Du Dich durch meine Doktorarbeit gequält hast ;-). Ich hätte mir keine bessere Mitdoktorandin wünschen können und bin dankbar, dass sich aus unserer Doktorandenzeit eine Freundschaft fürs Leben entwickelt hat. Ich weiß, dass Du auf jeden Fall Großartiges in Deinem Leben erreichen wirst und wünsche Dir von ganzem Herzen nur das Beste!

Then I would also like to thank you from the bottom of my heart, dear **Carina**! Thanks for always having my back, for everything you taught me, for always being there for me, for your kind and good-willed

nature. Thank you for being able to talk honestly about everything together and for always supporting each other. I can't imagine a better colleague and it was/is an honor to work with you! You are amazing! I am really looking forward to sharing not only the scientist's journey, but also the mom's journey with you in the future!

Tausend Dank auch an **Alice** und **Gabi**, die besten TAs überhaupt! Danke, dass ich immer von Eurem Erfahrungsschatz und Wissen profitieren durfte, ich Euch immer alles Fragen konnte, Ihr mir alles Mögliche gezeigt habt und mich auch bei großen Experimenten selbstverständlich unterstützt habt. Alice, Du beeindruckst mich immer wieder mit Deinem Pragmatismus und Deiner effizienten Arbeitsweise, da konnte ich mir wirklich viel abkucken und Gabi, Du imponierst mir immer wieder, Du bist die ‚Etablierungsqueen' und bist an Sorgfältigkeit und Deinen ‚Magic Hands' nicht zu übertreffen. Vielen Dank auch an **Moni**, auch wenn Du nicht mehr direkt bei uns warst, bist Du trotzdem immer da. Du bist einfach die gute Seele der Labore – danke für alles und vor allem für alles, was Du immer selbstlos im Hintergrund tust und an Aufgaben übernimmst! Vielen Dank auch an Dich **Marcus**. Du standst immer für ein nettes Gespräch bereit und hast stets Deine Hilfe angeboten! Vielen Dank auch an **Dr. Peter Siska**, für Deine unzähligen Überlebensanalysen, die fachlichen Diskussionen, Deinen Input und alle Ideen für meine Experimente und Paper!

Außerdem möchte ich auch noch Dir, liebe **Tina,** danken! Danke für die Zeit, die ich noch mit Dir zusammenarbeiten durfte und alles was Du mir gezeigt und gelernt hast! Danke für Deine liebe Art, Dein Wohlwollen und Deine selbstlose Hilfsbereitschaft! Ich wünsche Dir nur das Allerbeste!

Danke auch an die neu dazu gestoßenen Jungs, **Flo** und **Michael**! Ich bin so happy über Euch zwei als neue Doktoranden, es macht riesen Spaß mit Euch zu arbeiten, wir matchen perfekt und sind alle auf einer Wellenlänge. Hirschberg wird mir vor allem auch dank Euch immer in schöner Erinnerung bleiben (danke, dass wir nicht gekentert sind) und ich hoffe auf weitere coole Kongresse mit Euch. Danke, dass Ihr gerade in letzter Zeit ganz selbstverständlich alles Mögliche im Labor für mich übernommen habt!

Zu guter Letzt möchte ich **meiner Familie** danken, ohne Euch wäre ich niemals da wo ich jetzt bin. Einen besonderen Dank an meine **Mama** für Deine bedingungslose Unterstützung, danke für Deine Wertschätzung und dass Du mich immer wieder aufbaust! Dank Dir konnte ich die Persönlichkeit, das Selbstbewusstsein und die innere Stärke entwickeln alles in meinem Leben mit Selbstvertrauen zu meistern. Und vor allem auch DANKE an meinen Ehemann **Jannis**. Danke, dass Du immer an mich glaubst, mir immer den Rücken freihältst und für einfach alles Verständnis hast! Du gibst mir das Urvertrauen und die Kraft, dass wir gemeinsam alles schaffen können. Du machst mein Leben komplett. Diese Dissertation widme ich dem größten Geschenk des Universums (und dem wohl besten ‚Endprodukt' meiner Doktorarbeitszeit), unserem gemeinsamen Sohn.